Graduate School ETD Form 9
(Revised 01/14)

PURDUE UNIVERSITY
GRADUATE SCHOOL
Thesis/Dissertation Acceptance

This is to certify that the thesis/dissertation prepared

By Peter B. Robertson

Entitled
Pt I: Neoacadian-Alleghanian foreland basin development & provenance, Pine Mtn thrust sheet;
Pt II: Structural configuration of a modified Mesozoic-Cenozoic forearc basin, south-central AK

For the degree of Master of Science

Is approved by the final examining committee:

Kenneth Ridgway

Christopher Andronicos

Jeffrey Trop

To the best of my knowledge and as understood by the student in the *Thesis/Dissertation Agreement. Publication Delay, and Certification/Disclaimer (Graduate School Form 32)*, this thesis/dissertation adheres to the provisions of Purdue University's "Policy on Integrity in Research" and the use of copyrighted material.

Kenneth Ridgway

Approved by Major Professor(s): _____

_____

Approved by: Indrajeet Chaubey 02/26/2014

Head of the Department Graduate Program Date

PART I: NEOACADIAN TO ALLEGHANIAN FORELAND BASIN DEVELOPMENT AND PROVENANCE IN THE CENTRAL APPALACHIAN OROGEN, PINE MOUNTAIN THRUST SHEET

PART II: STRUCTURAL CONFIGURATION OF A MODIFIED MESOZOIC TO CENOZOIC FOREARC BASIN SYSTEM, SOUTH-CENTRAL ALASKA

A Thesis

Submitted to the Faculty

of

Purdue University

by

Peter B. Robertson

In Partial Fulfillment of the

Requirements for the Degree

of

Master of Science

May 2014

Purdue University

West Lafayette, Indiana

ProQuest LLC.
789 East Eisenhower Parkway
P.O. Box 1346
Ann Arbor, MI 48106 - 1346

"The mountains are calling and I must go, and I will work on while I can, studying incessantly."

"We are now in the mountains and they are in us, kindling enthusiasm, making every nerve quiver, filling every pore and cell of us."

- John Muir

ACKNOWLEDGEMENTS

It seems fitting to first thank those that initially encouraged me to pursue a Master's Degree in geology during my studies in the Department of Earth, Atmospheric, and Planetary Sciences at the University of Tennessee in Knoxville, TN. I am sincerely thankful for the interactions with and research opportunities provided by several of the professors and students there who fostered my passion for the geosciences, a long list of friends which includes Bob Hatcher, Nancy Meadows, Linda Kah, Colin Sumrall, Chris Fedo, Michael McKinney, Will Atwood, Rene Shroat-Lewis, Mike DeAngelis, Phil Derryberry, Andrea Hughes, Noah McDougall, Emily Napier, and many others. I would also like thank my family for their support and encouragement throughout my education. Without these people, none of the adventures that I have had the privilege of experiencing during this most recent chapter of my life at Purdue University would have been possible.

My research endeavors at Purdue University certainly would not have been possible without the guidance and support of my advisor, Ken Ridgway. From the start, Ken has focused on my development as an individual and as a team member in our research group and has contributed to my academic and professional growth throughout my time at Purdue. Ken has provided me with the necessary knowledge and tools to properly investigate my research in Alaska and in the Appalachians with seemingly unwavering patience. I thoroughly appreciate Ken for his ability to evaluate problems from multiple perspectives and for his philosophy of keeping a healthy balance between school and personal life. For all of these things, I am truly grateful. Thank you, Ken.

For their service as indispensible members of my thesis committee, I am grateful for Chris Andronicos and Jeff Trop. Without their help, many of the key research questions and discussions for each chapter and for future work would not have come to fruition. Chris and Jeff were particularly instrumental in helping me integrate my research findings and ideas into the big-picture context in both the Appalachian foreland basin system and in the Matanuska forearc basin system of south-central Alaska. I appreciate their patience and guidance and all of the time they have volunteered to improve upon my thesis work.

The culmination of work presented in Chapter 2 of this thesis was significantly impacted and improved upon by several individuals with whom I have had the fortune and distinct pleasure of working and coming to know during my thesis work at Purdue University. I would like to express gratitude to the Arizona LaserChron Center for the preparation of our detrital zircon samples and data formatting, as well as the National Science Foundation for transportation and lodging reimbursement during detrital zircon analyses. I sincerely appreciate the field and labwork assistance from Tommy Lovell, Andrea Stevens, Kate Verner, Bianca Maibauer, Kim Davis, and Ken Ridgway. I am grateful for meaningful discussions with Tom Becker regarding detrital zircon datasets for the Appalachian basin, William Andrews involving the emplacement history of the Pine Mountain thrust sheet, Don Chesnut and Steve Greb regarding terminology in the central Appalachian basin, Frank Ettensohn regarding the Late Devonian submarine fan systems of the basin, and Bob Hatcher regarding timing of, amount of shortening during, and provenance trends of the Alleghanian orogeny and the provenance in the Appalachian foreland basin. I also appreciate correspondence with Kim Hlava and her assistance with thin sections made from the measured section and Colin Sumrall for his assistance in fossil identification. This study also benefited from the wide range of perspectives provided by members of the Geology and Geophysics group and the Lithospheric Tectonics and Basin Research group in the Department of Earth, Atmospheric, and Planetary Sciences at Purdue University.

I would also like to recognize several individuals for their assistance in the completion of Chapter 3 of this thesis, including: Dwight Bradley and his family for accommodating our field crew during the 2011 field season; Chris Andronicos for his expertise and instruction that have significantly contributed to my understanding of some of the fundamental theories and techniques in structural geology, as well as for his guidance in the construction and interpretations of the cross-sections provided in this thesis; Christine Kassab for her help in providing literature suggestions, meaningful conversations about the Matanuska Valley region, and drafting assistance; Bruce Idleman for field work and medical assistance, as well as for lending me his camera in the field; Jeff Trop for field assistance, correspondence, and suggestions that have significantly contributed to the construction of the text, geologic maps, and cross-sections of Chapter 3; Kyle Kissock and Erin Donaghy for field assistance and correspondence during the course of the study; and meaningful conversations with Terry Pavlis and Sarah Roeske regarding the geologic evolution and structure of the Matanuska Valley region.

Lastly, I would like to acknowledge my friends and family for their support throughout my time at Purdue. The graduate school experience entails many difficult and overwhelming experiences, whether presented in research, coursework, or personal endeavors, and I owe many thanks to those that have been there for me in both my times of victory and defeat. For helping to improve the quality of life, I acknowledge Kim Davis, Darryl Reano, Ruth Aronoff, Ian Pope, Paul Acosta, Alex Gonzalez, Aaron Goldner, Robin Blomdin, Casey Beel, Jerry Bollinger, Rachel Gipe, Bianca Maibauer, Maide Barisciano, Jackie Schrader and many of the employees of Greyhouse Coffee and Supply Co. who are always smiling, Kristen Footo, Noah McDougall, Emily Napier, Haylee Dickinson, and Tommy Lovell. Thank you all.

This research was funded by grant money awarded by the National Science Foundation for the Arkose Ridge Project. I am grateful to the Department of Earth, Atmospheric, and Planetary Sciences at Purdue University for financial support in the form of several

teaching assistantships and various monetary awards provided by the department, alumni, and financial supporters of the department.

TABLE OF CONTENTS

Page

Page

LIST OF TABLES

LIST OF FIGURES

Figure Page

Appendix Figure

ABSTRACT

Robertson, Peter B. M.S., Purdue University, May 2014. Part I: Neoacadian to Alleghanian Foreland Basin Development and Provenance in the Central Appalachian Orogen, Pine Mountain Thrust Sheet; Part II: Structural Configuration of a Modified Mesozoic to Cenozoic Forearc Basin System, South-central Alaska. Major Professor: Kenneth Ridgway.

Foreland and forearc basins are large sediment repositories that form in response to tectonic loading and lithospheric flexure during orogenesis along convergent plate boundaries. In addition to their numerous valuable natural resources, these systems preserve important geologic information regarding the timing and intensity of deformation, uplift and erosion history, and subsidence history along collisional margins, and, in ancient systems, may provide more macroscopic information regarding climate, plate motion, and eustatic sea level fluctuations. This thesis presents two studies focused in the Paleozoic Appalachian foreland basin system along the eastern United States and in the Mesozoic to Cenozoic Matanuska forearc basin system in south-central Alaska.

Strata of the Appalachian foreland basin system preserve the dynamic history of orogenesis and sediment dispersal along the east Laurentian margin, recording multiple episodes of deformation and basin development during Paleozoic time. A well-exposed, >600 m thick measured stratigraphic section of the Pine Mountain thrust sheet at Pound Gap, Kentucky affords one of the most complete exposures of Upper Devonian through Middle Pennsylvanian strata in the basin. These strata provide a window into which the foreland basin's development during two major collisional events known as the Acadian-Neoacadian and the Alleghanian orogenies can be observed. Lithofacies analysis of four major sedimentary successions observed in hanging wall strata record the upward transition from (1) a submarine deltaic fan complex developed on a distal to proximal

prodelta in Late Devonian to Middle Mississippian time, to (2) a Middle to Late Mississippian carbonate bank system developed on a slowly subsiding, distal foreland ramp, which was drowned by (3) Late Mississippian renewed clastic influx to a tidally influenced, coastal deltaic complex to fluvial delta plain system unconformably overlain by (4) a fluvial braided river complex. Four samples of Lower Mississippian to Middle Pennsylvanian sandstone were collected from the hanging wall (n = 3) and footwall (n = 1) of the Pine Mountain thrust sheet at Pound Gap to determine sediment provenance in this long-lived foreland basin system. Paleocurrent indicators considered in the context of the regional foreland basin system suggest transverse regional drainage during the development of Early and Late Mississippian delta complexes. Eustatic fall during the early stages of the Alleghanian orogeny to the east saw a shift in regional drainage with the development of a southwestward-flowing and axial braided river system in Early Pennsylvanian time followed by Middle Mississippian transgression of a fluvio-deltaic complex. Detrital zircon U-Pb age data from Lower Mississippian to Lower Pennsylvanian sandstone support regional interpretations of sediment sourcing from probably recycled foreland basin strata along the east Laurentian margin, whereas compositionally immature Middle Pennsylvanian sediment was sourced by a limited distribution of east Laurentia sources reflecting thrust belt migration into the adjacent foreland basin system during Alleghanian orogenesis.

In addition, the stratigraphy of the foreland basin system in the central Appalachian basin is significantly different compared to the stratigraphic record that is typified for foreland basin systems and suggests that the Carboniferous Appalachian foreland basin system investigated in this study does not fit the typical foreland basin model that is used widely today for both ancient and modern systems. Possible factors that produce the observed discrepancies between the central Appalachian and typical foreland basin systems may include differences in the timing, type, and frequency of orogenic events leading to foreland basin development, related variations in the rheology of the underlying lithosphere, and whether forebulge migration is mechanically static or mobile.

The Cordilleran margin of south-central Alaska is an area of active convergence where the Pacific plate is being subducted at a low angle beneath the North American plate. In the Matanuska Valley of south-central Alaska, the geology of the Mesozoic to Cenozoic Matanuska forearc basin system records a complex collisional history along the margin from Cretaceous to Miocene time and provides an opportunity to study how shallow-angle subduction affects upper plate processes. Paleocene-Eocene low-angle subduction of an eastward migrating spreading ridge and Oligocene oceanic plateau subduction caused uplift, deformation, and slab window magmatic intrusion and volcanism in the Matanuska Valley region, thereby modifying the depositional environment and structure of the forearc system. In this study, detailed field mapping in the Matanuska Valley region and structural analysis of Paleocene-Eocene nonmarine sedimentary strata are utilized to better understand the structural response of the forearc basin system to multi-stage flat-slab subduction beneath an accreted continental margin, a process observed along multiple modern convergent margins. Four geologic maps and structural cross-sections from key areas along the peripheries of the Matanuska Valley area and one regional cross-section across the forearc system are presented to delineate its local structural configuration and to contribute to a more complete understanding of how sedimentary and tectonic processes along modern convergent margins may be or have been impacted by shallow-angle type and related subduction processes.

CHAPTER 1. INTRODUCTION

1.1 Introduction to the Central Appalachian Orogen

The Appalachian foreland basin is a northeast-southwest trending Paleozoic basin that spans from Alabama to New York in the southern and central Appalachians of the eastern United States (Fig. 2.1a). This basin is subdivided into three sub-basins referred to as the southern, central, and northern Appalachian basins, each of which is characterized by a distinct stratigraphic record and natural resources (e.g., hydrocarbons, coal, groundwater, fertile soils, etc.) essential to the eastern United States and beyond. The study presented in Chapter 2 of this thesis concerns the Late Devonian to Middle Pennsylvanian depositional history of the central Appalachian basin from strata of the Pine Mountain thrust sheet exposed at Pound Gap, Kentucky (Fig. 2.1b).

The central Appalachian foreland basin contains the thickest Carboniferous stratigraphic section in the Appalachian foreland basin system (~2500 m; Ettensohn et al., 2002) and preserves the axis of the Alleghanian foreland basin with >1,200 m of Pennsylvanian strata along the Kentucky-Virginia border (Greb et al., 2002, their figure 1). Exposures of Mississippian strata are limited to areas along the outskirts of the central Appalachian basin, which is dominantly characterized by Pennsylvanian strata forming its desiccated surficial landscape (Fig. 2.1a), or in the weakly deformed thrust sheets of the Valley and Ridge Province (e.g., Greb et al., 2002). Mississippian and older strata are otherwise buried at depths of ~600 m in the Valley and Ridge and thus conceal the depositional history of the central Appalachian basin.

Regional studies have recognized that Mississippian carbonate strata are thickest in the thrust sheets toward the southeast (<1,200 m; Nelson and Read, 1990) and thin

northwestward to ~30 m thick over the Waverly Arch (Ettensohn, 1980; Nelson and Read, 1990; Chesnut, 1992; Al-Tawil and Read, 2003), which remained a topographic high into the Pennsylvanian period (Dever, 1999). Whereas Pennsylvanian strata overlie progressively older Mississippian strata toward the Cincinnati Arch, upper Devonian clastic (Ettensohn and Elam, 1985) and Mississippian carbonate strata (Grabowski, 1986; Dever, 1999) of the central Appalachian basin thin onto the structural high, which was active episodically throughout the Paleozoic (Fig. 2.2). Upper Mississippian strata are separated from underlying Upper Devonian and Lower Mississippian strata by a Late Mississippian unconformity formed during reactivation of the structure and accelerated uplift to the east of the basin (Fig. 2.2) (de Witt and McGrew, 1979; Dever, 1999).

The Blue Ridge and Piedmont physiographic provinces comprise the crystalline core of the Appalachian orogen which lies parallel to the basin to the east and formed as the result of multiple episodes of Paleozoic accretion to the eastern Laurentian margin (Fig. 2.1a) (see Hatcher, 2010). As it contains the thickest Carboniferous strata along the origin, the central Appalachian basin preserves the best record of fluctuating basin dynamics in response to tectonism during arc-collision of the Late Devonian Neoacadian orogeny and continental-collision of the Late Mississippian to Permian Alleghanian orogeny.

1.2 Study Area and Historical Background

Pound Gap is located on the border of Kentucky and Virginia in Jefferson National Forest where U.S. Route 23 passes through Pine Mountain (Fig. 2.1b). Historically, this natural gap provided passage to early settlers in the Appalachians, including Daniel Boone, across Pine Mountain and was later the site of the Battle of Pound Gap in which a young Brigadier General James A. Garfield led Union troops to victory during the Civil War. Today, this battle and the Union and Confederate soldiers who lost their lives are commemorated at the Brothers Once More war monument.

The earliest known geologic description of Pound Gap was made by Owen (then referred to as ‘Sounding gap’; 1856, p. 229-230) in the first geologic survey of Kentucky. Over a

century later, Wilpolt and Marden (1959) described the section there as part of a larger study to assess the oil and gas potential of Mississippian strata in the central Appalachian Basin. The geology of and stratigraphy of the Jenkins West quadrangle (Pound quadrangle of Wilpolt and Marden, 1959) was later mapped and described by Rice (1973). Other known work at Pound Gap has focused on creating a field guide for the exposure the year it was revealed for the Kentucky Society of Professional Geologists (Chesnut et al., 1998), sequence stratigraphy and late Mississippian climatic variation evidenced in the Pennington Formation (Kahmann-Robinson, 2008), diagenetic alteration of carbonate rhizocretions in the Pennington Formation (Ober, 2003), and analyzing the carbonate petrography, lithofacies, depositional environments, and sequence stratigraphy of the Newman Limestone (Demmin, 1999; Johanson, 2000; Al-Tawil and Read, 2003). The exposure was also included in a study in the central Appalachian basin which used exposures of Mississippian strata in other areas of the Pine Mountain thrust sheet in order to reinterpret the stratigraphy, depositional environments, and tectonic framework of the basin (Ettensohn et al., 2002). These authors mainly use the regional stratigraphy to support a flexural relaxation model for the basin during the late Mississippian, whereas Greb et al. (2002, same volume) proposed the exposure at Pound Gap as a new reference section for Mississippian stratotypes and boundaries on Pine Mountain. The section was most recently included in a study on the Borden-Grainger-Fort Payne deltaic system in the central Appalachian basin of Kentucky (Udgata, 2011), from which descriptions were included in a field guide that included stops throughout the basin and at Pound Gap (Ettensohn et al., 2012). Today, the Pound Gap exposure is frequently visited by universities across the nation and serves as a valuable stage where budding and seasoned geoscientists alike may learn hands-on some of the fundamental geologic features and processes that are studied in our science. As a testament to this, I myself had visited the exposure at least five times prior to the inclusion of this study in my thesis work as part of classes undertaken at the University of Tennessee and at Purdue University.

1.3 Objectives

The recent bloom of scientific inquiries at Pound Gap reflects upon the quality of the exposure and the importance of several aspects of the strata. However, a detailed scientific investigation of the depositional systems and their individual components in the context of foreland basin system dynamics remains lacking. Chapter 2 of this thesis presents a detailed, bed-by-bed description of the lithologies, bedforms, bedding architecture, ichnofacies, and fossil content of the >600 m thick measured section, in addition to paleocurrent data, to infer local depositional conditions and interpret the depositional environments as they evolved in the Late Paleozoic central Appalachian foreland basin. This objective is approached by separating the lithologic data into lithofacies and lithofacies associations using the scientific community's most up-to-date understanding of depositional systems and facies models.

Furthermore, new detrital zircon U-Pb age data are presented from four sandstones deposited in separate clastic wedges to infer patterns in sediment sourcing to the basin from Early Mississippian to Middle Pennsylvanian time. These data are especially important because they provide insight into the previously uninvestigated provenance of sediment deposited in the most distal part of the Appalachian foreland basin system. Detrital zircon U-Pb age peak data from this study and published data from several others in the proximal Appalachian foreland basin are then compared to infer regional provenance patterns along the orogen.

Lastly, interpretations of the local depositional systems, paleocurrent data, and detrital zircon age spectra presented in this study are integrated with other regional studies to reconstruct the depositional and tectonic evolution of the central Appalachian foreland basin system from the final stages of the Neoacadian orogeny into the early stages of the Alleghanian orogeny. The paleogeographic reconstructions included in this work illustrate the central Appalachian basin as dynamic foreland basin system *sensu* DeCelles and Giles (1996) and provide three-dimensional models of basin sedimentation in response to changes in flexural subsidence and clastic influx during periods of tectonic

activity and quiescence along the crystalline components of the orogen. The stratigraphy and development of this system are then compared against a typical foreland system to demonstrate how the central Appalachian foreland basin system varies from the foreland basin model currently applied to convergent plate margins.

1.4 Introduction to the Matanuska forearc basin system, south-central Alaska

The Matanuska Valley is a northeast-southwest trending Mesozoic to Cenozoic forearc basin system that lies north of Cook Inlet in south-central Alaska (Fig. 3.1). The valley is situated between the Talkeetna Mountains to the north and the Chugach Mountains to the south, which run parallel to the basin. The key components of the Matanuska forearc basin system are the Jurassic to Paleocene Talkeetna magmatic arc, the Mesozoic to Cenozoic Matanuska forearc basin, and the Chugach Mesozoic subduction complex, which are separated by the Castle Mountain Fault and the Border Ranges Fault System, respectively (Figs. 3.1 and 3.11). This study focuses on four key areas along the Castle Mountain and Border Ranges fault systems to understand the structural configuration of the forearc basin system and its response to multi-stage normal, spreading ridge, and oceanic plateau subduction.

Previous investigations in the Matanuska Valley have focused on the plutonic and volcanic rocks in the trench and forearc regions and the igneous and high-temperature low-pressure metamorphic rocks in the accretionary prism to support hypothesis of Paleocene-Eocene spreading ridge subduction beneath the southern Alaskan margin (Fig. 3.2). Geophysical studies have also demonstrated that the active margin is currently undergoing flat-slab subduction of the Yakutat microplate, an oceanic plateau (e.g., Fuis et al., 2008), which has been supported in recent integrative studies of stratigraphic, provenance, geochronologic, and thermochronologic data from the upper plate above the area where subduction is occurring (Finzel et al., 2011). However, in general, the sedimentary record of these relatively common processes is poorly understood and has received little attention globally. Chapter 3 of this thesis presents some of the research conducted as part of a collaborative research effort between Bucknell University, Lehigh

University, and Purdue University, whose focus is to characterize and better understand this record in the Matanuska Valley area.

1.5 Study Area

The study presented in Chapter 3 is focused on the northern and southern peripheries of the Matanuska forearc basin system along the Castle Mountain Fault and the Border Ranges Fault System (Fig. 3.1). Along the Castle Mountain Fault in the southern Talkeetna Mountains, the areas included in this study are: the Government Peak area, south of Hatcher Pass and Bald Mountain Ridge, along the western margin of the Matanuska Valley; the Lonesome Mine area, just east of Government Peak and north of Arkose Ridge along the eastern slopes of the Susitna River; and the Lava Mountain-Sheep Valley-Red Hill (LSR) area, west of Kings River and Castle Mountain (Fig. 3.1). Along the Border Ranges Fault System, the study focuses on the Gravel Creek area, west of the Matanuska Glacier in the Chugach Mountains (Fig. 3.1), where I conducted field work during the summer of 2011 with several members of our research collaboration.

1.6 Objectives

Field observations made by the Bucknell-Lehigh-Purdue research group from the four key areas along the Castle Mountain Fault and Border Ranges Fault System are presented in geologic maps and structural cross-sections provided in Chapter 3. In addition, a northwest-southeast-trending structural cross-section across the Matanuska Valley region from northwest of the LSR area in the Talkeetna Mountains to the Chugach Mountains is provided as an interpretation of the subsurface structural configuration of the Matanuska forearc basin system, incorporating the remnant arc, forearc, and accretionary prism (Fig. 3.11). The geologic maps, cross-sections, and interpretations provided in Chapter 3 of this thesis will contribute to our research group's understanding of how sedimentation in forearc systems are affected by second order processes observed along several convergent plate boundaries.

CHAPTER 2. NEOACADIAN TO ALLEGHANIAN FORELAND BASIN DEVELOPMENT AND PROVENANCE IN THE CENTRAL APPALACHIAN OROGEN, PINE MOUNTAIN THRUST SHEET

2.1 Introduction

The Cumberland Plateau and adjacent Valley and Ridge Province are composed of strata that were deposited as part of the Paleozoic central Appalachian foreland basin, which contains many resources including hydrocarbons, coal, groundwater, and fertile soils essential to communities in the region. The boundary between these two geologic provinces is defined by the northeast-southwest oriented ridge of Pine Mountain, which is comprised of gently inclined strata of the Pine Mountain thrust sheet (Fig. 2.1a). These strata are well exposed in an >600 m thick section along U.S. Route 23, providing a spectacular exposure of Upper Devonian through Lower Pennsylvanian strata in the hanging wall of the Pine Mountain thrust fault (Fig. 2.1b). The Pine Mountain thrust sheet represents the leading-edge of the Alleghanian fold-and-thrust belt. The purpose of this study is to characterize the strata at Pound Gap to provide interpretations of local changing depositional environments from lithofacies analysis and paleocurrent data, and to analyze detrital zircon U-Pb age data from this section to determine the provenance of sediment in the central Appalachian basin. Syntheses of these datasets allow us to place our new data into a more regional context of late Acadian-Neoacadian to early Alleghanian foreland basin development.

Previous work in age-equivalent strata of the central and southern parts of the Appalachian foreland basin has lead to a broad understanding of foreland basin deposystems affected by end-Acadian through early-Alleghanian orogenesis. Many of these studies focused on the lower Pennsylvanian coal-bearing sandstone such as those of the Pennington-Lee clastic wedge and Breathitt Group (e.g., Rice, 1985; Archer and Greb,

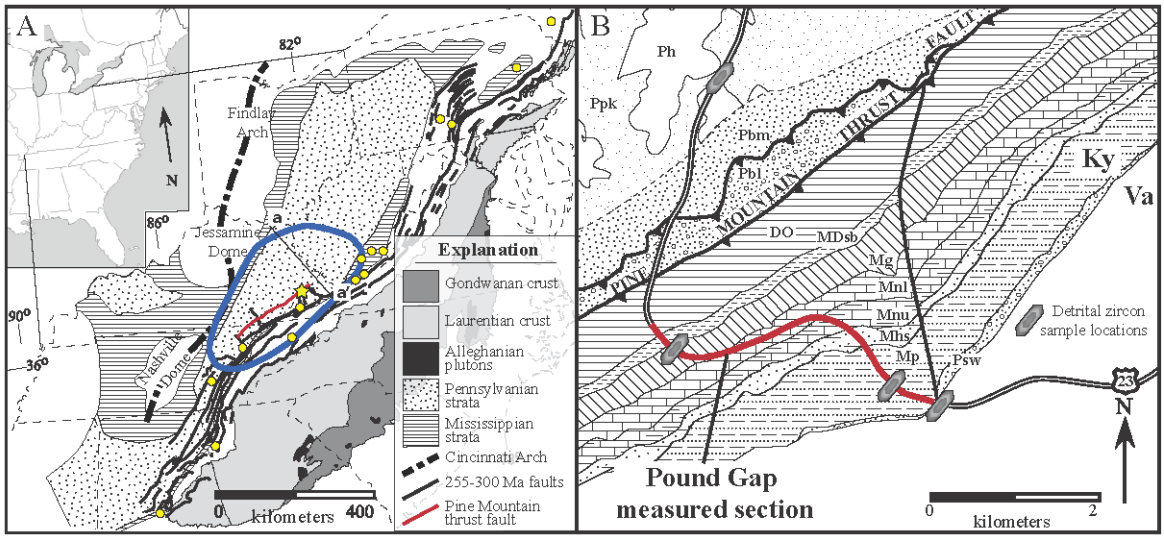

Figure 2.1: (**A)** Simplified geologic map showing study area (yellow star) and approximate regions of exposed basement and Carboniferous strata in the Appalachian foreland basin. Modified from Chesnut (1991), Becker et al. (2005, 2006)'s adaptation of previous authors' work (references compiled therein), Pashin and Gastaldo (2009) after Thomas (1988), and Greb and Chesnut (2009). Yellow circles = detrital zircon sandstone sample locations from previous published studies compared to new data presented in this study. Line of section a-a' shown in Figure 2.2a. (**B)** USGS 1:24,000 geologic map of Kentucky from kgs.uky.edu. Do = Devonian Ohio Shale, MDsb = Devonian-Mississippian Berea Sandstone, Bedford Shale, and Sunbury Shale, Mg = Mississippian Grainger Formation, Mnl = Mississippian lower Newman Lime- stone, Mnu = Mississippian upper Newman Limestone, Mhs = Mississippian Stony Gap/Hinton Member of Pennington Formation, Mp = Mississippian Pennington Formation, Psw = Pennsylvanian Warren Point/Sewanee Formation undivided, Pbl = Lower Pennsylvanian Breathitt Group undivided, Pbm = Middle Pennsylvanian Breathitt Group undivided, Ppk = Middle Pennsylvanian Pikeville Formation of the Breathitt Group, Ph = Middle Pennsylvanian Hyden Formation of the Breathitt Group.

1995; Greb and Chesnut, 1996). Previous research of Devonian black shales, which in eastern Kentucky account for 98% of the state's total gas production (Schepers et al., 2009), have provided a framework for natural gas exploration (e.g., Roen, 1984; Ettensohn and Barron, 1981; Ettensohn, 1992). Previous studies of the Pine Mountain thrust sheet strata in our field area include investigations into the depositional environments, petrography, diagenesis, and sequence stratigraphy of discrete portions of the Upper Devonian to Lower Pennsylvanian exposure (Demmin, 1999; Johanson, 2000; Al-Tawil and Read, 2003; Ober, 2003; Kahmann-Robinson, 2008). Observations from the Pound Gap exposure (Chesnut et al., 1998) and others in the central Appalachian basin have been utilized to reinterpret the stratigraphic and tectonic framework of the basin (Ettensohn et al., 2002; Greb et al., 2002). The approach taken in our study is based on a detailed bed-by-bed measured stratigraphic section that focuses on interpreting

depositional conditions and environments as they relate to regional foreland basin development and tectonics.

Our study is also the first to utilize detrital zircon U-Pb geochronology of sandstones to better understand the provenance of Paleozoic strata in the Pine Mountain thrust sheet. Previous detrital zircon geochronology studies have also contributed to our understanding of contemporaneous synorogenic clastic wedge provenance in the Appalachian foreland basin but in general have focused on strata located most proximal to the Alleghanian crystalline thrust front to infer basin-fill provenance (Thomas et al., 2004; Becker et al., 2005) and orogenic activity along the east Laurentian margin (Becker et al., 2005; Park et al., 2010). The objective of our study is to better define the development of the Late Devonian to Middle Pennsylvanian central Appalachian foreland basin by integrating sedimentologic and provenance data to infer depositional conditions, environments, local systems, and their sediment sources. We use this integration, along with findings from previous studies, to discuss both the local and regional evolution of the central Appalachian foreland basin system.

2.2 Regional Geologic Setting

The Appalachian foreland basin system has been the site of deposition during three main periods of subsidence induced by major episodes of island-arc or continental collision against the southern-central Laurentian margin following ~565 Ma rifting of the supercontinent Rodinia (Hatcher, 2005). The Grenville orogeny (1250-950 Ma; Rainbird et al., 2012), the Taconic orogeny (490-440 Ma; Thomas et al., 2004; Becker et al., 2005), the Acadian-Neoacadian orogeny (410-345 Ma; Hatcher, 2010 and references therein), and the Alleghenian orogeny (325-265 Ma; Hatcher, 2005) each contributed to the tectonic growth of Laurentia through the addition of crust conventionally referred to as having Laurentian or Gondwanan affinity. These tectonic processes resulted in a diverse amalgamation of source terranes in an orogenic belt that today spans from Alabama to Newfoundland and in the Paleozoic supplied over 2,292,500 km^3 of

preserved sediment (de Witt, 1993) that accumulated to thicknesses over 13,700 m in parts of the Appalachian foreland basin (de Witt and Milici, 1989).

This study is focused in the central Appalachian foreland basin, an oblong, northeast-southwest-trending regional basin generally located in eastern Kentucky, southern West Virginia, southwestern Virginia, and northeastern Tennessee (Fig. 2.1a). The basin is bound by several structural (and geographic) elements, the most important of which are the Cincinnati Arch to the west and the Alleghany Front to the east (Fig. 2.1a) (Chesnut, 1991; Archer and Greb, 1995; Ruppert and Rice, 2001; Adams, 1984; Greb and Martino, 2005). Stratigraphic nomenclature in this part of the foreland basin is historically inconsistent due to similarities in many of its Carboniferous units, alternate stratigraphic terms between the Kentucky Geological Survey (KGS) and the Virginia Division of Geology and Mineral Resources (DGMR), and discontinued terms that persist in recent literature. The stratigraphic terminology utilized herein is consistent with that defined by Chesnut (1992), with references to terms used by the Virginia DGMR and previous studies where necessary.

The stratigraphy in the central Appalachian basin along Pine Mountain includes the Middle Pennsylvanian Breathitt Group, exposed in the dissected Cumberland Plateau, and extends in the subsurface to the Cambrian Rome Formation for a total stratigraphic thickness of ~2 km (Figs. 2.2 and 2.3). The main sedimentary sequences comprise three synorogenic clastic wedges of the Taconic, Acadian-Neoacadian, and Alleghanian orogenies (e.g., Meckel, 1970; Hatcher et al., 1989; Ettensohn, 2008). The stratigraphy of the Pine Mountain thrust sheet exposed along and south of Pine Mountain (Figs. 2.1b, 2.2, and 2.3) is described by Rice (1973) and consists of four main sequences: (1) an Upper Devonian to Middle Mississippian, 376-413 m thick siliciclastic sequence consisting of the Ohio Shale, the Berea Sandstone, the Bedford Shale, the Sunbury Shale, and the Grainger Formation; (2) the 168-232 m thick Middle Mississippian Newman Limestone, consisting of a lower member characterized by micritic and fossiliferous limestone and an upper member characterized by calcareous siltstone, shale, sandstone,

and fossiliferous limestone; (3) the 232-277 m thick Pennington Formation, which consists of wavy bedded sandstone and siltstone of the Stony Gap Sandstone member and siltstone, shale, sandstone, limestone, and coal of the Upper Pennington member. (4) The basal Lee Formation (now termed the Warren Point Sandstone of the Breathitt Group) in part forms the uppermost stratigraphy on the Pine Mountain thrust sheet. This formation consists of 122-177 m of pebbly, quartz sandstone beds and thin, discontinuous coal beds. The middle and upper members of Rice's (1973) Lee Formation are not exposed in the hanging wall stratigraphy at Pound Gap (Fig. 2.1b). The footwall stratigraphy exposed north of Pine Mountain (Fig. 2.1b) consists of mainly siltstone, shale, and coal of the Lower and Middle Pennsylvanian Breathitt Formation (Rice, 1973).

The hanging wall stratigraphic sequences exposed along Pine Mountain have been interpreted as Late Devonian to Middle Mississippian deep-marine and prodeltaic to delta-front clastic strata (Ohio Shale through Grainger Formation; Hasson, 1972; Rice, 1984), Middle Mississippian to Upper Mississippian carbonate bank strata (Newman Limestone; e.g., Dever, 1977; Grabowski, 1986; Al-Tawil and Read, 2003), and Upper Mississippian to Middle Pennsylvanian nearshore and transitional marine, fluvio-deltaic strata (Pennington and Lee-equivalent Formations; e.g., Martin, 1975; BeMent, 1976; Rice, 1984; Ettensohn and Chesnut, 1985). These sequences thin and shallow northwestward above Precambrian Laurentian basement toward the Cincinnati Arch as part of the mostly undeformed subsurface stratigraphy of the Cumberland Plateau (see de Witt, 1993, fig. 5).

The stratigraphy plays an important role in the geometry of the Pine Mountain thrust sheet (Fig. 2.3). Rich (1934) proposed that the Pine Mountain thrust propagated along bedding from the rheologically weak shale and sandstone of the Rome Formation upward to the basal Devonian Chattanooga Shale (Miller, 1973; equiv. Ohio Shale), cutting obliquely through the more competent beds between these glide planes before surfacing. This resulted in a ramp-like fault geometry which transported overlying hanging wall strata cratonward in response to "a great plunger moving from the southeast" (Rich,

Figure 2.2. Left: Line of section (a-a') indicated in Figure 2.1, showing downwarped Devonian and Mississippian strata, the regional Pennsylvanian-Mississippian erosive unconformity, and thickening-hinterward pattern that defines the geometry of the central Appalachian foreland basin stratigraphy. Modified from Ches- nut and Greb (2009). Right: Timeline of events and stratigraphic column of units exposed at Pound Gap, Kentucky. Modified from Chesnut (1991) with information compiled by Ettensohn (2004, 2008), Dennis and Wright (1997), and Dennis (2007). Minor structural features penecontemporaneous with the Pennsylvanian- Mississippian unconformity include minor subsurface normal faults in eastern Kentucky of unidentified origin whereas major structural features correspond to mostly post-Pennsylvanian faults such as the Russell- Fork, Jacksboro, and Pine Mountain faults (Chesnut, 1991).

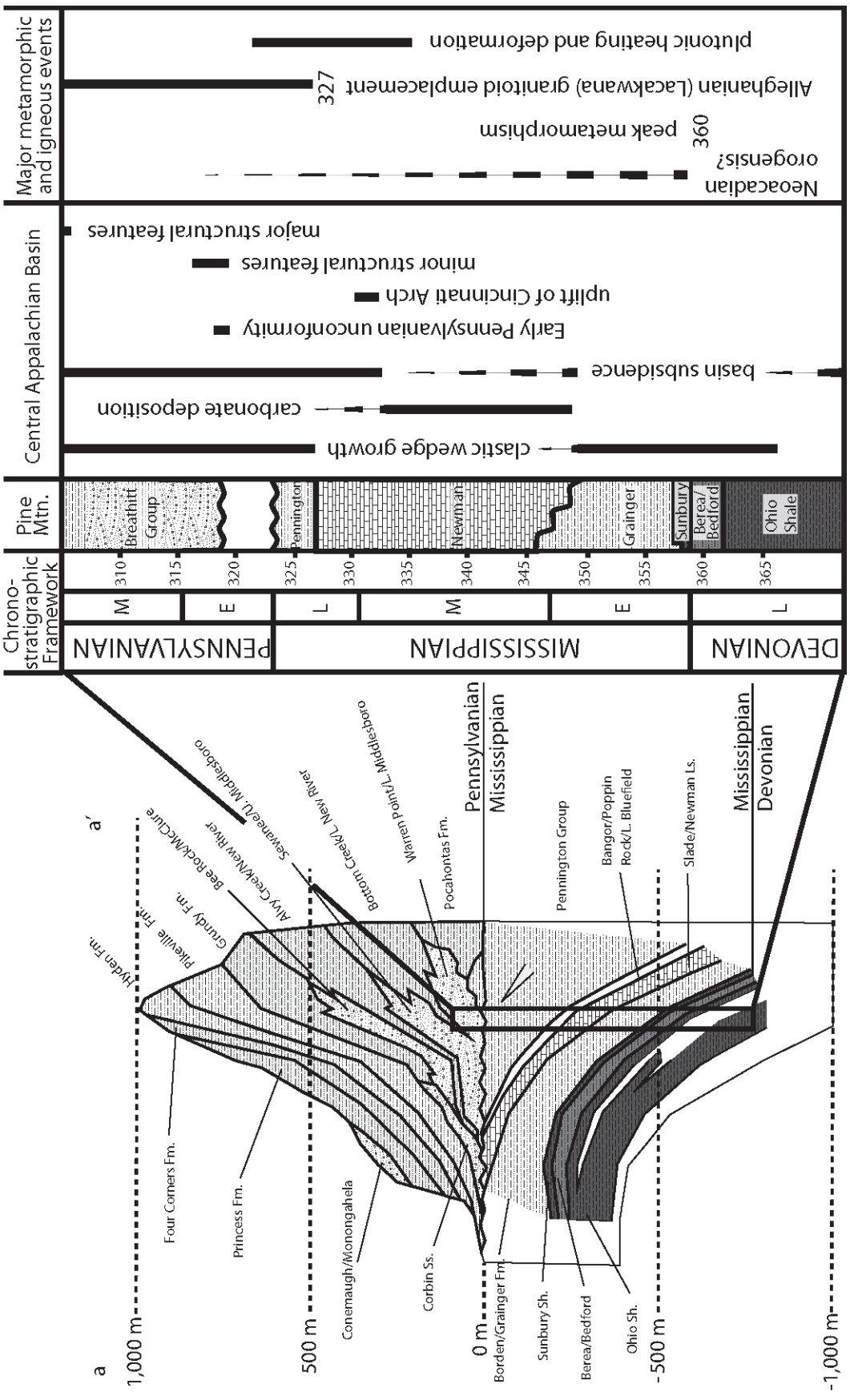
Major metamorphic and igneous events
Neocadian orogensis?
peak metamorphism
360
Alleghanian (Lacakwana) granitoid emplacement
327
plutonic heating and deformation
Central Appalachian Basin
major structural features
minor structural features
uplift of Cincinnati Arch
Early Pennsylvanian unconformity
basin subsidence
carbonate deposition
clastic wedge growth
Pine Mtn.
Breathitt Group
Pennington
Newman
Grainger
Sunbury
Berea/ Bedford
Ohio Shale
Chrono-stratigraphic Framework
PENNSYLVANIAN
MISSISSIPPIAN
DEVONIAN
M
E
L
M
E
L
310
315
320
325
330
335
340
345
350
355
360
365
a
a'
1,000 m
500 m
0 m
-500 m
-1,000 m
Hyden Fm.
Pikeville Fm.
Grundy Fm.
Alvy Creek/New River
Bee Rock/McClure
Sewanee/L. Middlesboro
Bottom Creek/L. New River
Warren Point/L. Mississippian
Pocahontas Fm.
Pennsylvanian
Mississippian
Pennington Group
Bangor/Poppin Rock/L. Bluefield
Slade/Newman Ls.
Mississippian
Devonian
Four Corners Fm.
Princess Fm.
Conemaugh/Monongahela
Corbin Ss.
Borden/Grainger Fm.
Sunbury Sh.
Berea/Bedford
Ohio Sh.

Figure 2.2

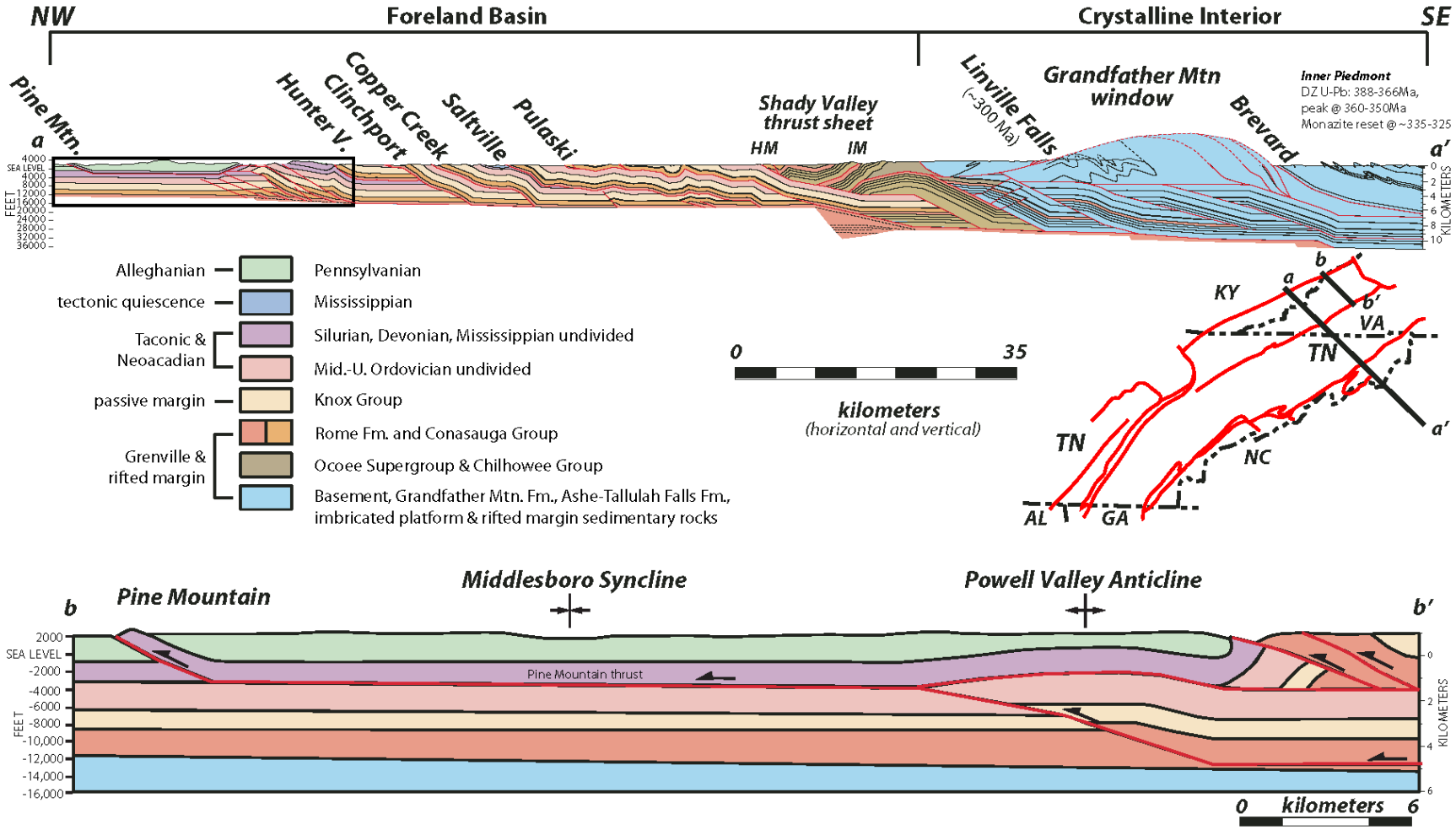

Figure 2.3: Cross-section a-a' from the undeformed Appalachian-Cumberland Plateau to the Coastal Plain of the eastern United States (from surface and seismic reflection data interpretation by Hatcher et al., 2007). Total shortening from Coastal Plain to Pine Mountain Thrust is interpreted to be 47% - 54% by Hatcher (1989). Timing of structures: Linville Falls thrust, Van Camp and Fullagar (1982) and Schedl et al. (1992) mylonitization ages (in Goldberg and Dallmeyer, 1997); Inner Piedmont, detrital zircon data summarized in Hatcher (2005), monazite U-Pb age data from Dennis and Wright

1934, p. 1596). This mechanism of emplacement and stair-step fault geometry is well-established and considered one of the fundamental structural elements of fold and thrust belts (Mitra, 1988). Coal virtrinite reflectance values indicate that the Pine Mountain thrust sheet was approximately three kilometers thick prior to erosion (O'Hara et al., 1990), and displacement along the Pine Mountain thrust varies from ~21 km to the southeast to ~3 km to the northwest (Mitra, 1988). At Pound Gap, the Pine Mountain thrust fault has been approximately traced along the gentle northern slopes of Pine Mountain (Rice, 1973), where overturned and faulted beds of Lower Pennsylvanian sandstone and shale provide some of the only direct evidence of the fault's location (Fig. 2.1b).

2.3 Lithofacies and Facies Associations

2.3.1 Measured Section and Lithofacies Classification

The exposure along Highway 23 (Fig. 2.1b) was measured using a Jacob's staff and utilized bed-by-bed descriptions of lithology, grain size relationships, color variation, bedding geometry, ichnofacies, and other fossil content (Fig. 2.4). Covered section was also calculated using a Jacob's staff and Brunton pocket transit. Thin sections were made from samples collected along the exposure for further lithologic information. Paleocurrent measurements were taken from sandstone beds throughout the measured section (Fig. 2.4). Groove casts, three-dimensional lateral accretion surfaces, and three- and two-dimensional exposures of foresets in trough and planar cross-stratified sandstone beds were measured for paleocurrent information using a Brunton pocket transit compass. Rose diagrams and stereonets were constructed using the stereographic projection software GEOrient (version 9.5.0; Rod Holcombe, ©2011) from three-dimensional measurements of lateral accretion surfaces, trough cross-stratified foresets, planar cross-stratified foresets, and two-dimensional trough and planar cross-strata foresets. Paleocurrent direction approximated from two-dimensional exposures of trough cross-stratification were determined by taking the intersection point between best-fit great circles of polar left-dipping and right-dipping foreset measurements, which produces an approximate mean trough orientation in lieu of data from more accurate three-

Figure 2.4. Simplified measured section of the hanging wall stratigraphy of the Pine Mountain thrust sheet represented in the Pound Gap exposure. Bed thicknesses and stacking patterns are representative of intervals observed and described in the detailed measured section but are not necessarily true to actual bed thicknesses within each interval. Paleocurrent measurements discussed in text. See Table 1 for locations of lithofacies in the measured section.

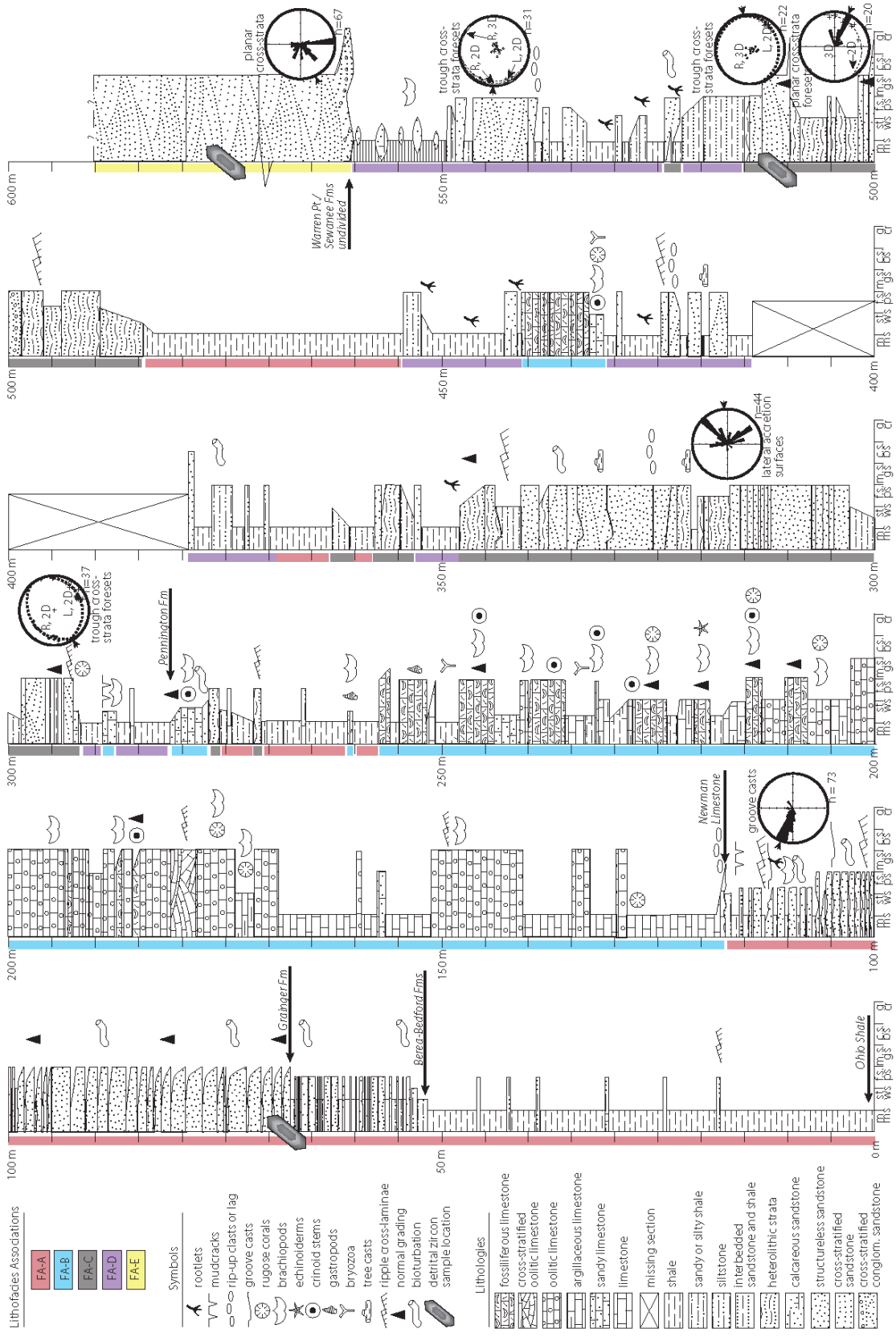
Lithofacies Associations
FA-A
FA-B
FA-C
FA-D
FA-E
Symbols
rootlets
mudcracks
rip-up clasts or lag
groove casts
rugose corals
brachiopods
echinoiderms
crinoid stems
gastropods
bryozoa
tree casts
ripple cross-laminae
normal grading
bioturbation
detrital zircon
sample location
Lithologies
fossiliferous limestone
cross-stratified oolitic limestone
oolitic limestone
argillaceous limestone
sandy limestone
limestone
missing section
shale
sandy or silty shale
siltstone
interbedded sandstone and shale
heterolithic strata
calcareous sandstone
structureless sandstone
cross-stratified sandstone
cross-stratified conglom. sandstone
Grainger Fm
Berea-Bedford Fms
Ohio Shale
Newman Limestone
Pennington Fm
Warren Pt./ Sewanee Fms undivided
groove casts
n= 73
trough cross-strata foresets
R, 2D
L, 2D
n=37
n=67
n=31
n=22
n=20
n=44
lateral accretion surfaces
planar cross-strata foreset
100 m
50 m
0 m
200 m
150 m
300 m
250 m
400 m
350 m
500 m
450 m
600 m
550 m

Figure 2.4

dimensional exposures. This method is adapted from the "biplanar method" of DeCelles et al., (1983) developed to determine mean trough orientation from measurements of trough cross-strata exposed on three-dimensional surfaces. All hanging wall paleocurrent data reported in this study has been restored to horizontal bedding from an attitude of 062°, 26°, an average which is consistent for inclined beds (n=35) from which paleocurrent measurements were taken continuously along the exposure.

The measured stratigraphic section is described here in terms of lithofacies, each of which is defined on the basis of grain size, sedimentary structures, ichnofacies, macrofossils, and bed geometries that share an interpreted depositional environment. Lithofacies with similar characteristics and interpreted depositional settings have been grouped into facies associations. Table 2.1 describes the characteristics of each lithofacies, where they occur in the measured stratigraphic section (Fig. 2.4), their depositional conditions, and their interpreted depositional environments. Figure 2.4 illustrates simplified stratigraphic relationships between each facies association, which may be supplemented by lithofacies descriptions and detailed occurrence intervals provided in Table 2.1 and the detailed measured section in Appendix A. Individual depositional environment interpretations from lithofacies in the following section are treated separately from the deposystem evolution interpreted from transitions between lithofacies and facies associations addressed in the discussion section.

2.3.2 Facies Association A: Lithofacies A1, A2, A3, A4, A5

Description

This facies association is dominated by shale to silty shale and structureless, planar-laminated, and ripple cross-laminated siltstone to fine sandstone beds which comprise lithologic packages organized here into Lithofacies A1-A5. Facies Association A (FA-A) is best developed at the base of the measured section in a 117 m thick, generally coarsening-upward sequence (Figs. 2.4 and 2.5a). The key identifying constituents of this facies association are couplets of shale and siltstone to fine sandstone which vary in shale to sand ratio; shale-dominated successions of Lithofacies A1 and A2 (Fig. 2.5b) are

Table 2.1: *Lithofacies described at Pound Gap, Kentucky*

Lithofacies	Sketch	Grain Size (Detrital)	Meters (Fig. 2.4)	Description	Transport and Depositional Process	Environment of Deposition
A1 - Laminated shale and structureless to ripple-laminated siltstone	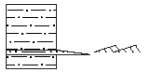	Clay to silt	0-18, 48-52, 357-369, 454-485	Thinly bedded shale; black to dark gray and nodular to well-laminated. Siltstone beds rare, < 9 cm thick, varying lateral thickness, and structureless to ripple cross-laminated with mud drapes; tan to gray.	Settling of clay- to silt-sized particles from low-density gravity flows and/or hemipelagic material in the water column. Equivalent to Bouma divisions Tc and Te (Bouma, 1962).	Distal prodelta basin plain
A2 - Laminated shale and structureless to ripple-laminated siltstone	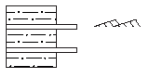	Clay to silt	18-48, 257-276, 284-288	Thinly bedded shale; black to medium gray. Siltstone beds common, < 9 cm thick, varying lateral thickness, and ripple-laminated with mud drapes; tan-brown to gray.	Settling of clay- to silt-sized particles from low-density gravity flows and/or hemipelagic material in the water column. Equivalent to divisions Tc and Te of Bouma, 1962.	Proximal prodelta basin plain
A3 - Interbedded laminated shale to silty shale and structureless to ripple cross-laminated siltstone to fine sandstone	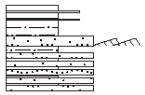	Clay to fine sand	52-68, 76-81, 83-86, 99-105	Mostly interbedded couplets of shale and siltstone to fine sandstone. Thinly laminated to nodular shale; dark gray to gray-green. Quartz sandstone well-sorted, subangular to rounded, structureless to cross-laminated, frequently bioturbated, tabular and well-laminated, contains some tool marks, 1-18 cm thick beds; tan-brown to gray.	Settling of clay- to fine sand-sized particles from freezing in low-density turbulent flows or sandy debris flows followed by hemipelagic settling.	Unconfined delta front outer fan (mud-rich)
A4 - Shale and normally graded to structureless, planar- or ripple cross-laminated sandstone and siltstone	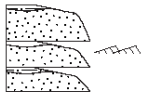	Clay to fine sand	67-76, 84-99	Mostly normally graded sequences. Thinly laminated to nodular shale; dark gray to gray-green. Quartz sandstone well-sorted, subangular to rounded, structureless to ripple cross-laminated, often bioturbated, tabular and well-laminated to wavy, some tool marks, 1 to >100 cm thick beds; tan-brown to gray.	Settling of clay- to sand-sized particles from low-density turbulent flows and/or freezing in sandy debris flows and hemipelagic settling. Equivalent to divisions Ta-Te of Bouma, 1962.	Unconfined delta front outer fan (sand-rich)
A5 - Shale, evaporite, and structureless, planar laminated, and ripple cross-laminated sandstone and siltstone		Clay to fine sand	105-117	Mostly interbedded sequences. Thinly laminated and fissile shale, sometimes with brachiopods and rare rootlets; tan-gray to red. Quartz sandstone well-sorted, subangular to rounded, structureless to ripple cross-laminated or hummocky cross-stratified, often bioturbated, tabular to wavy, abundant tool marks, 1-< 50 cm; red-brown to gray. Evaporite rare.	Settling from low-density combined turbulent flows or freezing in sandy tempestites. Upper beds deposited above storm wave base and subaerially exposed.	Storm-dominated abandoned deltaic complex
B6 - Lime mudstone, dolostone, and cherty limestone		--	117-126, 128, 130-132, 135-140, 142	Structureless micritic limestone with finely laminated yellow partings, rare cherty horizons, and dolomitic horizons. Planar to wavy bedding contacts with common karstified surfaces. Gray to brown. Solitary rugose corals present.	Settling and accumulation of lime mud in calm water conditions.	Shallow, peritidal mudflat or lagoon
B7 - Oolitic grainstone to wackestone		Very fine to very coarse sand	126-129, 132-134, 140-149, 151, 159-161, 168-170, 175-207, 210-212, 240	Structureless and well-laminated, grain-supported ooids in varying amounts of lime mudstone matrix. Scouring contacts, trough cross-bedded grainstone, chert, solitary rugose corals, brachiopods, dolostone, and rip-up clasts of oolitic grainstone are subordinate.	Migration of bedload-dominated 3D oolitic dunes and high-velocity sheets in open-marine tropical waters less than 100 meters deep.	Oolitic shoals and sheets
B8 - Sandy wackestone, fossiliferous sandy wackestone, and shale		Clay to fine sand	156-157, 240-243, 283-284, 287-288, 292, 350	Micritic limestone with varying abundance of quartz sand grains. Structureless to well-laminated, sometimes displaying lateral thickness variations. May be normally graded or contain interbeds of shale; red-brown to white.	Settling of carbonate mud and sand grains from suspension from the water column and cementation by secondary calcic fluids.	Marginal marine channels or sheets
B9 - Argillaceous lime mudstone and interbedded lime mudstone with shale	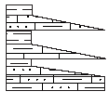	Clay	149, 150, 155, 171-175, 185, 203-204, 215-218, 221-225, 227-231	Structureless to poorly laminated shale with lime mudstone interbeds or micritic matrix in 20 cm - 4 m beds containing articulate to disarticulate crinoids, bryozoans (*Archimedes*), and solitary rugose corals.	Suspension settling of clay-sized particles in murky water conditions that limited carbonate development above 100 m water depth but below wave base.	Open marine carboante bank below wave base

Table 2.1: *Lithofacies described at Pound Gap, Kentucky, continued*

Lithofacies	Sketch	Grain Size (Detrital)	Meters (Fig. 2.4)	Description	Transport and Depositional Process	Environment of Deposition
B10 - Lime mudstone and limey shale		Clay	204, 232-235	Poorly laminated to structureless, weakly calcareous shale and lime mudstone containing bryozoans and limestone nodules.	Suspension settling of clay-sized particles in murky water conditions that limited carbonate development.	Deep, open marine carbonate bank
B11 - Fossiliferous packstone, calcareous sandstone, lime mudstone, and shale		Clay to fine sand	187, 192, 207-210-210, 212-214, 218-220, 223-227, 232, 234-240, 243-257, 260, 276-281, 433-440	Structureless to normally graded packstone (disarticulated brachiopods, crinoid stems, *Archimedes*, blastoids, horn corals, and rare gastropods) in 20 cm beds with micritic matrix fining upward to calcareous sandstone, shale, or lime mudstone. Rare articulated brachiopod beds.	High- to low-density gravity flows followed by suspension settling of clay to fine sand sized grains, likely representing storm events; fed by proximal carbonate source.	Open marine and shoaled carbonate bank
C12 - Heterolithic bedding of sandstone, siltstone, and shale	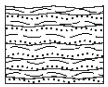	Clay to fine sand	271, 273, 276, 289-302, 316-320, 326-328, 337-348, 341-348, 353-357, 484-498, 502-510, 514-515	Flaser-, wavy-, and lenticular-bedded quartz sandstone with shale, frequently in ~10-20 cm, rhythmically thickening- or thinning-upward bundled cosets with ~2-3 cm thick beds. Bedforms may be wavy or tabular.	Alternating periods of bedload transport and sand ripple formation with clay deposition via suspension settling in slack-water conditions. Varying tidal influence.	Tidally influenced delta front to lower delta plain systems
C13 - Symmetric ripple cross-laminated and planar to trough cross-stratified sandstone, shale, and coal	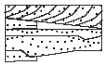	Clay to pebble	295-296, 302-316, 319-326, 328-341, 360-363, 498-502, 510-515, 523-525	Fine-grained quartz arenite beds tabular and scouring, interbedded with organic-rich shale and coal containing lycopsid tree fragments, often with lateral facies transitions. Symmetric ripple-laminated sandstone occurs in 15-40 cm amalgamated bedsets. Lateral accretion surfaces common. Siderite pebble lags, mud intraclasts, and *Skolithos* are rare.	Channel incision and abandonment, bedload-dominated 2D ripple and point bar migration, alternating sand and clay deposition under varying tidal and fluvial influence, and 2D ripple lamination in sheeted sands reworked by bidirectional wave and tidal currents.	Wave to tidally to fluvially influenced delta front to lower delta plain systems
D14 - Pedogenic mudstone and coal		Clay	282-284, 348-351, 369, 370-378, 414-417, 421-432, 441-453, 514, 522-537, 538-539, 546-548	Mudstones are generally poorly indurated and soily, but may be silty or grade into siltstone; variegated and gray-tan to green-maroon. Rootlets, rhizocretions, nodules, pedogenic slickensides, and coal to organic-rich horizons common. Sphenophyte tree fragments uncommon.	Accumulation of clay-sized particles and nutrients into paleosols deposited in low-energy conditions, sometimes utilized by plants	Interdistributary floodplain and overbank
D15 - Structureless to cross-stratified sandstone, shale, and coal	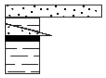	Clay to pebble	350, 352, 370, 372, 374-376, 417-424, 441-442, 452-454, 533-548	Shale poorly indurated and may grade into coal or paleosols of D14. Sandstone to siltstone frequently discontinuous, often structureless, rarely sublithic, low-angle ripple cross-laminated or planar to trough cross-stratified, weakly calcareous, or conglomeratic. Lycopsid and Sphenophyte tree fragments uncommon.	Accumulation of clay-sized particles in low-energy levels and overbank areas between migrating, bedload-dominated fluvial channels and levees.	Fluviatile upper delta plain distributary channels and overbanks
D16 - Thinly interbedded sandstone and shale	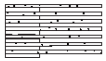	Clay to very fine sand	515-522	Thinly interbedded, tabular, non-rhythmic very fine sandstone and interbedded shale. Sandstone is structureless and may be discontinuous or display lateral thickness variations.	Alternating settling of sand and clay-sized particles in low-energy, potentially hypersaline water conditions inhospitable for burrowing fauna.	Lake or interdistributary floodplain
D17 - Carbonaceous shale, and siltstone and calcareous sandstone		Clay to very fine sand	548-561	Carbonaceous siltstone grades into fissile, black carbonaceous shale with discontinuous lenses of calcareous sandstone up to 20 cm thick and ~1 m across. Brachiopods may be present in sandstone lenses.	Settling of silt-clay sized particles and plant matter from suspension in calm, likely brackish waters. Sandstone lenses filled local depressions after transport during storm events.	Coastal marsh
E18 - Planar cross-stratified and structureless conglomeratic sandstone and coal	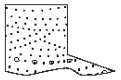	Fine sand to pebble	561-590+	Dominantly planar cross-stratified conglomeratic quartz sandstone with quartz granule to pebble lags in scouring beds up to 2.5 m thick; white weathering tan-brown. *In situ* coalified trees are present and may crosscut bedding. Very rare shaley horizons.	Migration of 2D dunes in sustained high-energy flows in scouring fluvial channels. Mud drapes from suspension settling of clay-sized particles following high-energy events.	Braided river system

Figure 2.5. Lithofacies of Facies Association A. (A) Basal exposure of FA-A showing coarsening-upward sequence from shale- to sandstone-dominated couplets characteristic of the facies association. (B) Ripple cross-laminated to structureless siltstone beds in well-laminated black to gray shale of Lithofacies A2. (C) Interbedded packages of Lithofacies A3 and A4. Note tabular bedding geometry and transitions between equally sandstone- and shale-rich couplets of Lithofacies A3 to sandstone-dominant couplets of Lithofacies A4. Person for scale (arrow). (D) Thickening-upward, sandstone-dominated package of Lithofacies A4 interbedded with thinly bedded, aggrading sandstone and shale couplets of Lithofacies A3. (E) Escape burrow structures (outlined) in ripple cross-laminated sandstone of Lithofacies A3. Quarter for scale (arrow). (F) Groove casts in basal sandstone surfaces above silty shale of Lithofacies A3. Paleocurrent direction here is from right to left. Arrows point to burrow structures. (G) Normally graded sandstone-shale couplet of Lithofacies A4, displaying structureless (Ta), planar-laminated (Tb), and ripple cross-laminated (Tc) sandstone to stiltstone capped by laminated silty shale (Td) as described by Bouma (1962).

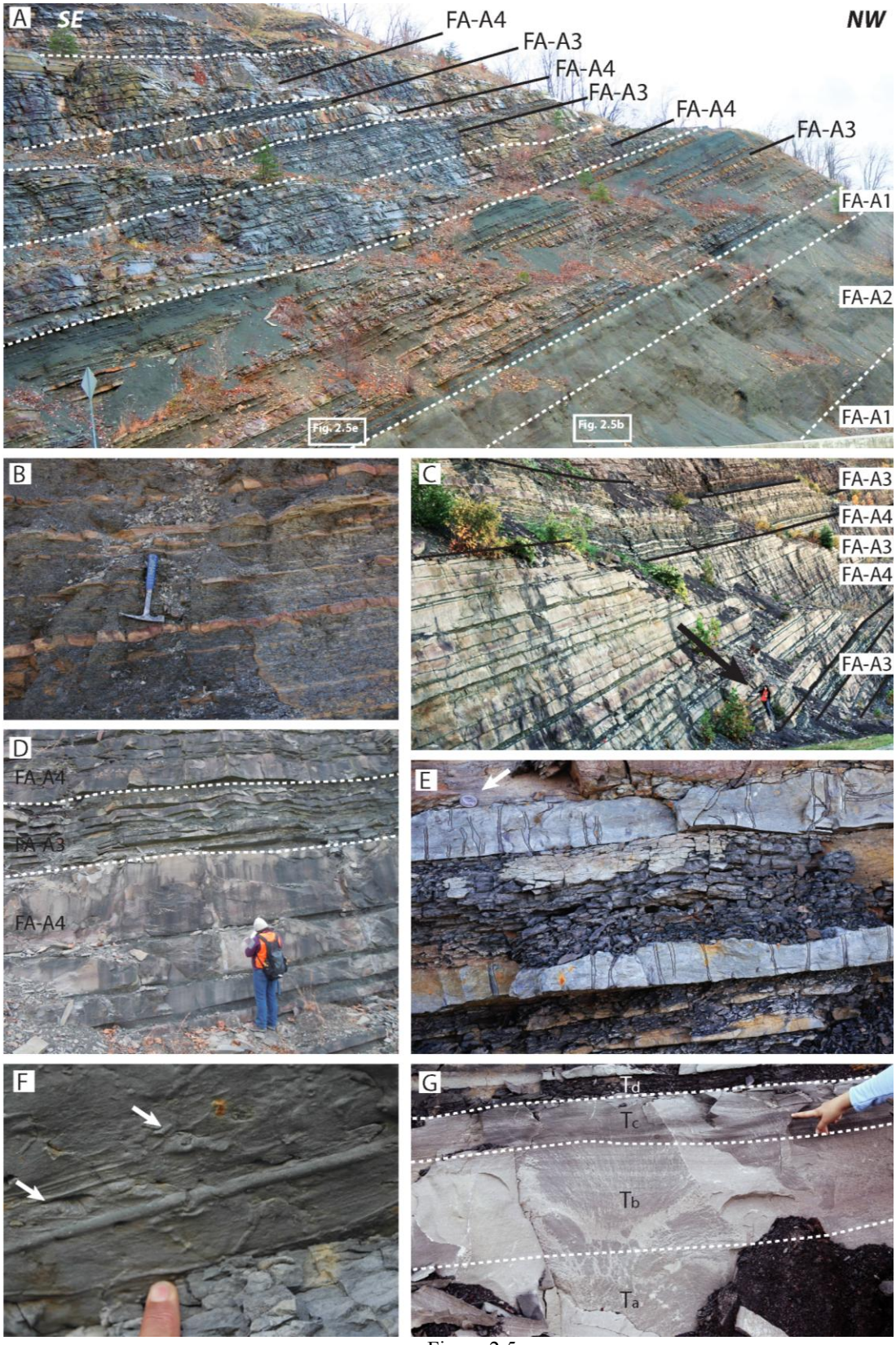
A
SE
NW
FA-A4
FA-A3
FA-A4
FA-A3
FA-A4
FA-A3
FA-A1
FA-A2
FA-A1
Fig. 2.5e
Fig. 2.5b
B
C
FA-A3
FA-A4
FA-A3
FA-A4
FA-A3
D
FA-A4
FA-A3
FA-A4
E
F
G
Td
Tc
Tb
Ta

Figure 2.5

comprised of mainly shale with thin, ripple cross-laminated siltstone beds of Lithofacies A1 and A2 (Fig. 2.5b), whereas Lithofacies A3 and A4 contain characteristically tabular, 1-1.63 m thick sandstone and siltstone beds which display constant thicknesses and are interbedded with or normally grade into shale to silty shale (Figs. 2.5c and 2.5d).

Lithofacies A1 is first present and thickest at the base of the measured section (Fig. 2.4) and is dominated by black to dark gray, moderately- to well-laminated but locally nodular and fissile shale to silty shale. Thin interbeds of siltstone are rare, tan to gray, display lateral thickness variations or may be discontinuous over a few meters, are mostly ripple cross-laminated with well-defined mud drapes, and do not exceed 9 cm in thickness. Similar packages of Lithofacies A2 are characterized by an increase in frequency and lateral continuity of ripple cross-laminated to structureless siltstone beds relative to Lithofacies A1 (Figure 2.5b).

Lithofacies A3 and A4 are present only in a 56 m thick succession beginning at meter 52 in the measured section (Fig. 2.4) and are characterized by interbedded and normally grading (respectively) very fine to fine sandstone and shale to silty shale. This interval contains multiple packages of tabular and laterally continuous sandstone and shale of Lithofacies A3 and A4 that vary in individual bed thickness and total thickness (Figs. 2.5a and 2.5c). The first sequence of Lithofacies A3 is 16 m thick (meters 52-68, Fig. 2.4) and contains light- to medium-gray, very fine-grained sandstone to siltstone beds averaging less than 10 cm in thickness, with a maximum thickness of 60 cm, which display tabular and continuous bedding geometries (Fig. 2.5d). Vertical (*Skolithos*?) and horizontal (*Zoophycus*?) burrow structures in siltstone to ripple cross-laminated sandstone (Fig. 2.5e) are common in this part of the measured section, and groove casts may be present (Fig. 2.5f). Sandstone is mostly interbedded with silty shale, forming sand-dominated, shale-dominated, and equally sand- and shale-rich couplets which rarely display normal grading. Very fine to fine sandstone beds may thin or thicken upward independent of shale interbed thickness, trends which may be observed between meters 60-63 and 79-84 (Fig. 2.4). Black to dark-gray or gray-green, moderately laminated to

nodular shale interbeds are more dominant in Lithofacies A3 than in Lithofacies A4 and are up to 60 cm thick, averaging less than 10 cm thick (Fig. 2.5e).

Lithofacies A4 is similar to A3 but contains fine sandstone beds up to 1.63 m thick (Fig. 2.5d), most of which are normally graded rather than interbedded, with many exceeding 50 cm in thickness. This lithofacies is present over meters 67-76 and 84-99 in the measured section, each interval containing several thickening- and thinning-upward sandstone-to-shale sequences (Figs. 2.4 and 2.5a). Burrow structures, groove casts, and siderite pebble lags are uncommon in sandstone beds. Fining-upward sandstone beds may display any number of several bedforms but typically transition upward from structureless to planar-laminated sandstone (usually present only in thicker beds) which in turn grade into ripple cross-laminated sandstone (ubiquitous), followed by either climbing ripple laminae in sandstone to siltstone or a direct transition to silty shale (Fig. 2.5g). Shale beds are black to dark gray, poorly laminated to nodular, and less than five centimeters thick. Normal grading between ripple cross-laminated sandstone and silty shale or shale most frequently occurs over a relatively thin interval and is best identified by changes in induration where silty shale is less well-indurated than fine sandstone. These bedding structures may be difficult to observe unless from directly on the exposure. Paleocurrent measurements from groove casts observed in Lithofacies A3 and A4 (n=73) are presented in Figure 2.4. Groove casts shallow unimodally toward an azimuth of 292° (±6.4° at 95% confidence interval).

Lithofacies A5 is also characterized by very fine sandstone to siltstone and shale couplets with rare evaporite beds, which may be interbedded or normally graded, but is distinguishable in the exposure (meters 105-117, Fig. 2.4) by the appearance of frequently ripple cross-laminated to hummocky cross-stratified, mostly very fine sandstone to siltstone beds with wavy tops, lateral thickness variations, frequent groove casts, and *Skolithos* and *Neonereites* burrows. Also present are infrequent dewatering structures, wood chips, and mud intraclasts. Thickening or thinning trends in siltstone to very fine sandstone exist but are less well-developed than in Lithofacies A3 and A4, with

sandstone beds ranging from 1-40 cm thick and averaging ~15 cm thick. Lithofacies A5 can be distinguished in the measured section by the appearance of rare brachiopods, desiccation cracks and silty rootlets in non-silty shale beds. Shale beds are gray to red or light tan immediately beneath siltstone to sandstone interbeds, are up to 85 cm thick and average less than 15 cm, and are slightly less abundant relative to siltstone to fine sandstone bed frequency.

Interpretation

Facies Association A reflects gradually changing depositional conditions in dominantly deep marine to briefly shallow and marginal marine settings. Black to dark gray shale beds of Lithofacies A1 were deposited with >1% organic content (see Tourtelot, 1979) by suspension settling in likely reducing bottom water conditions, though, without geochemical analyses, a wide range of possible processes and conditions may have contributed to the high organic content present (e.g., DeMaison and Moore, 1980; Myrow, 1990; Canfield, 1994; Murphy et al., 2000). Transitions between Lithofacies A1, A2, and A3 from black shale and non-bioturbated siltstone to gray-green shale with bioturbated siltstone and sandstone interbeds may reflect changes in organic content (Potter et al., 1980) due to fluctuating primary productivity (e.g., Pedersen and Calver, 1980), sedimentation rates, and/or fluctuations between anaerobic and dysaerobic conditions, respectively (see Canfield, 1994**)**. The depth oxygen stratification can occur in basins with water depths 150 meters or greater (e.g., Ettensohn and Elam, 1985). Mud-draped, ripple cross-laminated to trough cross-stratified siltstone interbeds of Lithofacies A1 and A2 were deposited during pulses of higher energy events creating low-density turbidity currents which transported silt particles into otherwise low-energy conditions and deposited silt and clay-sized sediment by mixed traction sedimentation and suspension fallout (Bouma, 1962) under lower flow regimes (Simons and Richardson, 1961). Structureless and ripple cross-laminated siltstone with mud drapes have been described by Bouma (1962) as constituents of low-density flows deposited by suspension, traction or a combination of suspension and traction sedimentation. Many of these beds are discontinuous with tabular basal contacts, perhaps reflecting localized current

conditions. These conditions persisted with the deposition of Lithofacies A2 but were more homogenous with less organic content deposited with clay-sized grain deposition between higher-energy depositional events, suggesting increased and more widespread influence of turbid water conditions in bathyl marine environments in which less organic content was preserved due to a number of potential reasons previously discussed (see Canfield, 1994).

Fluctuations in sedimentation rate, primary productivity, or bottom-water O_2 levels persisted during the deposition of Lithofacies A3 and A4, during which black to gray-green shale was deposited from hemipelagic fallout, suspension fallout in turbulent flows (i.e., Bouma, 1962; Lowe, 1982) and/or sandy debris flows (Shanmugam, 2000) of silt to fine sand in sheets. Structureless and ripple to trough cross-laminated sandstone bedforms present in Lithofacies A3 have been described elsewhere in previous studies and interpreted as bedforms created during traction sedimentation, frictional freezing and suspension fallout of sand and silt from waning high- to low-density turbulent flows (Bouma, 1962; Lowe, 1982) or sandy debris flows (Shanmugam, 2000). These bedforms and depositional processes have primarily been described in ancient submarine fan deposits (see Covault, 2011; Mattern, 2005; Shanmugam, 2000).

Burrow structures (*Zoophycus* and *Skolithos*?) in Lithofacies A3 and (less commonly) A4 indicate high levels of current or wave energy were present following deposition of fine sandstone during storm events (Pemberton et al., 1992; Hampson, 2008). *Skolithos* burrow structures have been reported in a wide range of environments from proximal offshore to upper shoreface (Pemberton et al., 1992) to deep-sea fan systems (e.g., Crimes et al., 1981), whereas *Zoophycus* trace fossils are characteristic of shelfal conditions below maximum wave base (Pemberton et al., 1992) and have been described in fan fringe, clastic ramp, channel axis, channel margin, lobe, and lobe fringe clastic deposits of the Middle Eocene Ainsa-Jaca basin in the Spanish Pyrenees (Heard and Pickering, 2008).

Groove casts observed along the basal surfaces of sandstone beds in Lithofacies A3 and A4 were created during high-energy events in which tools scoured the muddy substrate as they were transported by turbidity currents downslope and basinward. These are common features of classic turbidite deposits (Posamentier and Walker, 2006). At Pound Gap, these measurements indicate that turbid currents flowed west-northwest (toward 292°) downslope into the foreland basin.

Thickening- and thinning-upward trends described in Lithofacies A3 and A4 are inferred to reflect repetitive energy events of increasing and decreasing duration, respectively, most likely reflecting storm events and fluctuating proximity to sediment distribution source. Fine-grained shale to silty shale interbeds consistently separate sandstone beds and were deposited during periods of low energy clay deposition from hemipelagic fallout (Lithofacies A3) and/or from low-density turbidity currents (Lithofacies A4). Mutti and Ricci Lucchi (1972) inferred that progradation of depositional lobes could explain similar thickening-upward sandstone and shale packages they described in the Late Cretaceous northern Apennine foredeep basin, whereas Lien et al. (2003) interpreted this pattern in the Upper Carboniferous Ross Formation of western Ireland to reflect spillover lobe deposition during lateral channel migration. The latter interpretation draws from a close association between thickening-upward sandstone and shale packages and channel fill deposits, a relationship which is not observed at Pound Gap given the absence of channelized bedding contacts.

The lithofacies described in this facies association match well with outer fan turbidite facies of the Late Cretaceous Punta Barrosa Formation described and interpreted by Fildani et al. (2007) in the Andean retroarc foredeep basin of southern Chile. In this study, the authors distinguished between multiple discrete, 10-15 m thick packages of massively bedded sandstone alternating with finer-grained turbidite packages containing Bouma sequences (T_b-$_d$), siltstones, and turbiditic shales. Sandstone and shale flysch deposits outlined in lithofacies described by Mutti and Ricci Lucchi (1972) in the Apennine foredeep basin were reevaluated by Mutti (1979) who interpreted these

lithofacies as unconfined outer lobe and basin plain deposits of an ancient distal delta, further distinguish these packages as outer lobe and interchannel deposits. In the Eocene to early Oligocene Pindos foreland basin of southwestern Greece, Konstantopoulos and Zelilidis (2013) interpret lithofacies nearly identical to Lithofacies A3 and A4 as interchannel and outer fan lobe deposits. Here we similarly interpret Lithofacies A3 and A4 to record alternating pulses of sandy and muddy low-density turbidity or debris flows in the outer lobes of an unconfined submarine fan system.

Lithofacies A5 also contains sandstone and shale couplets, groove casts, and vertical (*Skolithos*?) burrow structures, but the presence of several other characteristics suggest a different range of possible depositional environments than those of Lithofacies A1-A4. *Neonereites* trace fossils of the *Cruziana* ichnofacies indicate deposition between lower shoreface to lower offshore environments above storm wave base (e.g., Pemberton et al., 1992). Rare brachiopods, rootlets, and red shale beds suggest aerobic conditions prevailed during periods of low-energy, with evaporite beds in the uppermost portion of the lithofacies suggesting periodic subaerial exposure in a peritidal environment (Demmin, 1999). Ripple cross-stratified fine sandstone beds record current and storm wave energy influence in lower shoreface to inner shelf settings (Clifton, 2006). The ratio of shale to sandstone increases upward and suggests that periods of low-energy deposition of clay-sized particles, likely from current suspension after storm events, increased in duration or that conditions favoring sand deposition were less available. These beds are similar to wave-dominated, lower shoreface deposits described and interpreted in the Cretaceous Blackhawk Formation of the Book Cliffs, Utah (e.g., Howard, 1966; Clifton, 2006).

Lithofacies A5 was deposited in aerobic conditions above storm wave base as part of a storm-dominated and subaqueous clastic deltaic complex. Sandstone was deposited during relatively high-energy events, likely storms, during which wave and/or current energies created groove marks filled by ripple and ripple cross-laminated sandstone composed of well-sorted, compositionally mature quartz sand. These beds are interpreted

here as storm-generated tempestites. Following these events, low-energy and shallow-water conditions permitted clay to settle from current suspension, rootlets to grow, brachiopods to suspension feed, and burrowing organisms to inhabit the sandy substrate. Wood chips and mud intraclasts in similar tabular sandstone sheets have been described in shelf-edge distributary delta deposits (Mellere et al., 2002) and were likely fed by sustained hyperpycnal turbidity currents during flooding events (Mulder and Syvitski, 1995) into this sandy storm-dominated, subaqueous deltaic system. Occasional exposure to subaerial conditions in peritidal waters permitted the formation of evaporites described in uppermost beds of the exposure of Lithofacies A5. These features may also suggest deposition as part of an abandoned deltaic system, similar to storm-dominated clastic shelves, which are characterized by similar estuarine-like characteristics during transgression (Boyd et al., 2006).

The combined depositional features and interpreted depositional conditions and environments suggest that FA-A was deposited as part of a subaqueous deltaic complex ranging from deep marine and bathyl to shallow marine and storm-dominated conditions (Table 2.1). The lithofacies interpreted here represent individual components of this complex and include mud-dominated basin plain deposits of a distal prodelta (Lithofacies A1 and A2), alternating mud- and sand-dominated, unconfined submarine fan deposits of a delta front (Lithofacies A3 and A4), and nearly equally mud- and sand-rich, wave- and current-influenced deposits of a periodically exposed, storm-dominated and subaqueous clastic deltaic complex (Lithofacies A5).

2.3.3 Facies Association B: B6, B7, B8, B9, B10, B11

Description

Facies Association B is characterized by carbonate sedimentary rocks displaying a wide range of bedforms and classifications (here following Dunham, 1962), including mainly structureless, lime mudstone, oolitic grainstone to wackestone, fossiliferous packstone, argillaceous lime mudstone, and subordinate interbeds of sandy wackestone, calcareous sandstone, and lime mudstone (see Table 2.1). FA-B dominates the measured section

between meters 117- 292, and 431-440 at Pound Gap (Fig. 2.6a), comprising two main sequences separated by siliciclastic beds of FA-A, FA-C, and FA-D (Fig. 2.4).

Lime mudstone of Lithofacies B6 is gray to brown where fresh, mostly structureless, and may contain discrete horizons of black chert, finely laminated yellow partings, or be dolomitized (Fig. 2.6b). Bedding contacts are mostly planar but may be wavy or karstified. Isolated solitary rugose corals, brachiopods, bryozoans, and other disarticulated shallow-marine fossils in matrix-supported assemblages are common constituents of Lithofacies B6. Fragments of trilobites, crinoid ossicles, bryozoans, solitary rugose corals, and ooids were also identified in thin section. This lithofacies is dominant in the lower portion of the basal sequence of FA-B (Fig. 2.4; Table 2.1).

Beds of Lithofacies B6 are frequently interbedded with gray to brown-gray, structureless, planar- to ripple cross-laminated or trough cross-stratified oolitic grainstone to wackestone beds of Lithofacies B7, sharing planar to rarely wavy, conformable bedding contacts (Fig. 2.6c). Rare large-scale trough cross-stratified to planar-laminated and sheeted oolitic grainstone beds scour into underlying beds of oolitic grainstone or lime mudstone (Fig. 2.6d) and may contain cannibalized, pebble-sized clasts of oolitic grainstone. Ooids are radial in thin section and range in grain size from very fine to very coarse sand (-1–4φ). Fossils were not observed in beds of this lithofacies. Lithofacies B7 is a major contributor in thickness to FA-B and occurs mainly in lower half of the first main sequence of FA-B described in the measured section (Fig. 2.4; Table 2.1).

Lithofacies B8 is characterized by interbedded light gray-brown to red-brown, sandy and occasionally fossiliferous wackestone with gray-black shale and is a minor contributor to the total thickness of FA- B. Sandy wackestone beds are usually thinly bedded and may contain rare brachiopods in intrinsically biogenic (autochthonous) concentrations (see Kidwell et al., 1986), solitary rugose corals, *Archimedes*, or crinoid ossicles, karstified horizons, oolitic horizons, ripple cross-laminae, and yellow to pink, swaley ribbons of

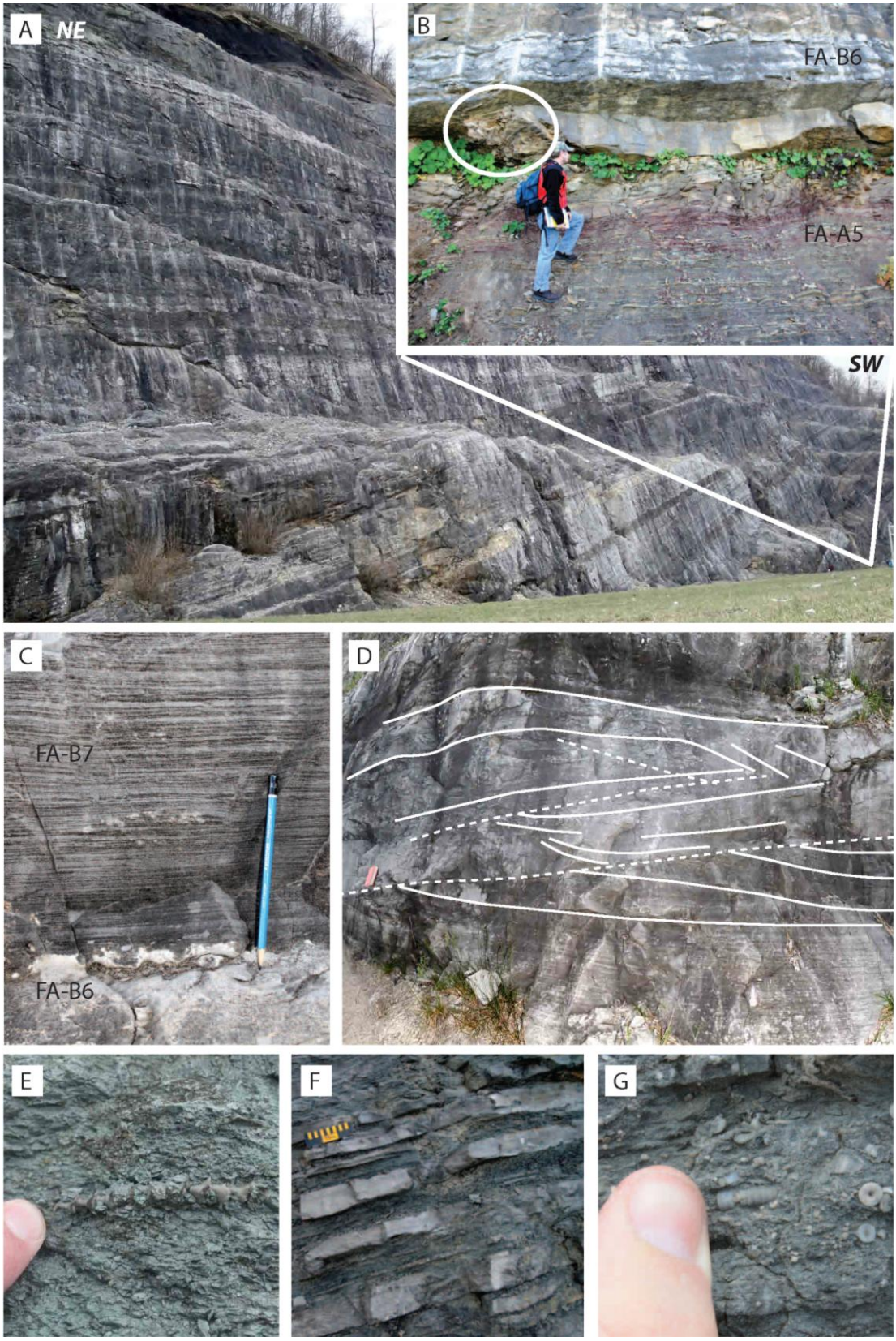

Figure 2.6

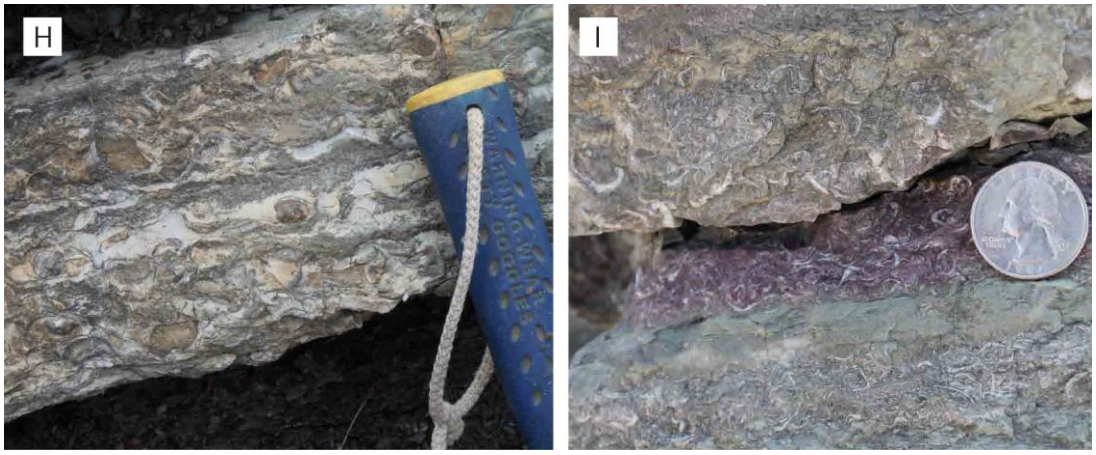

Figure 2.6: Lithofacies of Facies Association B. (A) Exposure of lowermost package of FA-B. (B) Contact is characterized by lime mudstone of Lithofacies B6 with isolated lenses of karstic breccia containing cobble- sized clasts of Lithofacies A5 sandstone and evaporite in lime mudstone matrix. (C) Well-laminated oolitic grainstone (Lithofacies B7) over cherty lime mudstone (Lithofacies B6). (D) Cross-stratified oolitic grain- stone. Solid lines follow laminae, dashed lines follow bedding contacts. (E) *Archimedes* stem in argillaceous limestone of Lithofacies B9. (F) Interbedded to normally graded fossiliferous packstone to shale packages. Scale card is 15 cm. (G) Bioclast-supported packstone of Lithofacies B11 containing parautochthonous and sedimentologic assemblages of crinoid ossicles and intact stems. (H) Disarticulated and unabraded brahio- pods. (I) Disarticulated and abraded brachiopod fragments.

sandy to silty limestone. In one isolated interval (meter 289, Fig. 2.4), desiccation cracks occur above sandy limestone containing brachiopods and ripple cross-laminae. Shale is uncommon but may separate thin beds of sandy wackestone in thinly interbedded packages, as at meter 431. Lithofacies B8 is most closely associated with fossiliferous packstone beds of Lithofacies B11.

Lithofacies B9 is characterized by gray to gray-tan, argillaceous lime mudstone and interbedded lime mudstone with dark- to light-gray or olive-green shale. Shale is generally poorly laminated and may also grade from weakly argillaceous lime mudstone frequently containing fossiliferous horizons of mostly matrix-supported but occasionally bioclast-supported, disarticulated to articulated crinoid stems, brachiopods, *Archimedes* (Fig. 2.6e), or solitary rugose corals. Lithofacies B9 comprises a significant amount of the total thickness of FA-B, occurring mostly between meters 149-185 and 203-231, most commonly in association with Lithofacies B7 and B11 (Fig. 2.4; Table 2.1).

Lithofacies B10 may be considered a subset of Lithofacies B9 but is separated here due to its distinct dark gray to black appearance and recessive nature in the measured exposure. This lithofacies is composed of weakly calcareous and structureless to poorly laminated lime mudstone with limey shale which frequently contains limestone nodules and rarely contains matrix-supported bryozoans. This unit occurs only in the upper half of the first main sequence of FA-B and is most closely associated with Lithofacies B9 and B11.

Packstone beds of Lithofacies B11 are gray to gray-tan, may be structureless and fossiliferous with gray shale beds separating limestone beds, or normally graded in < 20 cm beds that fine from packstone to dark-gray, frequently fossiliferous shale (Fig. 2.6f). Structureless, bioclast-supported packstone beds may contain crinoid ossicles (e.g., meters 187, 213-215, 244; Fig. 2.6g) and disarticulated brachiopod fragments (e.g., meters 237-240, 280; Figs. 2.6h and 2.6i) with less abundant assemblages containing solitary rugose corals (e.g., meters 208, 224, 247), *Archimedes* (e.g., meters 248-250),

blastoids (e.g., meter 220), rare gastropods (meters 254, 260), or diverse fossil assemblages (e.g., meters 219-221, 232, Fig. 2.4) in a micritic matrix. Fossil concentrations may be autochthonous and biogenic, in which concentrations result from biologic processes, but are mostly parautochthonous and sedimentologic, resulting from physical (usually hydraulic) processes controlling fossil concentrations (see Kidwell et al., 1986). Fossiliferous packstone beds may fine upward to calcareous sandstone, shale, or lime mudstone. Packstone to mudstone beds display mostly tabular to occasionally wavy bedding contacts and rare bioturbated bedding (e.g., meters 278-280, Fig. 2.4). Fossiliferous grainstone beds (lacking mud) are rare. Lithofacies B11 is a major constituent of FA-B, is most closely associated with Lithofacies B7, B8, and B9, and appears mainly over meters 187-281 and 433-440 (Fig. 2.4; Table 2.1).

Interpretation

The lithofacies of Facies Association B are broadly interpreted as carbonate bank strata deposited in tropical waters which received varying amounts of siliciclastic influx in calm to turbid water conditions. Lime mudstone beds of Lithofacies B6 were deposited in calm, clear water conditions which permitted limited fauna to inhabit the muddy carbonate substrate. Solitary solitary rugose corals without calcareous algae suggest well-lit water depths less than 100 meters in low latitudes (Hadding, 1933). The lateral continuity of these beds suggests calm-water conditions were widespread. These conditions may have been made possible in part by oolitic shoals of Lithofacies B7, which could have baffled wave energy and created low-energy, protected areas for carbonate mud to accumulate from hemipelagic settling of organic or inorganic calcic particles from the water column. Poorly fossiliferous lime mudstone beds have also been interpreted as ancient tidal flat and low energy lagoonal deposits from this stratigraphic unit in the central Appalachian basin (Al-Tawil and Read, 2003). Lime mudstone may also be deposited in deeper water, euxinic settings below fair-weather wave base, but these beds are typically composed of deeper marine fossil assemblages (Wilson, 1969), whereas thin sections of Lithofacies B6 reveal a muddy carbonate matrix with minor ooids and shallow marine fossil assemblages. In situ, isolated solitary solitary rugose

corals identified along the exposure suggest calm, shallow water conditions. Where karstic surfaces appear to be filled by overlying limestone facies of FA-B, these beds may have been either periodically exposed, creating karstic surfaces above which lime mudstone deposition continued. Where locally karstic surfaces are cavernous, lime mudstone may have been secondarily karstified by secondary fluids which infiltrated the subsurface.

Ooids of Lithofacies B7 formed in calcium-supersaturated, tropical waters between 24.0-25.7°C (Bathurst, 1972). Ooids are generally well-rounded and well-sorted, indicating transportation in high-energy, intertidal currents. Structureless, planar-laminated, and trough cross-stratified bedforms of oolitic grainstone to wackestone suggest traction sedimentation in water conditions devoid of or too turbid to permit deposition of finer clay-sized material. Planar-laminated oolitic sheets were deposited under upper flow regime conditions, whereas trough cross-stratified beds were deposited in lower flow regime conditions (Simons and Richardson, 1961). Beds of Lithofacies B7 are laterally continuous and are similar to those described by Al-Tawil and Read (2003) in eastern Kentucky, therein interpreted as large, occasionally migrating oolitic sheets on a medium- to high-energy carbonate bank influenced by tidal currents and lesser wave action. Cannibalized rip-up clasts of oolitic limestone and erosional contacts between intervals of planar-laminated oolitic grainstone to lime mudstone further support a consistently high-energy marine depositional environment affected by wave action and tidal currents.

Sand content in wackestone of Lithofacies B8 and shale content in argillaceous lime mudstone of Lithofacies B9 and lime mudstone of B10 indicate that siliciclastic influx into the shallow marine system occurred during and limited carbonate bank development. Autochthonous (intrinsically biogenic) concentrations of epifaunal, filter-feeding organisms such as articulate brachiopods, solitary rugose corals, *Archimedes* bryozoans, and crinoid fragments described in matrix-supported, infrequent beds of Lithofacies B8 support deposition in shallow conditions (e.g., Bambach, 1983) such as tidal flat,

lagoonal, or other inner shallow marine environments (e.g., Kidwell et al., 1986). The absence of smaller, silt- to clay-sized grains in sandy wackestone beds of Lithofacies B8 may indicate that current velocity was too high for finer particles to be deposited and that carbonate growth was unhindered by the murky water conditions that likely persisted during deposition of clay-rich beds described in Lithofacies B9 and B10.

In clay-rich beds of Lithofacies B9 and B10, silicic clay-sized particles likely settled from suspension in calm water conditions. Shaley laminae in beds of Lithofacies B9 are usually cyclically interbedded with lime mudstone, probably resulting from autocyclic forces such as tidal cycles, storm events, or seasonal variations in sediment supply (Al-Tawil and Read, 2003). Wilson (1969) suggested a deeper water, downslope or basinal depositional environment for similar, relatively thinly interbedded lime mudstone and shale. The close association of argillaceous lime mudstone beds with coarser deposits such as fossiliferous packstone beds of Lithofacies B11, and less commonly with oolitic grainstones to wackestones of B7, suggests deposition in highly fluctuating, bimodal energy environments. Where these packstones and coarser interbeds are absent, argillaceous lime mudstone beds may have been deposited in calm water conditions to which distal pulses of fine-grained sediment were introduced and settled from suspension below fair-weather wave base where *Archimedes* could colonize. Alternatively, these beds could reflect lagoonal deposition affected by storm events, though this seems less likely given the absence of bioturbation and extensive lateral continuity along the exposure.

Similar carbonate lithofacies reported by Al-Tawil and Read (2003) in eastern Kentucky occur in extensive sheets seaward of oolitic grainstone shoals equivalent in this study to Lithofacies B8. These authors interpret that argillaceous wackestone beds occur closely with skeletal packstone beds (graded to structureless; equivalent here to Lithofacies B11) in open marine conditions between fair-weather and storm wave base on a carbonate ramp seaward of oolitic grainstone shoals and skeletal grainstone beds (Al-Tawil and Read, 2003). Similar argillaceous lime mudstone beds described in the Mississippian

Barnett Shale by Loucks and Ruppel (2007), who interpreted the beds to reflect suspension settling of clay-sized particles from dilute turbidity currents or hemipelagic mud plumes sourced from deltas following storms (*sensu* Bates, 1953), but these authors infer a deep-water, anaerobic depositional environment below storm-wave base similar to those discussed by Wilson (1969). Here we infer that green-gray argillaceous lime mudstone and shale beds reflect deposition in calm, dysaerobic water conditions above storm wave base given their close association to higher-energy fossiliferous packstone beds of Lithofacies B11 and occasional oolitic grainstone to wackestone beds of Lithofacies B7. Dark gray to black lime mudstone beds of Lithofacies B10 may reflect deposition in deeper water, anaerobic conditions, but these infrequent beds also occur in close proximity to fossiliferous packstone beds and are poorly understood.

Parautochthonous concentrations of disarticulated fossil fragments in structureless to normally graded packstone beds of Lithofacies B11 indicate high energy currents transported and disarticulated shallow-marine, mostly epifaunal filter feeders. Similar shelly packstones (Kreisa, 1981) and turbiditic, fossiliferous limestones (Tucker, 1969) have been described and interpreted respectively as storm-generated deposits in carbonate platform and deeper water, bathyal environments. Normal grading in a micritic matrix to shale or calcareous sandstone is similar to bedding structures observed in turbidites described in Lithofacies A4 and indicates deposition in waning energy conditions, partly by freezing from debris flows and partly by settling from low-density turbulent flows generated by gravity (Bouma, 1962; Kreisa, 1981; Lowe, 1982) wave-action (Kreisa, 1981) during storms. These beds are continuous along the outcrop and are widespread in the central Appalachian basin, interpreted by Al-Tawil and Read (2003) as high-energy open marine sheets deposited above storm-wave base. Where packstone beds dominated by disarticulated brachiopod shells and lesser crinoid ossicles grade into shale, deposition likely occurred from turbidity or debris flows during repetitive, waning-energy events, such as storms.

Where beds of Lithofacies B11 contain crinoid stems and mostly intact body fossils of brachiopods, bryozoans, and solitary rugose corals, deposition occurred in relatively calm water conditions where they were protected from disarticulation after transport and deposition during storm events. Barriers such as shoals or banks may have created calm water conditions where high energy currents and wave action processes, including storm events, may have had minimal impact on deposition. Alternatively, these beds may have been deposited below storm-wave base. The presence of the bryozoan *Archimedes*, which inhabited quiet bottom waters immediately leeward of shoals and which were widespread in this area during the Late Mississippian (McKinney and Gault, 1980), suggests deposition in or near back-barrier, shallow-marine setting for interbedded fossiliferous packstone and shale beds. Lagoons may also serve as suitable depositional settings for interbedded packstone storm deposits and low-energy shale beds, especially where these beds are bioturbated (Fig. 2.6g). Where packstones occur in close stratigraphic proximity to oolitic grainstone beds of Lithofacies B7, deposition may have occurred in continuous, coarse-grained shoals or as banks outboard of shoals.

The collective depositional features and interpreted depositional conditions and environments provided here suggest that FA-B was deposited as part of a carbonate bank on which deposition occurred in open to restricted marine conditions. The lithofacies interpreted here represent individual components of this carbonate bank system which included muddy, to lagoonal environments (Lithofacies B6), medium- to high-energy open marine oolitic, sandy, and fossiliferous packstone sheets and shoals (Lithofacies B7, B8, and B11), and low-energy, deeper open marine lime mudstone sheets receiving fine-grained siliciclastic influx (Lithofacies B9 and B10).

2.3.4 Facies Association C: C12, C13

Description

Facies Association C is characterized by interbedded, often laterally thickening or thinning clastic lithofacies that are primarily composed of arenitic sandstone beds with rounded quartz grains. Common components of FA-C include heterolithic strata, ripple

cross-laminated and planar to trough cross-stratified sandstone, shale, and coal. Beds of FA-C may be commonly interbedded with carbonate beds of Lithofacies B, paleosols of Lithofacies D14, and less commonly with shale beds of FA-A, first appearing at meter 270 in the measured section (Figs. 2.4 and 2.7a).

Heterolithic sandstone beds of Lithofacies C12 are common in this facies association, varying from flaser- (Fig. 2.7b) to lenticular-bedded sandstone/siltstone-shale couplets (Fig. 2.7c) that display poorly (Fig. 2.7d) to well-developed symmetric, two-dimensional rippled bedforms with ripple wavelengths generally less than 10 cm, sometimes with multiple rhythmic thickening and thinning trends over ~10-20 cm intervals (e.g., meters 485-494, Figs. 2.4 and 2.7b). These beds may thicken laterally with interbedded intervals of Lithofacies C13 (especially over meters 321-330, Fig. 2.4) or may be present as discontinuous lenses in shale (meters 515-516, Fig. 2.4). Discontinuous and planar cross-stratified, fine sandstone beds up to ~15 cm thick are uncommonly interbedded with heterolithic strata of Lithofacies C12, exhibit mud drapes on sandstone foresets dipping 30°, and may be slightly calcareous (meters 505-510, Fig. 2.4). Apart from mud laminae in flaser- to lenticular-bedded intervals, sandstone to siltstone beds of Lithofacies C12 are fine-grained, quartzose, well-sorted, and white in the initial main sequence of FA-C (meters 271-357), but appear moderately sorted and tan to green-gray in the upper part of the measured section (meters 484-515, Fig. 2.4).

Fine quartz sandstone and siltstone beds of Lithofacies C12 are mostly 1-3 cm thick in frequently laterally thickening or thinning packages up to two meters thick (e.g., meters 326-329, 344-345, Fig. 2.4), which in turn may contribute to amalgamated heterolithic-bedded intervals up to eight meters thick. Though most intervals of Lithofacies C12 are architecturally consistent in bedding structure (e.g., meters 355-356, 496-499, Fig. 2.4), gradual vertical transitions are relatively common and may occur between mud-dominated (wavy-bedded) to siltstone- or sandstone-dominated (flaser-bedded) sequences (e.g., meters 317-319, 345-358, Fig. 2.4). Tan-gray sandstone and dark gray shale beds of

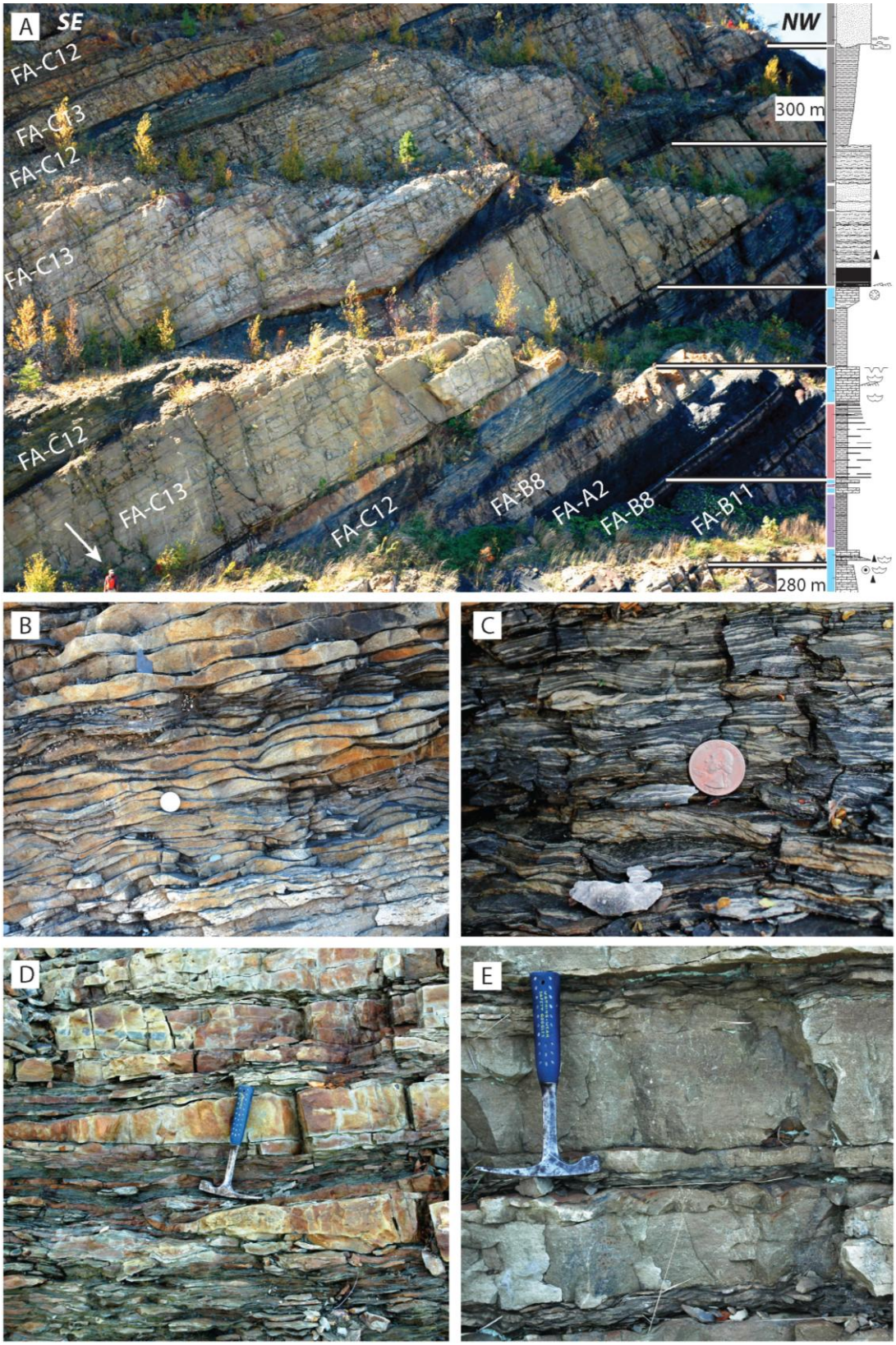
A
SE
NW
FA-C12
FA-C13
FA-C12
FA-C13
FA-C12
FA-C13
FA-C12
FA-B8
FA-A2
FA-B8
FA-B11
300 m
280 m
B
C
D
E

Figure 2.7

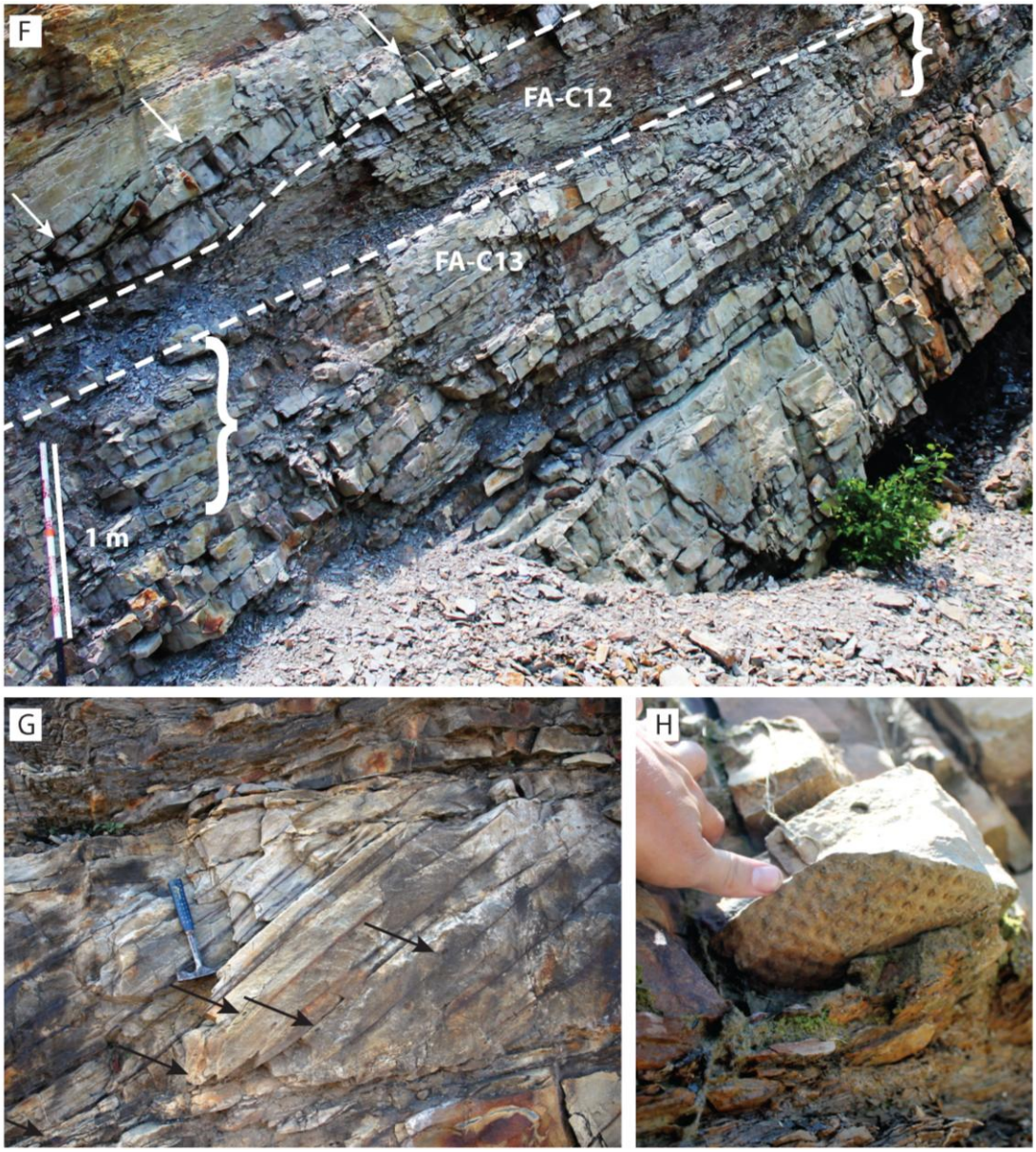

Figure 2.7: Lithofacies of Facies Association C. (A) Lower exposure of FA-C with detailed measured section illustrating planar to channelized contacts between Lithofacies C12 and C13 and interbedded lithofacies of FA-A, FA-B, and FA-D. Colors by stratigraphic column correspond to facies associations in key provided in Figure 2.4. Person in lower left corner for scale (arrow). (B) Well-developed, rhythmically thickening and thinning flaser-bedded heterolithic stratum of Lithofacies C12 interpreted as tidal rhythmites. Quarter for scale. (C) Lenticular-bedded heterolithic stratum of Lithofacies C12. (D) Intercalating flaser- to wavy-bedded heterolithic strata of Lithofacies C12 and laterally thickening amalgamated bedsets of symmetrically ripple cross-laminated sandstone of Lithofacies C13. (E) Multipe amalgamated bedsets of symmetrically ripple cross-laminated sandstone of Lithofacies C13. (F) Meters 321-326 in the measured section. Dashed lines separate laterally thickening amalgamated bedsets of thick-bedded ripple cross-laminated sandstone (FA-C13) and thin-bedded, flaser-bedded heterolithic sandstone (FA-A12). Brackets show thickness changes within packages of Lithofacies C13. Discontinuous horizon of sigmoidal lateral accretion surfaces of FA-C13 indicated by arrows. (G) Planar cross-stratified sandstone of Lithofacies C13 with sideritized mud intraclasts (arrows) in tangential bottomsets. (H) *Lepidodendron* tree cast in sandstone of Lithofacies C13 above organic-rich, lenticular-bedded stratum of Lithofacies C12.

Lithofacies C12 first appear in thin intervals beginning at meters 271, 273, and 276 in the measured section and commonly occur over meters 289-357 and 484-515 (Fig. 2.4). Field observations and thin sections (sampled from sandstones at meters 293, 318, 344, 356, and 487) of heterolithic beds indicate that sandstone is cemented by quartz except from meters 484-498 and 502-510 (Fig. 2.4), where they are cemented by calcite.

Heterolithic strata of Lithofacies C12 are interbedded with and may transition laterally to scouring and planar or trough cross-stratified sandstone, tabular and structureless sandstone, or amalgamated intervals of ripple cross-laminated and well-sorted fine sandstone beds of Lithofacies C13 (Figs. 2.7a and 2.7d). This sandstone-dominated lithofacies is characterized by significant lateral thickness variations, but beds are typically 15-50 cm thick and may be up to two meters thick. Scouring contacts may be localized between two beds or may persist across multiple beds over several meters of section (Fig. 2.7a).

Where symmetrically ripple cross-laminated sandstone beds are well-sorted without mud drapes, these beds are usually capped by low-angle, symmetrically wavy (and occasionally flaser-bedded) bedforms in 15-40 cm amalgamated bedsets (especially meters 303-338, Figs. 2.4 and 2.7e). Herringbone cross-stratification and vertical (*Skolithos*?) burrow structures (e.g., meters 335-337, Fig. 2.4) were rarely observed in these beds.

Fine sandstone beds of Lithofacies C13 may contain mud-draped, inclined foresets which appear sigmoidal in geometry or, where topsets are eroded, contain bottomsets which gradually become tangential in relation to their basal bedding surfaces (Fig. 2.7f). These beds are identified as lateral accretion surfaces, which are generally less than 50 cm thick but may approach one meter in thickness (most common between meters 315-341, Fig. 2.4), and frequently pinch out over tens of meters or less laterally. Similar but less frequent planar cross-stratified sandstone beds may also contain continuous, planar mud-drapes, but these foresets maintain a consistent angle of inclination (~30°), have bedding-

parallel upper and lower bounding surfaces, and are generally continuous along the exposure (e.g., meters 312-314, 498-502, Figs 2.4 and 2.7g). These cross-strata may also contain basal siderite pebble lags or mud intraclasts (or perhaps sideritized mud intraclasts) and average less than 30 cm thick, but may approach one meter in thickness.

Trough cross-strata in fine- to medium-grained sandstone are uncommon but may display mud drapes on low-angle foresets (e.g., meters 295-296, Fig. 2.4). One interval of trough cross-stratified medium-grained sandstone in the upper part of the measured section (meters 510-515, Fig. 2.4) is slightly calcareous, gray-green weathering white-gray, and sublithic, containing siderite pebbles or sideritized mud intraclasts on its lowermost bedding surface which scours into heterolithic strata of Lithofacies C12. Trackways of burrowing organisms, fish, and/or reptiles were observed on this sandstone interval's top bedding surfaces.

Other features observed in fine sandstone beds of Lithofacies C13 are a well-preserved, over two meter long tree trunk cast, and frequent *Lepidodendron* and *Stigmaria* fossilized tree fragments. Though uncommon, thin coal layers less than five centimeters thick and frequently organic-rich shale beds up to ~50 cm thick typically overlie heterolithic strata of Lithofacies C12 and may be overlain by scouring sandstone beds which may contain tree casts (Fig. 2.7h).

Sandstone, shale, and thin coal beds of Lithofacies C13 are most common between meters 295-341, but reappear in thinner intervals the upper part of the measured section (360-363, 498-525, Fig. 2.4). Restored paleocurrent data from sandstone beds in FA-C are presented in Figure 2.4. Measurements of foresets from two-dimensional, vertical surfaces displaying trough cross-stratification in lower sandstone beds of Lithofacies D13 (meters 295-296) dip an average of 06° toward an azimuth of 238° (n=37). Three-dimensional lateral accretion surfaces measured between meters 315-327 (n=44) dip an average of 08° toward 081° with a vector mean of 085° representing a bimodal distribution of northeastward and southeastward dipping surfaces. Foresets of planar

cross-strata measured between meters 498-502 dip an average of 18° toward 107° with a vector mean azimuth of 113° (three-dimensional exposure, n=11) and 24° toward 155° (two-dimensional vertical exposure, n=9). Right-dipping and left-dipping foresets of trough cross-strata in sublithic sandstone beds between meters 510-513 were measured separately owing to poor exposure of three-dimensional surfaces with left-dipping foresets. Right-dipping foresets measured from three-dimensional exposures dip an average of 07° toward 030° (n=12), whereas the calculated best-fit great circle through left-dipping foresets measured from two-dimensional vertical surfaces yields an average dip of 16° toward 166° (n=10). The intersection point between these great circles suggests an approximated average trough orientation dipping 05° toward 091°.

Interpretation

Deposition of Facies Association C occurred in a wide range of coastal environments that varied significantly in flow velocity and sediment supply. Symmetric, two-dimensional ripples in fine sandstone beds of heterolithic strata in Lithofacies C12 are classically attributed to depositional settings influenced by lower flow regime (Blatt et al., 1980, p. 137) oscillatory tidal currents or sinusoidal wave activity (Clifton and Dingler, 1984; Clifton, 2006). Following alternating wave and current activity resulting in sand to silt ripple formation by traction or suspension sedimentation, or potentially by residual sediment accumulation, clay particles settled from suspension in slack-water conditions and covered sand ripple laminae in beds of Lithofacies C12 (see Reineck and Wunderlich, 1968). Where mud drapes do not cover crests of fine sandstone ripples, mud was eroded by the next current and flaser beds were created; where mud dominates with minor connected or single sandy to silty rippled lenses, pulses of higher energy sand deposition punctuated otherwise low-energy, slack-water conditions and created lenticular beds (Reineck and Wunderlich, 1968). Conditions suitable for the formation of these coset bedforms are common in subtidal and intertidal zones in environments such as estuaries, tidal flats, distributary channels and tidal creeks, and similar tidally influenced environments (e.g., Reinson, 1979; Horne and Ferm, 1978; Dalrymple, 1992; Willis, 2005). Miller and Eriksson (1997) described fine-grained tidal rhythmites in

Upper Mississippian prodeltaic strata of the southern West Virginia central Appalachian basin. They have also been described in fluvial-tidal transition zones as tidal flat deposits in upper channel margin successions containing inclined heterolithic strata and may be best developed during times of low river flow (see Dalrymple and Choi, 2007, p. 166). Rhythmic thickening and thinning bundled cosets are interpreted as neap and spring tidal rhythmites which reflect synodically (moon phase) or tropically (moon declination) driven changes in tidal energies (see Kvale, 2006). Factors such as tidal influence, sediment supply, wave amplitude and wavelength, and water depth may have resulted in the observed variance in development and composition of heterolithic strata in this lithofacies.

Amalgamated intervals of well-sorted, fine sandstone beds characterized by two-dimensional, symmetrically rippled bedforms in Lithofacies C13 indicate deposition in similar conditions to those present during the deposition of heterolithic strata of Lithofacies C12, but without periods of low-energy slack-water deposition of clay-sized material. These wavy sandstone bedforms are common in offshore positions above fair-weather wave base where they are sometimes bioturbated (see Clifton, 2006). Symmetric ripples have also been described in the swash zone where swash and back-wash operate, in which sand is deformed into ripples by a thin sheet of water without eddies (Tanner, 1967). Where two-dimensional ripples are asymmetric (uncommon), depositional conditions were influenced by unidirectional or asymmetric orbital currents influenced by passing breakers (Evans, 1941) typically landward of deeper settings producing symmetric two-dimensional ripples in the offshore to nearshore position (Clifton, 2006), though wind-influenced asymmetric ripple marks have also been described in coastal settings (see Tanner, 1967). Clifton and Dingler (1984) summarize that there may be other possible contributors to these symmetric and asymmetric bedforms, such as combined oscillatory currents and unidirectional flow caused by tidal, rip, or longshore currents, but the amount of data required to determine these is beyond the scope of this study.

The dominance of well-sorted and well-rounded sand grains in sandstone beds of Lithofacies C12 and C13 is evidence of extensive physical and chemical weathering and sediment reworking processes that yielded compositionally and texturally mature sediment. Compositionally and texturally mature sandstone is commonly associated with beach and nearshore environments that are dominated by tidal and wave processes that rework coastal plain sediment and remove the less stable minerals and finer clastic fractions (e.g., Roy, 1977; Horne, 1979).

Wavy bedforms and interbedded sandstone containing lycopsid tree casts and carbonaceous-rich horizons have been described and interpreted elsewhere as shallow to emergent, wave-dominated shoreface and beach deposits (Falcon-Lang, 2004). *Skolithos* burrow structures in fine sandstone beds of Lithofacies C13 similarly indicate deposition in proximal offshore to upper shoreface environments (Pemberton et al., 1992), whereas herringbone cross-stratification has been described primarily in tidally influenced delta front environments and estuaries (Dalrymple, 1992).

Planar cross-stratified fine sandstone beds were created during migration of two-dimensional, straight-crested sand dunes under lower flow regimes (Simons and Richardson, 1961) in tidal channels and have been described as point bar (see Bridge, 2003) to upper shoreface deposits (Bhattacharya and Walker, 1991). Tangential foresets with coarser pebbles in bottomsets indicate high sediment-transport rates (e.g., Reesink and Bridge, 2007) or channel water depth (Smith, 1972) under lower flow regime conditions. Continuous mud drapes on foresets of planar cross-strata are identical to descriptions of inclined heterolithic strata of Thomas et al. (1987), who suggested that most of these deposits form during point bar migration in alternating high- and low-energy flow conditions generated by tidal processes in freshwater, tidally influenced rivers or creeks stemming from intertidal mudflats.

However, two-dimensional sand dunes can form in a wide range of environments, and further interpretation should rely on the context of its associated facies (Bhattacharya and

Walker, 1991). Where interbedded with scour-based intervals of amalgamated, wavy sandstone displaying lateral thickness variations (Lithofacies C13, meters 312-314), thinning-upward planar cross-strata were deposited in intertidal creeks which incised sheet-like and amalgamated shoreface deposits of symmetrically ripple-bedded sandstone. Where interbedded with thin beds of heterolithic, flaser- to lenticular-bedded sandstone beds (meters 498-502), planar cross-stratified sandstone beds were deposited in tidal creeks flanked by mud or tidal flats (see Wang, 2012, and Tessier, 2012).

The same can be said for similar trough cross-stratified sandstone beds with siderite pebble lags: though we can infer that they were deposited as three-dimensional, sinuous-crested sand dunes under low flow regimes (Simons and Richardson, 1961), these bedforms form in a wide variety of depositional environments and are best considered in the context of surrounding facies. The trough cross-stratified and fine-grained arenitic to sublitharenite (micaceous) beds between meters 295-296 and 510-515 in the measured section are bedded in close stratigraphic association with tidal flat deposits of heterolithic beds (Lithofacies C12). Here, we infer that planar and trough cross-stratified units of Lithofacies C13 were deposited in tidal creeks or channels flanked by tidal flats. Similar sequences defined by scour-based sandstones containing pebble lags and overlying fining-upward and planar to trough cross-stratified sequences have been reported in tidal inlet deposits (see FitzGerald et al., 2012), though these deposits may be difficult to identify in the ancient record. Increasing-upward micaceous content in these beds indicates that either an absence of the same physical reworking processes present in other tidally influenced delta plain and estuarine environments of FA-C due to periodic deposition in dominantly fluvial currents with minimal tidal current influence, or, less likely, that clastic detritus was derived from a different source relative to other sandstone beds of the facies association. Similar sandstone beds observed between meters 523-525 contains vertical (*Skolithos*?) burrow structures along upper bedding surfaces and bifurcates laterally, separated by reddish paleosols of Lithofacies D14 of FA-D. Calcareous cement in these sandstone beds may indicate infiltration of sea water during high tide or periods of marine transgression.

Paleocurrent data collected from cross-stratified sandstone beds in Lithofacies C13 vary in results along the exposure (Fig. 2.4) and suggest fluctuating sediment transport pathways through time in response to varying influences of tidal and fluvial processes. Lowermost trough cross-stratified sandstone beds over meters 295-296 were deposited in tidal creeks or channels which flowed southwestward. Planar cross-stratified tidal creek deposits preserved over meters 498-502 record a southeastward paleocurrent direction. Trough cross-stratified tidal creek or distributary channel deposits further upsection (meters 510-513) preserve a transition toward an eastward sediment transport direction. Whether paleocurrent directions from planar and trough cross-strata correspond to ebb- or flood-tidal or perhaps longshore current orientations typical of tidally influenced deltas is not immediately apparent and further such interpretations require re-evaluation of the data in the context of regional basinal trends considered in the discussion section of this manuscript.

Lateral accretion surfaces (epsilon-cross-stratified units of Allen, 1963, p. 102; principal type of inclined heterolithic strata of Thomas et al., 1987) described in the section result from point bar migration oblique to net sediment-transport direction and deposition on planar erosional surfaces produced during erosion of the floor and outer bank of a channel. Fine sand foresets and separating, continuous mud drapes were produced by fluctuating tidal current strength (Allen, 1963). At Pound Gap, paleocurrent measurements suggest that point bars migrated northeastward and southeastward. Unfortunately, since point bars migrate orthogonal to net channel flow direction, the possible flow directions are northwest or southeast and northeast or southwest. It is unlikely that the average migration direction toward 081° would yield a valid channel flow direction given the lack of lateral accretion surfaces dipping in this direction. This data is probably best interpreted when considered in the context of regional drainage trends established in previous studies. These bedforms are common features of distributary mouth bars (Dalrymple and Choi, 2007, p. 168), tidal bars (Longhitano et al., 2012) and the overwhelming majority of published examples of inclined heterolithic strata (including lateral accretion surfaces) are reported in freshwater, tidally influenced

meandering channels, rivers, and creeks draining intertidal mudflats (Thomas et al., 1987).

Transitions to fine sandstone and siltstone may record channel migration or abandonment which gave way to levee, crevasse-splay or inter-distributary channel development (e.g., Fisher et al., 1969; Bridge, 2006), and these deposits may be scoured by channelized sandstone from adjacent fluvial channels. Carbonaceous, organic-rich horizons and lycopsid tree casts of *Lepidodendron* and their *Stigmaria* roots, commonly at the base of fine sandstone above relatively mud-rich intervals of Lithofacies C12 and C13, preserve vegetated levees or shallow abandoned channels with canopy trees that commonly inhabited poorly drained, clastic substrates in ever-wet bottomlands (see DiMichele et al., 2001).

Similar lithofacies have been described by Boyd et al., (2006), who interpreted planar cross-stratified, flaser-bedded, and tidally bedded sandstone beds as bayhead-delta distributary-channel deposits. Where sandstone beds exhibit scouring basal contacts and contain planar cross-stratification with pebble lag, trough cross-stratification, carbonaceous detritus, current ripples, low-angle ripple laminae, mud intraclasts, and bioturbation, these beds are characteristic of incised valley fill deposits (see Boyd et al., 2006 and Suter, 2006). However, Willis (2005) notes that erosive-based sandstones are becoming increasingly recognized in tide-influenced depositional settings. Similar beds containing wave ripples, bioturbation, and trough cross-stratification may be characteristic of shelfal to shoreface environments (see Suter, 2006). At Pound Gap, the combined bedforms and features of FA-C are therefore interpreted to reflect deposition in a variety of mainly tidally influenced, coastal environments that more broadly comprise a delta front to lower delta plain system (Table 2.1). In this system, the delta front is comprised of the tidally and wave-influenced shoreface and foreshore environments, whereas the lower delta plain includes tidally influenced environments including tidal flats, interdistributary bays and channels, and lagoons affected by tidal incursion of sea water (see Fisher et al., 1969; Bhattacharya, 2006). Heterolithic sandstone beds of

Lithofacies C12 were deposited in intertidal to subtidal conditions and potentially fluvial-tidal transition zones, which may include tidal flats, distributary channels and tidal creeks, and other tidally influenced, low-energy estuarine environments that may persist in delta front to lower delta plain environments. Higher energy bedforms and interpreted depositional conditions of Lithofacies C13 persisted in proximal offshore to wave-dominated shoreface environments of a delta front system, whereas migrating channels and vegetated levees or shallow abandoned channels were deposited as part of a fluvial to estuarine lower to deltaic plain system.

2.3.5 Facies Association D: D14, D15, D16, D17

Description

Facies Association D is dominated by shale and texturally soily, variegated mudstone paleosols punctuated by fine-grained sandstone to siltstone beds. Soily mudstone and thin coal beds of Lithofacies D14 dominate the facies association and are separated by intervals of shale, arenitic to sublithic sandstone sometimes containing mud-draped ripple cross-laminae, planar and trough cross-stratified sandstone, and thin coal beds of Lithofacies D15, thinly interbedded shale and structureless sandstone of Lithofacies D16, and carbonaceous shale to siltstone with calcareous sandstone lenses of Lithofacies D17. This facies association is restricted to the upper part of the exposure at Pound Gap, first appearing at meter 281 and last appearing at meter 560 in the measured section (Fig. 2.4), and is punctuated by intervals of FA-A, FA-B, and FA-C (Fig. 2.8a).

Lithofacies D14 is characterized by clay-rich, variegated beds which are typically poorly indurated and texturally soily and may contain organic-rich layers or thin (<5 cm) coal beds. Soily mudstones are typically gray-green or red-gray (Fig. 2.8b) and may contain fossil fragments of the sphenophyte *Calamites* and other plant fragments, pedogenic slickensides in red, clay-rich beds (e.g., meters 424-428, Figs. 2.4 and 2.8c), abundant rootlets and red to tan rhizocretions commonly >30 cm in height and replaced by silt (Fig. 2.8d), and concretions (e.g., meters 349, 444-446, 547, Fig. 2.4). Individual soily mudstones range in thickness from ~10 cm to several meters and may contribute to ~10

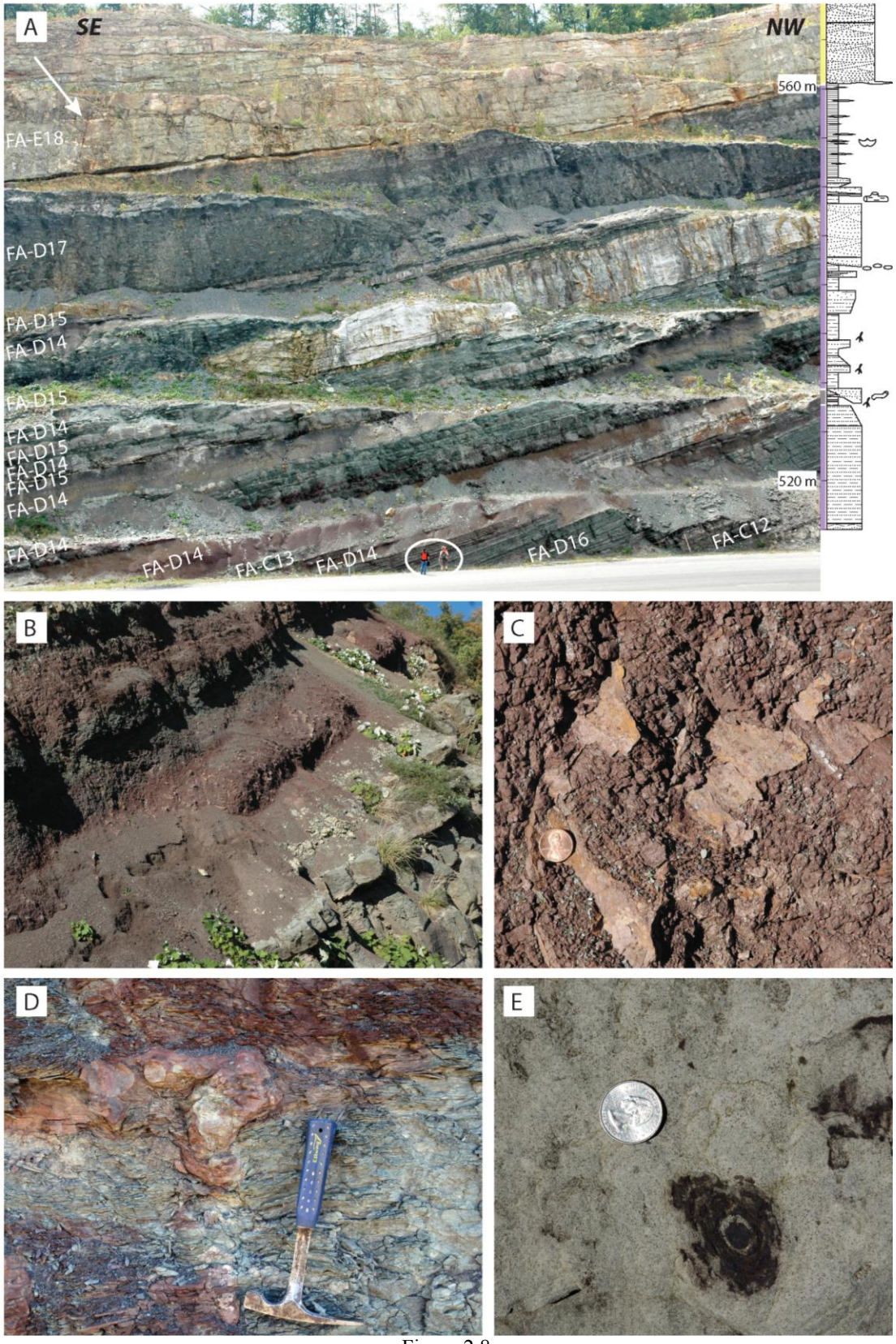
A
SE
NW
560 m
520 m
FA-E18
FA-D17
FA-D15
FA-D14
FA-D15
FA-D14
FA-D15
FA-D14
FA-D15
FA-D14
FA-D14
FA-D14
FA-C13
FA-D14
FA-D16
FA-C12
B
C
D
E

Figure 2.8

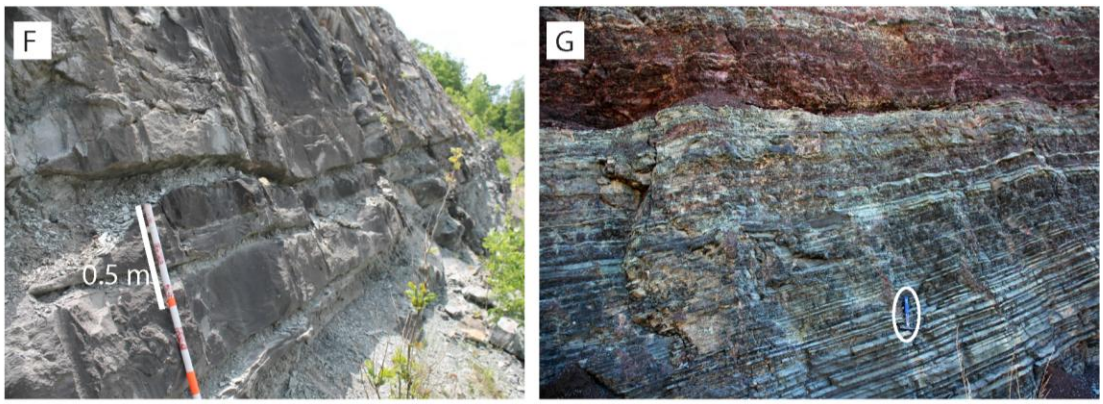

Figure 2.8: Lithofacies of Facies Association D. (A) Representative exposure with detailed measured section illustrating interbedded lithoacies of FA-D with FA-A and FA-C and truncation by FA-E. Colors correspond to facies associations in key provided in Figure 2.4. Minor faults occur in this interval with minor reverse displacement. Persons for scale (circled). White arrow indicates major scouring surface discussed in FA-E description. (B) Red paleosols of Lithofacies D14 above tabular, ripple-laminated sandstone of Lithofacies D15. Sandstone bed is approxiately 50 cm thick. (C) Pedogenic slickensides in paleosol of Lithofacies D14. (D) Deep-rooted rhizocretion in paleosol of Lithofacies D14. (E) Upper bedding surface of sandstone show- ing cross-sectional view of root cast. (F) Example of interbedded light gray paleosols of Lithofacies D14 with lenticular to tabular beds of trough cross-stratified sublithic sandstone of Lithofacies D15. Interval shown corresponds to meters 538-541 in the measured section. (G) Thinly interbedded, continuous, and structureless sandstone and shale of Lithofacies D16. Note thinning-upward trend of sandstone beds and abrupt transition to overlying paleosol of Lithofacies D14. Rock hammer for scale (circled).

m thick amalgamated intervals of soily mudstones (meters 442-452, Fig. 2.4), transitioning in color and texture abruptly or gradually. Variegated mudstones rarely contain calcareous, sandy intervals or limey, silty interbeds (meters 429-431, Fig. 2.4) or may grade into weakly calcareous siltstone intervals above rooted soily mudstones (meters 526-530, Fig. 2.4). Lithofacies D14 dominates the measured section over meters 348-378, 414-453, and 514-548 in the measured section (Fig. 2.4; Table 2.1).

Clay-rich, texturally soily beds of Lithofacies D14 frequently grade upward from shale beds of Lithofacies D15, which are interbedded with arenitic to sublithic and often calcareous sandstone to siltstone beds and rare, thin (<10 cm thick) coal beds. Root casts may be visible in cross-section on upper bedding surfaces of sandstone beds (Fig. 2.8e). Sandstone beds are typically very fine- to fine-grained, continuous but may bifurcate, separated by soily beds of Lithofacies D14 or shale of Lithofacies D15 (meters 418-419, 538-539, Figs. 2.4 and 2.8f), and may display significant lateral thickness changes (e.g., meters 523-524, 547-548, Fig. 2.4). Sandstone to siltstone beds are typically tan-brown weathering light gray to brown, may be ripple cross-laminated (e.g., meters 423, Fig. 2.4) or planar (meters 420, 542-544, Fig. 2.4) to trough cross-stratified (meters 423-425, 539-546, Fig. 2.4), and may contain mud intraclasts (e.g., meters 423, 539, Fig. 2.4) or rare burrow (*Skolithos*?) structures (meter 375, Fig. 2.4). Sandstone beds are frequently cemented by calcite (meters 350, 352-353, 441-443, 452-454, 535-536, 547-548, Fig. 2.4). Beds are typically less than one meter thick and stacked in sequences less than two meters thick (except from meters 539-546, Fig. 2.4), though may comprise intervals approaching five meters thick where interbedded with shale such as that described over meters 417-421, Fig. 2.4). Thin coal layers may be present beneath planar-based to scouring sandstone beds, and well-laminated, black to light gray shale contains fragments of lycopsid *Stigmaria* roots and sphenophyte trunks of *Calamites*.

More frequently, siltstone to fine sandstone beds are interbedded with thicker sequences of variegated mudstones of Lithofacies D14. The uppermost succession of Lithofacies D15 (meters 537-548, Fig. 2.4) is characterized by typically light gray soily mudstone

beds separating tabular to discontinuous or bifurcating beds of ripple cross-laminated to trough cross-stratified sandstone (Fig. 2.8f). Trough cross-stratified sandstone beds may be 10-30 cm thick in single to multistory complexes of sandstone up to seven meters thick. Where scouring, basal sandstone surfaces may contain mud intraclasts. Three-dimensional surfaces of trough cross-strata over meters 539-546 (Fig. 2.4) are poorly exposed and display only left-dipping foresets (n=16) which an average dip of 08° toward 310°. Two-dimensional vertical surfaces displaying both right- and left-dipping foresets (n=15) were measured for paleocurrent direction. Best-fit great circles through each foreset group are oriented nearly identically (right foresets dipping 09° toward 274°, left foresets dipping 15° toward 276°) and suggest an average westward-dipping trough orientation.

Lithofacies D16 is characterized by thinly interbedded very fine sandstone and shale beds and is restricted to one seven meter interval in the upper part of the measured exposure (meters 515-522, Fig. 2.4). These beds transition gradually from underlying lenses of flaser-bedded to ripple cross-laminated, slightly calcareous sandstone in shale. Thin sandstone beds are light gray, structureless to planar-laminated, continuous, have a tabular bedding geometry, and decrease in ratio with shale from ~80% to ~40% upward (Fig. 2.8g). Sandstone interbeds gradually become decreasingly well-indurated and thin upward from a maximum of ~8 to <1 cm, whereas shale interbeds maintain a consistent thickness of ~1-3 cm throughout. Shale beds become increasingly pedogenic and less well-indurated upward, especially below an overlying rooted red, soily mudstone beds of Lithofacies D14.

Lithofacies D17 is also limited to one ~12 m interval along the Pound Gap exposure (meters 548-561, Figs. 2.4 and 2.8a) and is characterized by a basal tan-orange to gray siltstone coalified plant fragments which after 50 cm grades sharply upward into laminated, black carbonaceous shale containing discontinuous lenses of fine-grained and structureless to laminated calcareous sandstone up to 20 cm thick and approximately one meter across. Further information regarding the geometry of these lenses is unfortunately

limited by the two-dimensionality of the exposure. Sandstone beds may contain brachiopods and are roughly spaced in two meter intervals, decreasing in frequency upsection.

Interpretation

Texturally soily, variegated, and typically poorly indurated mudstone beds of Lithofacies D14 are interpreted here as paleosols. Paleosols and thin organic-rich to coalified beds of Lithofacies D14 were deposited in low-energy overbank, floodplain, or marsh-like environments where clay and nutrients acted as a substrate for lycopsid and sphenophyte trees and other rooted vegetation. The color, texture, amount of organic content, and types of rootlets observed in individual paleosols can provide such information as the climate and drainage conditions of the depositional environment, but interpretations to this detail are beyond the scope of this study and have already been described and interpreted in detail by Ober (2003) and Kahmann-Robinson (2008).

Pedogenic slickensides in red, clayey paleosols formed during swelling and contraction of expansive clay soils during seasonal wetting and drying of the soil profile (Ciolkosz et al., 1979). Similar beds containing calcareous concretions and rootlets have been described in Vertisols of age-equivalent strata (Mauch Chunk Formation, Pennsylvania) in the Appalachian basin by Gray and Nickelson (1989), who interpreted a probable floodplain or delta plain origin for these beds.

Sublithic to arenitic and frequently calcareous sandstone beds of Lithofacies D15 were deposited in scouring, bed load-dominated meandering fluvial channels in which two- and three-dimensional dunes migrated under lower flow regimes (Simons and Richardson, 1961). These channels incised surrounding low-energy overbank and floodplain deposits of Lithofacies D14 and, where sandstone beds fine upward or bifurcate, separated by overbank shale or paleosol beds, migrated or were temporarily abandoned. Similar 1-5 m thick, sheet-like, erosionally based, pebbly and medium- to fine-grained cross-stratified to rippled sandstones described in a compilation of work

summarized by Boyd et al. (2006) from the Lower Cretaceous Basal Quartz Formation (Caramangay unit) in southern Alberta and northwestern Montana, where they are often capped by green, waxy paleosols. These beds have been interpreted as braided-fluvial to coarse-grained meandering-fluvial systems which scoured into fine-grained overbank deposits (Boyd et al., 2006, p. 210).

Planar cross-stratified or ripple cross-laminated sandstone beds characterized by non-channelized, tabular bedding geometries that thicken or thin laterally and are overlain and underlain by overbank shale or paleosol beds are likely either sandy levee or crevasse splay deposits deposited on the flanks of channels where depositional energy decreased with distance from the channel. Coarsening upward rooted paleosols of Lithofacies D14 that transition vertically to thinly bedded, planar cross-stratified and calcareous siltstone containing siderite nodules (meters 450-454, 533-536) are also tentatively interpreted as crevasse splay deposits formed during progradation of sediment bodies into flood basins or lakes (e.g., Bridge, 2006). Bridge (2006) also notes that crevasse splay deposits may contain similar bedforms to levee or channel fill deposits and thus may be difficult to correctly indentify. Except from meters 539-546, these beds are mostly isolated (single-story and encased by floodplain mudstone beds) rather than amalgamated, similar to ribbon-like channel and sheet-like crevasse splay deposits described and interpreted from the Horsefly sandstone of the Lower Cretaceous Basal Quartz Formation (Horsefly unit; see Boyd et al., 2006 and references therein). Where these sandstone beds gradually transition from tabular to lenticular and discontinuous with interbedded light gray paleosols and are capped by multistory trough cross-stratified sandstone (meters 539-546), this interval is interpreted to reflect transition from crevasse splay (tabular) to levee (lenticular) to channel-fill (scouring and irregular-based) deposits. Paleocurrent data suggest that fluvial channels transported sediment westward. Channel switching resulted in a return to low-energy conditions and deposition of the overlying paleosol beds containing tree casts.

Thinly interbedded very fine quartz sandstone and shale beds of Lithofacies D16 are structureless and continuous along the exposure, suggesting deposition in sheet-like bodies during repetitive pulses of medium-energy events in an otherwise low-energy depositional environment. These pulses appear to have been repetitive and characterized by consistent energy levels, though the upward thinning of sandstone beds upward may suggest decreasing duration or proximity to sediment sources. The transition to these beds from flaser-bedded and calcareous sandstone beds of interpreted tidal flat or tidally influenced interdistributary origin (Lithofacies C12) and into rooted paleosols of Lithofacies D14 may suggest that beds of Lithofacies D16 were deposited in floodplain or lacustrine environments that lost tidal influence through time. Lakes lack tidal influence and are therefore restricted to upper delta plain systems (Bhattacharya, 2006). However, Bridge (2006, p. 115) notes that distinguishing deltaic lacustrine deposits from levee and crevasse splay deposits overlain by muddy floodbasin deposits may be difficult. The absence of desiccation cracks in these deposits suggests the depositional system was consistently subaqueous or under moist conditions in a humid environment.
Carbonaceous siltstone grading to carbonaceous black shale of Lithofacies D17 was deposited in low energy, vegetated and reducing environments in which very fine sandstone filled troughs perhaps generated during storm events. Rare brachiopods and calcite cement in these sandstone lenses suggests that sea water covered the depositional environment either consistently or during periods of marine inundation. Carbonaceous shale has been described and frequently attributed to deposition in coastal brackish and salt marsh environments. The absence of coal may suggest that fresh to perhaps brackish waters were periodically discharged and that conditions were unfavorable for deposition of high-quality organic content (Kosters and Suter, 1993).

Lithofacies of FA-D were deposited in mostly low-energy conditions in floodplain to overbank (Lithofacies D14), levee and crevasse splay to fluvial meandering distributary channel (Lithofacies D15), lacustrine or floodplain (Lithfoacies D16), and marsh (Lithofacies D17) environments. Though tidal and wave action processes did not affect these environments, fluvial sandstones of Lithofacies D15 are frequently interbedded

with tidally influenced deposits of FA-C, suggesting that deposition of Facies Association D occurred in environments not far removed from tidal influence. This may explain why sandstones of FA-D may be arenitic to sublithic, whereas sandstone beds of FA-C contain texturally and compositionally mature quartz sand which was reworked wave action and tidal currents. In the Upper Mississippian central Appalachian basin of southeastern West Virginia, Kirkpatrick (1994) described similar lithofacies to those observed in FA-C and FA-D of this study and interpreted a convergence of fluvial and marine environments led to their deposition in a prograding deltaic system. Similarly, we interpret that lithofacies of FA-D were deposited in upper delta plain environments just removed from tidal influence.

2.3.6 Facies Association E: E18

Description

Facies Association E consists of only Lithofacies E18, which is characterized by structureless and planar to trough cross-stratified, medium to coarse quartz sandstone and granule to pebble conglomerate exposed at the top of the measured section (meters 561-590+, Fig. 2.4; Table 2.1). Packages of arenitic sandstone are typically ~5-8 meters thick with internal bedsets of up to two-meter-thick planar cross-stratified medium sandstone separated by mostly planar bedding surfaces, which are in turn frequently bound by major scouring contacts with thin basal quartz pebble conglomerates and irregular or planar to trough-like geometries over several meters (Fig. 2.9a). Quartz sandstone is white where fresh and weathers tan-yellow to red-brown. Planar cross-stratified foresets mostly display continuous bottomsets characterized by tangential relationships to basal bedding surfaces (Figs. 2.9b and 2.9c) and are sometimes defined by dark mud drapes (Fig. 2.9d) with rare ripple cross-laminated (<6 cm thick) beds toward the upper contacts of large-scale, tangential cross-stratified beds (Fig. 2.9c). Scour-and-fill structures containing granule to pebble conglomerate are common (Fig. 2.9e) and may be crosscut by horizontal coalified tree horizons (Figs. 2.9c and 2.9f). Quartz granules and pebbles are

Figure 2.9: Lithofacies 18 of Facies Association E. (A) Exposure of Lithofacies E18 demonstrating 5-8 meter thick composite packages of planar cross-stratified sandstone beds up to ~2.5 m thick. Solid line traces follow cross-laminae whereas dashed line traces follow bedding surfaces. (B) Thickly bedded planar cross-stratified sandstone displaying tangentially shallowing bottomsets. (C) Thinner beds of planar cross-stratified to ripple cross-laminated sandstone typically restricted to upper parts of thickly bedded cross-stratified packages. (D) Mud-draped laminae in stacked planar cross-strata. (E) Scour-and-fill structure in planar cross-stratified sandstone containing well-rounded quartz granules to pebbles. (F) In situ coalified tree cross-cutting planar cross-strata.

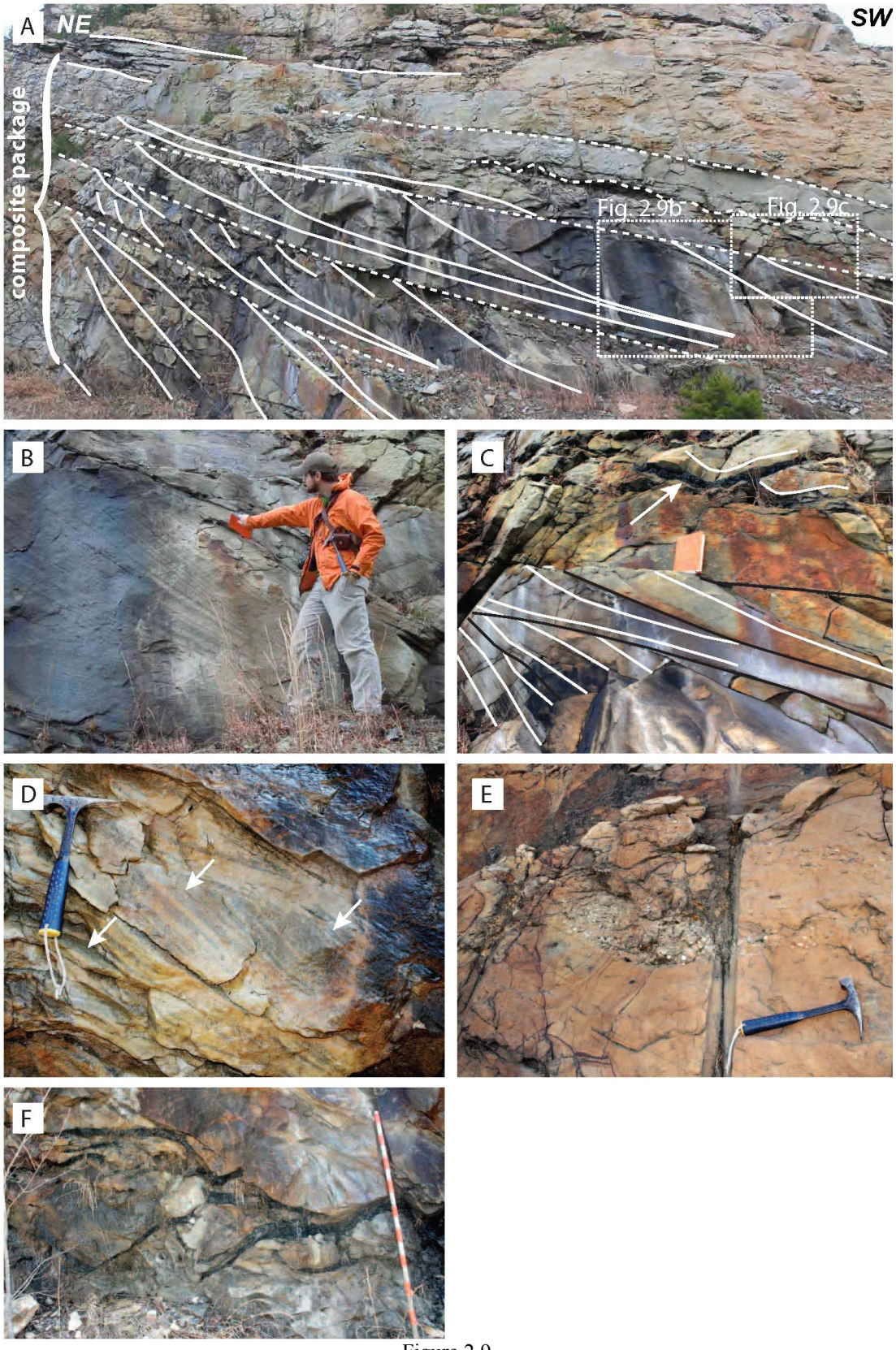

Figure 2.9

well-rounded, spherical to oblate, up to 4 cm across, and are sometimes imbricated where oblate.

The lowermost exposure of Lithofacies E18 (meters 560-572) appears tan and thickly bedded with pebble conglomerates transitioning abruptly to medium sandstone. This interval contains at least one major incising surface, which separates contrasting tan and more oxidized tan-purple sandstone, resulting in lateral thickness variations of ~2-8 m for this section (Fig. 2.8a, white arrow). Lower packages of Lithofacies E18 below this highly visible contact are stacked in ~5-8 m intervals of thickly bedded and planar cross-stratified sandstone transitioning upward to thinner beds of planar cross-stratified sandstone. Above these beds, a ~5-8 m interval consists of more thinly bedded, tan-gray to light gray sandstone weathering purple-tan that onlap the channelized basal contact. These beds are less accessible but clearly demonstrate low-angle planar erosive contacts between laterally thickening and thinning packages of sandstone (Fig. 2.8a, uppermost sandstone unit). Wizevich (1992) described similar 5-10 m thick packages discussed below in stratigraphically equivalent rocks in southeastern Kentucky.

Paleocurrent data collected from three-dimensional surfaces of planar cross-strata of Lithofacies E18 (n=67) are presented in Figure 2.4. Foresets dip in a ~270° range of dip directions from north-northeast to south-southeast, with measurement data most concentrated in the north, south, and southwest directions, averaging 18° toward 294° with a vector mean azimuth of 245°. None of the foresets measured dip eastwardly.

The upper extent of Lithofacies E18 is not exposed at Pound Gap, which, combined with faulting in the Pound Gap fault zone, complicate total thickness estimates for this unit. Here, we infer a minimum thickness of ~30 m to the top of the measured stratigraphic section (Fig. 2.4).

Interpretation

The coarser grain size, compositional maturity, dominance of two-dimensional lower flow regime bedforms, and scouring basal surfaces between sandstone beds in Lithofacies

E17 indicate consistently high depositional energy conditions were present during deposition. Planar cross-stratified sandstone beds containing conglomeratic scour-and-fill structures were formed during high-energy, channelizing events which scoured into underlying sandstone beds and deposited quartz pebbles from bed-load transport in turbulent flows. Large-scale planar cross-strata frequently displaying long, tangential bottomsets were deposited respectively as two-dimensional straight-crested and sinuous-crested subaqueous dunes under lower flow regimes (Simons and Richardson, 1961) and, where foresets contain well-rounded pebbles at their bases, were deposited rapidly (e.g., Reesink and Bridge, 2007). Though lower foreset angles are traditionally attributed to increasing depositional flow velocity, Smith (1972) demonstrated that foreset angle is also inversely correlated to crest depth of active transverse bars (migrating, planar-topped dunes) or may change in apparent angle along an exposure due to lateral changes in flow direction.

Mud drapes on foresets of planar cross-strata in some beds of Lithofacies E17 are characteristic of inclined heterolithic strata (Thomas et al., 1987) and suggest deposition as migrating transverse or longitudinal bars and dunes in alternating high- and low-energy flow conditions, which may be generated by tidal forces. Multistory channelized bedforms and laterally continuous architectural elements suggest depositional conditions were consistent and widespread, consistent with those present in braided river systems. Where lenticular in geometry, successions of planar cross-stratified to structureless sandstone were deposited in laterally shallowing channels with wedge-shaped geometry typical of curving channels adjacent to braid bars or larger mouth bars in fluvial systems (see review by Bridge, 2006, Fig. 2.10). Thinner packages of planar cross-stratified sandstone beds lacking scoured basal contacts may have been deposited as two-dimensional dunes on transverse or longitudinal bars.

Wizevich (1992) described planar cross-strata and large-scale tangential and giant tangential cross-strata in packages of the stratigraphically equivalent Lee Formation utilizing architectural elements defined by Miall (1985). The author described major

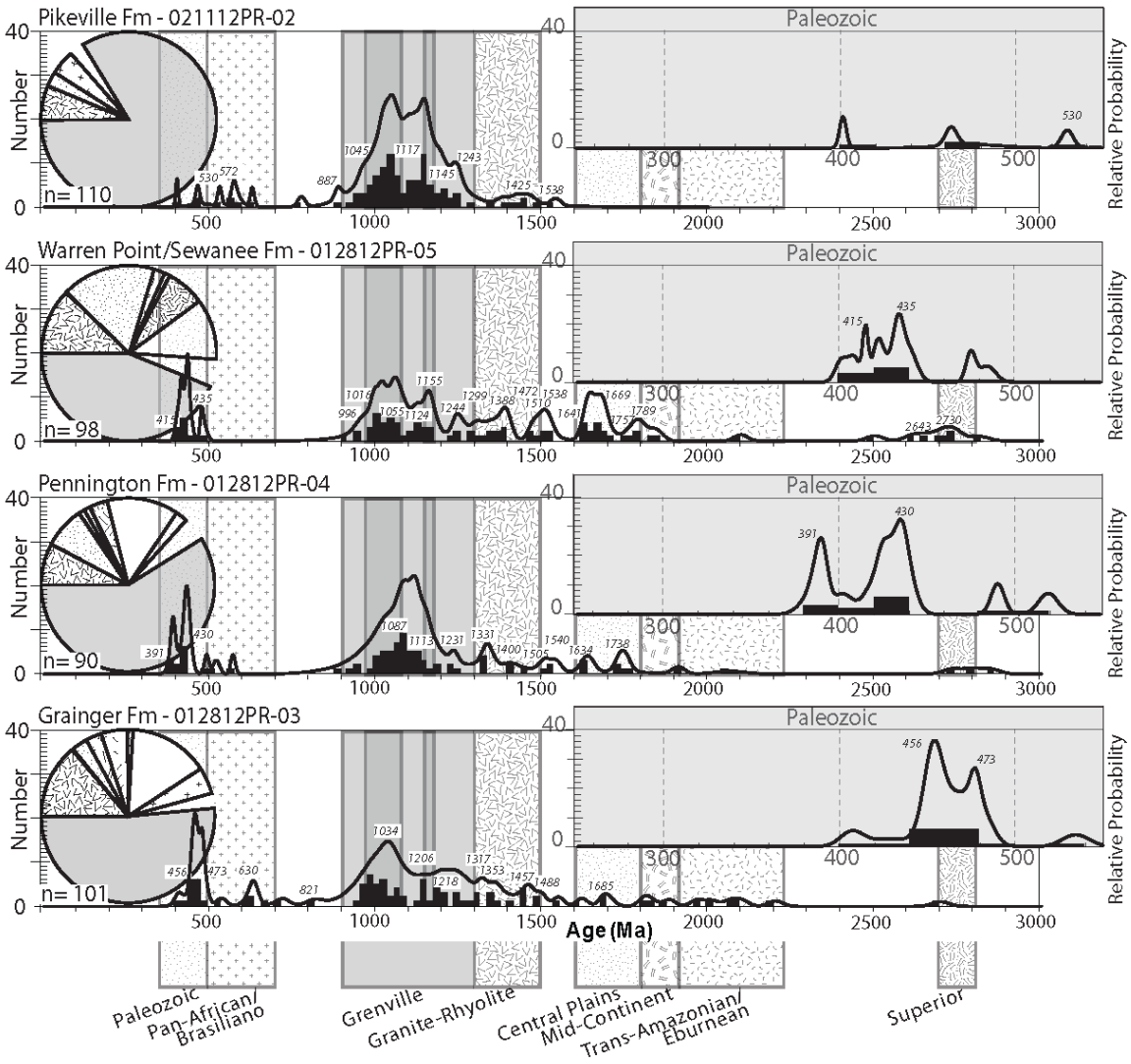

Figure 2.10: Detrital zircon age frequency histograms and normalized relativity plots with inset normalized probability plots of Paleozoic age associations from samples selected from Pound Gap, Kentucky.

channel elements which are defined by erosive surfaces above which foresets dip unidirectionally and beds fine upward from basal conglomerates into coarse- to fine-grained sand. Within major channel elements, Wizevich (1992) discriminated between Type 1 and Type 2 downflow-accretion elements. Type 1 downflow-accretion elements are mainly defined by basal thin-bedded conglomerates and large-scale planar or tangential cross-beds with small- and medium-scale cross-beds capping these 5-10 m sequences. These descriptions match well with those outlined for beds of Lithofacies E18 at Pound Gap. Following Wizevich (1992), we interpret that thin conglomerates represent

channel-floor deposits, planar cross-strata were deposited in lower flow velocities in broader, constricted areas of the channel, large-scale, long-bottomset tangential cross-strata were deposited in higher flow velocities in the areas of maximum channel velocity (Jopling, 1965), and small- and medium-scale cross-stratified bedforms represent macroform top deposits on migrating dunes in a deep, low-sinuosity, bed load-dominated fluvial channels. Type 2 downflow-accretion elements are primarily composed of giant tangential cross-strata interpreted as 7-8 m thick foresets up to 25 m long deposited in high-velocity channel-fill dunes (Wizevich, 1992). Type 2 downflow accretion elements were not observed at Pound Gap.

A fluvial depositional system interpretation for Lithofacies E18 is further supported by the absence of marine fossils and the presence of in situ coalified trees. Whereas Wizevich (1992) inferred a single-channel braid complex for the Lee Formation, this interpretation was mostly based on unimodal paleocurrent data. At Pound Gap, our paleocurrent data suggest that channels were highly sinuous and varied ~270° from their mean flow azimuth toward 248°.

2.4 Pikeville Formation

The Middle Pennsylvanian Pikeville Formation has been eroded from the hanging wall stratigraphy of the Pine Mountain thrust sheet exposed at Pound Gap and is thus not included in the lithofacies descriptions documented in this study. However, this unit is included in this study in order to understand the depositional and provenance record of the central Appalachian foreland basin system through the Middle Pennsylvanian time. An exposure of the Pikeville Formation in the footwall of the Pine Mountain thrust sheet (Fig. 2.1) is characterized by 12-30+ m thick, laterally continuous sequences of scour-based, compositionally immature (muscovite-rich) sandstone beds (7-30+ m thick) containing pebbles lags of sideritized mud intraclasts and abundant carbonaceous plant matter, including lycopsid casts of *Stigmaria* roots and *Lepidodendron* tree fragments (Appendix A). These medium sublithic sandstone beds transition sharply upward to carbonaceous shale, coal, and siltstone. Similar sequences of the Pikeville Formation

described in the central Appalachian basin have been interpreted to reflect deposition in fluvial to estuarine depositional environments (e.g., Aitken and Flint, 1994; Greb and Chesnut, 1996; Greb and Martino, 2005) that were present outboard (foreward) of those preserved in the Pine Mountain thrust sheet. Paleocurrent measurements taken from trough cross-strata in undeformed sandstone beds along U.S. Route 23 north of Pound Gap suggest that these rivers flowed west-northwestward toward an azimuth of 285° (Appendix A).

2.5 Detrital Zircon Geochronology

2.5.1 Detrital Zircon Preparation and Analysis

Samples of the units analyzed as part of this study were collected from along the Highway 23 road exposure, washed to prevent contaminants from affecting the integrity of the study, and sent to the Arizona LaserChron Center (ALC) for detrital zircon separation and preparation following the methods of Gehrels et al. (2011) and software of Gehrels et al. (2006) and Ludwig (2003) available on the ALC's website. Detrital zircons were then analyzed by LA-MC-ICP-MS using a New Wave UP193HE laser with a 30-μm spot size for all zircons in samples of the Pennington Formation and Warren-Point/Sewanee Sandstone, a 20-μm spot size for all zircons in samples of the Grainger Formation due to their finer grain size, and a 30-μm spot size for all zircons of the Pikeville Formation. Two R33 (Black et al., 2004) and five Sri Lanka (Gehrels et al., 2008) large zircons of known ID-TIMS ages [419.3 ± 0.4 Ma and 563.5 ± 2.3 Ma (2σ), respectively] were ablated prior to and after each run of 105 zircon analyses for each sample, with one Sri Lanka zircon ablated after every five unknown zircons, to monitor the accuracy of the system and to ensure the fidelity of data collected as part of this study. Zircon cores were chosen for laser ablation utilizing back-scattered electron (BSE) images in order to acquire ages faithful to each zircon's initial cooling age rather than later overprinting manifested in metamorphic rims. Isotopic measurements for ^{238}U, ^{232}Th, ^{208}Pb, and ^{206}Pb were made using Faraday detectors, with ^{204}Pb measurements made using an ion-counting Channeltron, in static mode.

Collected data was then reviewed for quality control using cutoffs recommended by the ALC, whereby zircons with >10% error for $^{206}Pb/^{238}U$ and $^{206}Pb/^{207}Pb$, >30% discordance, and >5% reverse discordance were not included in the study. Zircon ages younger than 900 Ma were calculated from $^{206}Pb/^{238}U$, whereas older zircon ages were calculated from $^{206}Pb/^{207}Pb$ ages. Peak ages were identified for our new data and for data from previous published studies for comparison (Fig. 2.13) by the Age Pick program of Gehrels and others (2006) which selects overlapping age ranges within 2-sigma error from at least three grains to objectively produce a robust peak age.

2.5.2 Detrital Zircon U-Pb Age Data

Histograms for each of the sandstone samples collected and analyzed for their detrital zircon U-Pb age spectra are presented in Figure 2.10 and are discussed below. Peak ages from each sample are italicized above each histogram and are compared in the regional deposystem discussion (Fig. 2.13) to peak ages from other studies' Appalachian foreland basin sandstone samples analyzed for detrital zircon U-Pb ages. The provenance of a detrital zircon is determined when its calculated U-Pb age overlaps with the bracketed cooling age history of a particular geochronologic province determined from previous studies. Geochronologic province age ranges utilized in this study are the same as those used and compiled by Park et al. (2010) and include the Superior (2700-2800 Ma), Trans-Amazonian/Eburnean (1900-2250 Ma), Trans-Hudson/Penokean ("Mid-Continent", 1800-1900 Ma), Yavapai/Mazatzal, ("Central Plains", 1600-1800), Granite-Rhyolite (1300-1400 Ma), Grenville (900-1300 Ma), Pan-African/Brasiliano (500-700 Ma), and Paleozoic (350-500 Ma) provinces (see references in Park et al., 2010).

The Lower Mississippian Grainger Formation (012812PR-03, n=101) contains detrital zircons derived from the Superior (0.99%), Trans-Amazonian/Eburnean (4.95%), Mid-Continent (2.97%), Central Plains (2.97%), Granite-Rhyolite (13.86%), Grenville (51.49%), Pan-African/Brasiliano (4.95%), and Paleozoic (14.85%) provinces, with 2.97% derived from unknown sources. These modalities are represented with respect to source terranes in pie-diagrams in Figure 2.10. The Grainger Formation is characterized

by age peaks of 456, 473, 821, 1034, 1206, 1218, 1317, 1353, 1457, 1488, and 1685 Ma calculated from detrital zircon age data.

The Upper Mississippian Pennington Formation (012812PR-04, n=90) contains detrital zircons derived from the Superior (3.33%), Trans-Amazonian/Eburnean (1.11%), Mid-Continent (1.11%), Central Plains (7.78%), Granite-Rhyolite (7.78%), Grenville (58.89%), Pan-African/Brasiliano (2.22%), and Paleozoic (13.33%) provinces, with 4.44% derived from unknown sources. These modalities are represented with respect to source terranes in pie-diagrams in Figure 2.10. Sandstone sampled from the Pennington Formation is characterized by age peaks of 391, 430, 1087, 1113, 1231, 1331, 1400, 1505, 1540, 1634, and 1738 Ma calculated from detrital zircon age data.

The Lower Pennsylvanian Warren Point/Sewanee Formation (012812PR-05, n=98) contains detrital zircons derived from the Superior (7.14%), Trans-Amazonian/Eburnean (1.02%), Mid-Continent (2.04%), Central Plains (17.35%), Granite-Rhyolite (12.24%), Grenville (43.88%), and Paleozoic (11.22%) provinces, with 5.1% derived from unknown sources. These modalities are represented with respect to source terranes in pie-diagrams in Figure 2.10. Sandstone sampled from the undivided Warren Point/Sewanee Formation include age peaks of 415, 435, 996, 1016, 1055, 1124, 1055, 1124, 1155, 1244, 1299, 1388, 1472, 1510, 1538, 1641, 1669, 1757, 1789, 2643, and 2730 Ma calculated from detrital zircon age data.

The Middle Pennsylvanian Pikeville Formation (021112PR-02, n=110) contains detrital zircons derived from the Granite-Rhyolite (6.36%), Grenville (83.64%), Pan-African/Brasiliano (4.55%), and Paleozoic (2.73%) provinces, with 2.73% derived from unknown sources. These modalities are represented with respect to source terranes in pie-diagrams in Figure 2.10. Sandstone sampled from the Pikeville Formation include age peaks of 391, 430, 1087, 1113, 1231, 1331, 1400, 1505, 1540, 1634, and 1738 Ma calculated from detrital zircon age data.

Detrital zircon U-Pb age spectra and age peaks are discussed below in the context of regional sediment dispersal trends and provenance evolution in the central Appalachian basin as they evolved through from Early Mississippian to Middle Pennsylvanian time. Paleocurrent data from this study and detrital zircon geochronologic data interpreted from other studies in the Appalachian foreland basin are also utilized to understand the basin's evolution in response to tectonic activity and quiescence along the Appalachian orogen.

2.6 Discussion

2.6.1 Depositional systems

Here, we discuss the depositional evolution between individual systems interpreted from the documented lithofacies measured from the base to the top of the exposed section. Collectively, the facies associations documented at Pound Gap represent a general up-section change from deep marine, to carbonate bank, to tidal, to fluvial depositional systems in the Appalachian foreland basin from Late Devonian through Early Pennsylvanian time. The interpreted local depositional systems are outlined in Table 2.1.

The base of the measured section a progradational clastic sequence dominated by a Late Devonian deepwater lithofacies shallowing upward to shallow-marine, peritidal evaporite, shale, and siltstone beds of FA-A (meters 0-117, Figs. 2.4 and 2.5). Within this sequence, storm-dominated subaqueous deltaic and shallow marine to peritidal, fine-grained clastic and evaporite strata prograde over unconfined submarine fan lobe and underlying bathyal prodelta strata deposited in alternating dysaerobic to anaerobic water conditions. This gradual transition from deep to shallow marine environments in this basal sequence of FA-A lacks both the discontinuous, coarse-grained, channelized, or slumped deposits typical of slope environments in detached shelf-margin deltaic complexes (*sensu* Mutti, 1992), which is an important piece of evidence that would help support a foreland basin depositional system for this sequence without previously established regional deposystem context. Paleocurrent data from groove casts (Fig. 2.4) indicate a west-northwestward dipping foreland ramp during Early Mississippian time. At Pound Gap, this initial package up to meter 117 in the measured section corresponds to

the Ohio Shale, Berea Sandstone and Bedford Shale (undivided), Sunbury Shale, and Grainger Formation (Fig. 2.4).

Shallow marine conditions prevailed into Middle Mississippian time but were met by a transition from clastic to carbonate deposition in tropical waters. This transgressive carbonate bank system transitioned from restricted to open marine, peritidal to wave-dominated and shallow-marine environments (represented by lime mudstone and oolitic grainstone sheets described over meters 117-215, Fig. 2.4) to deeper marine conditions dominated by gravity-driven processes below storm-wave influence (represented by fossiliferous packstone and interbedded argillaceous limestone beds of FA-B capped by shale-dominated beds of FA-A described over meters 215-257, Fig. 2.4). Locally karstified horizons in the lime mudstone beds in the base of this carbonate bank sequence, such as the one containing framework-supported lenses of angular siltstone and evaporite cobbles preserved immediately above the first 117 m thick sequence of FA-A (Figs. 2.4 and 2.6b), were created when secondary waters infiltrated planes of weakness in lime mudstone and dissolved the carbonate mud. These waters may have been occasionally magnesium rich, creating the locally dolomitized limestone beds observed in this part of the measured section. Many of the lithofacies described in this study match those of Al-Tawil and Read (2003) from Mississippian carbonate strata of the Appalachian foreland in West Virginia, suggesting that this carbonate system was widespread. This carbonate bank sequence is separated in the stratigraphy of the Pine Mountain thrust sheet into the shaley and sandy Upper and mostly micritic Lower members of the Newman Limestone (Fig. 2.4) (Rice, 1973).

The uppermost section of this thick carbonate bank sequence is punctuated by intervals of clastic sediment of FA-A and FA-C (meters 257-292), marking the basinward development of a coastal deltaic complex and the end of carbonate production in the Appalachian foreland basin by Late Mississippian time. A succession dominated by paleosols and shale with thin intervals of articulated brachiopod packstone beds, calcareous sandstone beds with brachiopods and desiccation cracks, and tidally

influenced sandstone beds (meters 281-292, Fig. 2.4) interpreted here as lagoonal to tidal flat and tidal creek deposits are similar to descriptions made by Horne and Ferm (1978), interpreted by the authors as lagoonal through back-barrier deposits, from along strike in the Appalachian foreland. This shallowing upward transition from carbonate to clay-rich beds is succeeded by quartz sand-dominated beds of FA-C which contain reworked sediment deposited in higher energy conditions heavily influenced by tidal processes. Tidal influence during deposition of these compositionally and texturally mature sandstone beds is documented by such bedforms as symmetrical ripple cross-laminae, rhythmically thickening and thinning tidal bundles, flaser- to lenticular heterolithic strata, and inclined heterolithic strata (Fig. 2.7). Paleocurrent indicators from tidal creek and distributary channel deposits of trough and planar cross-stratified sandstone (meters 295-296, 498-502, 510-513, Fig. 2.4) suggest a gradual transition from southwestward to southeastward to eastward tidal currents through time. Alternatively, distributary channel sandstone beds may have been deposited in the meandering section the "straight"-meandering-"straight" channel morphology observed universally in tidal estuaries (Dalrymple, 1992), which would suggest that the "straight" portions that comprise most of the channel system would have flowed north to south into the basin. As previously discussed, whether these paleocurrent directions correspond to flood-tide, ebb-tide, or longshore sediment transport directions is unknown and requires consideration of these lithofacies in the context of regional foreland basin system development established in previous studies. Similarly, little can be said of the northeastward- to southeastward-migrating point bars interpreted from discontinuous lateral accretion horizons (meters 315-327) without their consideration in the context of regional drainage patterns.

Lower and upper delta plain strata of FA-C and FA-D dominate the upper half of the section measured at Pound Gap (meters 295-560) and reflect further coastal regression from marine to fluviatile depositional realms within a deltaic complex; packages of tidally influenced deltaic sandstone to shale beds of FA-C are interbedded with and become subordinate upsection to meandering channel, overbank, and lacustrine to floodplain sandstone, siltstone, soily mudstone beds interpreted as paleosols, and shale

beds of fluviatile upper delta plain packages of FA-D. The 35 meters of missing section near the base of this transition (meters 379-414) likely represents an eroded sequence of rheologically weak mudstone and/or paleosol beds of FA-D, but is not included in the discussion for this facies association. A sequence of shallow-marine, fossiliferous packstone storm deposits of FA-B punctuate lowermost fine-grained delta plain strata (meters 430-441) and preserve a brief marine transgression which perhaps reflects a period of increased basin subsidence. This transgression is immediately followed by regressive fine-grained paleosols and shale of FA-C and lesser shale of FA-A interpreted by others as incised valley fill deposits (Boyd et al., 2006; Kahmann-Robinson, 2008).

The combined interpreted lithofacies of FA-D indicate that this Late Mississippian upper delta plain hosted distributary channels which meandered through vegetated floodplains outside of tidal influence. Tidal processes which reworked sediment in the adjacent lower delta plain were out of range in this system, resulting in dominantly fluvial bedforms in sublithic sandstone. Paleocurrent measurements from trough cross-stratified, sublithic, fluvial sandstone near the top of the upper delta plain sequence indicate flow was directed westward toward into the foreland. Brackish marine waters periodically inundated fluvial channels, floodplains, and later coastal marshes preserved in the uppermost calcareous sandstone, paleosols, and carbonaceous shale beds of FA-D. The stratigraphy described from meters 281-560 in the measured section, dominated by lower and upper delta plain deposits of FA-C and FA-D, are ascribed to the Upper Mississippian Pennington Formation (Fig. 2.4).

The contact between uppermost carbonaceous shale beds of FA-D and basal planar cross-stratified conglomeratic sandstone beds of FA-E is unconformable and characterized by irregular, scouring sandstone over bleached shale. Alternating thick- and thin-bedded packages are comprised of compositionally and texturally mature quartz sandstone preserved in lower flow regime bedforms (dominantly planar cross-stratified sandstone with tangential bottomsets) of interpreted fluvial origin and are separated by scouring, channelized contacts (Fig. 2.9). These beds mark the development of a broad, braided

river system in which large, two-dimensional sand dunes migrated southwestward in Early Pennsylvanian time (Fig. 2.4). The wide range of paleocurrent directions suggests that these were highly anastomosing channels. Alternatively, this paleocurrent distribution may reflect a dominantly southwestward regional paleoslope temporarily affected by tectonic downwarping of the basin during the early stages of the Alleghanian orogeny, consistent with penecontemporaneous submergence of the Cincinnati Arch to the northwest (e.g., Ettensohn, 2005), during which periods sediment dispersal was toward the northwest. Sandstone beds of FA-E correspond to the undivided Warren Point/Sewanee Formation previously described by Rice (1973) in the Pine Mountain thrust sheet stratigraphy as the Lower Pennsylvanian Lee Formation.

2.6.2 Provenance and sediment transport

Detrital zircon U-Pb age signatures, peaks, and inferred provenance are compared between samples in this study (Fig. 2.10) and age peaks calculated from other Appalachian foreland basin sandstones analyzed for detrital zircon U-Pb ages in other studies (Fig. 2.13). Detrital zircons analyzed from the Lower Mississippian Grainger Formation are characterized by a broad distribution in U-Pb ages, from which we infer provenance from several source terranes, especially those along eastern Laurentia (Pan-African/Brasiliano, Paleozoic, Grenville, Granite-Rhyolite, and Superior provinces). This distribution suggests that detritus received in this part of the foreland basin was sourced from mainly eastern source terranes or older basins uplifted and exposed during the final stages of the Acadian-Neoacadian orogeny.

Sandstone sampled from the lower Pennington Formation displays similar U-Pb age spectra to that of the Grainger Formation in this study, suggesting that the Late Mississippian lower delta plain received a diversely sourced contribution of sediment as it prograded basinward, effectively shutting off carbonate production in the central Appalachian foreland basin in response to the earliest stages of the Alleghanian orogeny along eastern Laurentia.

Although broadly similar to those of the Grainger and Pennington Formations, the U-Pb age signature of the Lower Pennsylvanian Warren Point/Sewanee Formation sandstone sampled at Pound Gap is unique in that less than half of the grains analyzed have ages associated with the Grenville province: the Central Plains, Granite-Rhyolite, and Paleozoic source terranes are well-represented, with additional age peaks correlated with the Superior province of the Canadian Shield. This age signature may suggest that Grenville source terranes were either buried by clastic wedges generated during the early Alleghanian orogeny, which seems unlikely given that these source terranes should have been uplifted during continental collision during this orogeny, or that Paleozoic and Granite-Rhyolite source terranes were uplifted and contributed more sediment in Early Pennsylvanian time than they had to previous clastic wedges in the central Appalachian basin. Regarding the relative abundance of U-Pb ages of Central Plains provincial affinity, it seems unlikely that river systems would have transported sediment directly sourced from uplifted regions in the Central Plains province given the likely topographic barrier presented by a forebulge uplifted during the early stages of the Alleghanian orogeny. These ages cannot be explained by uplift along eastern Laurentia unless they were previously concentrated in older sedimentary basins uplifted during the Alleghanian orogeny.

Detrital zircons analyzed from the Middle Pennsylvanian Pikeville Formation are characterized by age peaks predominantly associated with Grenville source terranes with notable absence of ages associated with Paleozoic, Central Plains, Mid-Continent, Trans-Amazonian/Eburnean, and Superior provinces. This signature is unique to the Pikeville Formation sandstone in this study and may suggest that many source terranes either were buried by clastic wedges generated during the early stages of the Alleghanian orogeny, sourced insignificant detritus in comparison to hinterward east Laurentian sources (Grenville, Granite-Rhyolite, and Pan-African/Brasiliano provinces) uplifted during the early stages of the Alleghanian orogeny, or are poorly represented in the Pikeville Formation due to a combination of these two processes.

Collectively, the detrital zircon signatures of sandstone samples collected from Pound Gap demonstrate contribution of detritus from a wide variety of source terranes in Early Mississippian through Lower Pennsylvanian clastic wedges, whereas Middle Pennsylvanian sandstones received a limited contribution of detritus from hinterward sources. Whether detrital zircons in each sandstone analyzed in this study were primarily sourced, or sourced directly from an exposed igneous province, is contestable. As an alternative to the provenance interpretations provided above, the wide range of U-Pb age populations represented in each sample are probably best explained in part by sediment recycling in the Appalachian basin, a hypothesis initially presented by Eriksson et al. (2004) and Thomas et al. (2004) for Alleghanian clastic wedge sandstone provenance. Support for sediment recycling in the basin was provided by Park et al. (2010), who suggested at least two cycles of Grenville zircon recycling are preserved in the Taconic through Alleghanian Appalachian foreland strata. This study does not hope to delineate the relative contributions of primary versus recycled detritus contributed to the central Appalachian basin but we acknowledge that each of these modes of sediment sourcing are viable. Here, we infer that it is more likely that the age signatures of the Grainger, Pennington, and Lee Formations reflect provenance from recycled basin strata generated during Cambrian passive margin development and ensuing Taconic foreland basin sedimentation in the Middle Ordovician to Silurian time. The strata that sourced each of these clastic stratigraphic units were then either uplifted and eroded during later orogenesis along the east Laurentian margin or were transported along strike of the basin after periods of exposure and erosion caused by eustatic fall.

2.6.3 Regional deposystem integration and tectonics

The depositional record interpreted for the central Appalachian foreland basin system draws from distinct lithofacies and facies associations documented in the Pine Mountain thrust sheet strata exposed at Pound Gap. The foreland basin system included (Stage 1) a Late Devonian-Early Mississippian submarine fan system (FA-A: Ohio Shale, Berea Sandstone, Bedford Shale, Sunbury Shale, and Grainger Formation) which transgressed from deep to shallow marine conditions, (Stage 2) an overlying Middle to Late

Mississippian, mainly regressive carbonate bank sequence (FA-B: Newman Limestone) deposited on a gradually subsiding outer foreland ramp which saw renewed siliciclastic influx in Late Mississippian time with the progradation of (Stage 3) a shallow marine to terrestrial clastic wedge characterized by tidally influenced marginal marine and delta plain environments (dominantly FA-C and FA-D: Pennington Formation), which is unconformably overlain by (Stage 4) channelized, cross-stratified quartzarenites (FA-E: Warren Point/Sewanee Formation) deposited in sinuous channels in a fluvial braid plain. A shift to immature and primarily east Laurentian-sourced Middle Pennsylvanian fluvial to estuarine delta plain strata of the Pikeville Formation (Stage 5) suggests significant influence by the building orogen to the southeast. The development of this broadly transgressive system is best considered in the context of regional deposystem and provenance trends and concurrent tectonic stages established in previous studies.

Age peak distributions are considered in the context of local paleocurrent trends and regional sedimentary dispersal trends to infer changing basinal drainage patters in response to crustal dynamics in the Appalachian foreland basin system during the final stages of Acadian-Neoacadian arc accretion through the initial stages of continental collision during the Alleghanian orogeny along the east Laurentian craton. Paleogeographic reconstructions for the central Appalachian basin are presented in this discussion utilizing local the deposystems documented in this study (roughly palinspastically restored in Figures 2.11, 2.12, 2.14, and 2.15) with the foreland basin deposystem model defined by DeCelles and Giles (1996). In this model, strata is deposited in the wedgetop depozone above active thrust sheets, the foredeep depozone between the structural front of the active fold and thrust belt and the relatively uplifted forebulge, the forebulge depozone where flexural uplift characterizes a broad area of low sediment accumulation and unconformity development, or the back-bulge depozone where flexural subsidence creates a broad and shallow area for sediment accumulation cratonward of the forebulge (DeCelles and Giles, 1996). The Cincinnati Arch has been classically regarded as long-lived structural high modeled as the uplifted forebulge (e.g., Quinlan and Beaumont, 1984) with debates revolving around whether the structure was

static (uplifting only vertically; e.g., Pope et al., 2009) or mobile (moving orthogonal to the orogen in response to tectonic loading; e.g., Quinlan and Beaumont, 1984). In the discussion below, the Cincinnati Arch is considered as a mobile feature during periods of differential tectonic loading in the Paleozoic, and shallowing- and deepening-upward sequences reflect changes in flexural subsidence in the foreland basin system rather than basin sedimentation outpacing subsidence.

2.6.3.1 Stage I – Late Devonian through Early Mississippian Acadian-Neoacadian foreland basin system

During Late Devonian time, Acadian-Neoacadian subsidence in the cratonic Appalachian foreland basin created deep water conditions in which deposition of five cycles of basinal black shale preceded successive clastic wedges which migrated axially and cratonward (e.g., Miller, 1973; Ettensohn, 1985; Ettensohn, 2008). Late Devonian to Early Mississippian uplift of the Virginia Promontory and the northeast Laurentian margin during docking of the Avalon-Carolina terrane (summarized in Hatcher, 2005) resulted in basinal downwarping outpacing sedimentation of the Ohio Shale, deep-water anaerobic conditions in the foredeep depozone which may have been between 39-375 m deep (Woodrow and Isley, 1983) or potentially up to 900 m deep in parts of the basin (Lundegard et al., 1980), and a transition from westward- to broadly southwestward-dipping foreland axis paleoslope (Fig. 2.11) (Ettensohn, 1985, 1987). Uplift along the New York promontory to the northeast during Acadian-Neoacadian arc collision sourced the extensive Devonian Catskill delta complex, which was in turn reworked during a eustatic lowstand to partly source the southwestwardly (axially) prograding uppermost Devonian Bedford-Berea subaqueous delta complex (Fig. 2.11) (Meckel, 1970; Pashin and Ettensohn, 1995). The Lower Mississippian Price-Pocono and Borden-Grainger delta complexes represent the terrestrial and subaqueous parts of a northwestward-prograding clastic wedge which emanated from the uplifted orogen to the east and prograded over the Bedford-Berea delta complex (Fig. 2.12) (e.g., Pepper et al., 1954; Kepferle, 1977; Rice, 1984; Ettensohn and Chesnut, 1985; Hatcher et al., 1989; Pashin and Ettensohn,

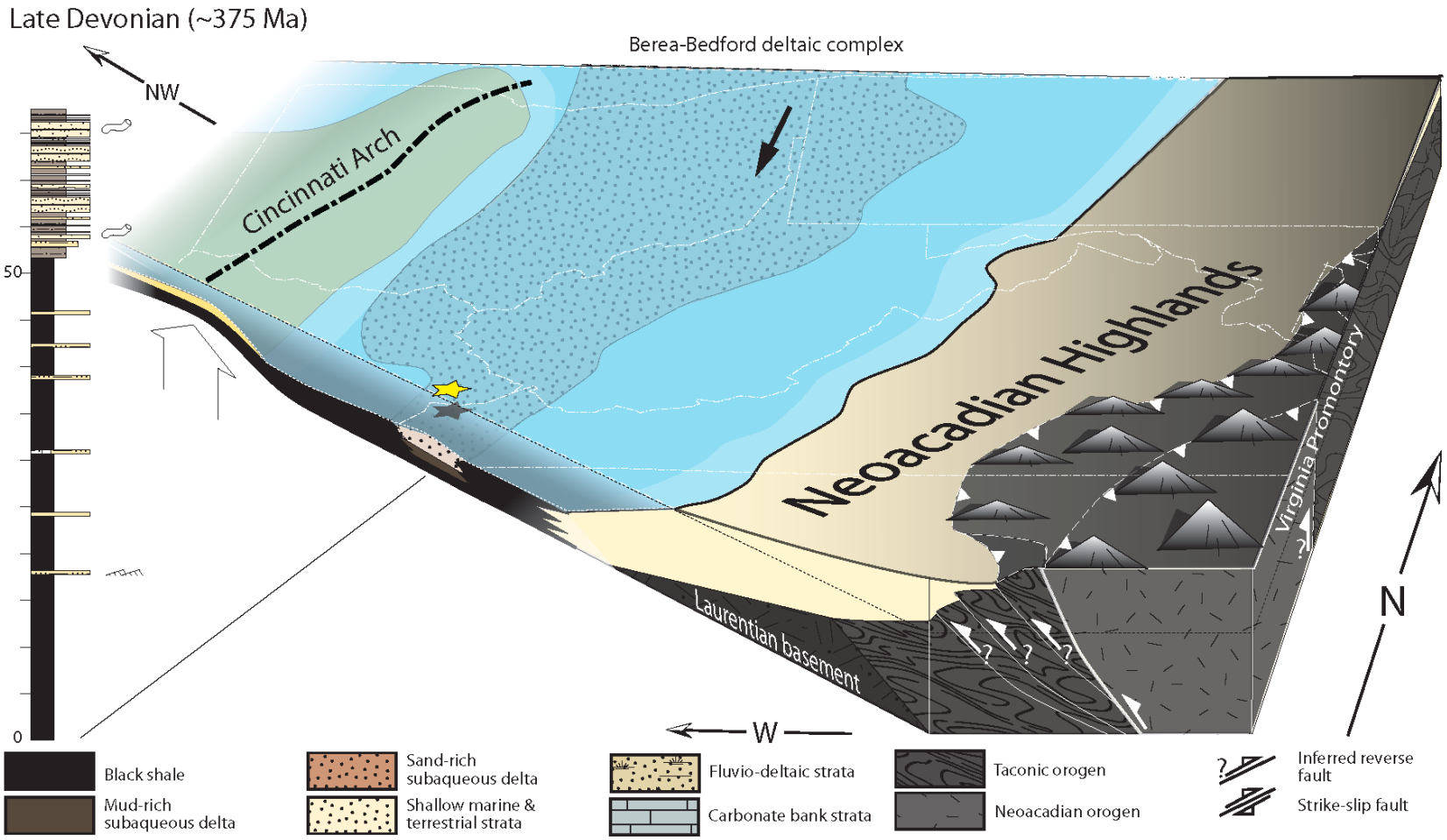

Figure 2.11: Late Devonian paleogeographic reconstruction for the central Appalachian foreland basin system. Late stages of the Acadian-Neoacadian orogeny to the east are synchronous with black shale deposition in an overdeepening foredeep, uplift of the forebulge (arrow beneath Cincinnati Arch; Ettensohn and Elam, 1985), and southwestward progradation of the Berea-Bedford subaqueous deltaic complex (after Ettensohn, 2004). Paleocurrent direction (solid black arrow) from Meckel (1970). Star corresponds to roughly palinspastically restored location of strata exposed in the Pine Mountain thrust sheet currently exposed at Pound Gap. Measured section comprises lower lithofacies of FA-A at Pound Gap. Approximate geomorphology after studies compiled by Blakey (2013).

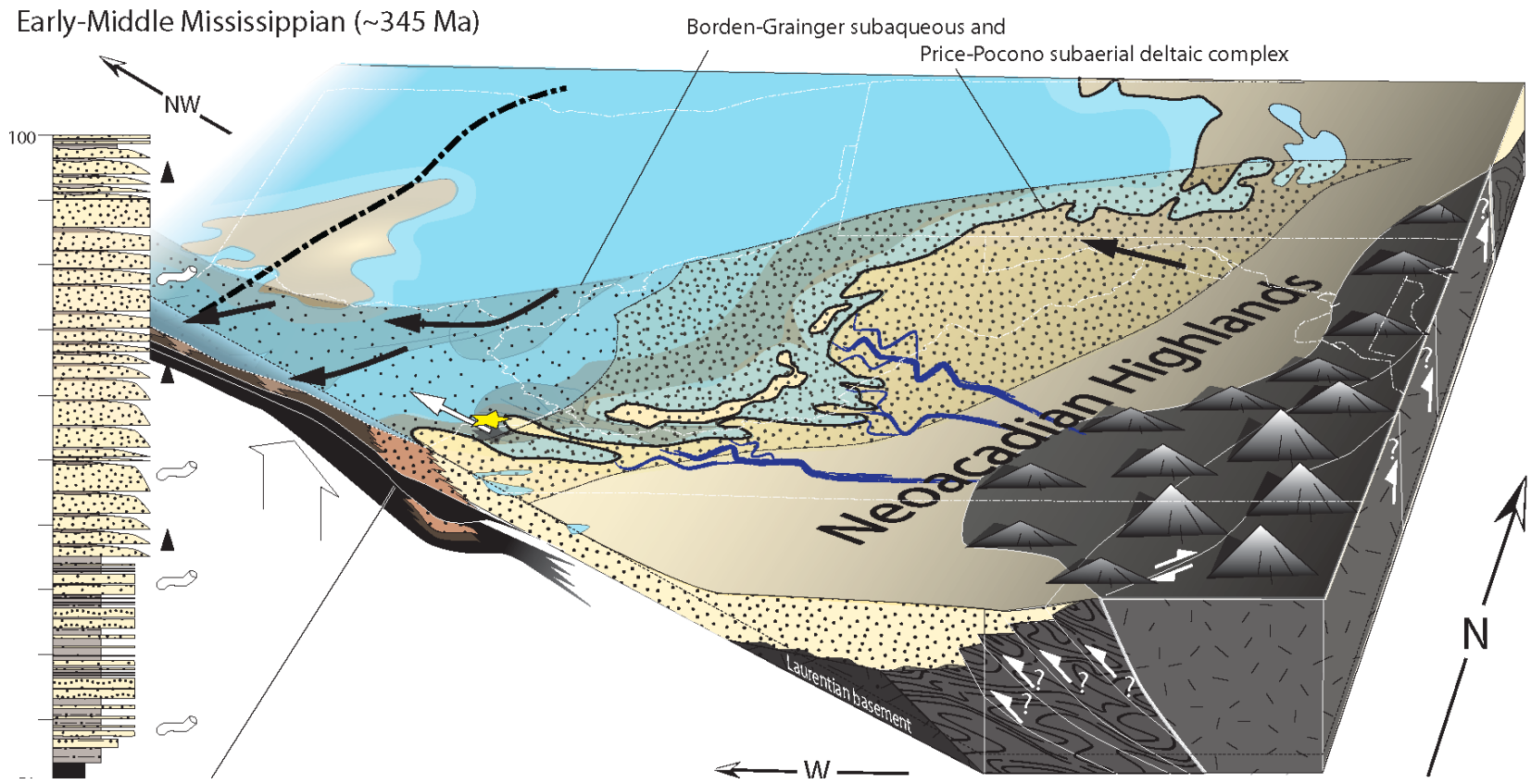

Figure 2.12: Early to Middle Mississippian paleogeographic reconstruction for the central Appalachian foreland basin system. Final stages of the Acadian- Neoacadian orogeny to the east sourced recycled clastic detritus to northwestward-prograding clastic deltaic complex, preserved in submarine fan deposits of the Grainger Formation at Pound Gap (star). Groove cast data from this study indicate west-northwestward flowing turbidity currents (white arrow). Measured section to left illustrates sand-rich outer fan lobe lithofacies of FA-A at Pound Gap. Paleocurrent directions (solid black arrows), Borden submarine fans, and river systems after Kepferle (1977). Hinterward forebulge migration from Ettensohn (1994). Approximate geomorphology after studies compiled by Blakey (2013). Clastic wedge boundaries depicted after Ettensohn (2004). See Figure 2.11 for key.

1995; Ettensohn, 2004). West-northwestward paleocurrent directions indicated from groove casts in the Lower Mississippian Grainger Formation of this study are consistent with the northwestward-prograding trend of the Borden-Grainger delta complex and record turbid gravity flows transporting sediment from the proximal foreland toward the basin's axis.

The mainly east Laurentian, likely recycled sediment provenance inferred from the detrital zircon U-Pb age spectra for the Grainger Formation analyzed in this study is concurrent with the eastern-derived, northwestward-prograding subaqueous delta complex described here and in previous studies for the Appalachian foreland basin. Age-equivalent samples of the Lower Mississippian Grainger Formation have been analyzed as part of a detrital zircon provenance study by Park et al. (2010) in the central and southern Appalachian foreland basin and include the Price and Grainger Formations (Fig. 2.13). Except for Pan-African peak ages and single grain U-Pb ages from detrital zircons, the U-Pb age signature reported in the Grainger Formation sampled at Pound Gap otherwise closely resembles those reported by Park et al. (2010), suggesting regionally consistent provenance and sediment dispersal patterns in separate deltaic complexes feeding the central and southern Appalachian foreland basins. The dominance of eastern source terrane signatures in diverse detrital zircon age spectra and age peaks in the Grainger Formation are consistent with interpretations of a southwestward-younging Acadian-Neoacadian clastic wedge (Catskill, Bedford-Berea, Price-Pocono, and Borden-Grainger delta complexes; Ettensohn, 2004) derived from the eastern Acadian-Neoacadian tectonic belts and Virginia promontory (Ettensohn and Chesnut, 1985) and more northeastern sources in New England and Canada (Rice, 1984). Alternatively, this "recycled" provenance signature may reflect sediment sourcing from older foreland basin strata uplifted during the late Acadian-Neoacadian orogeny.

In the central Appalachian basin, the Borden and Grainger Formations reflect the distal, subaqueous parts of an Early Mississippian delta complex (Ettensohn, 2004) or probably two separate delta complexes (Grabowski, 1986) which extended into the adjacent

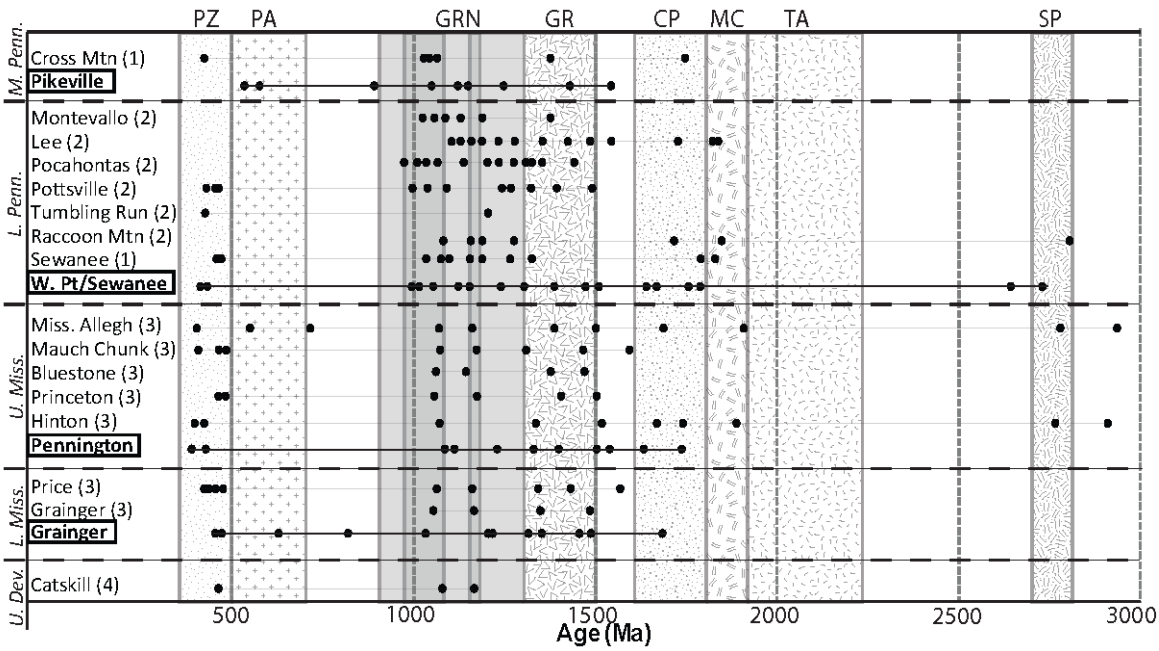

Figure 2.13: Age peak distribution plots for Carboniferous sandstones in the Appalachian basin. Samples included in this study are boxed. Other samples analyzed for detrital zircon U-Pb ages include (1) Thomas et al., 2004; (2) Becker et al., 2005; (3) Park et al., 2010; (4) McLennan et al., 2001. Age peaks of "Miss. Allegh (3)" represent all Mississippian Alleghanian clastic wedge sandstones analyzed by Park et al. (2010). Note abundance of Grenville-aged age peaks in Lower Pennsylvanian sandstone samples, likely recording uplift of Laurentian basement along the Alleghanian hinterland.

Illinois basin (Fig. 2.12). Delta front deposits of the Grainger Formation transition gradually to peritidal red shale and evaporites of the upper Grainger Formation (Fig. 2.5b) (e.g., Udgata, 2011) directly below the overlying carbonate bank limestones of the Newman Limestone, a transgression that temporally correlates to a major shift from long-term dry, subhumid conditions in mid-latitudes to humid climatic conditions in subtropical latitudes (Cecil et al., 2004; Blakey, 2008; Ettensohn, 2008). By Middle Mississippian time, these widespread deltaic complexes loaded the foreland basin and caused an eastward migration of the peripheral bulge (Fig. 2.12) (Ettensohn, 1994; Ettensohn et al., 2012). These fine-grained peritidal beds have been correlated across the basin and reflect deposition on and along the margins of the forebulge of the foreland basin (Ettensohn, 2004; Ugata, 2011; Ettensohn et al., 2012). This observation, paired with west-northwestward-dipping paleoslopes into the foreland basin, suggests that peritidal clastic beds of the Grainger Formation (uppermost beds of Lithofacies A5) preserved at Pound Gap were deposited on the northwestern slopes of the forebulge

(frequently referred to in foreland basin studies as the 'peripheral bulge') which migrated parallel with the basin's axis eastward into Virginia, West Virginia, and Tennessee by Middle Mississippian time (Fig. 2.12) (Udgata, 2011; Lane and Dubar, 1983; Kepferle, 1977, Ettensohn, 1994). The karstified, irregular contact between the upper Grainger Formation and lower Newman Limestone described in this study (Fig. 2.5b) is a regionally extensive unconformity that records further eastward forebulge migration during unloading-type flexural relaxation (Ettensohn, 1994). This boundary at Pound Gap is particularly significant because it signifies post-Acadian-Neoacadian tectonism and lack of clastic influx during the transition to stable carbonate bank development on a gently subsiding outer foredeep ramp in a tectonically inactive foreland basin system.

2.6.3.2 Stage II—Middle through Late Mississippian tectonic quiescence and carbonate bank development

Many of the carbonate lithofacies described at Pound Gap (FA-B) have been observed along strike in the foreland basin and record deposition in shallow water conditions on a slowly subsiding, gently to-the-southeast-dipping ramp that lay just northwest of the thickness hinge line that separates the distal and proximal parts of the foreland basin (Al-Tawil and Read, 2003; Al-Tawil et al., 2003; Kelleher and Smosna, 1993). Peritidal and shallow marine carbonate lithofacies documented in the measured section (Figs. 2.4 and 2.6) contribute to the basin's record of tectonic quiescence which suggests that the foreland was covered in shallow, tropical waters of an epicontinental sea as the Laurentian craton migrated northward to equatorial latitudes in Middle Mississippian time (Scotese, 2003; Blakey, 2013). The basin was bounded to the northeast and east by the remnant Acadian highlands and adjacent alluvial plain, to the north by a low-lying landmass, and to the northwest and west by the uplifted Cincinnati Arch (Kelleher and Smosna, 1993). Oolitic grainstone to wackestone beds of Lithofacies B7 documented in this study at Pound Gap and by Al-Tawil and Read (2003) in southern West Virginia suggest that the tectonically inactive, distal foreland ramp was characterized by large, periodically exposed, migrating ooid and sand belts similar to those found in the modern

Bahaman banks (Johanson, 2000). Regional observations of these elongate belts indicate that they were oriented downdip to the southeast into the filling foreland, suggesting deposition on a tidally dominated shelf (Kelleher and Smosna, 1993; McKinney and Gault, 1980) on the outer foreland ramp of the foredeep depozone, onlapping the Cincinnati Arch to the northwest.

Widespread shallow- to open-marine carbonate mud (Lithofacies B6) and oolitic shoal (Lithofacies B7) development was limited by a shift to humid conditions in Late Mississippian time, causing a transition to an open marine, skeletal-dominated carbonate system (Lithofacies B11) (Ettensohn et al., 1988; Al-Tawil and Read, 2003). Though developed during a period of tectonic quiescence, this carbonate system's growth was locally limited by uplift along the Waverly Arch and Kentucky River fault system (Dever et al., 1977; Dever, 1980, 1999) associated with continued Middle Mississippian forebulge migration in response to unloading and erosion of the Acadian-Neoacadian highlands (Ettensohn, 2004).

Increasingly shaley to sandy carbonate strata described at Pound Gap (Lithofacies B9-11) are also documented along strike in the basin and record increasingly frequent pulses of clastic sediment which significantly limited carbonate production in the foreland and mark renewed tectonic loading and basinal subsidence (Chesnut, 1994; Chesnut, 1996; Ettensohn, 1994; Al-Tawil and Read, 2003). By Late Mississippian time, carbonate strata filled the basin, reaching up to 1200 m in thicknesses in the proximal foreland preserved in the fold and thrust belt of Virginia to the southeast (Nelson and Read, 1990) to achieve equilibrium with the adjacent beveled orogen to the east (Ettensohn, 1994).

2.6.3.3 Stage III—Late Mississippian early Alleghanian foreland basin system

Mixed clastic and carbonate strata observed in the Pennington Formation at Pound Gap record Late Mississippian progradation of the Pennington-Mauch Chunk clastic wedge (Cooper, 1948; Ettensohn and Chesnut, 1985), represented by the shallowing-upward

transition from deep, open marine skeletal turbidites to lagoonal carbonates (FA-B) of the Newman Limestone to tidally influenced lower delta plain strata (FA-C) (Figs. 2.7 and 2.14). This gradual regression has been described regionally for the Pennington Formation (e.g., Martin, 1975) and marks the earliest progradation of the "Alleghenian clastic wedge", a more encompassing term describing the most extensive of the Appalachian clastic wedges, into the rapidly subsiding foreland basin (Hatcher et al., 1989).

Sedimentation on the Late Mississippian east Laurentian craton was driven by a climatic shift to icehouse conditions, subsequent eustatic sea level change (Kahmann-Robinson, 2008), and Milankovitch long-term eccentricity forcing (Al-Tawil and Read, 2003), with lesser tectonic influence on deposition in the filled foreland basin (Kahmann-Robinson, 2008). However, the Alleghenian clastic wedge is widely believed to have been generated in response to uplift during the initial stages of the Alleghanian orogeny (Hatcher et al., 1989). Multiple lines of evidence supporting a Late Mississippian onset for the Alleghanian orogeny along the east Laurentian margin include syndepositional paleoseismites in southeastern West Virginia Late Mississippian thrust sheet strata equivalent to the lower Pennington Formation (Stewart et al., 2002; Bartholomew and Whitaker, 2010), coeval or immediately subsequent amphibolite-facies metamorphism, polyphase deformation, and plutonism along the east Laurentian margin (southern New England and Virginia to Alabama; see Hatcher, 2010), and a ca. 335-325 Ma thermal event in the Inner Piedmont to the southeast (Figs. 2.2 and 2.3) (Dennis and Wright, 1997; Dennis, 2007).

Late Mississippian deltas drained toward the northwest into the Appalachian foreland basin (Fig. 2.14) (e.g., Meckel, 1970; McKinney and Gault, 1980). Paleocurrent data from lower delta plain strata of the Pennington Formation (FA-C) suggest either that the gradual change from southwestward- to southeastward- to eastward-flowing tidal creeks and distributary channels reflects changing sediment transport directions, or, more likely, that southeastward and eastward paleocurrent directions in tidal creek and distributary

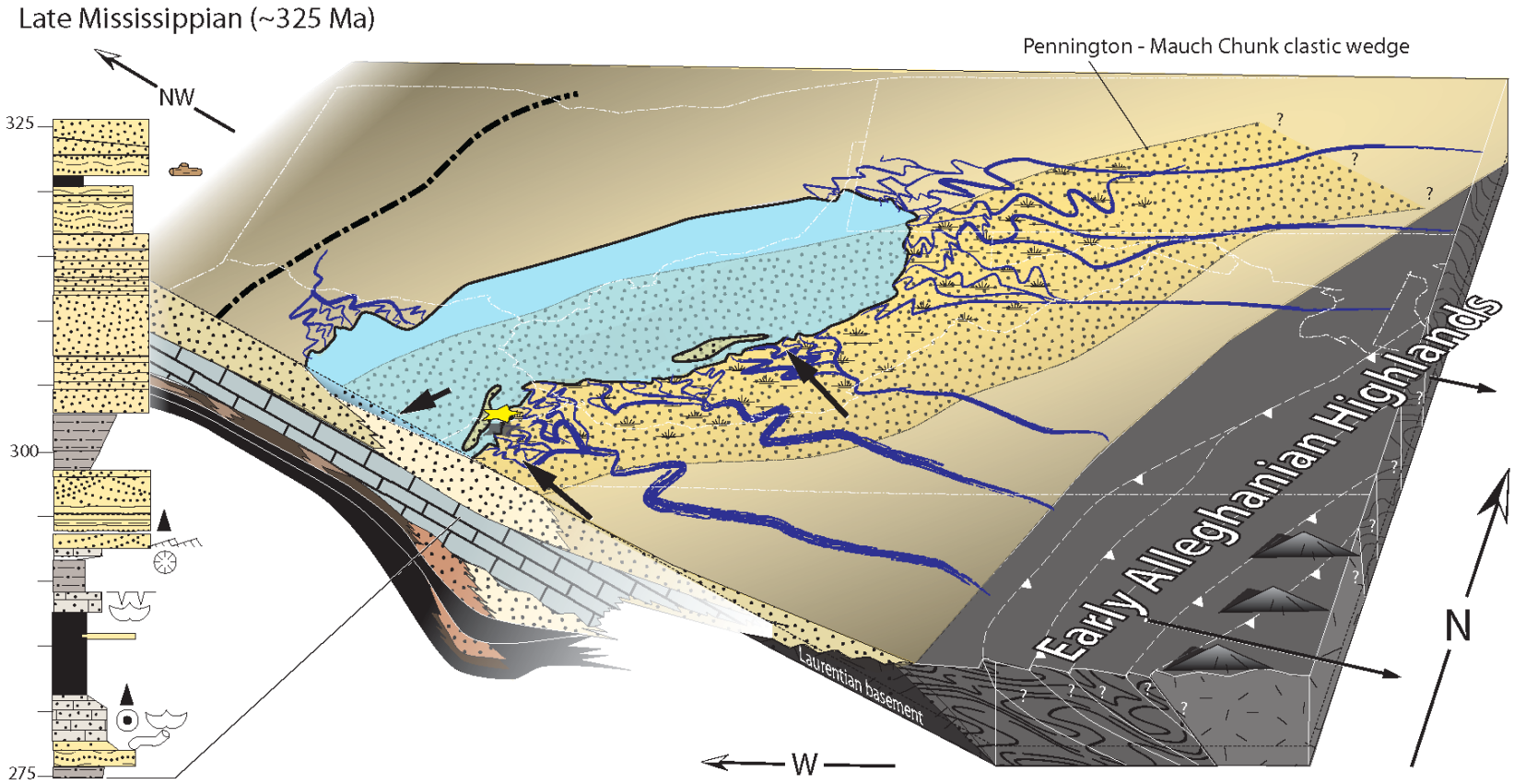

Figure 2.14: Late Mississippian paleogeographic reconstruction for the central Appalachian foreland basin system. Earliest stages of the Alleghanian orogeny to the east sourced recycled clastic detritus to a mixed carbonate and clastic deltaic complex prograding northwestward over Middle to Late Mississippian carbonate bank strata. This system is preserved in lower delta plain lithofacies of FA-C in the Pennington Formation and underlying FA-B lithofacies of the Newman Lime- stone at Pound Gap (star). Paleocurrent data from this study indicate a tidally influenced west-northwestward facing coastline. Measured section to left illustrates sand-rich lithofacies of FA-C and carbonate lithofacies of FA-B at Pound Gap. Paleocurrent directions (solid black arrows) after Meckel (1970) and Ettensohn and Chesnut (1985). River systems after McKinney and Gault (1980). Approximate geomorphology after studies compiled by Blakey (2008). Clastic wedge boundar- ies depicted after Ettensohn (2004). See Figure 2.11 for key.

channel deposits record the flood-tide direction, whereas southwestward paleocurrent indicators from lowermost tidal creek deposits would then correspond to longshore current directions parallel to the basin's axis. In the context of northwestward, transverse drainage, northeastward migrating point bars (FA-C) likely preserve northwestward flowing rather than southeastward flowing channels, whereas southeastward migrating point bars may record channel flow southwestward or northeastward, parallel to the axis of the foreland basin.

Alternatively, inferring a shift from southwestward to southeastward and eastward drainage in this deltaic system may carry implications of a locally northeast-southwest oriented coastline with a southeastward slope. However, many deltas are known for having semiradial sediment dispersal pattern or for having sinuous channels (see Dalrymple and Choi, 2007 for examples) whose flow directions may vary significantly from the mean flow direction in the delta; the channels in this portion of the delta plain may have flowed nearly perpendicularly to the net drainage direction of the delta. Whatever the case, the transition into dominantly floodplain, overbank, and meandering channel deposits of FA-D (Fig. 2.8) is accompanied by a shift to west-northwestward drainage preserved in uppermost meandering channel sandstone beds of the Pennington Formation at Pound Gap. The gradual shallowing-upward sequence and west-northwestward net sediment transport direction for fluvial channels of upper delta plain strata interpreted here is consistent with the northwestward drainage pattern and progradation of the Alleghenian clastic wedge observed in the deltaic systems stemming from the uplifted highlands to the southeast (Fig. 2.14) (McKinney and Gault, 1980; Hatcher et al., 1989). Paleosols at Pound Gap have been interpreted by Kahmann-Robinson (2008) to reflect deposition in alternating wet (poorly drained paleosols) and dry (well-drained paleosols) conditions in a progressively wetter climate through the Late Mississippian.

The broad contribution of mostly east Laurentian (and likely recycled) sediment sources interpreted from detrital zircon U-Pb age data observed from the lower Pennington

Formation sandstone analyzed in this study (Fig. 2.10) is concordant with an eastern origin of the Alleghanian clastic wedge in response to orogenesis along the eastern cratonic margin. Age-equivalent sandstones to the Pennington Formation sampled in the Appalachian basin have been analyzed in detrital zircon U-Pb age studies and include the Hinton, Mauch Chunk, Bluestone, and Princeton Formations sampled from the northern and central Appalachian basins (Fig. 2.13) (Park et al., 2010). Detrital zircon age peak distributions for these sandstones are similar, varying mostly in content of Mid-Continent, Central Plains, and Superior province associated age peaks. The detrital zircon grain age peak distributions reported from these sandstones are dominated by Paleozoic, Grenville, and Granite-Rhyolite age associations, which is consistent with the signature observed in the Pennington Formation of this study. The similar signatures observed across these upper Mississippian sandstones suggest that provenance and regional sediment distribution patterns were consistent across both the central and northern Appalachian basin. This observation is interpreted to reflect the relative homogeneity of the Late Mississippian Alleghenian clastic wedge, which was characterized by a semiradial, cratonward progradation pattern and a southwestward net sediment transport direction (Fig. 2.14) (see Hatcher et al., 1989; Ettensohn, 2004).

The progradational pattern of the mainly terrestrial Alleghenian clastic wedge and shallow nature of the foreland basin is attributed to a dispersed tectonic load imposed by the expansive advancing Alleghanian fold and thrust belt (Fig. 2.14) (e.g., Tankard, 1986; Ettensohn, 2004). Using the most recent chronostratigraphic ages for the Mississippian-Pennsylvanian boundary (Gradstein et al., 2012) and conodont biostratigraphy from the basal Pennington Formation (Collinson et al., 1971), deposition of mixed carbonate and siliciclastic strata of the Pennington Formation (dominated by FA-C and FA-D at Pound Gap) lasted as long as 12.8 Myr in coastal-plain to transitional-marine environments (e.g., Greb and Eble, 1998).

2.6.3.4 Stage IV—Early Pennsylvanian braided river system development

Widespread coastal floodplains, marshes, and meandering channel systems of the Late Mississippian upper delta plain (FA-D, Fig. 2.8) were brought to an end with widespread sea level fall and tectonic tilting and uplift along eastern Laurentia (Beaumont et al., 1987; Wizevich, 1993; Chesnut, 1992). This transition is marked by the Kaskaskia-Absoroka supersequence boundary (Sloss, 1963), over which regionally extensive, texturally and compositionally mature beds of quartzarenites of the central Appalachian Warren Point Formation (FA-E of this study, Fig. 2.9), often referred to as "Lee-type" sandstones in older literature, lie unconformably. Early Pennsylvanian time saw the development of a southwest-flowing, braided, fluvial river system (e.g., Miller, 1974; BeMent, 1976; Rice, 1984; Rice, 1985; Greb and Chesnut, 1996) in the central Appalachian basin (Fig. 2.15) that has been correlated widely across the Appalachian foreland basin stratigraphy and represents part of an Amazon-scale longitudinal drainage system stemming from northeastern Canada to the Ouachita basin of the southeastern U.S., straddling the uplifted forebulge (Cincinnati Arch) along the western margin of the Appalachian foreland basin (Archer and Greb, 1995). The variation in flow direction recorded in foresets of planar cross-strata in the Warren Point/Sewanee Formation in this study (FA-E) indicates that this was a braided rivers were highly sinuous and flowed in a net southwestward direction. Stratigraphically equivalent sandstones to conglomeratic, mostly planar cross-stratified quartzarenites described in this study (Fig. 2.9) contain recycled Paleozoic quartz sand and pebbles derived from Canada, were weathered in tropical climates (BeMent, 1976; Rice, 1984; Thomas et al., 2004), and interfinger eastward with sharply contrasting, lithic-rich sandstone, shale, and coal beds of the Breathitt Group (Figs. 2.2 and 2.15).

The combined contribution of paleocurrent measurements, lithofacies descriptions, and interpreted broad contribution of detrital zircon sources data from the Warren Point/Sewanee Formation interpreted here indicate northeastern sources, textural and compositional sediment reworking during long-distance transport or locally consistent hydraulic energies, and sourcing from mainly east Laurentian source terranes (Figs. 2.8

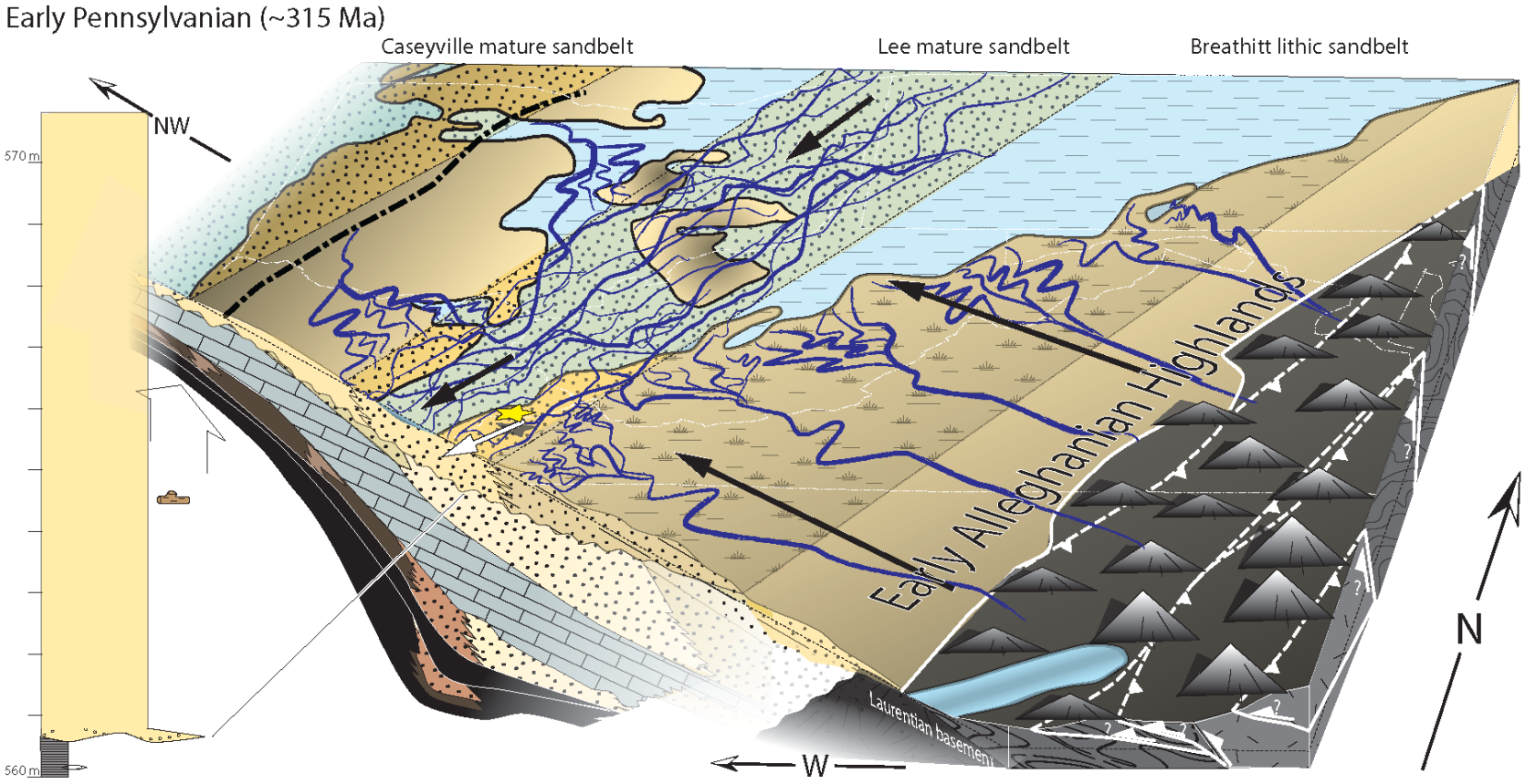

Figure 2.15: Early Pennsylvanian paleogeographic reconstruction for the central Appalachian foreland basin system. Alleghenian clastic wedge strata deposited in axial braid plain systems flowing southwest (FA-E of this study; white arrow) and in intertonguing, transverse fluvio-deltaic strata similar to that of the Pikeville Formation described in the footwall of the Pine Mountain thrust sheet at Pound Gap. Measured section to left illustrates Late Devonian through Early Pennsylva- nian strata exposed at Pound Gap (star). Paleocurrent directions (solid black arrows) from Meckel (1970). Forebulge uplift from Ettensohn (1994). Approximate geomorphology after studies compiled by Blakey (2013). Caseyville, Lee, and Breathitt sandbelts after Chesnut (1994). See Figure 2.11 for key.

and 2.10). This interpretation fits well into regional descriptions of an axial drainage system stemming from the Canadian Shield (Fig. 2.15) (e.g., Rice, 1984; Archer and Greb, 1995). The Early Pennsylvanian longitudinal river system would have received detritus from transverse drainage systems fed by source terranes adjacent to and along the east Laurentian margin. Several detrital zircon geochronologic studies have focused on age-equivalent sandstones in the Appalachian foreland basin, which have included the Tumbling Run Member of the Pottsville (Becker et al., 2005), the Pottsville, (Gray and Zeitler, 1997; Becker et al., 2005), and the Mauch Chunk (Park et al., 2010) Formations of the northern Appalachian basin, the Sewanee (Thomas et al., 2004), Lee, and Pocahontas (Becker et al., 2005) Formations of the central Appalachian basin, and two sandstones from the Montevallo coal zone of the Pottsville Formation and the Raccoon Mountain Formation in the southern Appalachian basin (Becker et al., 2005). These sandstones are consistently dominated by concentrated populations of Grenville and Granite-Rhyolite age peak signatures (Fig. 2.13), interpreted here as having sources in multiple terranes along strike of the foreland basin (including the Superior province). This matches well with interpretations from our and other studies' paleocurrent data which suggest an axial drainage system carrying sediment along strike of the basin toward the southwest (Fig. 2.14) (e.g., Miller, 1974; BeMent, 1976; Rice, 1984; Rice, 1985; Greb and Chesnut, 1996). Inconsistent distributions of peak ages sourced from other terranes (i.e., Paleozoic, Central Plains, Mid-Continent source terranes) may reflect a potential bias caused by insufficient data, minor differential provenance and/or local drainage patterns along strike of the Appalachian basin, or signatures affected by potentially several, currently incalculable, episodes of sediment recycling.

2.6.3.5 Stage V—Middle Pennsylvanian fluvio-deltaic transgression and later thrust sheet advancement

Carbonaceous and muscovite-rich sandstone to shale beds of the Pikeivlle Formation in this study interpreted as marsh or poorly drained delta plain strata match regional descriptions of a fluvio-deltaic system (e.g., Aitken and Flint, 1994; Greb and Chesnut,

1996; Greb and Martino, 2005) deposited in a rapidly subsiding foreland basin heavily influenced by the building orogen to the southeast (Chesnut, 1994). Paleocurrent measurements made in this study suggest west-northwestward drainage into the foreland basin. Detrital zircon U-Pb age spectra for the Pikeville Formation (Figs. 2.4 and 2.10) suggest that immature clastic sediment was primarily sourced from east Laurentian crystalline basement rocks incorporated into thrust sheets to the southeast, which is consistent with paleocurrent directions and suggests deposition of the Pikeville Formation at Pound Gap in a proximal fluvio-deltaic system stemming from the hinterland (Fig. 2.14). When compared with detrital zircon age peaks from a sample of stratigraphically equivalent sandstone from the Cross Mountain Formation of the southern Appalachian foreland basin in Tennessee (Thomas et al. 2004), it is apparent that the dominant influence of Grenville source terranes continued into the Middle Pennsylvanian time. Sediment sourcing from Paleozoic and Pan-African/Brasiliano source terranes to the east is consistent with paleocurrent data suggesting drainage from the southeast. The presence of age peaks of Central Plains affinity in the Cross Mountain Formation may indicate either differential sediment dispersal between the southern and central Appalachian basins or that our analyses of the Pikeville Formation lacked sufficient data ("drowning-out" signature of Grenville-sourced detrital zircons).

Our compositional, paleocurrent, and detrital zircon U-Pb age data support previous conceptions of foreland basin fill sourced by the advancing, low-grade metamorphic thrust sheets to the southeast (Houseknecht, 1980; Rice, 1985; Rice and Schwietering, 1988), suggesting sediment dispersal via transverse drainage systems. Continued advancement of the thrust sheets to the southeast provided large volumes sediment to the foreland, outpacing subsidence and filling the central Appalachian foreland basin system by Middle Pennsylvanian time (Fig. 2.15) (Chesnut, 1994). Interfingering members of the Breathitt Group, including the "Lee-type" quartzarenites of braided fluvial river origin and immature, lithic sandstones of fluvio-deltaic origin, are the principal components of the foredeep stratigraphy. These intertwined Pennsylvanian sediment dispersal networks documented in the Pine Mountain thrust sheet hanging wall and footwall strata in this

study coexisted as axial and transverse drainage systems, connecting the early Alleghanian hinterland to the foreland basin system which thickened in the axial direction into the Black Warrior Basin southwestward (Fig. 2.15) (see Ettensohn, 2008). In the Alleghanian foreland basin system, axial braided river systems dominated the foreland basin during glacio-eustatic lowstands, flowing to the southwest, and were limited to the western margin during transgression of northwestward-flowing transverse drainage systems stemming from wedge-top depozone strata above active thrust sheets to the southeast during glacio-eustatic highstands (e.g., Chesnut, 1994; Greb and Chesnut, 1996; Greb and Martino, 2005; Bodek, 2006; Grimm et al., 2013).

The strata exposed at Pound Gap were incorporated into the Pine Mountain thrust sheet and emplaced over undeformed foredeep strata of the Appalachian Plateau province during the final deformational stage of the Alleghanian orogeny (Bartholomew and Whitaker, 2010), during which collisional events continued into Permian time (see Hatcher, 2010). The thrust fault migrated northwestward in a stair-step geometry, propagating subparallel to bedding in the shaley Cambrian Rome Formation, obliquely through overlying competent clastic and carbonate strata, and subparallel to bedding in the Ohio Shale (Rich, 1934). Thickness models of the thrust sheet's original maximum thickness determined from coal vitrinite reflectance data range from 1-3 km thick and depend on variables such as the assumed rate of uplift after thrust sheet emplacement and the relative rate of erosion to thrusting pace for the thrust sheet (O'Hara et al., 1990).

2.6.4 The central Appalachian foreland basin system: a typical foreland basin?

As a foreland basin system, it is important to understand how the central Appalachian foreland basin as defined in this study compares to the widely accepted foreland basin system model of DeCelles and Giles (1996). The typical foreland basin stratigraphy as outlined by Mutti et al. (2003) is characterized by a transition from coarsening-upward deposition in marine to nonmarine conditions (Fig. 2.16). This first-order assessment matches the stratigraphic sequence outlined in this study from the Pine Mountain thrust sheet, and each of the depositional systems outlined in the typical foreland basin

sequence have been interpreted in the central Appalachian foreland basin stratigraphy described in this study. However, there are several key differences. In the typical foreland basin model, deposition of basinal turbidites in the outer to axial to inner foredeep depozone and successive deposition in mixed deposystems of the wedge-top postdate carbonate deposition on the outer ramp during passive margin development. In the central Appalachian foreland basin, deposition of basinal turbidites preceded carbonate bank development and ensuing mixed clastic and carbonate deposition (Fig. 2.16). Whereas the typical model reflects deposition in increasingly proximal parts of the foredeep depozone, the stratigraphy of the Pine Mountain thrust sheet interpreted in this study reflects deposition in increasingly distal parts of the foredeep depozone. The discrepancy between the relative timing of basinal turbidite systems and carbonate development is probably best explained by timing differences in tectonic processes for each system: carbonate bank development in the central Appalachian orogen reflects tectonic quiescence between orogenic events rather than passive margin development after rifting. This interpretation of tectonic quiescence reflected in carbonate development is widely accepted in the Appalachian basin system (e.g., Ettensohn and Chesnut, 1985; Chesnut, 1991; Ettensohn et al., 2002; Al-Tawil and Read, 2003), though carbonate systems in active foreland basin systems do occur (e.g., the Tully Limestone deposited during active Acadian tectonism as part of the otherwise clastic Catskill Delta as suggested by Heckel, 1973; the submerged outer ramp to forebulge of the western Persian Gulf; the Central Basin Platform of the Permian Basin in Texas). This distinction also bears complications such as lithospheric rheology differences that are important in understanding how long-lived convergent margins such as the Appalachian orogen differ from single-orogeny convergent margins.

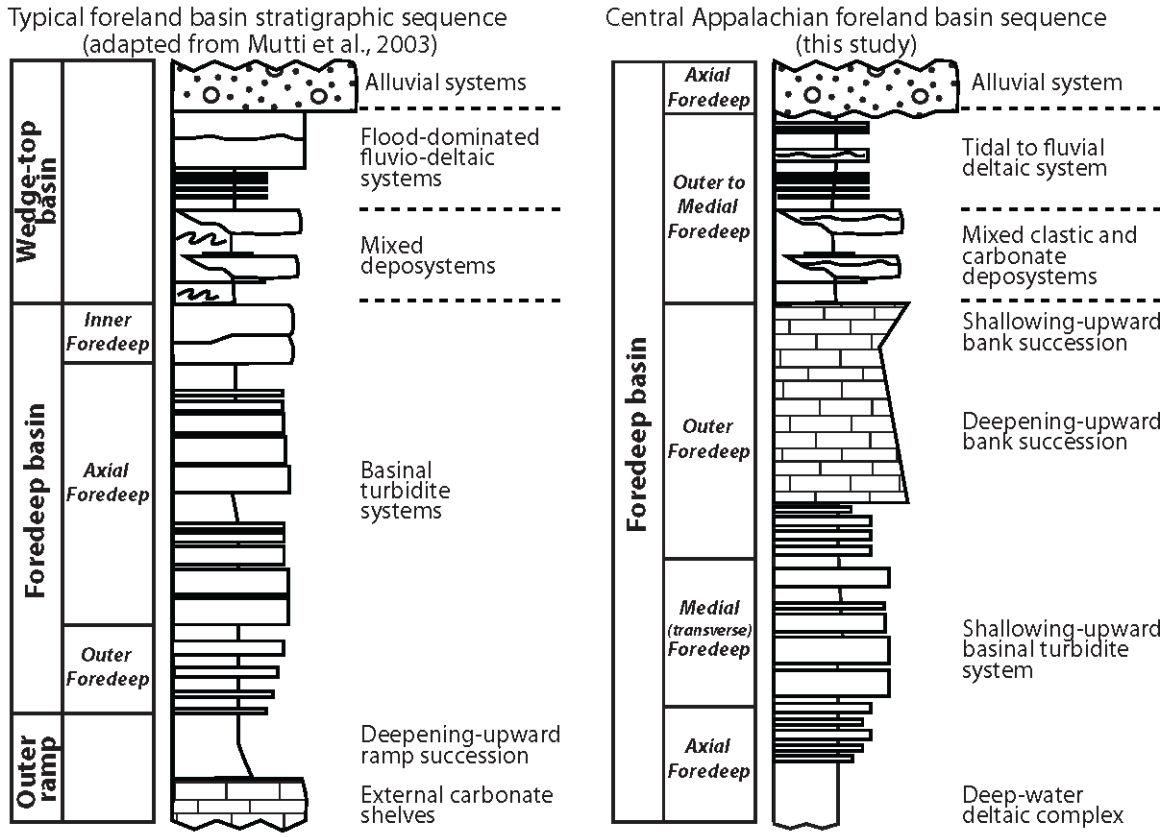

Figure 2.16: Comparison of typical foreland basin stratigraphic sequence adapted from Mutti et al., 2003 (left, inspired by Eocene of the south-central Pyrenees) to the stratigraphy of the central Appalachian foreland basin interpreted from the Pine Mountain thrust sheet in this study (right). Note that each of the depositional systems that characterize the outer ramp, foredeep, and wedge-top basins in typical foreland basin systems are present in the central Appalachian basin stratigraphy but are interpreted here as depositional systems local to the foredeep depozone. Vertical scale is not representative of relative thickness or time.

Deposition in mixed deposystems is succeeded by fluvio-deltaic and alluvial deposition in the wedge-top depozone of typical foreland basin systems (Fig. 2.16). However, deposition of mixed carbonate and clastic lower delta plain strata, fluviatile upper delta plain strata, and alluvial braided river system strata of the central Appalachian foreland basin are each interpreted in this study as deposits of the foredeep depozone. Moreover, the foredeep systems interpreted from the Pine Mountain thrust sheet strata, though coarse-grained and fluvial, were deposited in the axial position of the foredeep. This interpretation is supported by studies of the Alleghanian foreland basin system which suggest that major structural features (such as the fold and thrust belt) generated during

the Middle Pennsylvanian to Permian main phase of the Alleghanian orogeny post-date Early Pennsylvanian braided river system development (Fig. 2.2). Sediment derivation from the uplifting orogen to the southeast, as interpreted from new detrital zircon provenance presented in this study, and lithic-rich fluvio-deltaic strata of the Middle Pennsylvanian Pikeville Formation in the footwall of the Pine Mountain thrust fault are consistent with compositionally and texturally immature strata typical of the proximal foredeep to distal wedge-top depozones transported via transverse drainage systems stemming from the actively deforming wedge-top depozone (DeCelles and Giles, 1996).

2.7 Conclusions

The Pound Gap exposure is one of the best in the Appalachian foreland basin to observe the depositional systems that filled the Carboniferous Appalachian foreland basin. The strata of the Pine Mountain thrust sheet have been characterized into distinct lithofacies from which inferred depositional conditions and processes have been used to interpret depositional environments in the end-Neoacadian to early Alleghanian central Appalachian foreland basin. Lithofacies with similar characteristics and interpreted depositional environments are grouped into facies associations which reflect changing depositional conditions in local systems (e.g., a tidally influenced lower delta plain) or changing local environments with consistent depositional processes (e.g., a deltaic submarine fan system). The documented transitions within and between facies associations of the Pine Mountain thrust sheet strata at Pound Gap record deposition in deep to shallow marine and terrestrial environments which, in the context of regional foreland basin development of the central Appalachian basin, are interpreted to reflect changing basin dynamics from the final phases of the Neoacadian orogeny through the early stages of the Alleghanian orogeny and deposition in the distal to medial foredeep depozone which received sediment via alternating axial and transverse drainage systems.

Paleocurrent and new detrital zircon data are utilized with the interpreted lithofacies to infer multiple shifts in local drainage patterns and are integrated into regional studies to support deposition in alternating axial and transverse systems and changing foreland

basin dynamics in response to waning and waxing tectonic loading and uplift along the east Laurentian margin from Late Devonian to Middle Pennsylvanian time. End-Neoacadian uplift and erosion along the orogen provided mostly recycled sediment to a deep marine prodelta which was succeeded by an axial, southwestward-prograding submarine fan complex, followed by a transverse, northwestward-prograding submarine fan complex from Late Devonian to Early Mississippian time. Sediment was derived from preexisting Appalachian basin strata uplifted during end-Neoacadian arc collision to the southeast. Carbonate bank development in Middle to Late Mississippian time occurred in tropical shallow and open marine conditions during a period of tectonic quiescence. Late Mississippian lower and upper delta plain deposits mark renewed clastic influx into the Appalachian foreland basin during the early stages of continental collision in the Alleghanian orogeny and was strongly influenced by tidal processes that gradually gave way to transverse, fluvial-dominated systems. Detritus in this deltaic complex was transported by transverse river systems from older basin strata uplifted during the early stages of the Alleghanian orogeny. Introduction of coarse and mature, likely recycled detritus in an axial, southwestward flowing braided river system during Early Pennsylvanian time occurred in the distal to medial foredeep depozone and was followed by northwestward-flowing fluvio-deltaic deposition in Middle Pennsylvanian time.

The stratigraphy of the Neoacadian to Alleghanian foreland basin system is demonstrated to be significantly different from that of the typical foreland basin system widely applied to convergent plate margins today. Explanations for this discrepancy should include such factors as the timing and frequency of orogenic events leading to foreland basin development, related rheologic properties of the underlying lithosphere, and whether forebulge migration is mechanically static or mobile.

The rocks exposed at Pound Gap provide a valuable opportunity to study foreland basin system development along convergent margins with long-lived, multi-stage collisional histories. The lithofacies framework and interpretations of the central Appalachian foreland basin system made from paleocurrent and provenance data presented in this

study draw support from regional structural, sedimentologic, stratigraphic, and geochronologic provenance studies from the Carboniferous Appalachian foreland basin system and may serve as a frame of reference for investigating the evolution of similar, less well-understood foreland basins globally. In particular, this study documents tidal lower delta plain depositional environments in the central Appalachian basin, environments which have historically received little attention because they are frequently eroded and redeposited in shelfal or deeper marine settings in ancient systems (see Bhattacharya, 2006; Tessier, 2012). In addition, this study provides detailed documentation and interpretations of unconfined subaqueous delta complexes deposited in a foreland basin setting, systems which have received far less attention in comparison to their continental shelf to abyssal plain counterparts explored in the petroleum industry, but which have clearly demonstrated significant hydrocarbon potential.

CHAPTER 3. STRUCTURAL CONFIGURATION OF A MODIFIED MESOZOIC TO CENOZOIC FOREARC BASIN SYSTEM, SOUTH-CENTRAL ALASKA

3.1 Introduction

Southern Alaska has been the site of continental growth through tectonic accretion and subduction-related processes throughout the Mesozoic and Cenozoic and is widely regarded as a classic area to study continent accretion (e.g., Plafker and Berg, 1994). However, only recently have we begun to realize some of the more complicated phenomena, such as ridge subduction and oceanic plateau subduction, that have affected and continue to dominate upper plate processes along this and other collisional plate margins (Herron et al., 1981; Cande et al., 1986; Behrmann et al., 1994; Bradley et al., 1998; D'Orazio et al., 2001; Sak et al., 2004; Taylor et al., 2005; Pedoja et al., 2006; Whittaker et al., 2007; Espinoza et al., 2008; Scalabrino et al., 2009; Ridgway et al., 2012). Forearc basins, magmatic arcs, and accretionary prisms comprise a geologic trinity which preserves a history of arc magmatism, accretionary prism growth, sedimentation, and deformation along collisional plate boundaries and are genetically linked to continental growth along collisional plate boundaries. However, several limiting factors, such as tectonic erosion, magmatism, metamorphism, etc., inherent to these types of margins notably reduce their preservation potential (see Dickinson and Seely, 1979), inhibiting our understanding of the nature and timing of processes that contribute to continental growth.

The Matanuska forearc basin of southern Alaska is situated between accreted Cretaceous to Paleocene plutons of the Talkeetna magmatic arc and Cretaceous to Paleocene accretionary prism rocks (Fig. 3.1). Cretaceous arc and marine forearc strata were deposited over accreted Jurassic remnant intra-oceanic arc plutons and volcaniclastic

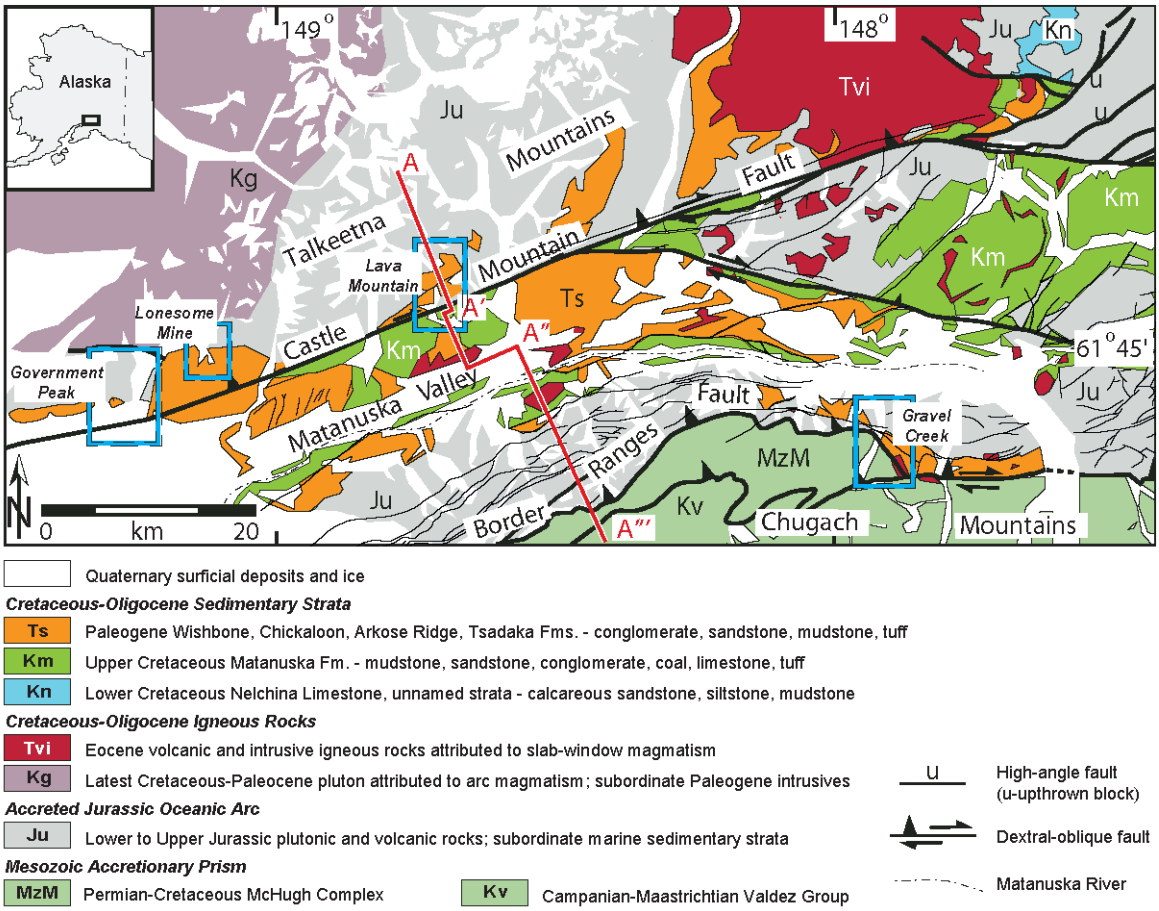

Figure 3.1: Simplified geologic map of the Matanuska Valley region along southern Alaska. Modified from Trop (2008) and Ridgway et al. (2012). Blue boxed areas along the Castle Mountain fault and the Border Ranges fault systems represent key areas discussed in this chapter where we discuss the structural record of Cenozoic subduction processes which modified the forearc system. Structural cross-section A-A''' presented in Figure 3.11.

rocks (Trop, 2008). The structures, up to six kilometers of strata, and younger igneous plutons in the Matanuska Valley region preserve a complex record of deformation, sedimentation, and plutonism in a marine to nonmarine forearc basin (e.g., Bruhn and Pavlis, 1981; Little, 1988; Little and Naeser, 1989; Bradley et al., 1998; Bunds, 2001; Pavlis and Roeske, 2007; Trop, 2008; Trop and Ridgway, 2007; Ridgway et al., 2012). Cretaceous strata and unconformably overlying Paleocene-Eocene nonmarine strata are deformed and intruded by Paleogene igneous plutons with a near-trench geochemical signature (e.g., Lytwyn et al., 2000). Previous investigations of the plutonic and volcanic rocks in the trench and forearc regions (Lytwyn et al., 2000; D'Orazio et al., 2001; Gorring and Kay, 2001; Cole and Stewart, 2008) and of the igneous and high-temperature

low-pressure metamorphic rocks in the accretionary prism (Sisson et al., 1989; Underwood et al., 1999; Iwamori, 2000) have demonstrated that Matanuska Valley region preserves a record of Paleocene-Eocene spreading ridge subduction (Fig. 3.2). In addition, southern Alaska is currently experiencing oceanic plateau subduction of the ~30 km thick Yakutat microplate, which has further affected the depositional and structural configuration of the margin (Fig. 3.2) (see Finzel et al., 2011; Ridgway et al., 2012). This chapter, as part of a larger investigation of the long term sedimentary record of ridge subduction processes in forearc basins, addresses how spreading ridge subduction modified the structural configuration of the Matanuska Valley forearc basin. Presented here are geologic maps and cross-sections from several key regions in the Matanuska Valley region (yellow boxed areas in Fig. 3.1) which will contribute to the scientific community's understanding of how second-order subduction processes such as spreading ridge and flat-slab subduction may impact the structural configuration of forearc basins.

3.2 Regional Geologic Setting

The Matanuska Valley and flanking Talkeetna and Chugach Mountain ranges host an intricate assemblage of complexly deformed forearc basin strata, magmatic arc plutons, and metamorphosed accretionary prism strata (Fig. 3.1). These have been subdivided into tectonostratigraphic terranes (see Plafker and Berg, 1994) that were added to the southern Alaskan margin beginning in Late Jurassic and Cretaceous time with the accretion of an intra-oceanic arc and oceanic plateau, collectively comprising the Wrangellia composite terrane (Nokleberg et al., 1985; Ridgway et al., 2002; Trop et al., 2005; Rioux et al., 2007). This accreted terrane was overprinted by Cretaceous Talkeetna arc magmatism during northward normal subduction along the margin (Plafker and Berg, 1994) and was accompanied by Matanuska marine forearc basin development (Fig. 3.2) (Trop, 2008) and Chugach accretionary prism growth (e.g., Plafker et al., 1994; Amato and Pavlis, 2010; Amato et al., 2013). Syndepositional displacement of alluvial-fluvial-lacustrine strata with lava and tuff of the Arkose Ridge, Chickaloon, and Wishbone Formations along the Castle Mountain and Border Ranges fault systems followed Paleocene regional uplift and erosion in response to ~58 Ma northeastward spreading ridge subduction (Cole

et al., 2006) and 61-50 Ma near trench plutonism in the Matanuska forearc basin (Fig. 3.2) (Bradley et al., 2003). Further uplift and erosion in the forearc basin is attributed to oceanic plateau subduction of the Yakutat microplate starting in Oligocene time (Finzel et al., 2011).

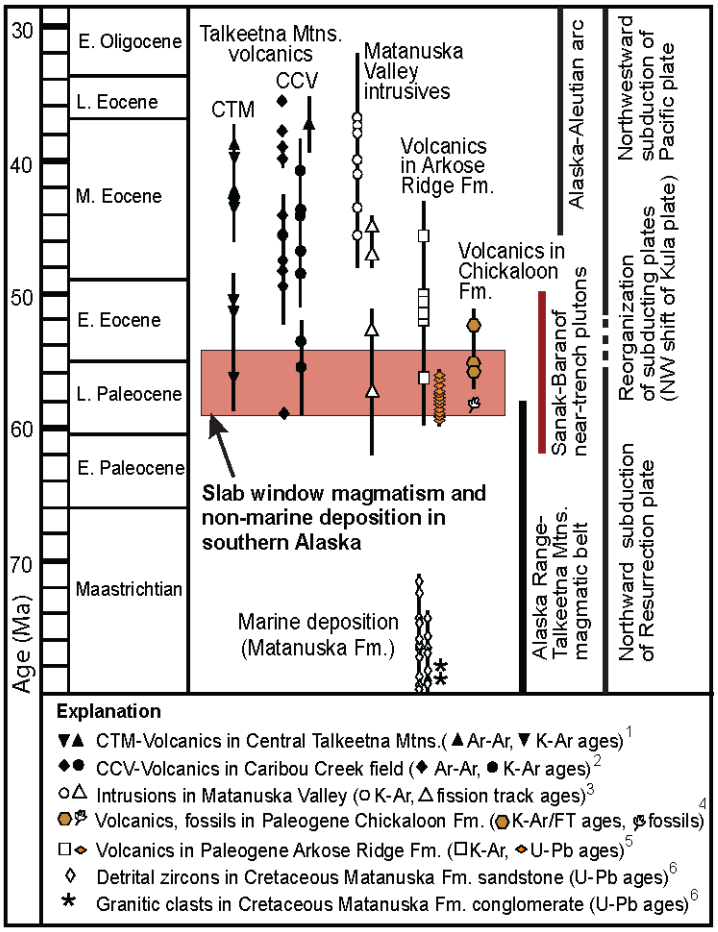

Figure 3.2: Age-event diagram showing isotopic ages from igneous rocks and igneous clasts in the Matanuska Valley and Talkeetna Mountains. Deposition of the Arkose Ridge and Chickaloon Formations is coeval with slab window plutonism and volcanism in the central Talkeetna Mountains (CTM) and the Caribou Creek volcanic field (CCV), as well as near-trench plutonism in the Mata- nuska Valley region, which are processes attributed to spreading ridge subduction beneath the southern Alaskan margin (Bradley et al., 2003). Modified from Kortnya et al. (2013) after Cole et al. (2006) who cite: 1 - Cjetsey et al. (1978), Adams et al., 1985), Little (1988), and R.B. Cole and P.W. Layer (2002, personal communication); 2 - Cole et al., (2006), Silberman and Grantz (1984), Panuska et al. (1990), and Trop et al., (2003); 3 - Silberman and Grantz (1984), Little (1988), and Little and Naeser (1989); 4- Triplehorn et al. (1984); 5 - Silberman and Grantz (1984); Idleman et al., 2013; 6 - Trop (2008).

Studies of Paleogene strata in the region have mainly focused on late Paleocene-Eocene strata of the Chickaloon and Wishbone Formations south of the Castle Mountain fault (e.g., Clardy, 1974; Little and Naeser, 1989; Flores and Stricker, 1993; Trop et al., 2003), but investigations north of this major transpressional structure have revealed several >1-km thick, well-exposed outcrops of age-equivalent and sedimentologically similar strata, separated into four lithofacies associations of the Arkose Ridge Formation, in thicknesses of 1800 to >2000 m (Kortyna et al., 2009; Kassab et al., 2009, Kortyna, 2011; Donaghy, 2012; Kortyna et al., 2013; Sunderlin et al., in press) which afford the opportunity to understand the timing and record of deposition along the margin during eastward-progressing spreading ridge subduction and associated slab window plutonism and volcanism (Kortyna et al., 2009; Idleman et al., 2011). This study is concerned with the potential record of syn- and post-depositional deformation of these strata along the northern and southern margins of the Matanuska Valley region.

3.3 Methodology

Geologic maps of four key areas presented in this chapter include field observations and data collected during the summers of 2008, 2009, 2010, 2011, and 2012 as part of a collaborative research project by Bucknell University, Lehigh University, and Purdue University. Ed Bauer, Erin Donaghy, Bruce Idleman, Kyle Kissock, Cullen Kortyna, Christine Kassab, Ken Ridgway, Tyler Szwarc, Jeff Trop, and I contributed to geologic mapping. Other data used in the construction of our geologic maps and structural cross-sections were derived from field data compiled in geologic maps by Detterman et al. (1976) and Winkler (1992) of the study area. Each local cross-section was constructed by interpolating calculated apparent dips for groups of bedding orientation data collected during geologic mapping reconnaissance work onto the plane(s) of section using fold axis calculations made for each group. This method inherently assumes kink fold geometry (e.g, Ramsay and Huber, 1984). Basement contacts with overlying strata were orthographically projected onto the plane of section assuming that the strata onlap the basement rock unconformably (i.e., buttress unconformity). Where data is lacking due to an exposure's inaccessibility (i.e., at Lava Mountain), we rely on photographs to guide

illustrations and interpretations of subsurface bedding attitudes. Unmeasured fault plane dips were estimated trigonometrically using fault traces with topographic elevation data. Stereographic representations of bedding data were constructed using the stereographic projection software GEOrient (version 9.5.0; Rod Holcombe, ©2011). In stereographic plots, solid great circles represent calculated girdles with corresponding beta axis poles (red β), whereas dashed great circles represent mean strike of bedding data.

Cross-section A-A" spans from the southern Talkeetna to the northernmost Chugach Mountains and was constructed using our new data in addition to previously published data from the Matanuska Valley region (Detterman et al., 1976; Winkler, 1992; Kortyna et al., 2009). Subsurface faults which do not daylight in the plane of section are inferred from local fault systems exposed laterally or are depicted to explain local deformed strata.

3.4 Geologic Maps and Structural Cross-Sections

3.4.1 Government Peak area

The Government Peak area is the westernmost studied area along the northern margin of the basin and lies north of the Castle Mountain Fault (Figs. 3.1 and 3.3). Most data in this area is from Winker (1992) and Bleick et al. (2012) with other data collected during a two-day traverse across the area. This area is characterized by Cretaceous pelitic schist (Kps) exposed along Bald Mountain Ridge which is bordered by Jurassic amphibolite and quartz diorite (Jma) to the east and is faulted (sense unknown) against the Late Cretaceous Willow Creek pluton (Kw) to the north (Fig. 3.3). Measurements of foliations in pelitic schist exposures produce an average foliation orientation of 280°, 24° with a calculated fold axis plunging 01° toward an azimuth of 098° (Fig. 3.3). Beds of sandstone and conglomerate with sparse mudstone of the Paleocene-Eocene Arkose Ridge Formation rest unconformably over Jurassic metamorphic rocks but are normally faulted at Government Peak with a southward dipping fault plane (Fig. 3.3). An east-west-trending fault has been traced in the Arkose Ridge Formation south of Government Peak and separates upthrown strata to the north and downthrown strata to the south. Additional

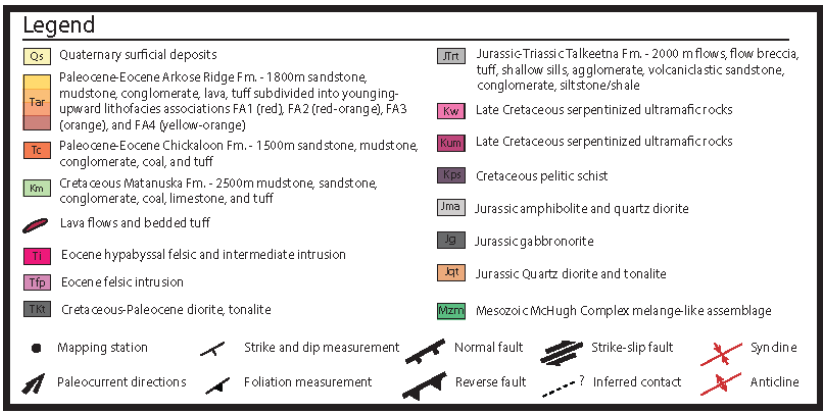

Figure 3.3: Geologic map of the Government Peak area north of the Castle Mountain fault. Poles to foliation planes of Cretaceous pelitic schist plotted in upper left corner yield average foliation orientation of 280°, 24° with a calculated fold axis plunging 01° toward 098°. Adapted from Bleick et al., 2012.

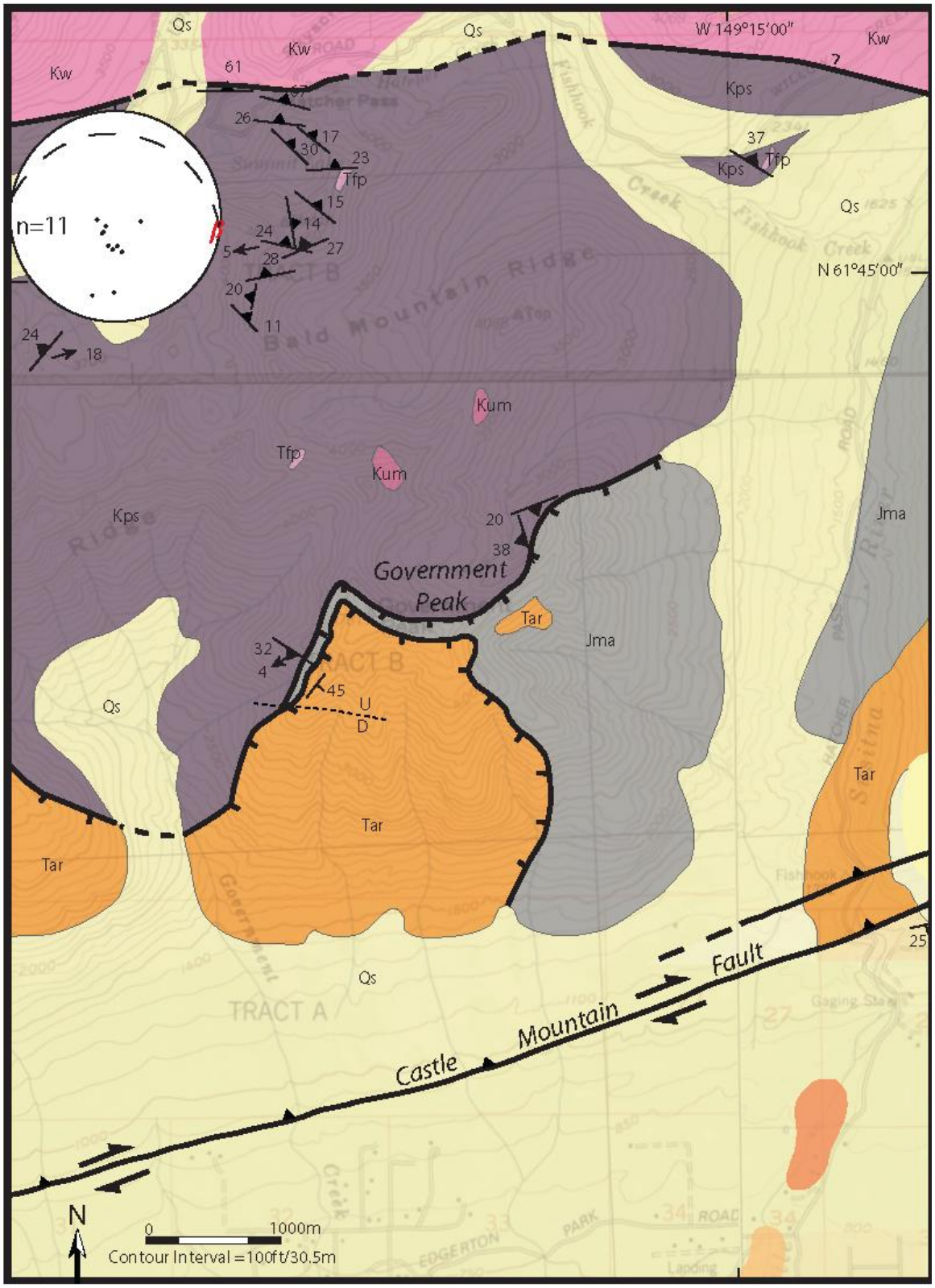
Qs
Kw
61
26
17
30
23
Tfp
15
14
24
27
5
28
20
11
24
18
n=11
Bald Mountain Ridge
Kum
Tfp
Kum
Kps
20
38
Government Peak
Tar
Jma
32
4
45
U
D
Qs
Tar
Tar
Qs
TRACT A
Castle Mountain Fault
W 149°15'00"
Kw
Kps
37
Tfp
Kps
Qs
N 61°45'00"
Jma
Tar
25
N
0
1000m
Contour Interval = 100ft/30.5m

Figure 3.3

knowledge of this area requires further field work but will improve upon our knowledge of how westernmost Paleogene strata in the Matanuska Valley region preserve the depositional record of uplift and subsidence associated with spreading ridge subduction.

3.4.2 Lonesome Mine area

Lonesome Mine is located north of the Castle Mountain fault and is characterized by fluvial-alluvial strata and discontinuous lava flows of the Arkose Ridge Formation lying unconformably over Cretaceous granite (Fig. 3.4). This area was mapped by Winkler (1992) and Kortyna et al. (2009; 2013). Here, lithofacies 1, 2, and 4 of the Arkose Ridge Formation have been mapped (terminology of Kortyna et al., 2009), with an upsection change from deposition in gravelly to sandy paleocanyons and braided channels (FA1) overlying incised Jurassic pelitic schist, to muddy floodplains and shallow channels/splays (FA2), to sandy fluvial channels with lava flows and bedded tuff (FA4) (Kortyna et al., 2009). Muddy floodplain pond and lake deposits of FA3 are not preserved in the Lonesome Mine area. Beds in the Arkose Ridge Formation generally strike east-northeast, dipping southeastward with an average bedding orientation of 072°, 29° and are weakly folded in a syncline plunging 22° toward an azimuth of 117° (Fig. 3.5).

Alluvial-fluvial strata and lava flows of the Arkose Ridge Formation were deposited during regional uplift and volcanism associated with spreading-ridge subduction beneath the Matanuska Valley region (Ridgway et al., 2012). Paleocurrent data from fluvial sandstone beds suggest south-southwestward-flowing rivers as part of the Paleogene southwestward-draining river system previously discussed (Kortyna et al., 2013**)**. Later deformation along the northern Matanuska Valley region and Castle Mountain fault uplifted and folded these strata into an open syncline which was then partly eroded. These events may have been synchronous with any of the several periods of deformation in the Matanuska Valley region discussed for the regional cross-section A-A'".

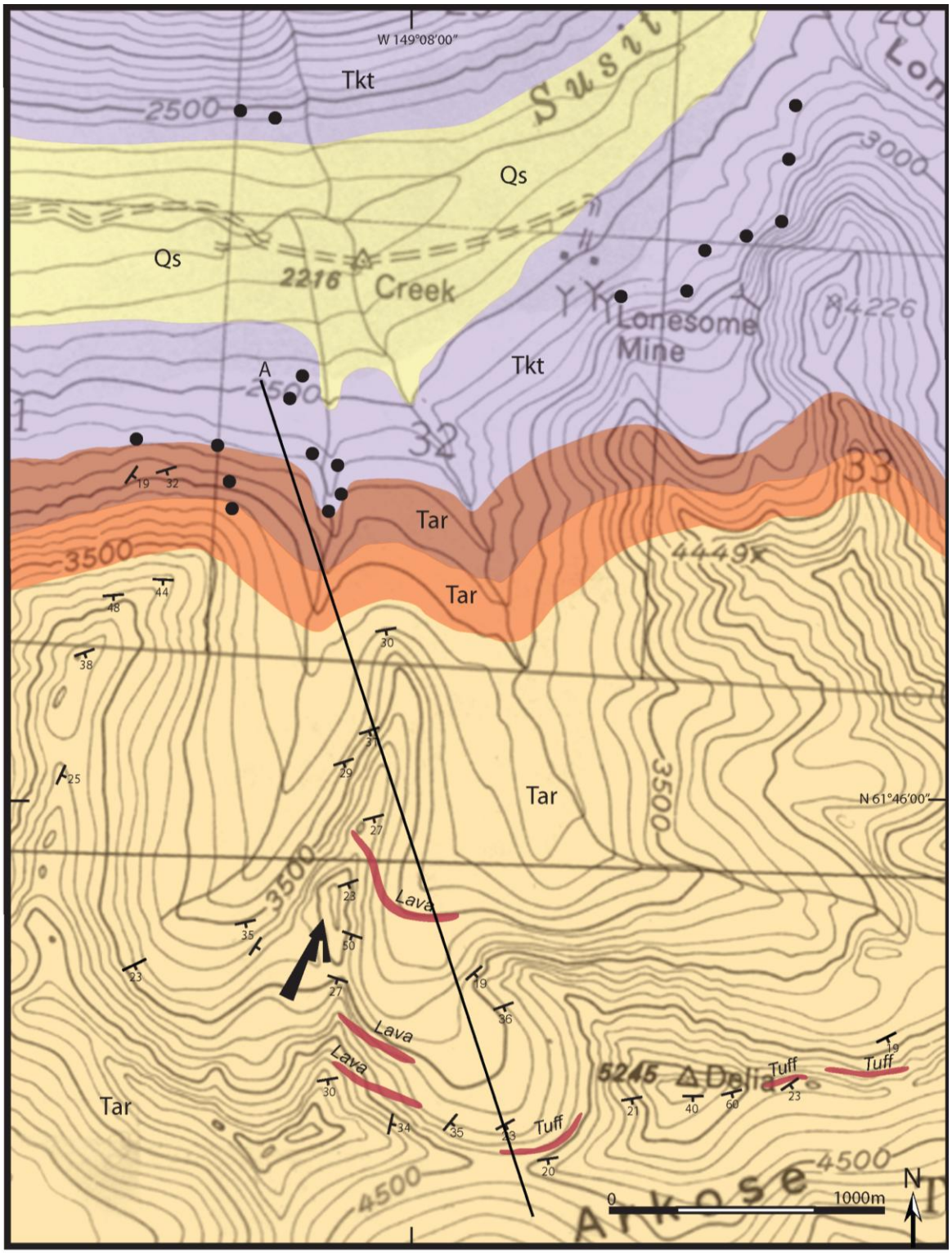

Figure 3.4: Geologic map of the Lonesome Mine area north of the Castle Mountain fault. Cross-section A-A' is presented in Figure 3.5. See Figure 3.3 for key.

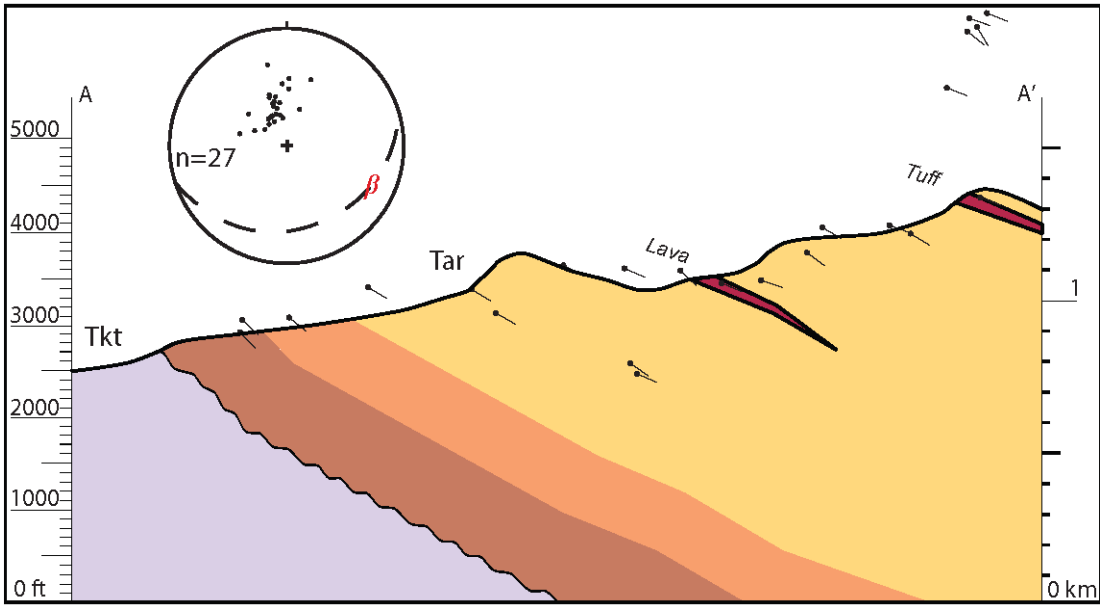

Figure 3.5: Cross-section A-A' of the Lonesome Mine area. Lithofacies F1, F2, and F4 rest unconformably (wavy line) above Cretaceous-Paleocene tonalite and diorite. Ball-and-stick symbols represent bedding data projected from strata measured in the mapped area in Figure 3.4. Stereographic plot depicts poles to bedding planes of the Arkose Ridge Formation with a calculated average strike of 072°, 29° and fold axis plunging 22° toward an azimuth of 117°. See Figures 3.3 and 3.8 for key.

3.4.3 Lava Mountain-Sheep Valley-Red Hill area

The Lava Mountain-Sheep Valley-Red Hill area (LSR) straddles the Castle Mountain Fault along the northern fringe of the Matanuska Valley (Fig. 3.6). Field observations have demonstrated a high-relief unconformable relationship between the Paleocene-Eocene Arkose Ridge Formation (Tar) and Jurassic gabbronorite basement (Jg). In the northeastward corner of the mapped area, the unconformable surface is onlapped by progressively younger fluvial to alluvial to lacustrine mudstone and sandstone of FA1, FA2, and FA4, respectively, of the Arkose Ridge Formation (Fig. 3.6) (Kortyna et al., 2009) and likely represents depositional onlap to a buttress unconformity. This contact is locally faulted north of Lava Mountain with down-to-the-southeast normal slip of unknown magnitude.

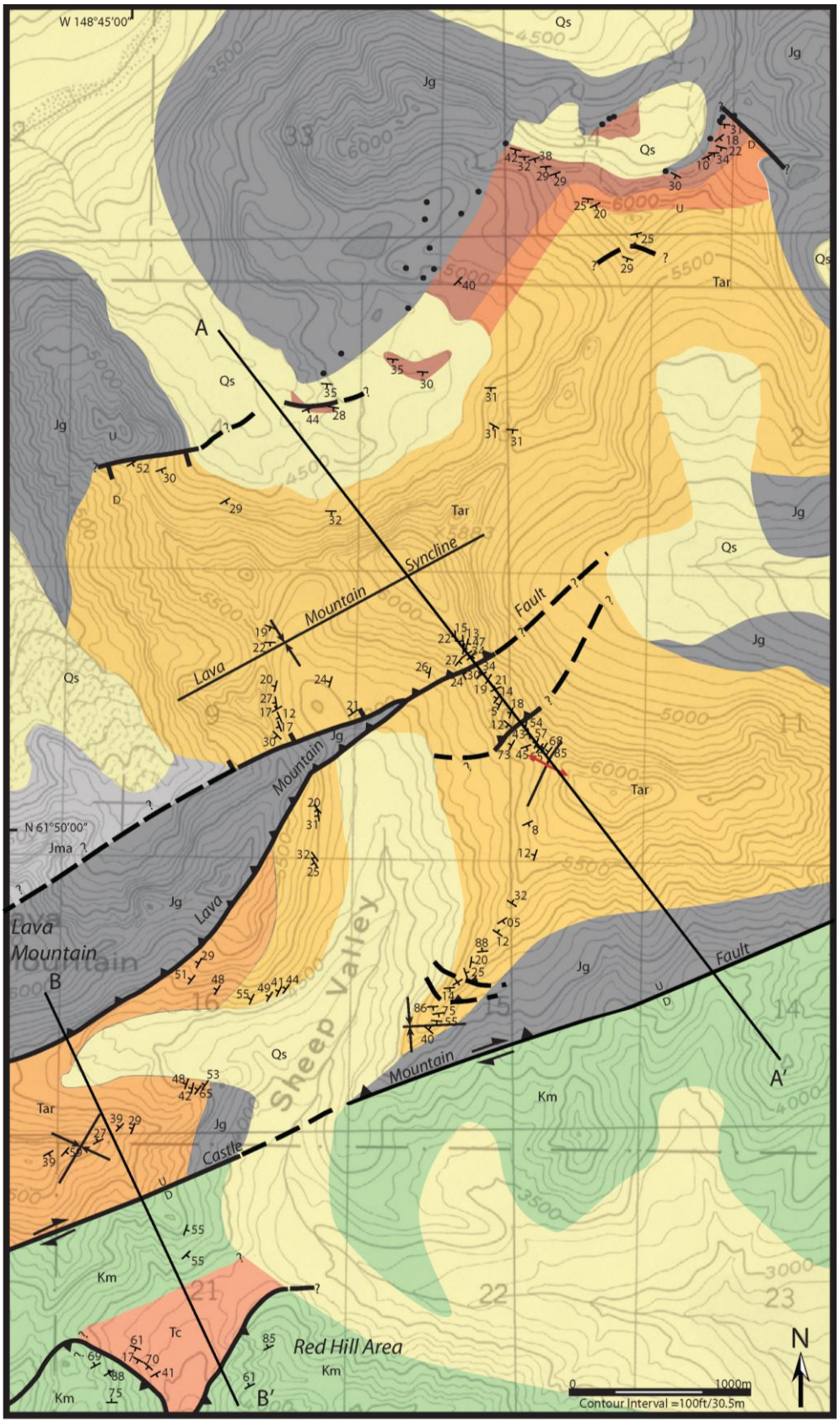

Figure 3.6: Geologic map of the Lava Mountain-Sheep Valley-Red Hill area along the Castle Mountain fault. Structural cross-sections A-A' and B-B' are presented in Figure 3.8. See Figure 3.3 for key.

Strata of the Arkose Ridge Formation and underlying basement are deformed by a series of northeast-striking, mostly reverse faults which dip northwestward in the Lava Mountain fault zone. We define this fault zone as the northeast trending set of faults that extend through Lava Mountain. North of the fault zone, strata of the Arkose Ridge Formation are folded in a broad, northeast-southwest trending syncline. The fault zone is characterized by two northwestward-dipping reverse faults, the northernmost of which emplaces Jurassic granite over Arkose Ridge Formation strata (Figs. 3.7a, 3.7b). The Lava Mountain fault, the most through-going reverse fault in the fault zone, which cross-cuts a northwestward-dipping normal fault separating Jurassic gabbronorite from Arkose Ridge Formation strata immediately west of the fault zone. Footwall strata of the Lava Mountain fault are box-folded and overlie the Lava Mountain splay fault (Fig. 3.7a), and measurements along the ridgeline above these folded strata do not reflect the complexity of the structure (Fig. 3.6). Footwall strata of the splay fault are tightly folded into a northeast-southwest-trending anticline which opens southeastward into a gentle syncline toward the Castle Mountain Fault (Fig. 3.7b).

The interpolated measurements from the LSR area are presented in the structural cross-section of the Lava Mountain fault zone in Figure 3.8a (A-A'). The average fold axis ascertained from bedding orientation data in the Arkose Ridge Formation plunges 13° toward an azimuth of 232°, varying in two areas: along the southeastern slopes of Sheep Valley, north of the Castle Mountain fault, folded and faulted strata plunge 14° toward an azimuth of 087° (measurements projected into granitic basement in Fig. 3.8a); south of Lava Mountain, folded strata plunge 06° toward 217° (Fig. 3.8b).

Structural cross-section B-B' (Fig. 3.8b) transects the folded and faulted Arkose Ridge Formation south of Lava Mountain and crosses the Castle Mountain fault into the Red Hill area in the southwestern part of the mapped area (Fig. 3.6). Around Red Hill, steeply northwestward-dipping Cretaceous marine turbidite strata of the Matanuska Formation (Km) are thrust over gently southwestward-dipping Paleocene-Eocene arkosic sandstone beds containing petrified logs of the Chickaloon Formation (Tc). Average bed

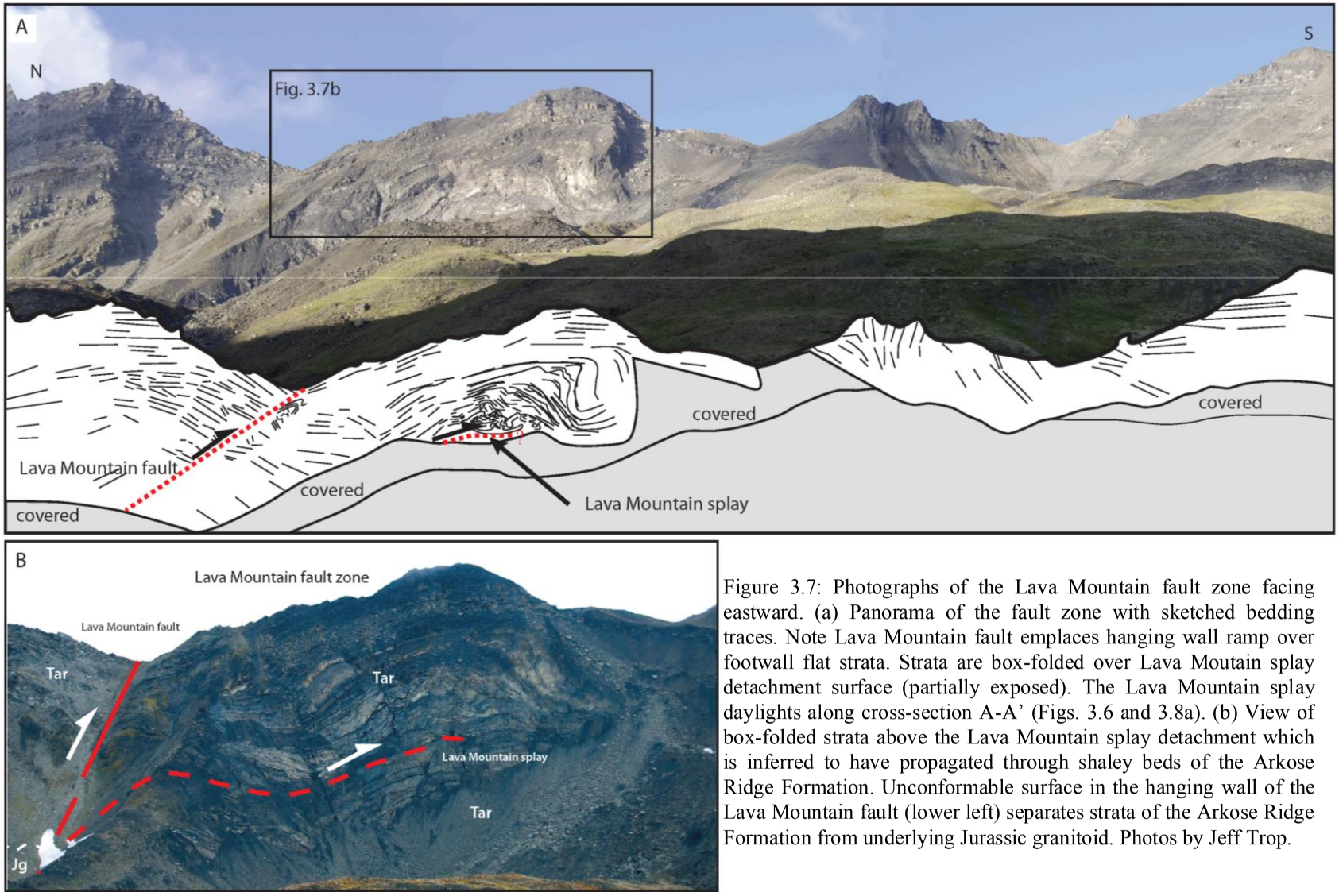

Figure 3.7: Photographs of the Lava Mountain fault zone facing eastward. (a) Panorama of the fault zone with sketched bedding traces. Note Lava Mountain fault emplaces hanging wall ramp over footwall flat strata. Strata are box-folded over Lava Moutain splay detachment surface (partially exposed). The Lava Mountain splay daylights along cross-section A-A' (Figs. 3.6 and 3.8a). (b) View of box-folded strata above the Lava Mountain splay detachment which is inferred to have propagated through shaley beds of the Arkose Ridge Formation. Unconformable surface in the hanging wall of the Lava Mountain fault (lower left) separates strata of the Arkose Ridge Formation from underlying Jurassic granitoid. Photos by Jeff Trop.

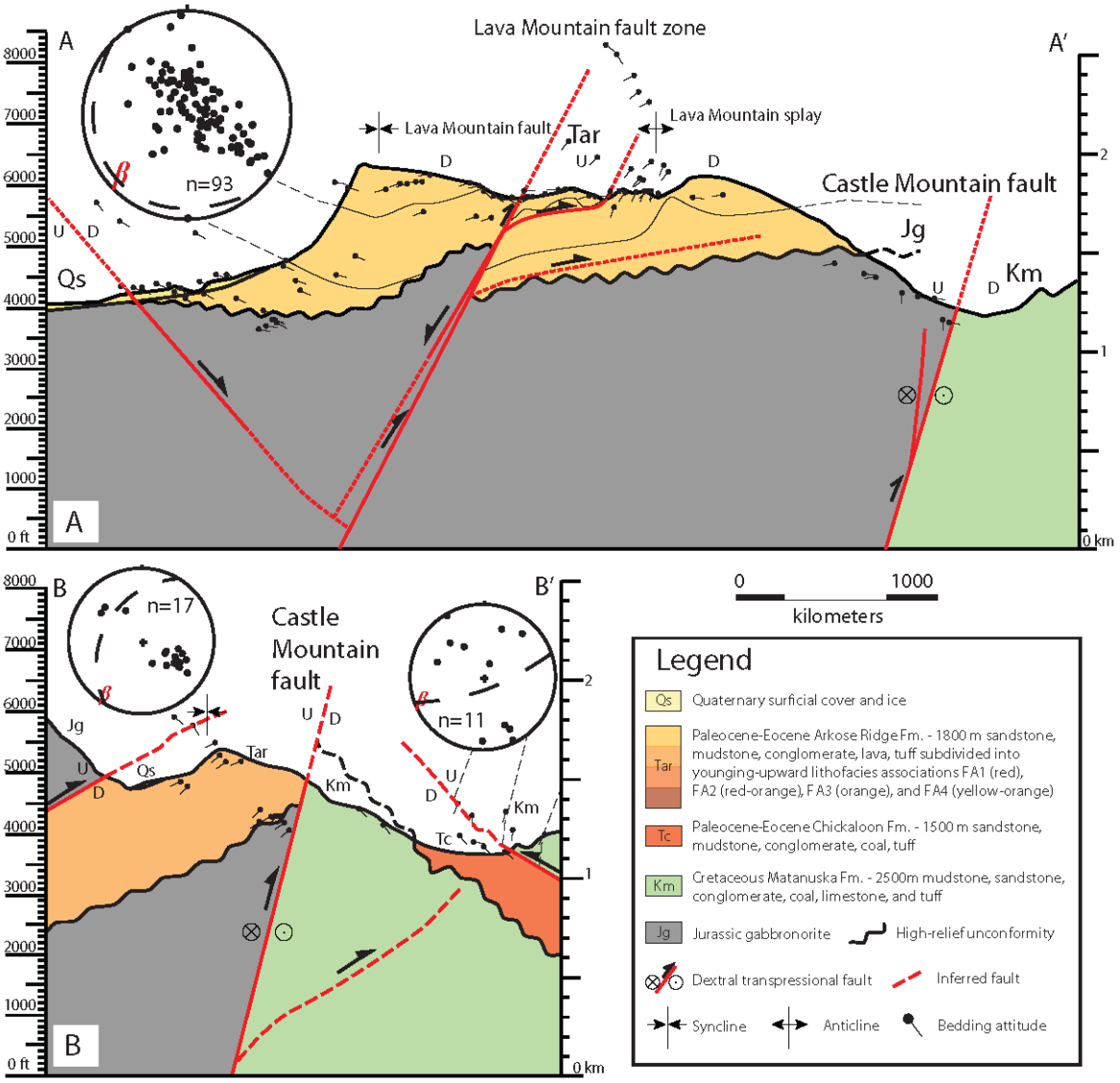

Figure 3.8: Structural cross-sections across the Lava Mountain-Sheep Valley-Red Hill areas. (A) Cross-section A-A' of the Lava Mountain fault zone is correlative with photograph presented in Figure 7b and illustrates deformed strata north of the fault zone forming a broad syncline bound by normal faults. In the fault zone, the Lava Mountain fault cross-cuts the southern normal fault of this graben structure and emplaces Jurassic gabbronorite over Arkose Ridge Formation strata (lower left corner in Fig. 3.7b.) The Lava Mountain splay soles into the Lava Mountain fault and contains box-folded strata over a detachment surface. Footwall strata of the Lava Mountain splay are folded into a tight anticline (explained by dashed blind detachment surface). (B) Cross-section B-B' of the Red Hill area demon- strates how strata dip away from the Castle Mountain Fault both to the north and south of the transpres- sional structure. South of the Castle Mountain fault, Matanuska Formation strata are emplaced over Chickaloon strata and are truncated at a high angle relative to the thrust fault plane, perhaps preserving a hanging wall ramp (Km) over footwall flat (Tc) geometry. Folding in footwall strata explained by blind reverse fault (dashed) splaying from the Castle Mountain fault.

orientations from the Arkose Ridge Formation north of the Castle Mountain fault yield an average orientation of 210°, 45° with a fold axis plunging 06° toward an azimuth of 217°. Toward Red Hill, south of the Castle Mountain Fault, bed orientations of the Chickaloon and Matanuska Formations average an orientation of 070°, 77° and produce an average fold axis plunging 08° toward an azimuth of 248° (Fig. 3.8b).

The broad syncline in strata of the Arkose Ridge Formation in the northwestern part of the mapped area (labeled Lava Mountain Syncline) is bound by two eastward-striking normal faults which dip toward each other (Figs. 3.6 and 3.8). This feature is interpreted as an extensional graben structure in which normal displacement along the northern periphery of this syncline occurred along the rheologically weak unconformity between Jurassic granite and strata of the Arkose Ridge Formation. Assuming that the unconformable surface is subparallel to bedding observed in this region, thickness estimates from exposed strata observed northwest of the Lava Mountain fault zone to the subsurface projection of the contact suggest a minimum thickness of ~2700 meters for FA3 alone. This finding may have significant implications for depositional rates of the Arkose Ridge Formation and uplift along the northern margin of the Matanuska Valley region but requires further understanding of the depositional duration of this formation's facies associations.

Normal faults between Lava Mountain and the Lava Mountain fault zone are cross-cut by reverse faults, suggesting that contraction in the LSR area followed extension. Box folds in the footwall strata of the Lava Mountain fault are interpreted as detachment folds which formed above the Lava Mountain splay fault. The anticline in the footwall of the Lava Mountain splay fault may have also formed by detachment folding and has been illustrated above a blind detachment fault stemming from the Lava Mountain fault (Fig 3.8a).

Kortyna et al. (2009; 2013) demonstrated that the Lava Mountain stratigraphic section was deposited as part of a Paleocene-Eocene southwestward-draining fluvial system

stemming from arc plutons of Late Cretaceous-Early Paleocene plutons of the Alaska Range-Talkeetna Mountains magmatic arc to the northeast. This river system drained into the axial position of the nonmarine Matanuska forearc as it was uplifted during slab-window magmatism and volcanism (e.g., Cole et al., 2006). Normal faulting of the Arkose Ridge Formation in the LSR area may have been synchronous with renewed subsidence in the forearc and subduction complex uplift, during which time the Chickaloon and Wishbone Formations were deposited over block-faulted and eroded basement of Jurassic arc plutons and Cretaceous subduction complex strata (Little and Naeser, 1989). Later reverse faulting may have occurred during transpression associated with Oligocene development of the oroclinal bend (Grantz, 1966; Freeland and Dietz, 1973; Little and Naeser, 1989), Miocene regional uplift and erosion of the forearc (Little and Naeser, 1989), Miocene minor dextral slip along the Castle Mountain fault (Grantz, 1966; Clardy, 1974; Detterman et al., 1976; Bruhn, 1979), and/or Oligocene to Reccent subduction of the Yakutat microplate (Fuis et al., 2008; Finzel et al., 2011).

3.4.4 Gravel Creek area

The Gravel Creek area is located just north of the Border Ranges fault along the southern margin of the Matanuska Valley region (Fig. 3.1). This area is characterized by several northwest-southeast-trending normal faults and faults with unknown sense of slip which juxtapose Paleogene mudstone, siltstone, conglomeratic sandstone, and tuff of the Chickaloon Formation against Jurassic quartz diorite and tonalite (Jqt), Triassic to Jurassic volcaniclastic and sedimentary strata of the Talkeetna Formation (JTrt), and mélange-like assemblages of the McHugh Complex (Fig. 3.9). An Eocene felsic intrusion (Tfp) was observed to the southwest along the contact between Chickaloon strata and assemblages of the McHugh Complex. This contact strikes northwestward and is normally faulted and cross-cuts the larger felsic intrusion with down-to-the-northeast sense of slip (Fig. 3.9). Another normal fault runs parallel just north of this structure across the center of the mapped area but with down-to-the-southwest sense of slip, bounding a package of Chickaloon Formation between these extensional structures. The footwall of this central fault contains weakly deformed Chickaloon strata with an average

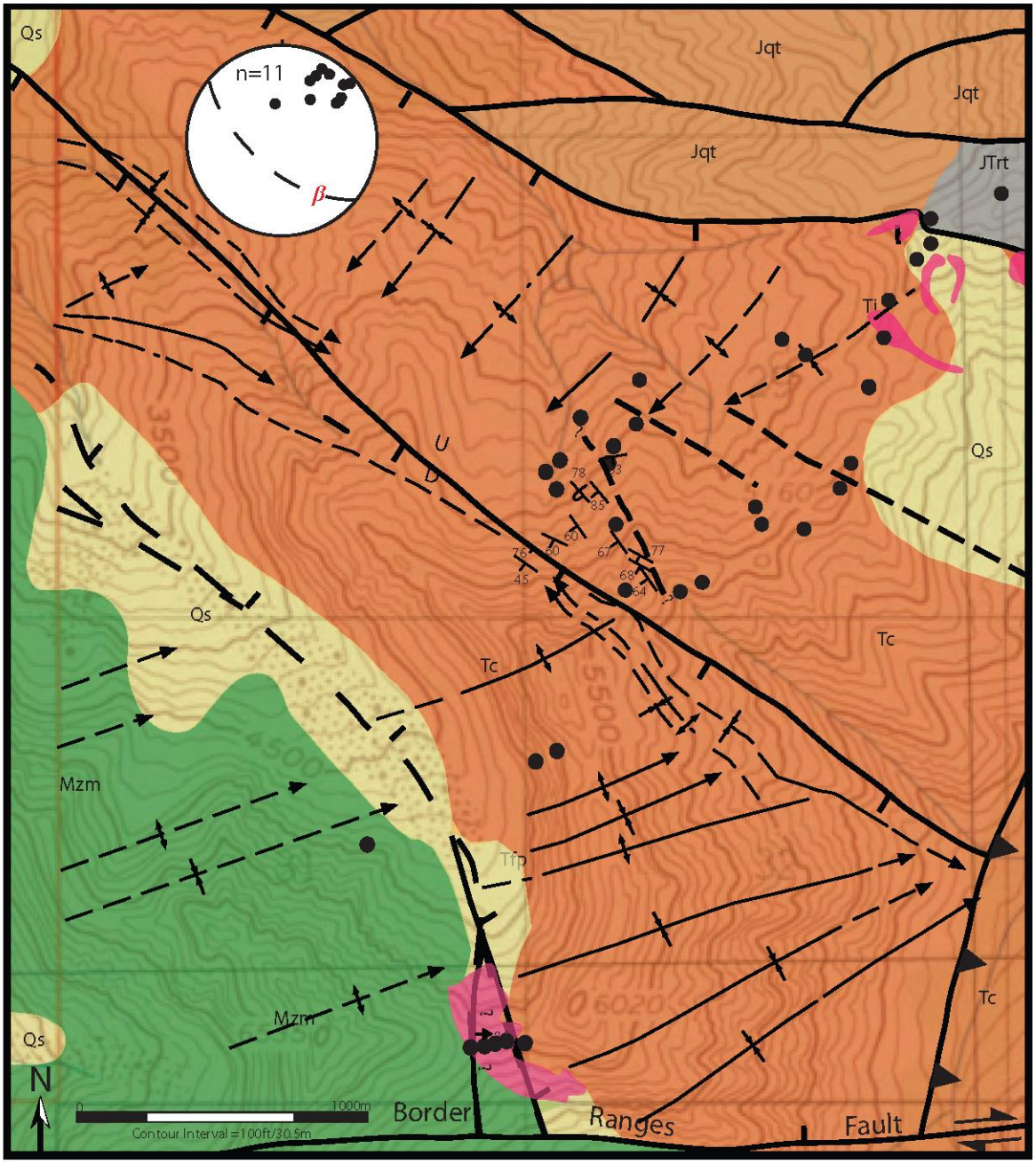

Figure 3.9: Geologic map of the Gravel Creek area north of the Border Ranges Fault along the southern periphery of the Matanuska Valley region (see Fig. 3.1 for location, Fig. 3.3 for key) with data from this study and from Little (1988). Chickaloon average bedding orientation strikes toward an azimuth of 130° dipping 64° degrees to the southwest with a calculated fold axis plunging 31° toward 146°.

bedding orientation striking toward an azimuth of 130° and dipping 64° degrees to the southwest. The calculated fold axis for these beds plunges 31° toward 146° (Fig. 3.9). These beds are intruded by an Eocene hypabyssal felsic intrusion (Ti) mapped in this study just south of the next and northernmost normal fault in the mapped area. This extensional structure trends parallel to the southern two normal faults and is characterized by down-to-the-southwest sense of slip. North of this fault is a series of faulted packages of Chickaloon Formation strata, Jurassic quartz diorite and tonalite, and Talkeetna Formation volcaniclastic and sedimentary strata.

Tuffs sampled from the Chickaloon Formation at Gravel Creek were analyzed for their geochronology in order to better understand the depositional timing for this unit and produce ca. 54 Ma detrital zircon U-Pb ages (Fig. 3.10c) (Trop et al., 2012). This study (Trop et al., 2012) reports that integration of these ages with stratigraphic, geochronologic, and provenance data indicate development of alluvial fan, fluvial, and lacustrine environments in strike-slip pull-apart basins along the southern margin of the forearc basin sourced from proximal uplifted assemblages of the McHugh Complex. These newly published datasets collected in coordination with the material presented in this chapter support multiple stages of forearc system uplift during normal subduction (ca. 75-60 Ma) and spreading ridge subduction (ca. 60-50 Ma; Trop et al., 2012). In addition, fossilized leaves were collected from the Chickaloon Formation to understand the paleogeography during deposition of the unit (Fig. 3.10d). These data will contribute to our understanding of the timing of slab window volcanism, uplift, and subsidence in response to spreading ridge subduction along the southern margin of the Matanuska Valley region.

Extensional structures in the Gravel Creek area overprint Eocene felsic intrusion into the Matanuska and Chickaloon Formations and may have formed coeval with one or multiple of several events that occurred along the region in Eocene time, including (1) strike-slip reactivation of the Border Ranges fault system from 55-45 Ma (Little, 1988; Little and Naeser, 1989); (2) Middle Eocene dextral wrench faulting during a time of transtension

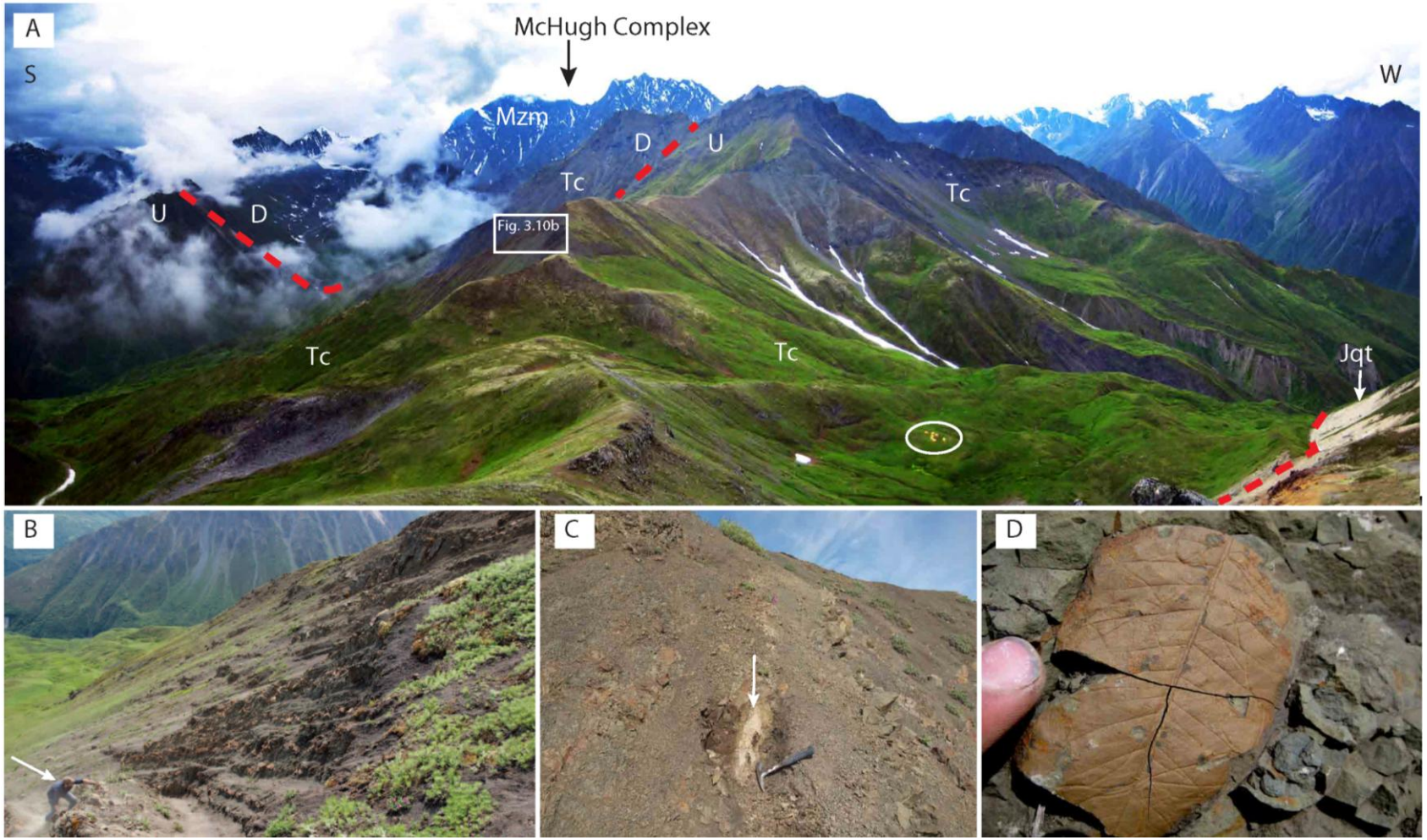

Figure 3.10: Photographs of the Gravel Creek area. (A) View of the Chugach Mtns. from station in NE-most mapped area (Fig. 3.9), looking SE toward normally faulted Chickaloon Fm. strata (dashed). Tents circled for scale. Fluvial-alluvial-lacustrine strata were deposited in strike-slip pull-apart basins sourced by proximal uplifted McHugh Complex (black arrow). Fault-bound packages of Jurassic quartz diorite and tonalite exposed to far right in picture. (B) Inclined sandstone, siltstone, and shale beds of the Chickaloon Fm. (crouching geologist for scale) containing (C) bedded tuff (arrow) with ca. 54 Ma detrital zircon U-Pb ages and (D) well-preserved leaf fossils.

(Little and Naeser, 1989); (3) 44-30 Ma uplift of the forearc basin, unconformity development, and folding of forearc strata into E-NE trending upright folds (Little and Naeser, 1989); (4) pre-late Oligocene development of the oroclinal bend along the Border Ranges fault system (Grantz, 1966; Freeland and Dietz, 1973; Little and Naeser, 1989); or (5) regional uplift of the forearc system during flat-slab subduction of the Yakutat microplate (Finzel et al., 2011).

3.5 Structural cross-section A-A'" of the Matanuska Valley region

Cross-section A-A'" transects the Talkeetna Mountains southeastward across the Matanuska Valley into the Chugach Mountains and thus depicts the structural configuration of the remnant magmatic arc-forearc basin-accretionary prism system (Fig. 3.1). Although the construction of this cross-section utilized bedding measurement data from along the Matanuska Valley region, subsurface interpretations of the remnant forearc basin's configuration are especially complicated by lack of data, along-strike transitions between Tertiary slab window intrusions and Cretaceous and Paleogene strata, and the complexity of fault-slivered igneous and metamorphic assemblages located between exposed strata in the basin (central block, Fig. 3.11) and the metasedimentary mélange of the McHugh Complex (southern block, Fig. 3.11).

The northern block is defined by Jurassic and Cretaceous plutons of the Talkeetna magmatic arc north of the Castle Mountain fault (Figs. 3.1 and 3.11). In the eastern Talkeetna Mountains, zircon U-Pb geochronology has established that the intraoceanic arc was active from 183-153 Ma above a north-dipping subduction zone and was then accreted to North America in Late Jurassic or Early Cretaceous time (Burns, 1985; Plafker et al., 1989; Rioux et al., 2003, 2007; Clift et al., 2005; Hacker et al., 2011). This arc massif is separated from strata of the Matanuska remnant forearc basin to the south by the >200-km-long Castle Mountain fault, northward-dipping, orogen-parallel and high-angle transpressional structure that has experienced at least 3-4 km of reverse slip (Grantz, 1966; Detterman et al., 1976; Bunds, 2001) and over 14 km of Tertiary dextral slip (Grantz, 1966; Fuchs, 1980). This structure is still active and may have originated as

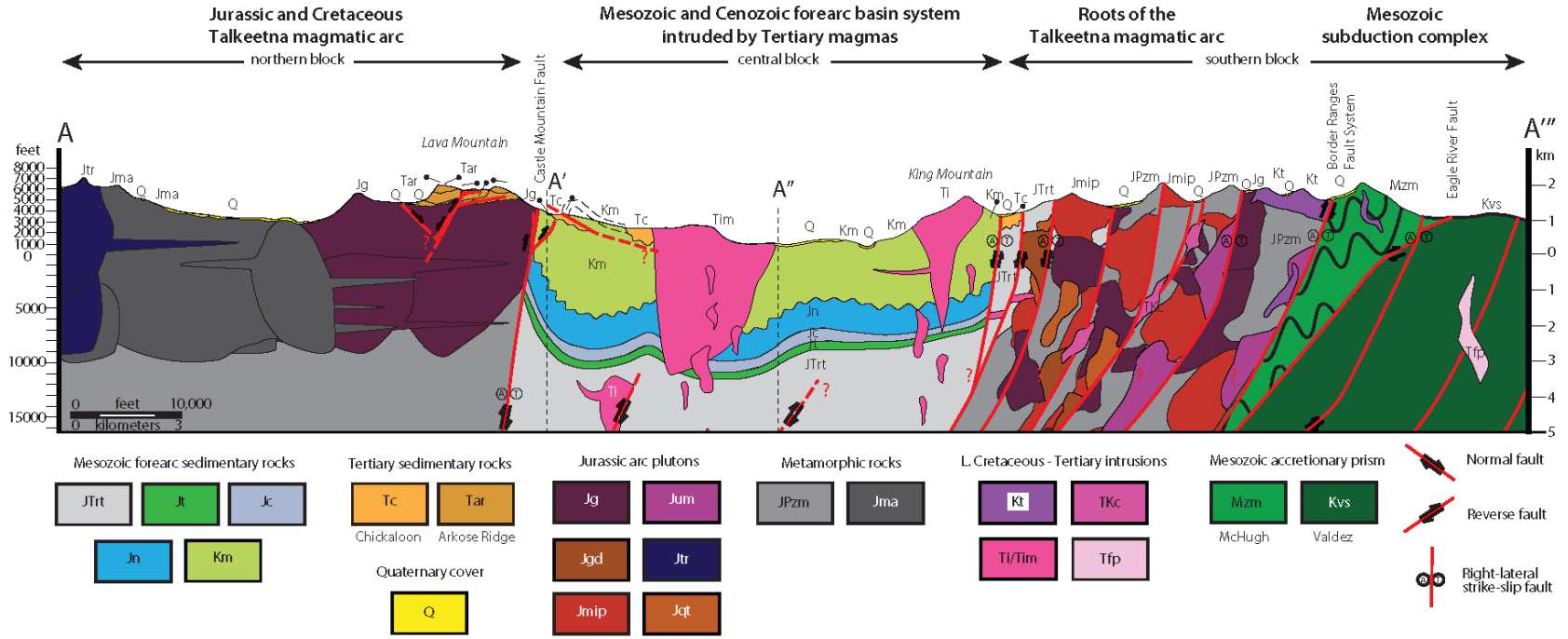

Figure 3.11: Schematic structural cross-section A-A" (see Fig. 3.1 for location) across the Matanuska Valley region from the Talkeetna to the Chugach Mountains. **Northern block**: Jurassic to Cretaceous plutons of the Talkeetna magmatic arc and overlying Paleogene nonmarine strata and volcanic rocks of the Arkose Ridge Formation. **Central block**: Deformed Triassic to Jurassic volcaniclastic and sedimentary strata (JTrt) to Cretaceous marine forearc basin turbidite strata unconformably overlain by Paleogene nonmarine strata and volcanic rocks of the Chickaloon and Wishbone Formations. Both Mesozoic and Tertiary stratigraphic sequences north and south of the Castle Mountain fault are intruded by slab window plutons generated during spreading ridege subduction. **Southern block**: Transpressional thrust slivers of Permo-Jurassic through Cretaceous plutons which comprise the basement of the Wrangellia Composite Terrane beneath the Matanuska remnant forearc basin to the north. Emplacement of these igneous and metamorphic assemblages into this belt of high-angle, mostly dextral strike-slip faults and over metasedimentary accretionary prism strata of the Mesozoic McHugh Complex (Mzm), followed by under-thrusting of the Cretaceous Valdez accretionary complex (Kvs) may reflect structural reconfiguration of the forearc basin system in response to multi-stage normal, spreading ridge, and oceanic plateau subduction beneath the southern Alaskan margin.

early as Late Cretaceous time (e.g., Lahr et al., 1986; Haeussler, 1994; Bunds, 2001; Willis et al., 2007).

Growth synclines in Paleocene-Eocene footwall strata of the Castle Mountain fault provide further evidence for Tertiary displacement (Ridgway et al., 2012). These strata are part of the central block (Fig. 3.11) which is characterized by marine turbidite strata of the Cretaceous Matanuska Formation locally and unconformably overlain by nonmarine strata of the Paleocene-Eocene Chickaloon and Wishbone Formations. These forearc strata are intruded by Tertiary slab window plutons and are deformed into east-northeast trending upright folds in the Matanuska Valley (Little and Naeser, 1989) and are juxtaposed against a fault-slivered, Early Jurassic to Cretaceous igneous and metamorphic assemblage which comprise the northern segment of the southern block (Figs. 3.1 and 3.11).

This faulted, mainly crystalline sequence contains the roots of the Talkeetna intraoceanic arc massif (Fig. 3.11) (Plafker et al., 1989) in an exceptionally well-preserved, 202-181 Ma magmatic arc complex (Hacker et al., 2011) containing sedimentary through volcanic strata and intrusive to mantle rocks (Burns, 1985; DeBari and Sleep, 1991). Fault-slivering of these rocks has been attributed to lateral shuffling within the belt in response to multiple episodes of intra-arc collision events and/or spreading ridge subduction (e.g., Pavlis and Roeske, 2007). This belt has been thrust over more intensely deformed Mesozoic rocks of the Chugach subduction complex to the south along the Border Ranges fault system (Little, 1992). The Border Ranges fault system has been interpreted as a paleosubduction thrust (Clift et al., 2005) which was reactivated as a Cenozoic strike-slip fault with hundreds of kilometers of dextral slip (Pavlis and Roeske, 2007). Tertiary slab window plutons locally intrude both metasedimentary rocks of the subduction complex and the Talkeetna magmatic arc's roots but are overprinted by pervasive strike-slip fault in the southern block (Figs 3.1 and 3.11).

Pavlis and Roeske (2007) have suggested that the Castle Mountain and Border Range fault systems are linked and have experienced ~130 km of Paleogene dextral offset. These authors note that episodic reactivation of this arc-forearc boundary is in part related to the mechanically contrasting rheologies of the crystalline massif of the arc and the accreted oceanic assemblages of the forearc accretionary complex (Pavlis and Roeske, 2007).

Cross-section A-A'" provides one potential explanation for the distribution of these elements in the central and southern blocks. In this schematic representation of the current forearc system, igneous and metamorphic basement assemblages and overlying forearc strata were uplifted, potentially over metasedimentary accretionary prism strata of the Mesozoic McHugh Complex (Mzm), and eroded during multi-stage normal, spreading ridge, and oceanic plateau subduction beneath the southern Alaskan margin. Further investigations of the Paleogene depositional and structural history of the basin need to be conducted in order to better understand how common processes such as spreading ridge and oceanic plateau subduction alter upper plate processes of convergent margins.

3.6 Conclusions

New geologic maps and cross-sections from the Matanuska Valley region of south-central Alaska are presented to contribute to our understanding of how separate periods of normal, spreading ridge, and oceanic plateau subduction have modified the depositional processes and structural configuration of the Matanuska Valley region. The findings of this study and related investigations along the south-central Alaskan convergent margin will provide valuable information regarding how upper plate processes along convergent margins are affected by common subduction processes such as spreading ridge and flat-slab subduction.

REFERENCES

REFERENCES

Adams, M.A., 1984, Geologic overview, coal resources, and potential methane recovery from coalbeds of the central Appalachian Basin—Maryland, West Virginia, Kentucky, and Tennessee. *In* Rightmire, C.T., Eddy, G.E., and Kirr, J.N., eds., Coalbed Methane Resources of the United States. *American Association of Petroleum Geologists Studies in Geology*, v. 17, p. 45–72.

Al-Tawil, A., and Read, J.F., 2003, Late Mississippian (Late Meramecian-Chesterian), glacio-eustatic sequence development on an active distal foreland ramp, Kentucky, U.S.A. *In* Harris, P.M., Morgan, W.A., and Somerville, I.D., eds., Permo-Carboniferous Carbonate Platforms and Reefs. *SEPM Special Publication 78 and American Association of Petroleum Geologists Memoir 83*, p. 35-55.

Al-Tawil, A., Wynn, T.C., and Read, J.F., 2003, Sequence response of a distal-to-proximal foreland ramp to glacio-eustasy and tectonics: Mississippian, Appalachian Basin, West Virginia-Virginia, USA. *In* Harris, P.M., Morgan, W.A., and Somerville, I.D., eds., Permo-Carboniferous Carbonate Platforms and Reefs. *SEPM Special Publication 78 and American Association of Petroleum Geologists Memoir 83*, p. 11-34.

Amato, J.M., and Pavlis, T.L., 2010, Detrital zircon ages from the Chugach terrane, southern Alaska, reveal multiple episodes of accretion and erosion in a subduction complex. *Geology*, v. 38, n. 5, p. 459-462.

Amato, J.M., Pavlis, T.L., Clift, P.D., Kochelek, E.J., Hecker, J.P., Worthman, C.M., and Day, E.M., 2013, Architecture of the Chugach accretionary complex as revealed by detrital zircon ages and lithologic variations: evidence for Mesozoic subduction erosion in south-central Alaska. *Geological Society of America Bulletin*, v. 125, n. 11/12, p. 1891-1911.

Archer, A.W., and Greb, S.F., 1995, An Amazonian-scale drainage system in the Early Pennsylvanian of central North America. *Journal of Geology*, v. 103, n. 6, p. 611-627.

Bambach, R.K., 1983, Ecospace utilization and guilds in marine communities through the Phanerozoic. *In* Tevesz, M. J. S., and McCall, P. L., eds., *Biotic Interactions in Recent and Fossil Benthic Communities*, New York, Plenum Press, p. 719–746.

Bartholomew, M.J., and Whitaker, A.E., 2010, The Alleghanian deformational sequence at the foreland junction of the central and southern Appalachians. *In* Tollo, R.P., Bartholomew, M.J., Hibbard, J.P., and Karabinos, P.M., eds., From Rodinia to Pangea: The Lithotectonic Record of the Appalachian Region. *Geological Society of America Memoir 206*, p. 431-454.

Bates, C.C., 1953, Rational theory of delta formation. *American Association of Petroleum Geologists Bulletin*, v. 37, p. 2119-2162.

Bathurst, R.G.C., 1972, *Carbonate sediments and their diagenesis: Developments in Sedimentology*, v. 12, Elsevier, New York, NY, 620 p.

Beaumont, C., Quinlan, G.M., and Hamilton, J., 1987, The Alleghenian orogeny and its relationship to the evolution of the eastern interior, North America. *In* Beaumont, C., and Tankard, A.J., eds., Sedimentary Basins and Basin-Forming Mechanisms, *Canadian Society of Petroleum Geologists Memoir 12*, p. 425-445.

Becker, T.P., Thomas, W.A., Samson, S.D., and Gehrels, G.E., 2005, Detrital zircon evidence of Laurentian crustal dominance in the lower Pennsylvanian deposits of the Alleghanian clastic wedge in eastern North America. *Sedimentary Geology*, v. 182, p. 59-86.

Becker, T.P., Thomas, W.A., and Gehrels, G.E., 2006, Linking late Paleozoic sedimentary provenance in the Appalachian basin to the history of Alleghanian deformation. *American Journal of Science*, v. 306, p. 777-798.

Behrmann, J.H., Lewis, S.D., Musgrave, R., Bangs, N., Boden, P., Brown, K., Collombat, H., Didenko, A.N., Didyk, B.M., Froelich, P.N., Golovchenko, X., Forsythe, R., Kurnosov, V., Lindsley-Griffin, N., Marsaglia, K., Osozawa, S., Prior, D., Sawyer, D., Scholl, D., Spiegler, D., Strand, K., Takahashi, K., Torres, M., Vega Faundez, M., Vergara, H., and Waseda, A., 1994, Tectonics and geology of spreading ridge subduction at the Chile triple junction; a synthesis of results from Leg 141 of the Ocean Drilling Program. *Geologische Rundschau*, v. 83.4, p. 832-852.

BeMent, W.O., 1976, Sedimentological aspects of Middle Carboniferous sandstone on the Cumberland overthrust sheet. Unpublished Doctoral dissertation, University of Cincinnati, Cincinnati, OH, 182 p.

Bhattacharya, J.P., 2006, Deltas. *In* Posamentier, H.W. and Walker, R.G., eds., Facies Models Revisited. *SEPM Special Publication 84*, p. 237-292.

Bhattacharya, J.P., and Walker, R.G., 1991, River- and wave-dominated depositional systems of the Upper Cretaceous Dunvegan Formation, northwestern Alberta. *Bulletin of Canadian Petroleum Geology*, v. 39, n. 2, p. 165-191.

Black, L., Kamo, S., Allen, C., Davis, D., Aleinikoff, J., Valley, J., Mundil, R., Campbell, I., Korsch, R., Williams, I., and Foudoulis, C., 2004, Improved 206Pb/238U microprobe geochronology by the monitoring of a trace-element-relaxed matrix effect; SHRIMP, ID-TIMS, ELA-ICP-MS and oxygen isotope documentation for a series of zircon standards. *Chemical Geology*, v. 205, p. 115-140.

Blakey, R., 2008, Paleogeography and geologic evolution of North America, http://cpgeosystems.com/nam.html.

Blakey, R., 2013, Key time slices of North American geologic history, http://cpgeosystems.com/namkeypaleogeography.html.

Blatt, H., Middleton, G.V., and Murray, R., 1980, *Origin of Sedimentary Rocks*, *2nd edition*, Prentice-Hall, Englewood Cliffs, N.J., 782 p.

Bleick, H.A., Till, A.B., Bradley, D.C., O'Sullivan, P.B., Wooden, J.L., Bradley, D.B., Taylor, T.A., Friedman, S.B., and Hults, C.P. , 2012, Early Tertiary exhumation of the flank of a forearc basin, southwest Talkeetna Mountains, Alaska. *U.S. Geological Survey Open-File Report 2012–1232*.

Bodek, R.J., Jr., 2006, Sequence stratigraphic architecture of early Pennsylvanian, coal-bearing strata of the Cumberland block: a case study from Dickenson County, Virginia. Unpublished Master's thesis, Polytechnic Institute and State University, Blacksburg, VA, 72 p.

Bouma, A.H., 1962, *Sedimentology of some flysch deposits: a graphic approach to facies interpretation*. Elsevier, Amsterdam, 168 p.

Boyd, R., Dalrymple, R.W., and Zaitlin, B.A., 2006, Estuarine and incised-valley fill models. *In* Posamentier, H.W. and Walker, R.G., eds., Facies Models Revisited. *SEPM Special Publication 84,* p. 171-235.

Bradley, D.C., Parrish, R., Clendenen, W., Lux, D., Layer, P.W., Heizler, M., and Donley, D.T., 1998, New geochronological evidence for the timing of Early Tertiary ridge subduction in southern Alaska. *Geological Studies in Alaska by the U.S. Geological Survey, U.S. Geological Survey Professional Paper 1615*, p. 5-21.

Bradley, D.C., Kusky, T.M., Haeussler, P.J., Goldfarb, R.J., Miller, M.L., Dumoulin, J.A., Nelson, S.W., and Karl, S. M., 2003, Geologic signature of early Tertiary ridge subduction in Alaska. *In* Sisson, V.B., Roeske, S.M., and Pavlis, T.L., Geology of a transpressional orogen developed during ridge-trench interaction along the north Pacific margin*, Geological Society of America Special Paper 371*, p. 19–49.

Bridge, J.S., 2003, *Rivers and floodplains: Forms, Processes, and Sedimentary Record*. Blackwell Publishing, Oxford, p. 504.

Bridge, J.S., 2006, Fluvial faces models: recent developments. *In* Posamentier, H.W. and Walker, R.G., eds., Facies Models Revisited, *SEPM Special Publication 84*, p. 85-170.

Bruhn, R.L., 1979, Holocene displacements measured by trenching the Castle Mountain Fault near Houston, Alaska. *Geological report, Alaska Division of Geological and Geophysical Surveys*, v. 61.

Bruhn, R.L., and Pavlis, T.L, 1981, Late Cenozoic deformation in the Matanuska Valley, Alaska: three-dimensional strain in a forearc region. *Geological Society of America Bulletin, Part I*, v. 92, p. 282-293.

Bunds, M. P., 2001, Fault strength and transpressional tectonics along the castle Mountain strike-slip fault, southern Alaska. *Geological Society of America Bulletin*, v. 113, n. 7, p. 908- 919.

Burns, L.E., 1985, The Border Ranges ultramafic and mafic complexes, south-central Alaska: Cumulate fractionates of island-arc volcanic. *Canadian Journal of Earth Sciences*, v. 22, p. 1020-1038.

Cande, S.C., and Leslie, R.B., 1986, Late Cenozoic tectonics of the southern Chile Trench. *Journal of Geophysical Research*, v. 91, p. 471-496.

Canfield, D.E., 1994, Factors influencing organic carbon preservation in marine sediments. *Chemical Geology*, v. 114, p. 315-329.

Cecil, C.B., Brezinski, D., and DuLong, F., 2004, The Paleozoic record of changes in global climate and sea level: central Appalachian basin. *In* Southworth, S., and Burton, W., eds., Geology of the National Capital Region—Field trip guidebook. *U.S. Geological Survey Circular 1264*, p. 77–135.

Chesnut, D.R., Jr., 1991, Timing of Alleghenian tectonics by central Appalachian foreland basin analysis. *Southeastern Geology*, v. 31, n. 4, p. 203-221.

Chesnut, D.R., Jr., 1992, Stratigraphic and structural framework of the Carboniferous rocks of the central Appalachian basin in Kentucky. *Kentucky Geological Survey*, ser. 11, bulletin 3, 42 p.

Chesnut, D.R., Jr., 1993, Eustatic and tectonic control of sedimentation in the Pennsylvanian strata of the Central Appalachian Basin, USA. *Douzieme Congres International de la Stratigraphie et geologie du Carbonifere et Permien, Buenos Aires, 22-27 Septembre 1991, Comptes Rendus*, v. 2, p. 421-430.

Chesnut, D.R., Jr., 1994, Eustatic and tectonic control of deposition of the Lower and Middle Pennsylvanian strata of the central Appalachian Basin. *In* Dennison, J.M., and Ettensohn, F.R., eds., Tectonic and Eustatic Controls on Sedimentary Cycles. *Society for Sedimentary Geology, Concepts in Sedimentology and Paleontology*, no. 4, p. 51–64.

Chesnut, D.R., Jr., 1996, Geologic framework for the coal-bearing rocks of the central Appalachian Basin. *International Journal of Coal Geology*, v. 31, p. 55–66.

Chesnut, D.R., Jr., Eble, C.F., Greb, S.F., and Dever, G.R., 1998, Geology of Pound Gap Roadcut, Letcher County, Kentucky. *Kentucky Society of Professional Geologists*, 169 p.

Ciolkosz, E.J., Petersen, G.W., and Cunningham, R.L., 1979, Landslide-prone soils of southwestern Pennsylvania. *Soil Science*, v. 128, p. 348-352.

Clardy, B.I., 1974, Origin of the lower and middle Tertiary Wishbone and Tsadaka Formations, Matanuska Valley, Alaska. Unpublished M.S. thesis, University of Alaska, Fairbanks, AK, 50 p.

Clift, P.D., Pavlis, T., DeBari, S.M., Draut, A.E., Rioux, M., Kelemen, P.B., 2005, Subduction erosion of the Jurassic Talkeetna-Bonanza arc and the Mesozoic accretionary tectonics of western North America. *Geology*, v. 33, n. 11, p. 881-884.

Clifton, H.E., 1976, Wave-formed sedimentary structures—a conceptual model. *In* Davis, R.A., and Ethington, R.L., eds., Beach and Nearshore Processes. *Society of Economic Paleontologists and Mineralogists Special Publication 24*, p. 126–148.

Clifton, H.E., and Dingler, J.R., 1984, Wave-formed structures and paleoenvironmental reconstruction. *In* Greenwood, B., and Davis, R.A., Jr., eds., Hydrodynamics and Sedimentation in Wave-Dominated Coastal Environments. *Marine Geology*, v. 60, p. 165-198.

Cole, R.B., and Stewart, B.S., 2008, Continental margin volcanism at sites of spreading ridge subduction: examples from southern Alaska and western California. *Tectonophysics*, v. 464, p. 118-136.

Cole, R.B., Nelson, S.W., Layer, P.W., and Oswald, P.J., 2006, Eocene volcanism above a depleted mantle slab window in southern Alaska. *Geological Society of America Bulletin*, v. 118 n. 1/2, p. 140–158.

Collinson, C.W., Rexroad, C.B., and Thompson, T.L., 1971, Conodont zonation of the North American Mississippian. *In* Sweet, W.C., and Bergstrom, S.M., eds., Symposium on Conodont Biostratigraphy. *Geological Society of America Memoir 127*, p. 353–394.

Cooper, B.N., 1948, Status of Mississippian stratigraphy in the central and northern Appalachian region. *Journal of Geology*, v. 56, n. 4, p. 255-263.

Covault, J.A., 2011, Submarine fans and canyon-channel systems: a review of processes, products, and models. *Nature Education Knowledge*, v. 3, iss. 10, n.4, 13 p.

Crimes, T.P., Goldring, R., Homewood, P., van Stuijvenberg, J., and Winkler, W., 1981, Trace fossil assemblages of deep-sea fan deposits, Gurnigel and Schlieren flysch (Cretaceous-Eocene), Switzerland. *Eclogae Geologicae Helvetiae*, v. 74, p. 953–995.

Dallmeyer, R.D., Wright, J.E., Secor, D.T., Jr., and Snoke, A.W., 1986, Character of the Alleghanian orogeny in the southern Appalachians: Part II. Geochronological constraints on the tectonothermal evolution of the eastern Piedmont in South Carolina. *Geological Society of America Bulletin*, v. 97, p. 1329-1344.

Dalrymple, R.W., 1992, Tidal depositional systems. *In* Walker, R.G., and James, N.P., eds., Facies Models: Response to Sea Level Change. *Geological Association of Canada, St. John's*, p. 195–218.

Dalyrmple, R.W., and Choi, K., 2007, Morphologic and facies trends through the fluvial–marine transition in tide-dominated depositional systems: a schematic framework for environmental and sequence-stratigraphic interpretation. *Earth-Science Reviews*, v. 81, p. 135-174.

DeBari, S.M., and Sleep, N.H., 1991, High-Mg, low-Al bulk composition of the Talkeetna island arc, Alaska: implications for primary magmas and the nature of arc crust. *Geological Society of America Bulletin*, v. 103, p. 37-47.

DeCelles, P.G., Langford, R.P., and Schwartz, R.K., 1983, Two new methods of paleocurrent determination from trough cross-stratification. *Journal of Sedimentary Petrology*, v. 53, n. 2, p. 629-642.

DeMaison, G.J., and Moore, G.T., 1980, Anoxic environments and oil source bed genesis. *Organic Geochemistry*, v. 2, p. 9-31.

Demmin, G.A., 1999, Lithofacies analysis of the Greenbrier Limestone in Frazier Quarry, southeastern West Virginia, and the Newman Limestone at Pound Gap, east-central Kentucky. Unpublished Master's thesis, University of Akron, Akron, OH, 74 p.

Dennis, A.J., 2007, Cat Square basin, Catskill clastic wedge: Silurian-Devonian orogenic events in the central Appalachians and the crystalline southern Appalachians. *In* Sears, J.W., Harms, T.A., and Evenchick, C.A., eds., Whence the Mountains? Inquiries into the Evolution of Orogenic Systems: A Volume in Honor of Raymond A. Price. *Geological Society of America Special Paper 433*, p. 313-329.

Dennis, A.J., and Wright, J.C., 1997, Middle and late Paleozoic monazite U-Pb ages, Inner Piedmont, South Carolina. *Geological Society of America Abstracts with Programs*, v. 29, no. 3, p. 12.

Detterman, R.L., Plafker, G., Russell, G.T., and Hudson, T., 1976, Features along part of the Talkeetna segment of the Castle Mountain–Caribou fault system, Alaska. *U.S. Geological Survey Miscellaneous Field Studies Map MF-738*, scale 1:63,360.

Dever, G.R., Jr., 1977, The lower Newman Limestone: Stratigraphic evidence for Late Mississippian tectonic activity. *In* Dever, G.R., Jr., Hoge, H.P., Hester, N.C., and Ettensohn, F.R., eds., Stratigraphic evidence for late Paleozoic tectonism in northeastern Kentucky (Guidebook and road log for field trip held in conjunction with the fifth annual meeting of the eastern section of the American Association of Petroleum Geologists and the 1977 field conference of the Geological Society of Kentucky). *Kentucky Geological Survey*, ser. 10, p. 8–18.

Dever, G.R., Jr., 1980, The Newman Limestone: an indicator of Mississippian tectonic activity in northeastern Kentucky. *In* Luther, M.K., ed., Proceedings of the Technical Sessions Kentucky Oil and Gas Association Thirty-sixth and Thirty-seventh Annual Meetings, 1972 and 1973. *Kentucky Geological Survey*, ser. 11, p. 42-54.

Dever, G.R., Jr., 1999, Tectonic implications of erosional and depositional features in upper Meramecian and lower Chesterian (Mississippian) rocks of south-central and east-central Kentucky. *Kentucky Geological Survey*, ser. 11, bulletin 5, p. 67-134.

Dever, G.R., Jr., Hoge, H.P., Hester, N.C., and Ettensohn, F.R., 1977, Stratigraphic evidence for late Paleozoic tectonism in northeastern Kentucky: field trip guidebook, Eastern Section, American Association of Petroleum Geologists, *Kentucky Geological Survey*, ser. 10, 80 p.

de Witt, W., Jr., 1993, Principal oil and gas plays in the Appalachian basin (province 131). *In* de Witt, W., Jr., ed., Evolution of Sedimentary Basins—Appalachian Basin. *U.S. Geological Survey Bulletin 1839–I*, 37 p.

de Witt, W., Jr., and McGrew, L.W., 1979, The Appalachian basin. *In* Craig, L.C., and Connor, C.W., coordinators, Paleotectonic Investigations of the Mississippian System in the United States. *U.S. Geological Survey Professional Paper 1010, Part I*, p. 59–106.

de Witt, W., Jr., and Milici, R.C., 1989, Energy resources of the Appalachian orogen. *In* Hatcher, R.D., Jr., Thomas, W.A., and Viele, G.W., eds., The Appalachian-Ouachita Orogen in the United States. *Geological Society of America, The Geology of North America*, v. F-2, p. 495-510.

Dickinson, W.R., and Seely, D.R., 1979, Structure and stratigraphy of forearc regions. *American Association of Petroleum Geologists Bulletin*, v. 63, p. 2-31.

DiMichele, W.A., Stein, W.E., and Bateman, R.M., 2001, Ecological sorting of vascular plants classes during the Paleozoic evolutionary radiation. *In* Allmon, W.D., and Bottjer, D.J., eds., *Evolutionary Paleoecology: The Ecological Context of Macroevolutionary Change*. Columbia University Press, New York, NY, p. 285–335.

Donaghy, E., 2012, Sedimentology, depositional age, and provenance of sedimentary and volcanic rocks exposed along Willow Creek, eastern Susitna Basin, south-central Alaska: implications for modification of a forearc basin by spreading ridge subduction. Unpublished B.S. thesis, Bucknell University, Lewisburg, PA.

D'Orazio, M., Agostini, S., Innocenti, F., Haller, J.J., Manetti, P., and Mazzarini, F., 2001, Slab window-related magmatism from southernmost south America: the Late Miocene mafic volcanic from the Estancia Glencross Area (52°S, Argentina-Chile). *Lithosphere*, v. 57, p. 67-89.

Dunham, R.J., 1962, Classification of carbonate rocks according to depositional texture. *In* Ham, W.E., Classification of Carbonate Rocks. *American Association of Petroleum Geologists Memoir 1*, p. 108-121.

Espinoza, F., Morata, D., Polve, M., Lagabrielle, Y., Maury, R.C., Guivel, C., Cotten, J., Bellon, H., and Suarez, M., 2008, Bimodal back-arc alkaline magmatism after ridge subduction; Pliocene felsic rocks from central Patagonia (47°S). *Lithosphere*, v. 101.3-4, p. 191-217.

Ettensohn, F.R., 1980, An alternative to the barrier-shoreline model for deposition of Mississippian and Pennsylvanian rocks in northeastern Kentucky: summary. *Geological Society of America Bulletin, Part. I*, v. 91, p. 130-135.

Ettensohn, F.R., 1985, The Catskill delta complex and the Acadian orogeny: a model. *In* Woodrow, D.L., and Sevon, W.D., eds., The Catskill Delta. *Geological Society of America Special Paper 201*, p. 39–49.

Ettensohn, F.R., 1987, Rates of relative plate motion during the Acadian orogeny based on the spatial distribution of black shales. *Journal of Geology*, v. 95, p. 572–582.

Ettensohn, F.R., 1992, Controls on the origin of Devonian-Mississippian oil and gas shales, east-central United States. *Fuel*, v. 71, p. 1487-1492.

Ettensohn, F.R., 1994, Tectonic control on formation and cyclicity of major Appalachian unconformities and associated stratigraphic sequences. *In* Dennison, J.M., and Ettensohn, F.R., eds., Tectonic and Eustatic Controls on Sedimentary Cycles. *SEPM Concepts in Sedimentology and Paleontology*, v. 4, p. 217–242.

Ettensohn, F.R., 2004, Modeling the nature and development of major Paleozoic clastic wedges in the Appalachian Basin, USA. *Journal of Geodynamics*, v. 37, p. 657–681.

Ettensohn, F. R., 2008, The Appalachian Foreland Basin in Eastern United States. *In* Hsü, K.J., ed., *Sedimentary Basins of the World, v. 5, The Sedimentary Basins of the United States and Canada*, Elsevier, Amsterdam, p. 105-179.

Ettensohn, F.R., and Barron, L.S., 1981, Depositional model for the Devonian-Mississippian black-shale sequence of North America: a tectono-climatic approach. *Technical Information Center, U.S. Department of Energy*, DOE/METC/12040-2, 80 p.

Ettensohn, F.R., and Chesnut, D.R., 1985, Depositional environments and stratigraphy of the Pennington Formation (Upper Visean-Namurian A), east-central and eastern Kentucky, U.S.A. *In* Escobedo, J.L., et al., eds., *Compte Rendu, Dixième Congrès International de Stratigraphic et de Géologie du Carbonifère, Madrid*, v. 3, p. 269-283.

Ettensohn, F.R., and Elam, T.D., 1985, Defining the nature and location of a Late Devonian-Early Mississippian pycnocline in eastern Kentucky. *Geological Society of America Bulletin*, v. 96, p. 1313-1321.

Ettensohn, F.R., Dever, G.R., and Grow, J.S., 1988, A paleosol interpretation for profiles exhibiting subaerial exposure "crusts" from the Mississippian of the Appalachian basin. *Geological Society of America Special Paper 216*, p. 49-80.

Ettensohn, F.R., and Chesnut, Jr., D.R., 1989, Nature and probable origin of the Mississippian-Pennsylvanian unconformity in the eastern United States. *In* Yugan, J., and Chun, L., eds., *Compte Rendu, Onzième Congrès International de Stratigraphie et de Géologie du Carbonifère*,.Nanjing University Press, Nanjing, v. 4, p.145–159.

Ettensohn, F.R., Greb, S.F., Chesnut, D.R., Jr., Harris, D.C., Mason, C.E., Eble, C.F., Howell, P.D., Watson, A.E., and Johnson, W.K., 2002, Mississippian stratigraphy, depositional environments, and tectonic framework of the central Appalachian basin, eastern Kentucky, U.S.A. *In* Hills, L.V., Henderson, C.M., and Bamber, E.W., eds., Carboniferous and Permian of the World. *Canadian Society of Petroleum Geologists Memoir 19*, p. 22-40.

Ettensohn, F.R., Lierman, R.T., Udgata, D.B.P., and Mason, C.E., 2012, The Early-Middle Mississippian Borden–Grainger–Fort Payne delta/basin complex: Field evidence for delta sedimentation, basin starvation, mud-mound genesis, and tectonism during the Neoacadian Orogeny. *In* Eppes, M.C., and Bartholomew, M.J., eds., From the Blue Ridge to the Coastal Plain: Field Excursions in the Southeastern United States. *Geological Society of America Field Guide 29*, p. 345–395.

Evans, O.F., 1941, The classification of wave-formed ripple marks. *Journal of Sedimentary Research*, v. 11, n. 1, p. 37-41.

Falcon-Lang, H.J., 2004, Early Mississippian lycopsid forests in a delta-plain setting at Norton, near Sussex, New Brunswick, Canada. *Journal of the Geological Society*, London, v. 161, p. 969-981.

Fildani, A., Shultz, M.R., Graham, S.A., and Leier, A., 2007, A deep-water amalgamated sheet system, Punta Barrosa Formation, Marina's Cliff, Chile. *In* Nilsen, T., Shew, R., Steffens, G., and Studlick, J., eds., Deep-water Outcrops of the World Atlas. *American Association of Petroleum Geologists Studies in Geology*, v. 56, p. 125-127.

Finzel, E.S., Trop, J.M., Ridgway, K.D., and Enkelmann, E., 2011, Upper plate proxies for flat-slab subduction processes in southern Alaska. *Earth and Planetary Science Letters*, v. 303, 13 p.

Fisher, W.L., Brown, L.F., Scott, A.J., and McGowen, J.H., 1969, Delta systems in the exploration for oil and gas, a research colloquium. *Texas Bureau of Economic Geology*, Austin, TX, 204 p.

FitzGerald, D., Buynevich, I., and Hein, C., 2012, Morphodynamics and facies architecture of tidal inlets and tidal deltas. *In* Davis, R.A., Jr., and Dalrymple, R.W., eds., *Principles of Tidal Sedimentology*, Springer Science+Business Media B.V., Netherlands, p. 301-334.

Flores, R.M., and Stricker, G.D., 1993, Early Cenozoic depositional systems, Wishbone Hill district, Matanuska coal field, Alaska. *U.S. Geological Survey Bulletin*, v. 1992, p. 101-117.

Freeland, G.L, and Dietz, R.S., 1973, Rotation history of Alaskan tectonic blocks. *Tectonophysics*, v. 18, n. 3-4, p. 322-332.

Fuchs, W. A., 1980, Tertiary tectonic history of the Castle Mountain–Caribou fault system in the Talkeetna Mountains, Alaska. Unpublished dissertation, University of Utah, UT, 150 p.

Fuis, G.S., Moore, T.E., Plafker, G., Brocher, T.M., Fisher, M. A., Mooney, W.D., Nokleberg, W.J., Page, R.A., Beaudoin, B.C., Christensen, N.I., Levander, A.R., Lutter, W. J., Saltus, R.W., and Ruppert, N.A., 2008, Trans-Alaska crustal transect and continental evolution involving subduction underplating and synchronous foreland thrusting. *Geology*, v. 36, p. 267–270.

Gehrels, G. E., Valencia, A., and Pullen, A., 2006, Detrital zircon geochronology by laser ablation multicollector ICPMS at the Arizona LaserChron Center. *In* Olszewski, T. ed., Geochronology: Emerging opportunities, *Paleontological Society Paper 12*, p. 67–76.

Gehrels, G.E., Valencia, V., and Ruiz, J., 2008, Enhanced precision, accuracy, efficiency, and spatial resolution of U-Pb ages by laser ablation-multicollector-inductively coupled plasma-mass spectrometry. *Geochemistry, Geophysics, Geosystems*, v. 9, Q03017.

Gehrels, G.E., Blakey, R., Karlstrom, K.E., Timmons, J.M., Dickinson, B., and Pecha, M., 2011, Detrital zircon U-Pb geochronology of Paleozoic strata in the Grand Canyon, Arizona. *Lithosphere*, v. 3, p. 183-200.

Goldberg, S.A., and Dallmeyer, R.D., 1997, Chronology of Paleozoic metamorphism and deformation in the Blue Ridge thrust complex, North Carolina and Tennessee. *American Journal of Science*, v. 297, p. 488-526.

Gorring, M.L., and Kay, S.M., 2001, Mantle processes and sources of Neogene slab window magmas from southern Patagonia, Argentina. *Journal of Petrology*, v. 42, p. 1067-1094.

Grabowski, G.J., Jr., 1986, Mississippian system. *U.S. Geological Survey Professional Paper 1151-H*, p. 19-31.

Gradstein, F.M., Ogg, J.G., Schmitz, M.D., and Ogg, G.M., 2012, *The Geologic Time Scale 2012*, Elsevier, 1176 p.

Grantz, A., 1960, Strike-slip faults in Alaska. *U.S. Geological Survey Open-File Report 66-53*, 82 p.

Gray, M.B., and Nickelson, R.P., 1989, Pedogenic slickensides, indicators of strain and deformation processes in redbed sequences of the Appalachian foreland. *Geology*, v. 17, p. 72-75.

Gray, M.B., and Zeitler, P.K., 1997, Comparison of clastic wedge provenance in the Appalachian foreland using U-Pb ages of detrital zircons. *Tectonics*, v. 16, n. 1, p. 151-160.

Greb, S.F., and Chesnut, D.R., Jr., 1996, Lower and lower Middle Pennsylvanian fluvial to estuarine deposition, central Appalachian basin—Effects of eustacy, tectonics, and climate. *Geological Society of America Bulletin*, v. 108, p. 303-317.

Greb, S.F., and Eble, C.F., 1998, The Mississippian-Pennsylvanian Boundary at Pound Gap. *In* Ettensohn, F.R., and Chesnut, D.R., Jr., eds., Geology of the Pound Gap Roadcut, Letcher County, Kentucky. *Kentucky Society of Professional Geologists*, p. 9-13.

Greb, S.F., Chesnut, D.R., Jr., Dever, G.R., Jr., Harris, D.C., Eble, C.F., Andrews, W.M., Ettensohn, F.R., Howell, P.D., Mason, C.E., Caudill, M.R., Houck, K,J., and Nelson, W., J., 2002, Pound Gap—A new reference section for Mississippian strata on Pine Mountain, central Appalachian basin, USA. *In* Hills, L.V., Henderson, C.M., and Bamber, E.W., eds., Carboniferous and Permian of the World. *Canadian Society of Petroleum Geologists Memoir 19*, p. 696-709.

Greb, S.F., and Martino, R.L., 2005, Fluvial-estuarine transitions in fluvial-dominant successions; examples from the Lower Pennsylvanian of the central Appalachian basin. *In* Blum, M., ed., Fluvial Sedimentology VII. *International Association of Sedimentologists Special Publication 35*, p. 425-452.

Greb, S.F., Pashin, J.C., Martino, R.L., Eble, C.F., 2008, Appalachian sedimentary cycles during the Pennsylvanian: changing influences of sea level, climate, and tectonics. *In* Fielding, C.R., Frank, T.D., and Isbell, J.L., eds., Resolving the Late Paleozoic Ice Age in Time and Space. *Geological Society of America Special Paper 441*, p. 235–248.

Grimm, R.P., Eriksson, K., and Carbaugh, J., 2013, Tectono-sedimentary evolution of early Pennsylvanian alluvial systems at the onset of the Alleghanian orogeny, Pocahontas basin, Virginia. *Basin Research*, v. 25, p. 450-470.

Hacker, B.R., Kelemen, P.B., Rioux, M., McWilliams, M.O., Gans, P.B., Reiners, P.W., Layer, P.W., Söderlund, U., and Vervoort, J.D., 2011, Thermochronology of the Talkeetna intraoceanic arc of Alaska: Ar/Ar, U-Th/He, Sm-Nd, and Lu-Hf dating. *Tectonics*, v. 30, 23 p.

Hadding, A.R., 1933, *The pre-Quaternary sedimentary rocks of Sweden: VI. Reef limestones*. Lund Universitet, Lund, Scania, Sweden, v. 37, n. 10, 88 p.

Haeussler, P.J., 1994, Possible active fault traces on or near the Castle Mountain Fault between Houston and the Hatcher Pass Road. *In* Till, A.B. and Moore, T.E., eds., Geologic Studies in Alaska by the U.S. Geological Survey, 1993. *U.S. Geological Survey Bulletin 2107*, p. 49-58.

Hampson, G.J., 2008, Recent advances in modeling siliciclastic shallow-marine stratigraphy. *In* Hampson, G.J., Steel, R.J., and Burgess, P.M., eds., *SEPM Society for Sedimentary Geology Special Publication 90*, 497 p.

Hasson, K.O., 1972, Lithostratigraphy of the Grainger Formation (Mississippian), northeast Tennessee. Unpublished Doctoral dissertation, University of Tennessee, Knoxville, TN, 143 p.

Hatcher, R.D., Jr., 2010, The Appalachian orogen: a brief summary. *In* Tollo, R.P., Bartholomew, M.J., Hibbard, J.P., and Karabinos, P.M., eds., From Rodinia to Pangea: The Lithotectonic Record of the Appalachian Region. *Geological Society of America Memoir 206*, p. 1–19.

Hatcher, R.D., Jr., 2011, Comparison of Appalachian and Himalayan foreland clastic wedges. *Geological Society of America Abstracts with Programs*, v. 43, n. 5, p. 44.

Hatcher, R.D., Jr., 1989, Tectonic synthesis of the U.S. Appalachians. *In* Hatcher, R.D., Jr., Thomas, W.A., and Viele, G.W., eds., The Appalachian-Ouachita Orogen in the United States. *Geological Society of America, The Geology of North America*, v. F-2, p. 511-535.

Hatcher, R.D., Jr., Thomas, W.A., Geiser, P.A., Snoke, A.W., Mosher, S., and Wiltschko, D.V., 1989, Alleghanian orogen. *In* Hatcher, R.D., Jr., Thomas, W.A., and Viele, G.W., eds., The Appalachian-Ouachita Orogen in the United States. *Geological Society of America, The Geology of North America*, v. F-2, p. 233-318.

Heard, T.G., and Pickering, K.T., 2008, Trace fossils as diagnostic indicators of deep-marine environments, Middle Eocene Ainsa-Jaca basin, Spanish Pyrenees. *Sedimentology*, v. 55, p. 809-844.

Heckel, P.H., 1973, Nature, origin, and significance of the Tully Limestone; an anomalous unit in the Catskill Delta, Devonian of New York. *Geological Society of America Special Paper 138*, 244 p.

Herron, E.M., Cande, S.C., and Hall, B.R., 1981, An active spreading center collides with a subduction zone: a geophysical survey of the Chile Margin triple junction. *Memoir of the Geological Society of America,* v. 154, p. 683-701.

Horne, J.C., 1979, The orthoquartzite problem. *In* Ferm, J.C., and Horne, J.C., eds., *Carboniferous Depositional Environments in the Appalachian Region*. University of South Carolina Department of Geology, Columbia, SC, p. 259-265.

Horne, J.C., and Ferm, J.C., 1976, *Carboniferous depositional environments in the Pocahontas basin, eastern Kentucky and southern West Virginia: a field guide*. University of South Carolina Department of Geology, Columbia, SC, 129 p.

Houseknecht, D.W., 1980, Comparative anatomy of a Pottsville lithic arenite and quartzarenite of the Pocahontas basin, southern West Virginia; petrogenetic, depositional, and stratigraphic implications. *Journal of Sedimentary Research*, v. 50, n. 1, p. 3-20.

Idleman, B.D., Trop, J.M., and Ridgway, K.D., 2011, Geochronological evidence for rapid forearc subsidence and sedimentation during Paleogene spreading ridge subduction along the southern Alaska convergent margin. *Geological Society of America Abstracts with Programs*, v. 43, p. 439.

Iwamori, H., 2000, Thermal effects of ridge subduction and its implications for the origin of granitic batholith and paired metamorphic belts. *Earth and Planetary Science Letters*, v. 181, p. 131–144.

Johanson, E.S., 2000, Petrography, facies stratigraphy and depositional environments of the Big Lime (Middle/Upper Mississippian) on the Pine Mountain overthrust, southeastern Kentucky. *Geological Society of America Abstracts with Programs*, v. 32, iss. 4, p. 19.

Kahmann-Robinson, J.A., 2008, Sequence stratigraphy of the Chesterian Pennington Formation, Pound Gap, KY, USA: an intertonguing marine-terrestrial succession. Unpublished Doctoral dissertation, Baylor University, Waco, TX, p. 78-113.

Kassab, C.M., Kortyna, C.D., Ridgway, K.D., and Trop, J.M., 2009, Sedimentology, structural framework, and basin analysis of the eastern Arkose Ridge Formation, Talkeetna Mountains, Alaska. *Geological Society of America Abstracts with Programs*, v. 41, n. 7, p. 304.

Kortyna, C.D., Donaghy, E., Trop, J.M., and Idleman, B.D., 2013, Integrated provenance record of a forearc basin modified by slab-window magmatism: detrital zircon geochronology and sandstone compositions of the Paleogene Arkose Ridge Formation, south-central Alaska. *Basin Research*, v. 25, 25 p.

Kortyna, C.D., 2011, Sedimentary record of the transition from Late Cretaceous arc magmatism to Eocene spreading ridge subduction in southern Alaska. Unpublished B.S. thesis, Bucknell University, Lewisburg, PA., 140 p.

Kortyna, C.D., Trop, J.M., Lecomte, A.A., Bauer, E., Kassab, C.M., Sunderlin, D., and Ridgway, K.D., 2009, Sedimentology, paleontology, and structural framework of the central Arkose Ridge Formation, Talkeetna Mountains, Alaska. *Geological Society of America, Abstracts with Programs*, v. 41, n. 7, p. 304.

Kreisa, R.D., 1981, Storm-generated sedimentary structures in subtidal marine facies with examples with examples from the Middle and Upper Ordovician of southwestern Virginia. *Journal of Sedimentary Petrology*, v. 51, n. 3, p. 823-848.

Kelleher, G.T., and Smosna, R., 1993, Oolitic tidal-bar reservoirs in the Mississippian Greenbrier Group of West Virginia. *In* Keith, B.D., and Zuppman, C.W., eds., Mississippian Oolites and Modern Analogs. *American Association of Petroleum Geologists, Studies in Geology*, n. 35, p. 163–173.

Kepferle, R.C., 1977, Stratigraphy, petrology, and depositional environments of the Kenwood Siltstone Member of the Borden Formation (Mississippian), Kentucky and Indiana. *United States Geological Survey Professional Paper 1007*, 49 p.

Kidwell, S.M., Fürisch, F.T., and Aigner, T., 1986, Conceptual framework for the analysis and classification of fossil concentrations. *Palaios*, v. 1, p. 228-238.

Kirkpatrick, J.W., IV, 1994, Sedimentology of the Stony Gap Sandstone (Upper Mississippian), Summers and Mercer counties, West Virginia. Unpublished Master's thesis, East Carolina University, Greenville, NC, 129 p.

Konstantopoulos, P.A., and Zelilidis, A., 2013, Sedimentation of submarine fan deposits in the Pindos foreland basin, from late Eocene to early Oligocene, west Peloponnesus peninsula, SW Greece. *Geological Journal*, v. 48, p. 335-362.

Kosters, E.C., and Suter, J.R., 1993, Facies relationships and systems tracts in the Late Holocene Mississippi delta plain. *Journal of Sedimentary Petrology*, v. 63, n. 4, p. 727-733.

Kvale, E.P., 2006, The origin of neap-spring tidal cycles. *Marine Geology*, v. 235, p. 5-18.

Lahr, J.C., Page, R.A., Stephens, C.D., and Fogleman, K.A., 1986, Sutton, Alaska, earthquake of 1984: evidence for activity on the Talkeetna segment of the Castle Mountain fault system. *Bulletin of the Seismological Society of America*, v. 76, n. 4, p. 967-983.

Lane, N.G., and Dubar, J.R., 1983, Progradation of the Borden Delta: new evidence from crinoids. *Journal of Paleontology*, v. 57, n. 1, p. 112-123.

Lien, T., Walker, R.G., and Martinsen, O.J., 2003, Turbidites in the Upper Carboniferous Ross Formation, western Ireland: reconstruction of a channel and spillover system. *Sedimentology*, v. 50, p. 113-148.

Little, T.A., 1988, Tertiary tectonics of the Border Ranges fault system, north-central Chugach Mountains, Alaska: sedimentation, deformation and uplift along the inboard edge of a subduction complex. Unpublished dissertation, Stanford University, Stanford, CA, 343 p.

Little, T.A., and Naeser, C.W., 1989, Tertiary tectonics of the Border Ranges fault system, Chugach Mountains, Alaska: deformation and uplift in a forearc setting. *Journal of Geophysical Research*, v. 94, n. B4, p. 4333-4359.

Longhitano, S.G., Mellere, D., Steel., R.J., and Ainsworth, R.B., 2012, Tidal depositional systems in the rock record: a review and new insights. *Sedimentary Geology*, v. 279, p. 2-22.

Ludwig, K.R., 2003, ISOPLOT 3.0: A geochronological toolkit for Microsoft Excel. *Special Publication 4*, Berkeley Geochronology Center, Berkeley, CA, 71 p.

Lundegard, P.D., Samuels, N.D., and Pryor, W.A., 1980, Sedimentology, petrology, and gas potential of the Brallier Formation – Upper Devonian turbidite facies of the central and southern Appalachians. *U.S. Department of Energy*, DOE/METC/5201-5, 220 p.

Lytwyn, J., Lockhart, S., Casey, J., and Kusky, T., 2000, Geochemistry of near trench intrusive associated with ridge subduction, Seldovia quadrangle, southern Alaska. *Journal of Geophysical Research*, v. 105, p. 27957-27978.

Martin, R.V., 1975, Petrology of the Carter Caves Sandstone, Mississippian, Northeastern Kentucky. Unpublished Master's thesis, University of Cincinnati, Cincinnati, OH, 66 p.

McKinney, F.K., and Gault, H.W., 1980, Paleoenvironment of Late Mississippian fenestrate bryozoans, eastern United States. *Lethaia*, v. 13, p. 127-146.

McLennan, S.M., Bock, B., Compston, W., Hemming, S.R., and McDaniel, D.K., 2001, Detrital zircon geochronology of Taconian and Acadian foreland sedimentary rocks in New England. *Journal of Sedimentary Research*, v. 71, n. 2, p. 305-317.

Meckel, L.D., 1970, Paleozoic alluvial deposition in the central Appalachians: a summary. *In* Fisher, G.W., Pettijohn, F.J., Reed, J.C., and Weaver, K.N, eds., *Studies of Appalachian Geology: Central and Southern*. John Wiley, New York, NY, p. 49–67.

Mellere, D., Plink-Björklund, P., Steel, R., 2002, Anatomy of shelf deltas at the edge of a prograding Eocene shelf margin, Spitsbergen. *Sedimentology*, v. 49, p. 1181-1206.

Merschat, A.J., Hatcher, R.D., Jr., and Davis, T.L., 2005, The northern Inner Piedmont, southern Appalachians, USA: kinematics of transpression and SW-directed mid-crustal flow. *Journal of Structural Geology*, v. 27, p. 1252–1281.

Miall, A.D., 1985, Architectural-element analysis: A new method of facies analysis applied to fluvial deposits. *Earth Science Reviews*, v. 22, p. 261-308.

Miller, R.L., 1973, Where and why of Pine Mountain and other major fault planes, Virginia, Kentucky, and Tennessee. *American Journal of Science*, v. 273-A, p. 353-371.

Miller, M.S., 1974, Stratigraphy and coal beds of Upper Mississippian and Lower Pennsylvanian rocks in southwestern Virginia, Charlottesville, Virginia, *Virginia Division of Mineral Resources Bulletin 84*, 211 p.

Miller, D.J., and Eriksson, K.A., 1997, Late Mississippian prodeltaic rhythmites in the Appalachian basin: a hierarchical record of tidal and climatic processes. *Journal of Sedimentary Research*, v. 67, n. 4, p. 653-660.

Mitra, S., 1988, Three-dimensional geometry and kinematic evolution of the Pine Mountain thrust system, southern Appalachians. *Geological Society of America Bulletin*, v. 100, p. 72-95.

Mulder, T., and Syvitski, J.P.M., 1995, Turbidity currents generated at river mouths during exceptional discharges to the world oceans. *Journal of Geology*, v. 103, p. 285-299.

Mutti, E., 1979, Turbidites et cones sous-marins profonds: 3me Cycle Romand Sciences de la Terre, Friourg. *Sedimentation Detritique*, p. 355-419.

Mutti, E., 1992, *Turbidite sandstones*. AGIP-Instituto di Geologia, Università di Parma, San Donato Milanese, 275 p.

Mutti, E., and Ricci Lucchi, F., 1972, Le torbiditi dell'Appennino settentrionale: Introduzione all'analisi di facies. *Memorie della Societa Geologica Italiana*, v. 11, p. 161–199.

Mutti, E., Tinterri, R., Benevelli, G., di Biase, D., and Cavanna, G., 2003, Deltaic, mixed and turbidite sedimentation of ancient foreland basins. *Marine and Petroleum Geology*, v. 20, p. 733-755.

Nelson, W.A., and Read, J.F., 1990, Updip to downdip cementation and dolomitization patterns in a Mississippian aquifer, Appalachians. *Journal of Sedimentary Petrology*, v. 60, n. 3, p. 379-396.

Nokleberg, W.J., Jones, D.L., and Silberling, N.J., 1985, Origin and tectonic evolution of the Maclaren and Wrangellia terranes, eastern Alaska Range, Alaska. *Geological Society of America Bulletin*, v. 96, p. 1251–1270.

Ober, E.G., 2003, Diagenetic alteration of carbonate phases in a rhizocretion from a well developed paleosol in the upper Pennington Formation, Pound Gap Kentucky. *Geological Society of America Abstracts with Programs*, v. 35, iss. 1, p. 55.

O'Hara, K., Hower, J. C., and Rimmer, S. M., 1990, Constraints on the emplacement and uplift history of the Pine Mountain thrust sheet, eastern Kentucky: evidence from coal rank trends. *Journal of Geology*, v. 98, 43-51.

Owen, D.D., 1856, *Report of the geological survey in Kentucky made during the years 1854 and 1855*, Hodges, A.G., state printer, 416 p.

Park, H. Barbeau, D.L., Jr., Rickenbaker, A., Bachmann-Krug, D., and Gehrels, G.E., 2010, Application of foreland basin detrital-zircon geochronology to the reconstruction of the southern and central Appalachian orogen. *Journal of Geology*, v. 118, p. 23-44.

Pashin, J.C., and Ettensohn, F.R., 1995, Reevaluation of the Bedford-Berea Sequence in Ohio and adjacent states: forced regression in a foreland basin. *Geological Society of America Special Paper 298*, 68 p.

Pavlis, T.A., and Roeske, S.M., 2007, The Border Ranges fault system, southern Alaska. *In* Ridgway, K.D., Trop, J.M., Glen, J.M.G., and O'Neill, J.M., eds., Tectonic Growth of a Collisional Continental Margin: Crustal Evolution of Southern Alaska. *Geological Society of America Special Paper 431*, p. 95-127.

Pedersen, T.F., and Calvert, S.E., 1990, Anoxia vs. productivity: what controls the formation of organic-carbon-rich sediments and sedimentary rocks? *American Association of Petroleum Geologists Bulletin*, v. 74, p. 454-466.

Pedoja, K., Ortlieb, L., Dumont, J.F., Lamonthe, M., Ghaleb, B., Auclair, M., and Laborusse, B., 2006, Quaternary coastal uplift along the Talara Arc (Ecuador, Northern Peru) from new marine terrace data. *Marine Geology*, v. 228, p. 73-91.

Pemberton, S.G., Van Wagoner, J.C., and Wach, G.D., 1992, Ichnofacies of a wave-dominated shoreline. *In* Pemberton, S.G., ed., Applications of Ichnology to Petroleum Exploration. *SEPM Core Workshop 17*, p. 339–382.

Pepper, J.F., de Witt, W., Jr., and Demarest, D.F., 1954, Geology of the Bedford Shale and Berea Sandstone in the Appalachian basin. *U. S. Geological Survey Professional Paper 259*, 111 p.

Perry, W.J., Jr., 1978, Sequential deformation in the central Appalachians. *American Journal of Science*, v. 278, p. 518-542.

Plafker, G., Nokleberg, W.J., and Lull, J.S., 1989, Bedrock geology and tectonic evolution of the Wrangellia, Peninsular, and Chugach terranes along the Trans-Alaskan Crustal Transect in the northern Chugach Mountains and southern Copper River basin, Alaska. *Journal of Geophysical Research*, v. 94, p. 4255-4295.

Plafker, G., and Berg, H.C., 1994, Overview of the geology and tectonic evolution of Alaska. *In* Plafker, G., and Berg., H.C., eds., The Geology of Alaska. *Geological Society of America, The Geology of North America*, v. G-1, p. 989-1021.

Ponten, A., and Plink-Björklund, P., 2007, Depositional environments in an extensive tide-influenced delta plain, Middle Devonian Gauja Formation, Devonian Baltic basin. *Sedimentology*, v. 54, p. 969-1006.

Pope, M.C., Holland, S.M., and Patzkowsky, M.E., 2009, The Cincinnati Arch: a stationary peripheral bulge during the Late Ordovician. *In* Swart, P.K., Eberli, G.P., McKenzie, J.A., Jarvis, I., and Stevens, T., eds., *Perspectives in Carbonate Geology: A Tribute to the Career of Robert Nathan Ginsburg*, John Wiley & Sons, Ltd., Chichester, West Sussex, UK.

Posamentier, H.W., and Walker, R.G., 2006, Deep-water turbidites and submarine fans. *In* Posamentier, H.W. and Walker, R.G., eds., Facies Models Revisited, *SEPM Special Publication 84*, p. 397-520.

Quinlan, G. M., and Beaumont, C., 1984, Appalachian thrusting, lithospheric flexure, and the Paleozoic stratigraphy of the eastern interior of North America. *Canadian Journal of Earth Science,* v. 21, p. 973-996.

Rainbird, R., Cawood, P.A., and Gehrels, G.E., 2012, The great Grenvillian sedimentation episode: record of supercontinent Rodinia's assembly. *In* Busby, C. and Azor, A., eds.,*Tectonics of Sedimentary Basins: Recent Advances*. Blackwell Publishing Ltd., p. 583-600.

Ramsay, J.G., and Huber, M.I., 1984, *The Techniques of Modern Structural Geology, Volume 1: Strain Analysis*. Academic Press Ltd., Oxford, UK., 307 p.

Reesink, A.J.H., and Bridge, J.S., 2007, Influence of superimposed bedforms and flow unsteadiness on formation of cross strata in dunes and unit bars. *Sedimentary Geology*, v. 202, p. 281-296.

Reineck, H., and Wunderlich, F., 1968, Classification and origin of flaser and lenticular bedding. *Sedimentology*, v. 11, p. 99-104.

Reinson, G.E., 1979, Facies models 14: barrier island systems. *Geoscience Canada*, v. 6, n. 2, p. 51-68.

Rice, C.L., 1973, Geologic map of the Jenkins West quadrangle, Kentucky-Virginia. *U.S. Geological Survey Geologic Quadrangle Map GQ-1126, scale 1:24,000.*

Rice, C.L., 1984, Sandstone units of the Lee Formation and related strata in eastern Kentucky. *U.S. Geological Survey Professional Paper 1151-G*, 53 p.

Rice, C.L., 1985, Terrestrial vs. marine depositional model; a new assessment of subsurface Lower Pennsylvanian rocks of southwestern Virginia. *Geology*, v. 13, p. 786-789.

Rice, C.L., and Schwietering, J.F., 1988, Fluvial deposition in the central Appalachians during the Early Pennsylvanian. *U.S. Geological Survey Bulletin 1839-B*, p. B1–B10.

Rich, J.L., 1934, Mechanics of low angle overthrust faulting as illustrated by Cumberland thrust block, Virginia, Kentucky, and Tennessee. *American Association of Petroleum Geologists Bulletin*, v. 18, p. 1584-1596.

Ridgway, K.D., Trop, J.M., Nokleberg, W.J., Davidson, C.M., and Eastham, K.D., 2002, Mesozoic and Cenozoic tectonics of the eastern and central Alaska Range: progressive basin development and deformation within a suture zone. *Geological Society of America Bulletin*, v. 114, p. 1480–1504.

Ridgway, K.D., Trop, J.M., and Finzel, E.S., 2012, Modification of continental forearc basins by flat-slab subduction processes: a case study from southern Alaska. *In* Busby, C.J., and Azor, A., eds., *Tectonics of Sedimentary Basins: Recent Advances*. John Wiley & Sons, Ltd, Chichester, UK, p. 327-346.

Rioux, M., Hacker, B., Mattinson, J., Kelemen, P.B., Hanghoj, K., and Plank, T., 2003, The role of intermediate to felsic plutonism in the accreted Talkeetna arc, south-central Alaska. *Geological society of America Abstracts with Programs*, v. 35, abs. 174-15.

Rioux, M., Hacker, B., Mattinson, J., Kelemen, P., Blusztajn, J., and Gehrels, G., 2007, The magmatic development of an intra-oceanic arc: high-precision U-Pb zircon and whole-rock isotopic analyses from the accreted Talkeetna arc, south-central Alaska. *Geological Society of America Bulletin*, v. 119, p. 1168–1184.

Roen, J.B., 1984, Geology of Devonian black shales of the Appalachian basin. *Organic Geochemistry*, v. 5, n. 4, p. 251-254.

Rodgers, J., 1970, *The tectonics of the Appalachians*. Wiley Interscience, New York, NY, 271 p.

Roy, P.S., 1977, Does the Hunter River supply sand to the New South Wales coast today? *Royal Society of New South Wales, Journal and Proceedings*, v. 110, p. 17–24.

Ruppert, L.F., and Rice, C.L., 2001, Chapter B—Coal resource assessment methodology and geology of the northern and central Appalachian Basin coal regions. *In* Northern and Central Appalachian Basin Coal Regions Assessment Team, 2000 resource assessment of selected coal beds and zones in the northern and central Appalachian Basin coal regions. *U.S. Geological Survey Professional Paper 1625–C*, CD-ROM, version 1.0.

Ryder, R.T., 1995, Appalachian Basin Province (067). *In* Gautier, D.L., Dolton, G.L., Takahashi, K.I., and Varnes, K.L., eds., National Assessment of United States Oil and Gas Resources - Results, Methodology, and Supporting Data. *U.S. Geological Survey Digital Data Series DDS-30*, 86 p.

Sak, P.B., Fisher, D.M., and Gardner, T.W., 2004, Effects of subduction seafloor roughness on upper plate vertical tectonism: Osa Peninsula, Costa Rica. *Tectonics*, v. 23, 16 p.

Scalabrino, B., Lagabrielle, Y., de la Rupelle, A., Malavieille, J., Polve, M., Espinoza, F., Morata, D., and Suarez, M., 2009, Subduction of an active spreading ridge beneath southern South America; a review of the Cenozoic geological records from the Andean Foreland, central Patagonia (46-47°S). *In* Lallemand, S., Funiciell, F., Brun, J.P., Oncken, O., Weissert, H., and Dullo, C., eds., *Subduction Zone Dynamics, Frontiers in Earth Sciences*. Springer-Verlag Berlin Heidelberg, p. 227-246.

Schepers, K., Nuttall, B., Oudinot, A., and Gonzalez, R., 2009, Reservoir modeling and simulation of the Devonian gas shale of eastern Kentucky for enhanced gas recovery and CO2 storage. *SPE International Conference on CO2 Capture, Storage, and Utilization*, SPE 126620-PP.

Scotese, C.R., 2003, Paleogeographic map archive. *PALEOMAP project*, Department of Geology, University of Texas, Arlington, TX.

Scotese, C.R., and McKerrow, W.S., 1990, Revised world maps an introduction. *In* McKerrow, W.S., and Scotese, C.R., eds., Palaeozoic palaeogeography and biogeography. *Geological Society of London Memoir 12*, p. 1–24.

Secor, D.T., Jr., Snoke, A.W., and Dallmeyer, R.D., 1986, Character of the Alleghanian orogeny in the southern Appalachians: Part III. Regional tectonic relations. *Geological Society of American Bulletin*, v, 97, p. 1345-1353.

Shanmugam, G., 2000, 50 years of the turbidite paradigm (1950s-1990s): deep-water processes and facies models—a critical perspective. *Marine and Petroleum Geology*, v. 17, p. 285-342.

Simons, D.B., and Richardson, E.V., 1961, Forms of bed roughness in alluvial channels, American Society of Civil Engineers Proceedings. *Journal of the Hydraulics Division*, v. 87, p. 87-105.

Simons, D.B., and Richardson, E.V., 1966, Resistance to flow in alluvial channels. *U.S. Geological Society Professional Paper 422-J*, p. J1-J61.

Sisson, V.B., Hollister, L.S., and Onstott, T.C., 1989, Petrologic and age constraints on the origin of a low-pressure/high-temperature metamorphic complex, southern Alaska. *Journal of Geophysical Research*, v. 94, p. 4392-4410.

Sloss, L.L., 1963, Sequences in the cratonic interior of North America. *Geological Society of America Bulletin*, v. 74, n. 2, p. 93-114.

Smith, N.D., 1972, Some sedimentological aspects of planar cross-stratification in a sandy braided river. *Journal of Sedimentary Petrology*, v. 42, n. 3, p. 624-634.

Stewart, K.G., Dennison, J.M., and Bartholomew, M.J., 2002, Late Mississippian paleoseismites from southeastern West Virginia and southwestern Virginia. *In* Ettensohn, F.R., Rast, N., and Brett, C.E., eds., Ancient Seismites. *Geological Society of America Special Paper 359*, p. 127–144.

Sunderlin, D., Trop, J.M., Idleman, B.D., Brannick, A., White, J.G., and Grande, L., in press, Paleoenvironment and paleoecology of a Late Paleocene high-latitude terrestrial succession, Arkose Ridge Formation at Box Canyon, southern Talkeetna Mountains, Alaska. *Palaeogeography, Palaeoclimatology, Palaeoecology*.

Suter, J.R., 2006, Facies models revisited: clastic shelves. *In* Posamentier, H.W. and Walker, R.G., eds., Facies Models Revisited. *SEPM Special Publication 84*, p. 339-397.

Tankard, A.J., 1986, Depositional response to foreland deformation in the Carboniferous of eastern Kentucky. *American Association of Petroleum Geologists Bulletin*, v. 70, n. 7, p. 853-868.

Tanner, W.F., 1967, Ripple mark indices and their uses. *Sedimentology*, v. 9, p. 89-104.

Taylor, F.W., Mann, P., Bevis, M.G., Edwards, R.L., Cheng, H., Cutler, K.B., Gray, S.C.,. Burr,. G.S., Beck, J.W., Phillips, D.A., Cabioch, G., and Recy, J., 2005, Rapid fore-arc uplift and subsidence caused by impinging bathymetric features; examples from the New Hebrides and Solomon arcs. *Tectonics*, v. 24, iss. 6, 23 p.

Tessier, B., 2012, Stratigraphy of tide-dominated estuaries. *In* Davis, R.A., Jr., and Dalrymple, R.W., eds., *Principles of Tidal Sedimentolog*y. Springer Science+Business Media B.V., Netherlands, p. 109-128.

Thomas, R.G., Smith, D.G., Wood, J.M., Visser, J., Calverley-Range, E.A., and Koster, E.H., 1987, Inclined heterolithic stratification – Terminology, description, interpretation and significance. *Sedimentary Geology*, v. 53, p. 123-179.

Thomas, W.A., Becker, T.P., Samson, S.D., and Hamilton, M.A., 2004, Detrital zircon evidence of a recycled orogenic foreland provenance for Alleghanian clastic-wedge sandstones. *Journal of Geology*, v. 112, p. 23-37.

Trop, J.M., 2008, Latest Cretaceous forearc basin development along an accretionary convergent margin: south-central Alaska. *Geological Society of America Bulletin*, v. 120, p. 207- 224.

Trop, J.M., and Ridgway, K.D., 2000, Sedimentology, stratigraphy, and tectonic importance of the Paleocene–Eocene Arkose Ridge Formation, Cook Inlet-Matanuska Valley forearc basin, Alaska. *In* Pinney, D.S. and Davis, P.K., eds., Short Notes on Alaskan Geology, 1999, Fairbanks, Alaska. *Division of Geological and Geophysical Surveys Professional Report*, v. 119, p. 129-144.

Trop, J.M., and Ridgway, K.D., 2007, Mesozoic and Cenozoic tectonic growth of southern Alaska: A sedimentary basin perspective. *In* Ridgway, K.D., Trop, J.M., Glen, J.M.G., and O'Neill, J.M., eds., Tectonic Growth of a Collisional Continental Margin: Crustal Evolution of Southern Alaska. *Geological Society of America Special Paper 431*, p. 55-94.

Trop, J.M., Ridgway, K.D., and Spell, T.L., 2003, Synorogenic sedimentation and forearc basin development along a transpressional plate boundary, Matanuska Valley-Talkeetna Mountains, southern Alaska. *In* Sisson, V. B., Roeske, S., and Pavlis, T.L., eds, Geology of a Transpressional Orogen Developed During Ridge-trench Interaction Along the North Pacific Margin. *Geological Society of America Special Paper 371*, p. 89–118.

Trop, J.M., Szuch, d.A., Rioux, M., and Blodgett, R.B., 2005, Sedimentology and provenance of the Upper Jurassic Naknek Formation, Talkeetna Mountains, Alaska: bearings on the accretionary tectonic history of the Wrangellia composite terrane. *Geological Society of America Bulletin*, v. 117, n. 5/6, p. 570-588.

Trop, J.M., Kissock, K., Donaghy, E., and Idleman, B.D., 2012, Sedimentary record of exhumation along a forearc basin-accretionary prism boundary during ridge subduction: Paleogene Chickaloon Formation, northern Chugach Mountains, southern Alaska. *Geological Society of America Abstracts with Programs*, v. 44, n. 7, p. 175.

Tucker, M.E., 1969, Crinoidal turbidites from the Devonian of Cornwall and their palaeogeographic significance. *Sedimentology*, v. 13, p. 281-290.

Udgata, D.B.P., 2011, Depositional and stratigraphic significance of marine, green-clay, mineral facies in the lower-middle Mississippian Borden and Fort Payne Formations, western Appalachian and eastern Illinois basins, Kentucky. Unpublished Doctoral dissertation, University of Kentucky, Lexington, KY, 257 p.

Underwood, M.B., Shelton, K.L., McLaughlin, R.J., Laughland, M.M., and Solomon, R.M., 1999, Middle Miocene paleotemperature anomalies within the Franciscan Complex of Northern California: thermo-tectonic responses near the Mendocino triple junction. *Geological Society of America Bulletin*, v. 111, p. 1448–1467.

Wang, P., 2012, Principles of sediment transport applicable in tidal environments. *In* Davis, R.A., Jr., and Dalrymple, R.W., eds., *Principles of Tidal Sedimentology*. Springer Science+Business Media B.V., Netherlands, p. 19-34.

Whittaker, J.M., Muller, R.D., Sdrolias, M., Heine, C., 2007, Sunda-Java trench kinematics, slab window formation and overriding plate deformation since the Cretaceous. *Earth and Planetary Science Letters*, v. 255, p. 445-457.

Willis, B.J., 2005, Deposits of tide-influenced river deltas. *In* Giosan, L., and Bhattacharya, J.P., eds., River Deltas—Concepts, Models, and Examples. *SEPM Special Publication 83*, p. 87-129.

Willis, J.B., Haeussler, P.J., Bruhn, R.L., and Willis, G.C., 2007, Holocene slip rate for the western segment of the Castle Mountain Fault, Alaska. *Bulletin of the Seismological Society of America*, v. 97, n. 3, p. 1019-1024.

Wilpolt, R.H., and Marden, D.W., 1959, Geology and oil and gas possibilities of Upper Mississippian rocks of southwestern Virginia, southern West Virginia, and eastern Kentucky. *U.S. Geological Survey Bulletin 1072-K*, p. 587-656.

Wilson, J.L., 1969, Microfacies and sedimentary structures in "deeper water" lime mudstones. *In* Friedman, G.M., ed., Depositional Environments in Carbonate Rocks. *SEPM Special Publication 14*, p. 4-19.

Winkler, G. R., 1992, Geologic map and summary geochronology of the Anchorage 1° × 3° quadrangle, southern Alaska. *U.S. Geological Survey Miscellaneous Investigations Series Map I-2283, scale 1:250,000*.

Wizevich, M.C., 1992, Sedimentology of Pennsylvanian quartzose sandstones of the Lee Formation, central Appalachian basin: fluvial interpretation based on lateral profile analysis. *Sedimentary Geology*, v. 78, p. 1-47.

Wizevich, M.C., 1993, Depositional controls in a bed load-dominated fluvial system: Internal architecture of the Lee Formation, Kentucky. *Sedimentary Geology*, v. 85, p. 537-556.

Woodrow, D.L., and Isley, A.M., 1983, Facies, topography, and sedimentary processes in the Catskill Sea (Devonian), New York and Pennsylvanian. *Geological Society of America Bulletin*, v. 94, p. 450-470.

Ziegler, A.M., Scotese, C.R., McKerrow, W.S., Johnson, M.E., and Bambach, R.K., 1979, Paleozoic paleogeography. *Annual Review of Earth and Planetary Sciences*, v. 7, p. 473- 502.

APPENDICES

Appendix A Detailed measured section of the Pound Gap exposure.

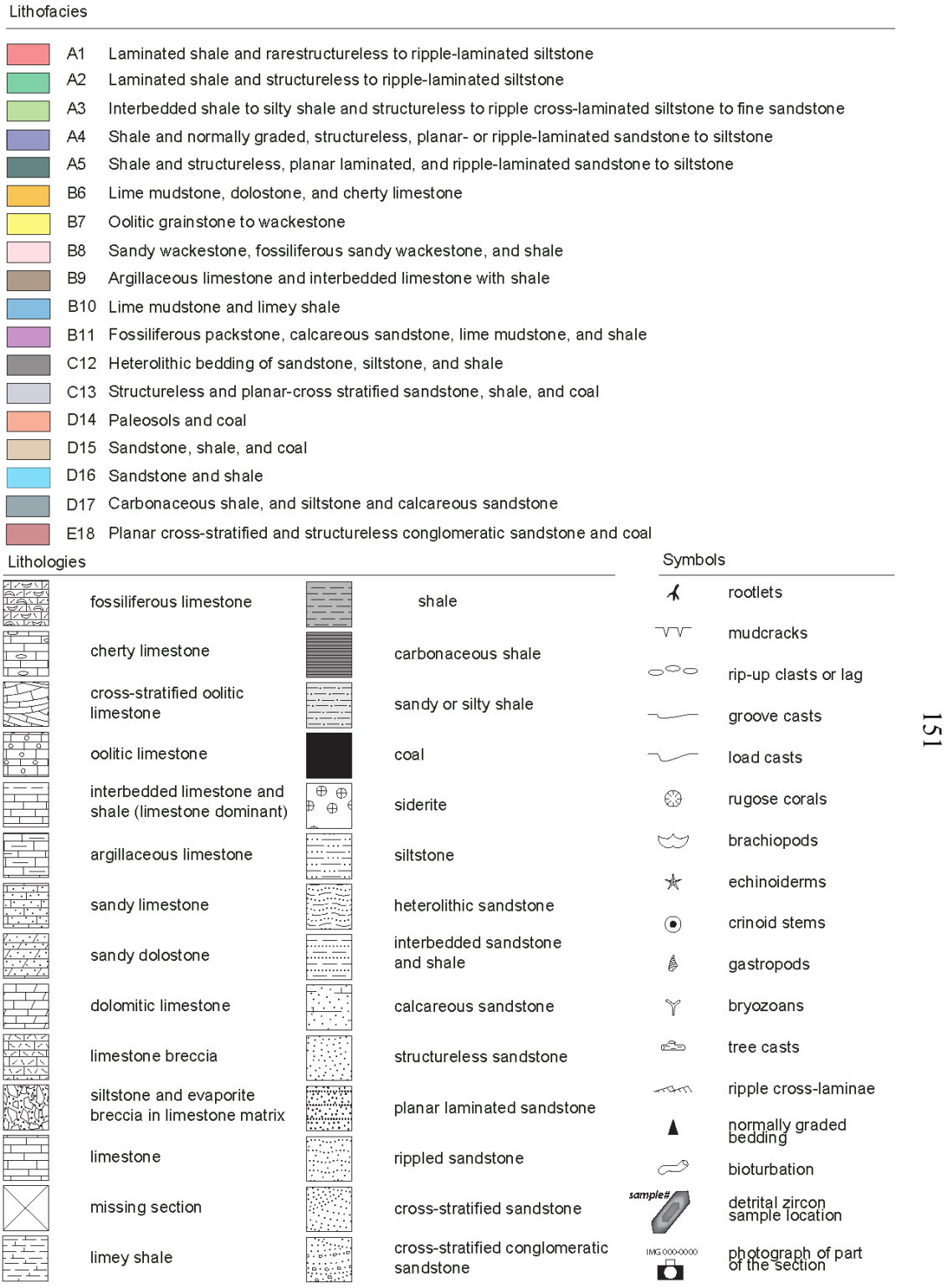

151

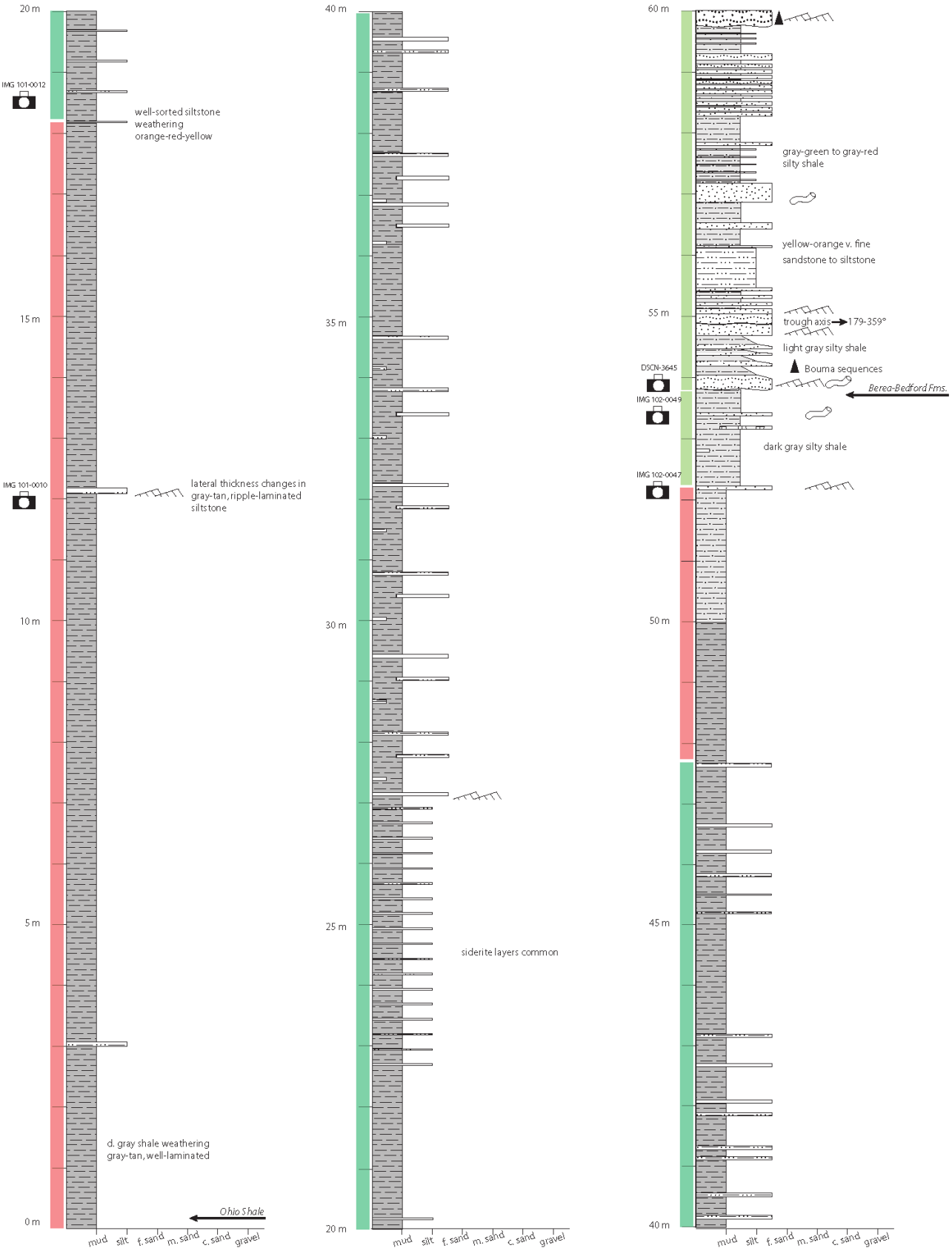
20 m
IMG 101-0012
well-sorted siltstone
weathering
orange-red-yellow
15 m
IMG 101-0010
lateral thickness changes in
gray-tan, ripple-laminated
siltstone
10 m
5 m
d. gray shale weathering
gray-tan, well-laminated
0 m
Ohio Shale
mud
silt
f. sand
m. sand
c. sand
gravel
40 m
35 m
30 m
25 m
siderite layers common
20 m
mud
silt
f. sand
m. sand
c. sand
gravel
60 m
gray-green to gray-red
silty shale
yellow-orange v. fine
sandstone to siltstone
55 m
trough axis
179-359°
light gray silty shale
DSCN-3645
Bouma sequences
Berea-Bedford Fms.
IMG 102-0049
dark gray silty shale
IMG 102-0047
50 m
45 m
40 m
mud
silt
f. sand
m. sand
c. sand
gravel

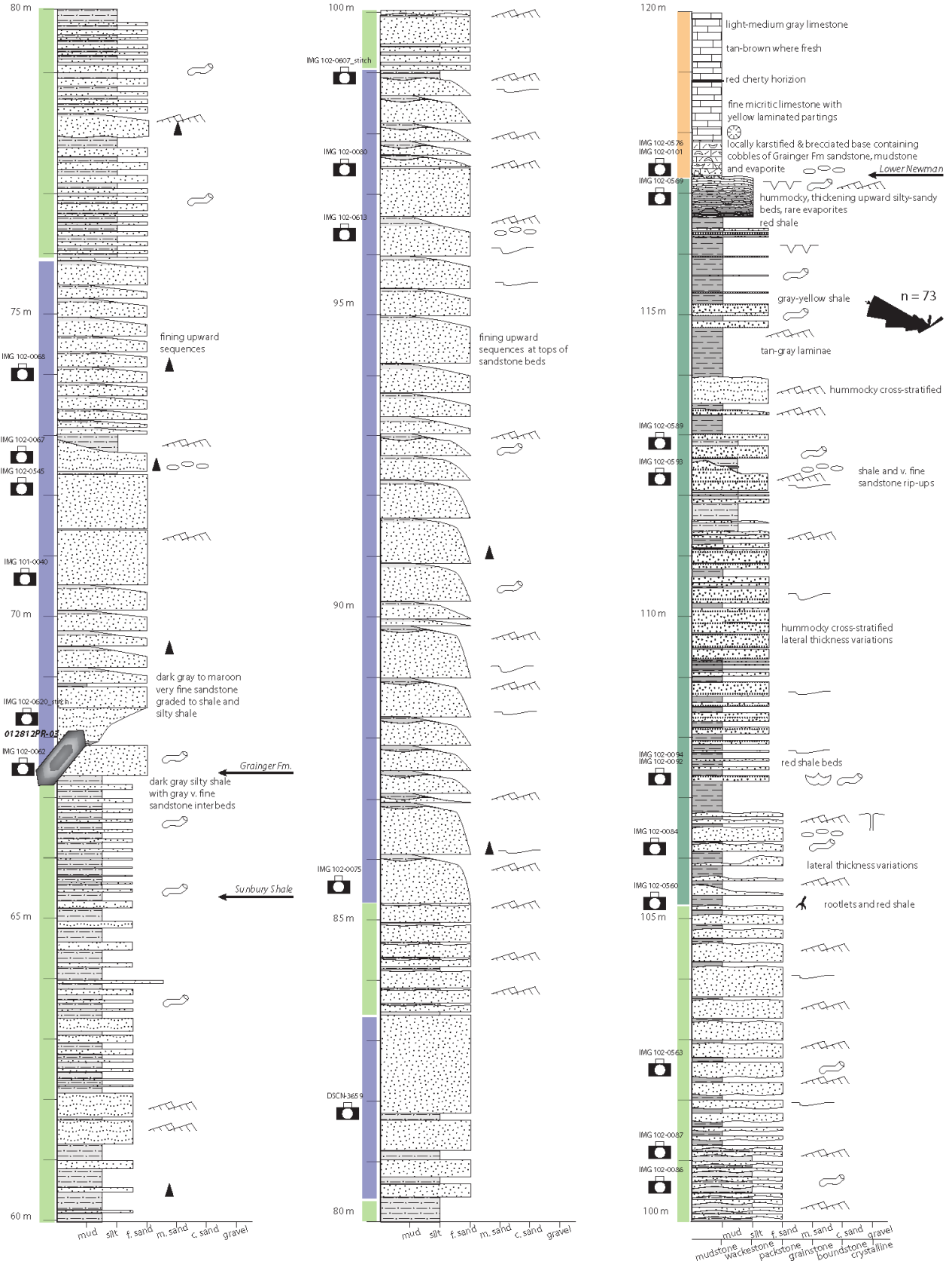
80 m
75 m
70 m
65 m
60 m
IMG 102-0068
IMG 102-0067
IMG 102-0545
IMG 101-0040
IMG 102-0820_stitch
012812PR-03
IMG 102-0062
fining upward sequences
dark gray to maroon very fine sandstone graded to shale and silty shale
Grainger Fm.
dark gray silty shale with gray v. fine sandstone interbeds
Sunbury Shale
mud
silt
f. sand
m. sand
c. sand
gravel
100 m
95 m
90 m
85 m
80 m
IMG 102-0607_stitch
IMG 102-0060
IMG 102-0613
IMG 102-0075
DSCN-3659
fining upward sequences at tops of sandstone beds
120 m
115 m
110 m
105 m
100 m
IMG 102-0576
IMG 102-0101
IMG 102-0589
IMG 102-0589
IMG 102-0593
IMG 102-0094
IMG 102-0092
IMG 102-0084
IMG 102-0560
IMG 102-0563
IMG 102-0087
IMG 102-0086
light-medium gray limestone
tan-brown where fresh
red cherty horizion
fine micritic limestone with yellow laminated partings
locally karstified & brecciated base containing cobbles of Grainger Fm sandstone, mudstone and evaporite
Lower Newman
hummocky, thickening upward silty-sandy beds, rare evaporites
red shale
gray-yellow shale
n = 73
tan-gray laminae
hummocky cross-stratified
shale and v. fine sandstone rip-ups
hummocky cross-stratified lateral thickness variations
red shale beds
lateral thickness variations
rootlets and red shale
mudstone
wackestone
packstone
grainstone
boundstone
crystalline

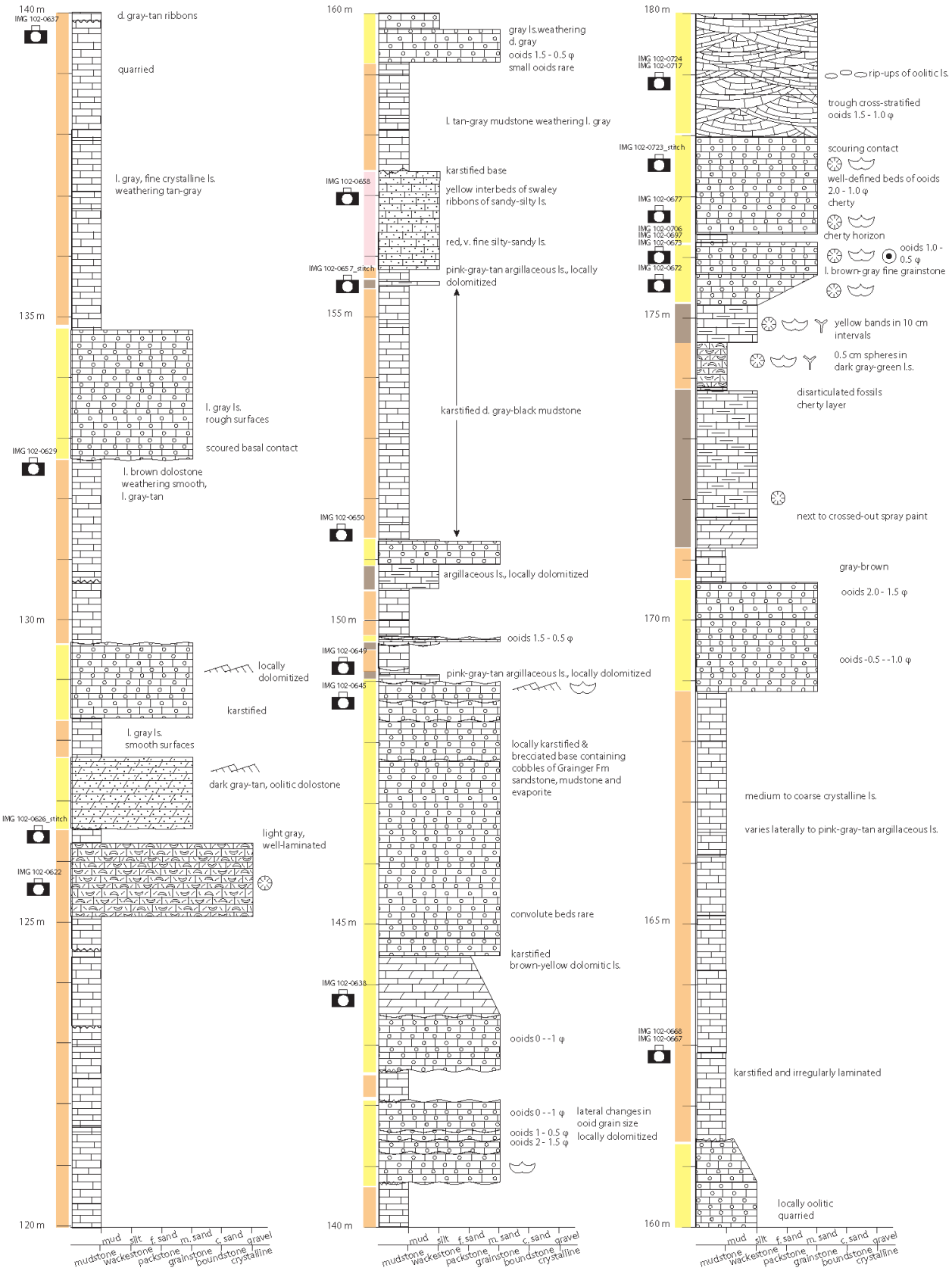
140 m
IMG 102-0637
d. gray-tan ribbons
quarried
l. gray, fine crystalline ls. weathering tan-gray
135 m
l. gray ls. rough surfaces
scoured basal contact
IMG 102-0629
l. brown dolostone weathering smooth, l. gray-tan
130 m
locally dolomitized
karstified
l. gray ls. smooth surfaces
dark gray-tan, oolitic dolostone
IMG 102-0628_stitch
light gray, well-laminated
IMG 102-0622
125 m
120 m
mud
silt
f. sand
m. sand
c. sand
gravel
mudstone
wackestone
packstone
grainstone
boundstone
crystalline
160 m
gray ls.weathering d. gray
ooids 1.5 - 0.5 φ
small ooids rare
l. tan-gray mudstone weathering l. gray
karstified base
IMG 102-0658
yellow interbeds of swaley ribbons of sandy-silty ls.
red, v. fine silty-sandy ls.
IMG 102-0657_stitch
pink-gray-tan argillaceous ls., locally dolomitized
155 m
karstified d. gray-black mudstone
IMG 102-0650
argillaceous ls., locally dolomitized
150 m
ooids 1.5 - 0.5 φ
IMG 102-0649
pink-gray-tan argillaceous ls., locally dolomitized
IMG 102-0645
locally karstified & brecciated base containing cobbles of Grainger Fm sandstone, mudstone and evaporite
convolute beds rare
145 m
karstified brown-yellow dolomitic ls.
IMG 102-0638
ooids 0 - -1 φ
ooids 0 - -1 φ
ooids 1 - 0.5 φ
ooids 2 - 1.5 φ
lateral changes in ooid grain size locally dolomitized
140 m
180 m
IMG 102-0724
IMG 102-0717
rip-ups of oolitic ls.
trough cross-stratified ooids 1.5 - 1.0 φ
IMG 102-0723_stitch
scouring contact
well-defined beds of ooids 2.0 - 1.0 φ cherty
IMG 102-0677
IMG 102-0706
IMG 102-0697
IMG 102-0673
cherty horizon
ooids 1.0 - 0.5 φ
IMG 102-0672
l. brown-gray fine grainstone
175 m
yellow bands in 10 cm intervals
0.5 cm spheres in dark gray-green l.s.
disarticulated fossils cherty layer
next to crossed-out spray paint
gray-brown
ooids 2.0 - 1.5 φ
170 m
ooids -0.5 - -1.0 φ
medium to coarse crystalline ls.
varies laterally to pink-gray-tan argillaceous ls.
165 m
IMG 102-0668
IMG 102-0667
karstified and irregularly laminated
locally oolitic quarried
160 m

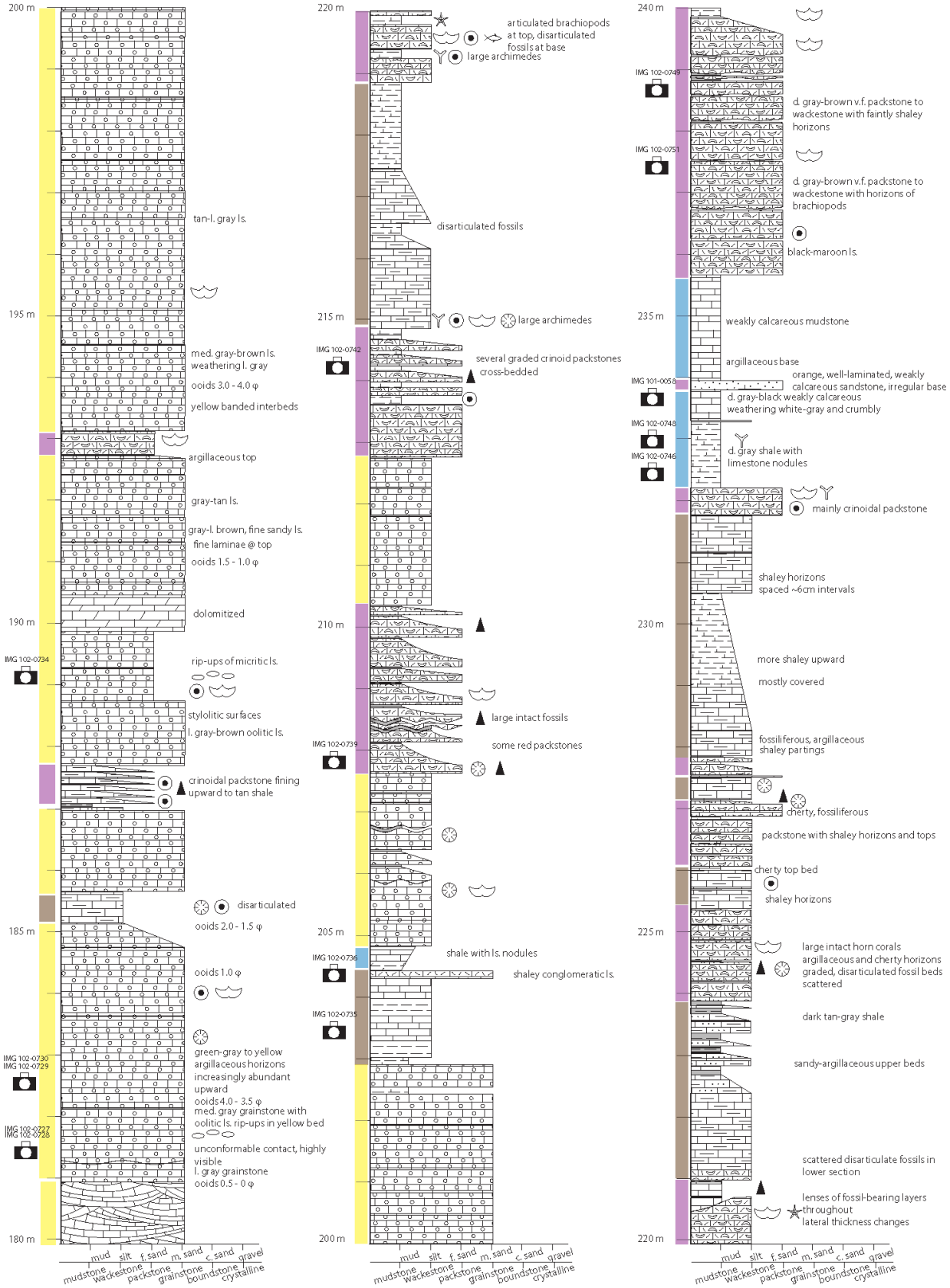
200 m
195 m
190 m
185 m
180 m
tan-l. gray ls.
med. gray-brown ls. weathering l. gray
ooids 3.0 - 4.0 φ
yellow banded interbeds
argillaceous top
gray-tan ls.
gray-l. brown, fine sandy ls.
fine laminae @ top
ooids 1.5 - 1.0 φ
dolomitized
IMG 102-0734
rip-ups of micritic ls.
stylolitic surfaces
l. gray-brown oolitic ls.
crinoidal packstone fining upward to tan shale
disarticulated
ooids 2.0 - 1.5 φ
ooids 1.0 φ
IMG 102-0730
IMG 102-0729
green-gray to yellow argillaceous horizons increasingly abundant upward
ooids 4.0 - 3.5 φ
med. gray grainstone with oolitic ls. rip-ups in yellow bed
IMG 102-0727
IMG 102-0728
unconformable contact, highly visible
l. gray grainstone
ooids 0.5 - 0 φ
mud
silt
f. sand
m. sand
c. sand
gravel
mudstone
wackestone
packstone
grainstone
boundstone
crystalline
220 m
215 m
210 m
205 m
200 m
articulated brachiopods at top, disarticulated fossils at base
large archimedes
disarticulated fossils
large archimedes
IMG 102-0742
several graded crinoid packstones
cross-bedded
large intact fossils
some red packstones
IMG 102-0739
shale with ls. nodules
IMG 102-0736
shaley conglomeratic ls.
IMG 102-0735
240 m
235 m
230 m
225 m
220 m
IMG 102-0749
d. gray-brown v.f. packstone to wackestone with faintly shaley horizons
IMG 102-0751
d. gray-brown v.f. packstone to wackestone with horizons of brachiopods
black-maroon ls.
weakly calcareous mudstone
argillaceous base
orange, well-laminated, weakly calcareous sandstone, irregular base
IMG 101-0058
d. gray-black weakly calcareous weathering white-gray and crumbly
IMG 102-0748
IMG 102-0746
d. gray shale with limestone nodules
mainly crinoidal packstone
shaley horizons spaced ~6cm intervals
more shaley upward
mostly covered
fossiliferous, argillaceous shaley partings
cherty, fossiliferous
packstone with shaley horizons and tops
cherty top bed
shaley horizons
large intact horn corals
argillaceous and cherty horizons
graded, disarticulated fossil beds scattered
dark tan-gray shale
sandy-argillaceous upper beds
scattered disarticulate fossils in lower section
lenses of fossil-bearing layers throughout
lateral thickness changes

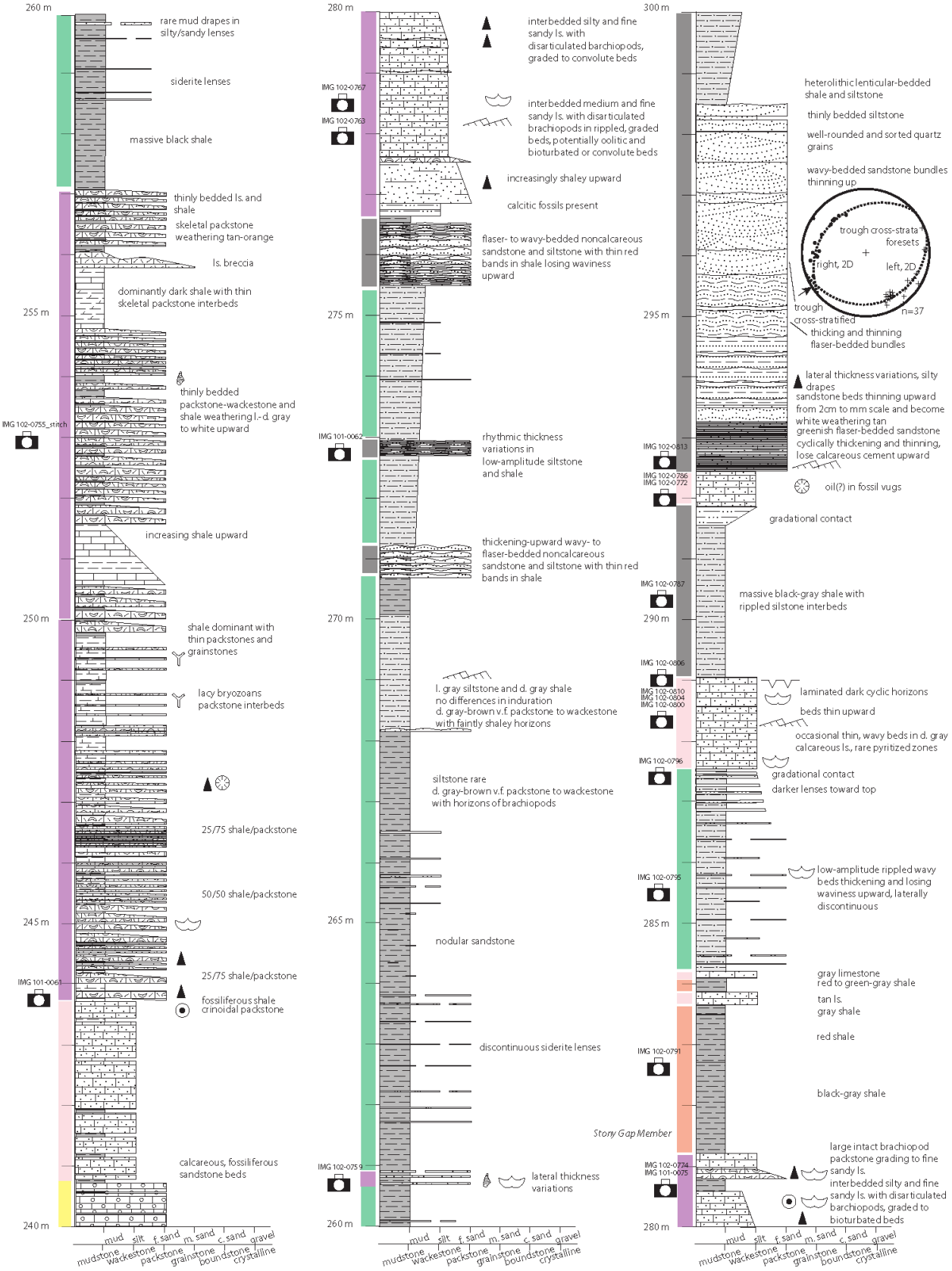
260 m
rare mud drapes in silty/sandy lenses
siderite lenses
massive black shale
thinly bedded ls. and shale
skeletal packstone weathering tan-orange
ls. breccia
dominantly dark shale with thin skeletal packstone interbeds
255 m
thinly bedded packstone-wackestone and shale weathering l.-d. gray to white upward
IMG 102-0755_stitch
increasing shale upward
250 m
shale dominant with thin packstones and grainstones
lacy bryozoans packstone interbeds
25/75 shale/packstone
50/50 shale/packstone
245 m
25/75 shale/packstone
IMG 101-0061
fossiliferous shale
crinoidal packstone
calcareous, fossiliferous sandstone beds
240 m
mud
silt
f. sand
m. sand
c. sand
gravel
mudstone
wackestone
packstone
grainstone
boundstone
crystalline
280 m
interbedded silty and fine sandy ls. with disarticulated barchiopods, graded to convolute beds
IMG 102-0767
IMG 102-0763
interbedded medium and fine sandy ls. with disarticulated brachiopods in rippled, graded beds, potentially oolitic and bioturbated or convolute beds
increasingly shaley upward
calcitic fossils present
flaser- to wavy-bedded noncalcareous sandstone and siltstone with thin red bands in shale losing waviness upward
275 m
IMG 101-0062
rhythmic thickness variations in low-amplitude siltstone and shale
thickening-upward wavy- to flaser-bedded noncalcareous sandstone and siltstone with thin red bands in shale
270 m
l. gray siltstone and d. gray shale no differences in induration
d. gray-brown v.f. packstone to wackestone with faintly shaley horizons
siltstone rare
d. gray-brown v.f. packstone to wackestone with horizons of brachiopods
265 m
nodular sandstone
discontinuous siderite lenses
IMG 102-0759
lateral thickness variations
260 m
mud
silt
f. sand
m. sand
c. sand
gravel
mudstone
wackestone
packstone
grainstone
boundstone
crystalline
300 m
heterolithic lenticular-bedded shale and siltstone
thinly bedded siltstone
well-rounded and sorted quartz grains
wavy-bedded sandstone bundles thinning up
trough cross-strata foresets
right, 2D
left, 2D
n=37
trough cross-stratified thicking and thinning flaser-bedded bundles
295 m
lateral thickness variations, silty drapes
sandstone beds thinning upward from 2cm to mm scale and become white weathering tan
greenish flaser-bedded sandstone cyclically thickening and thinning, lose calcareous cement upward
IMG 102-0813
IMG 102-0786
IMG 102-0772
oil(?) in fossil vugs
gradational contact
IMG 102-0767
290 m
massive black-gray shale with rippled siltstone interbeds
IMG 102-0806
IMG 102-0810
IMG 102-0804
IMG 102-0800
laminated dark cyclic horizons
beds thin upward
occasional thin, wavy beds in d. gray calcareous ls., rare pyritized zones
IMG 102-0796
gradational contact
darker lenses toward top
IMG 102-0795
low-amplitude rippled wavy beds thickening and losing waviness upward, laterally discontinuous
285 m
gray limestone
red to green-gray shale
tan ls.
gray shale
red shale
IMG 102-0791
black-gray shale
Story Gap Member
large intact brachiopod packstone grading to fine sandy ls.
interbedded silty and fine sandy ls. with disarticulated barchiopods, graded to bioturbated beds
IMG 102-0774
IMG 101-0075
280 m
mud
silt
f. sand
m. sand
c. sand
gravel
mudstone
wackestone
packstone
grainstone
boundstone
crystalline

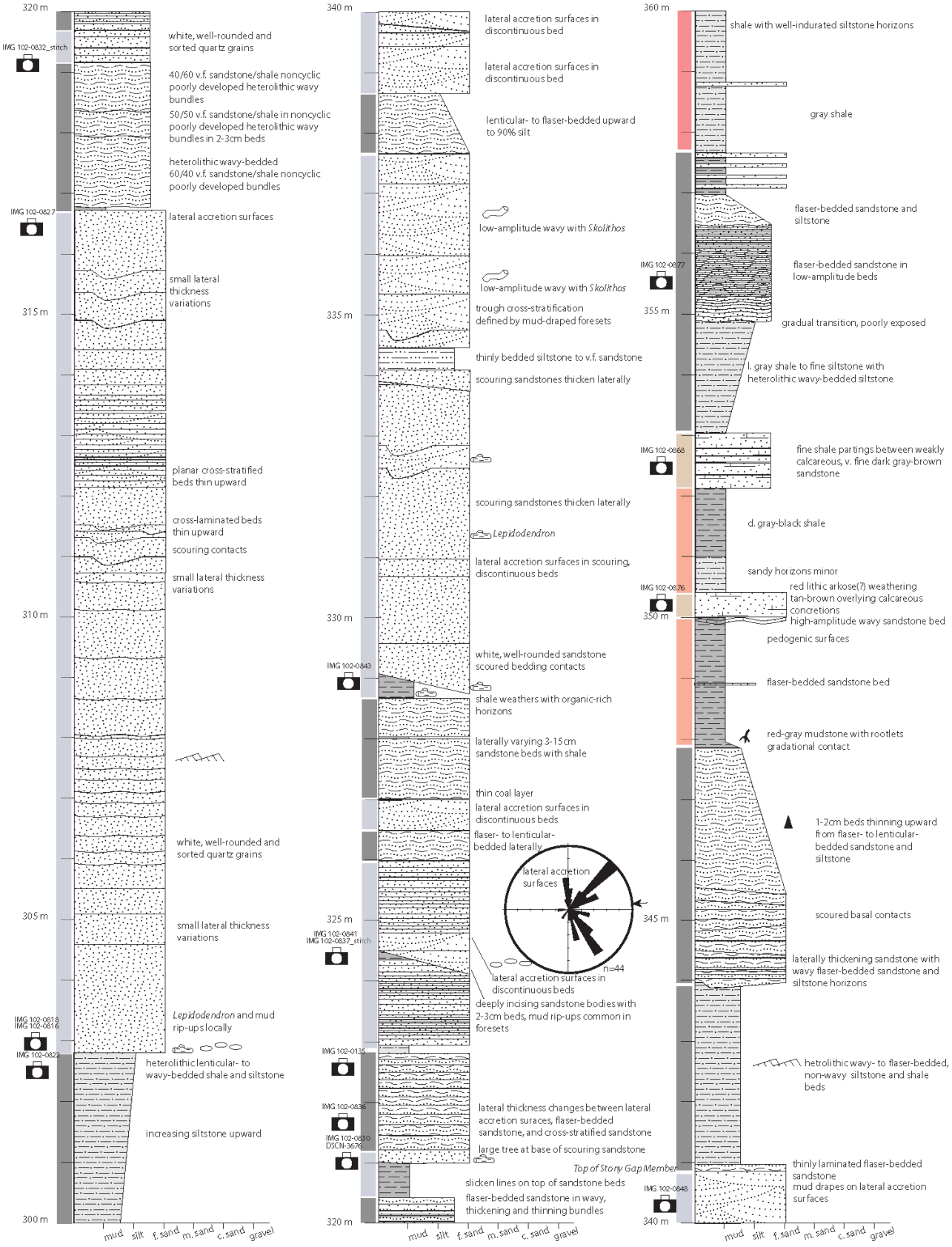
320 m
IMG 102-0832_stitch
white, well-rounded and sorted quartz grains
40/60 v.f. sandstone/shale noncyclic poorly developed heterolithic wavy bundles
50/50 v.f. sandstone/shale in noncyclic poorly developed heterolithic wavy bundles in 2-3cm beds
heterolithic wavy-bedded 60/40 v.f. sandstone/shale noncyclic poorly developed bundles
IMG 102-0827
lateral accretion surfaces
small lateral thickness variations
315 m
planar cross-stratified beds thin upward
cross-laminated beds thin upward
scouring contacts
small lateral thickness variations
310 m
white, well-rounded and sorted quartz grains
305 m
small lateral thickness variations
IMG 102-0818
IMG 102-0816
Lepidodendron and mud rip-ups locally
IMG 102-0822
heterolithic lenticular- to wavy-bedded shale and siltstone
increasing siltstone upward
300 m
mud
silt
f. sand
m. sand
c. sand
gravel
340 m
lateral accretion surfaces in discontinuous bed
lateral accretion surfaces in discontinuous bed
lenticular- to flaser-bedded upward to 90% silt
low-amplitude wavy with Skolithos
low-amplitude wavy with Skolithos
335 m
trough cross-stratification defined by mud-draped foresets
thinly bedded siltstone to v.f. sandstone
scouring sandstones thicken laterally
scouring sandstones thicken laterally
Lepidodendron
lateral accretion surfaces in scouring, discontinuous beds
330 m
IMG 102-0843
white, well-rounded sandstone scoured bedding contacts
shale weathers with organic-rich horizons
laterally varying 3-15cm sandstone beds with shale
thin coal layer
lateral accretion surfaces in discontinuous beds
flaser- to lenticular-bedded laterally
lateral accretion surfaces
n=44
325 m
IMG 102-0841
IMG 102-0837_strich
lateral accretion surfaces in discontinuous beds
deeply incising sandstone bodies with 2-3cm beds, mud rip-ups common in foresets
IMG 102-0835
IMG 102-0836
lateral thickness changes between lateral accretion suraces, flaser-bedded sandstone, and cross-stratified sandstone
IMG 102-0830
DSCN-3676
large tree at base of scouring sandstone
Top of Stony Gap Member
slicken lines on top of sandstone beds
flaser-bedded sandstone in wavy, thickening and thinning bundles
320 m
mud
silt
f. sand
m. sand
c. sand
gravel
360 m
shale with well-indurated siltstone horizons
gray shale
flaser-bedded sandstone and siltstone
IMG 102-0877
flaser-bedded sandstone in low-amplitude beds
355 m
gradual transition, poorly exposed
l. gray shale to fine siltstone with heterolithic wavy-bedded siltstone
IMG 102-0868
fine shale partings between weakly calcareous, v. fine dark gray-brown sandstone
d. gray-black shale
sandy horizons minor
IMG 102-0876
red lithic arkose(?) weathering tan-brown overlying calcareous concretions
high-amplitude wavy sandstone bed
350 m
pedogenic surfaces
flaser-bedded sandstone bed
red-gray mudstone with rootlets gradational contact
1-2cm beds thinning upward from flaser- to lenticular-bedded sandstone and siltstone
345 m
scoured basal contacts
laterally thickening sandstone with wavy flaser-bedded sandstone and siltstone horizons
hetrolithic wavy- to flaser-bedded, non-wavy siltstone and shale beds
thinly laminated flaser-bedded sandstone
mud drapes on lateral accretion surfaces
IMG 102-0848
340 m
mud
silt
f. sand
m. sand
c. sand
gravel

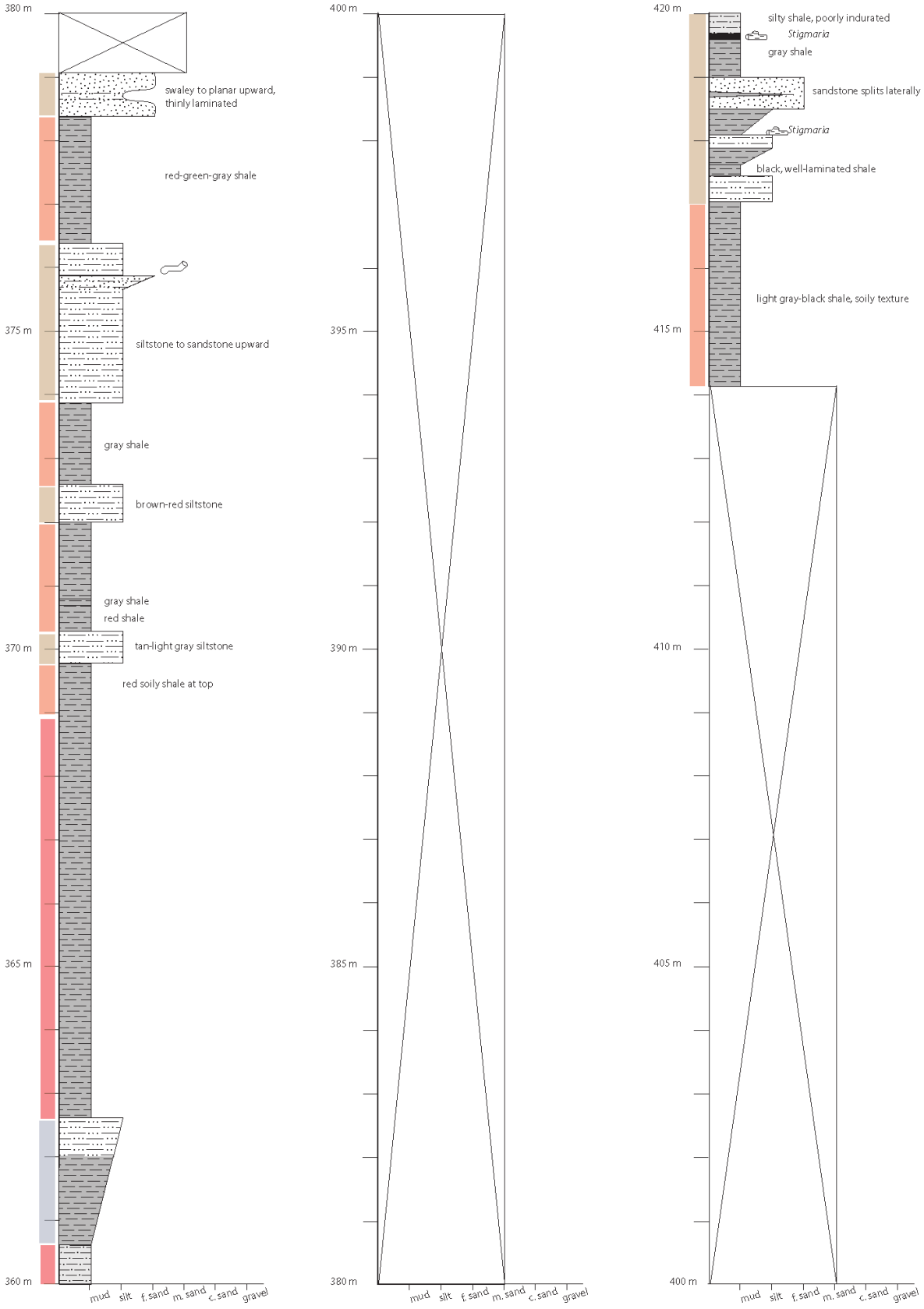
380 m
swaley to planar upward, thinly laminated
red-green-gray shale
375 m
siltstone to sandstone upward
gray shale
brown-red siltstone
gray shale
red shale
370 m
tan-light gray siltstone
red soily shale at top
365 m
360 m
mud
silt
f. sand
m. sand
c. sand
gravel
400 m
395 m
390 m
385 m
380 m
mud
silt
f. sand
m. sand
c. sand
gravel
420 m
silty shale, poorly indurated
Stigmaria
gray shale
sandstone splits laterally
Stigmaria
black, well-laminated shale
light gray-black shale, soily texture
415 m
410 m
405 m
400 m
mud
silt
f. sand
m. sand
c. sand
gravel

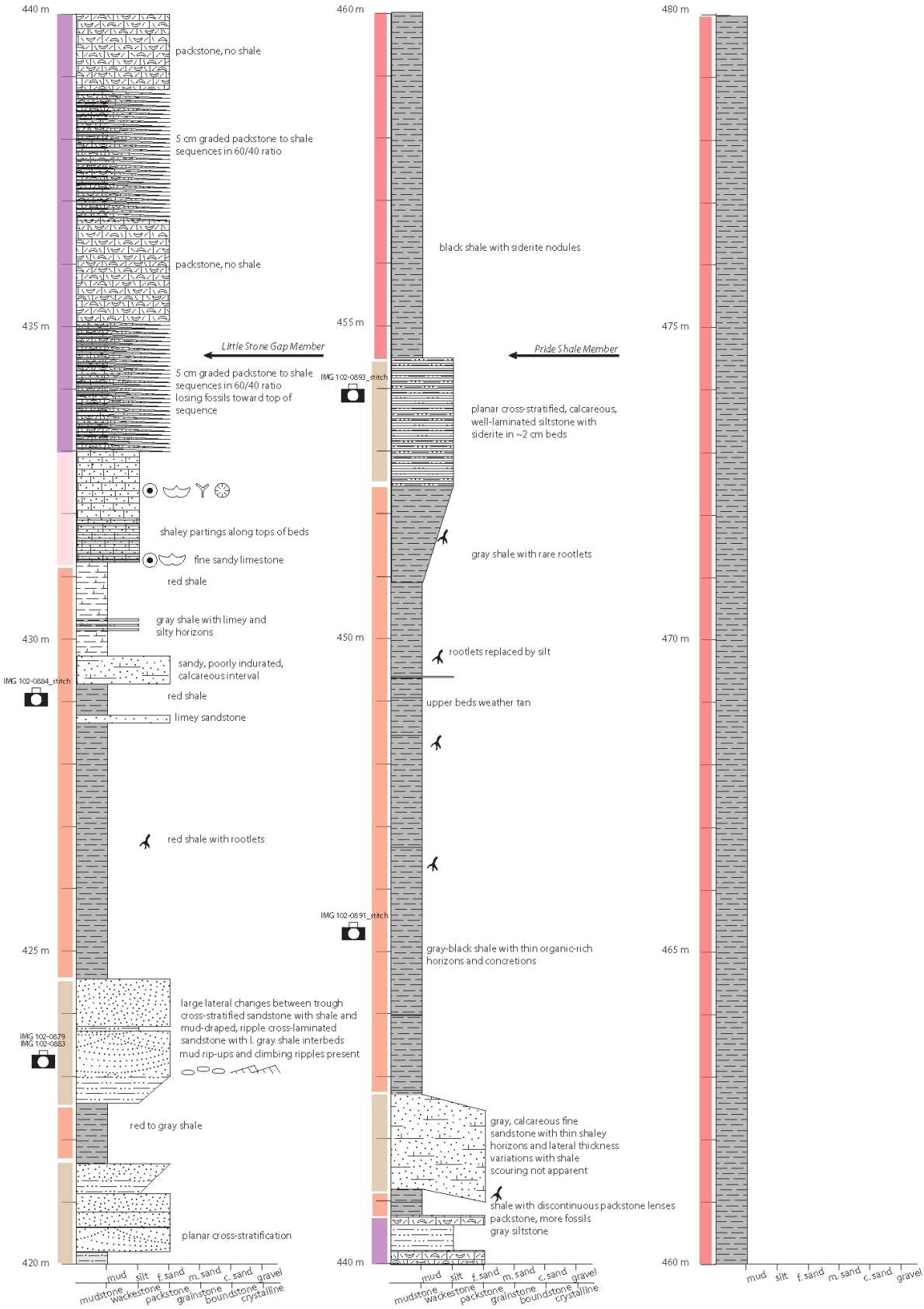
440 m
packstone, no shale
5 cm graded packstone to shale sequences in 60/40 ratio
packstone, no shale
435 m
Little Stone Gap Member
5 cm graded packstone to shale sequences in 60/40 ratio losing fossils toward top of sequence
shaley partings along tops of beds
fine sandy limestone
red shale
gray shale with limey and silty horizons
430 m
sandy, poorly indurated, calcareous interval
IMG 102-0884_stitch
red shale
limey sandstone
red shale with rootlets
425 m
large lateral changes between trough cross-stratified sandstone with shale and mud-draped, ripple cross-laminated sandstone with l. gray shale interbeds mud rip-ups and climbing ripples present
IMG 102-0879
IMG 102-0883
red to gray shale
planar cross-stratification
420 m
460 m
black shale with siderite nodules
455 m
Pride Shale Member
IMG 102-0893_stitch
planar cross-stratified, calcareous, well-laminated siltstone with siderite in ~2 cm beds
gray shale with rare rootlets
450 m
rootlets replaced by silt
upper beds weather tan
IMG 102-0891_stitch
gray-black shale with thin organic-rich horizons and concretions
gray, calcareous fine sandstone with thin shaley horizons and lateral thickness variations with shale scouring not apparent
shale with discontinuous packstone lenses
packstone, more fossils
gray siltstone
440 m
480 m
475 m
470 m
465 m
460 m
mud
silt
f. sand
m. sand
c. sand
gravel
mudstone
wackestone
packstone
grainstone
boundstone
crystalline

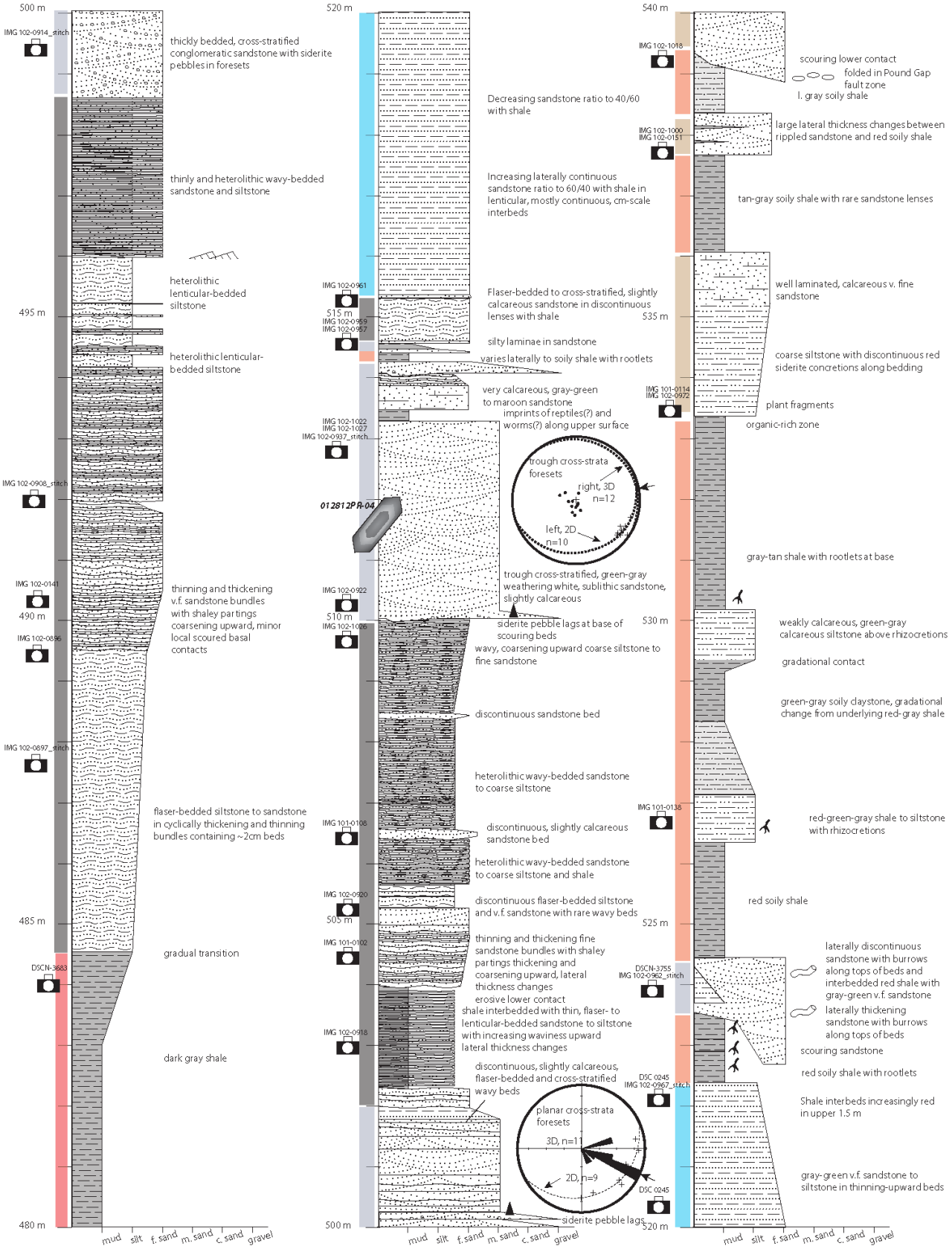
500 m
IMG 102-0914_stitch
thickly bedded, cross-stratified conglomeratic sandstone with siderite pebbles in foresets
thinly and heterolithic wavy-bedded sandstone and siltstone
heterolithic lenticular-bedded siltstone
495 m
heterolithic lenticular-bedded siltstone
IMG 102-0908_stitch
IMG 102-0141
thinning and thickening v.f. sandstone bundles with shaley partings coarsening upward, minor local scoured basal contacts
490 m
IMG 102-0896
IMG 102-0897_stitch
flaser-bedded siltstone to sandstone in cyclically thickening and thinning bundles containing ~2cm beds
485 m
gradual transition
DSCN-3683
dark gray shale
480 m
mud
silt
f. sand
m. sand
c. sand
gravel
520 m
Decreasing sandstone ratio to 40/60 with shale
Increasing laterally continuous sandstone ratio to 60/40 with shale in lenticular, mostly continuous, cm-scale interbeds
IMG 102-0961
Flaser-bedded to cross-stratified, slightly calcareous sandstone in discontinuous lenses with shale
515 m
IMG 102-0959
IMG 102-0957
silty laminae in sandstone
varies laterally to soily shale with rootlets
very calcareous, gray-green to maroon sandstone
imprints of reptiles(?) and worms(?) along upper surface
IMG 102-1022
IMG 102-1027
IMG 102-0937_stitch
trough cross-strata foresets
right, 3D n=12
left, 2D n=10
012812PR-04
trough cross-stratified, green-gray weathering white, sublithic sandstone, slightly calcareous
IMG 102-0922
510 m
siderite pebble lags at base of scouring beds
IMG 102-1026
wavy, coarsening upward coarse siltstone to fine sandstone
discontinuous sandstone bed
heterolithic wavy-bedded sandstone to coarse siltstone
IMG 101-0108
discontinuous, slightly calcareous sandstone bed
heterolithic wavy-bedded sandstone to coarse siltstone and shale
IMG 102-0920
505 m
discontinuous flaser-bedded siltstone and v.f. sandstone with rare wavy beds
IMG 101-0102
thinning and thickening fine sandstone bundles with shaley partings thickening and coarsening upward, lateral thickness changes
erosive lower contact
shale interbedded with thin, flaser- to lenticular-bedded sandstone to siltstone with increasing waviness upward lateral thickness changes
IMG 102-0918
discontinuous, slightly calcareous, flaser-bedded and cross-stratified wavy beds
planar cross-strata foresets
3D, n=11
2D, n=9
DSC 0245
siderite pebble lags
500 m
mud
silt
f. sand
m. sand
c. sand
gravel
540 m
IMG 102-1018
scouring lower contact
folded in Pound Gap fault zone
l. gray soily shale
IMG 102-1000
IMG 102-0151
large lateral thickness changes between rippled sandstone and red soily shale
tan-gray soily shale with rare sandstone lenses
well laminated, calcareous v. fine sandstone
535 m
coarse siltstone with discontinuous red siderite concretions along bedding
IMG 101-0114
IMG 102-0972
plant fragments
organic-rich zone
gray-tan shale with rootlets at base
530 m
weakly calcareous, green-gray calcareous siltstone above rhizocretions
gradational contact
green-gray soily claystone, gradational change from underlying red-gray shale
IMG 101-0138
red-green-gray shale to siltstone with rhizocretions
red soily shale
525 m
DSCN-3755
IMG 102-0962_stitch
laterally discontinuous sandstone with burrows along tops of beds and interbedded red shale with gray-green v.f. sandstone
laterally thickening sandstone with burrows along tops of beds
scouring sandstone
red soily shale with rootlets
DSC 0245
IMG 102-0967_stitch
Shale interbeds increasingly red in upper 1.5 m
gray-green v.f. sandstone to siltstone in thinning-upward beds
520 m
mud
silt
f. sand
m. sand
c. sand
gravel

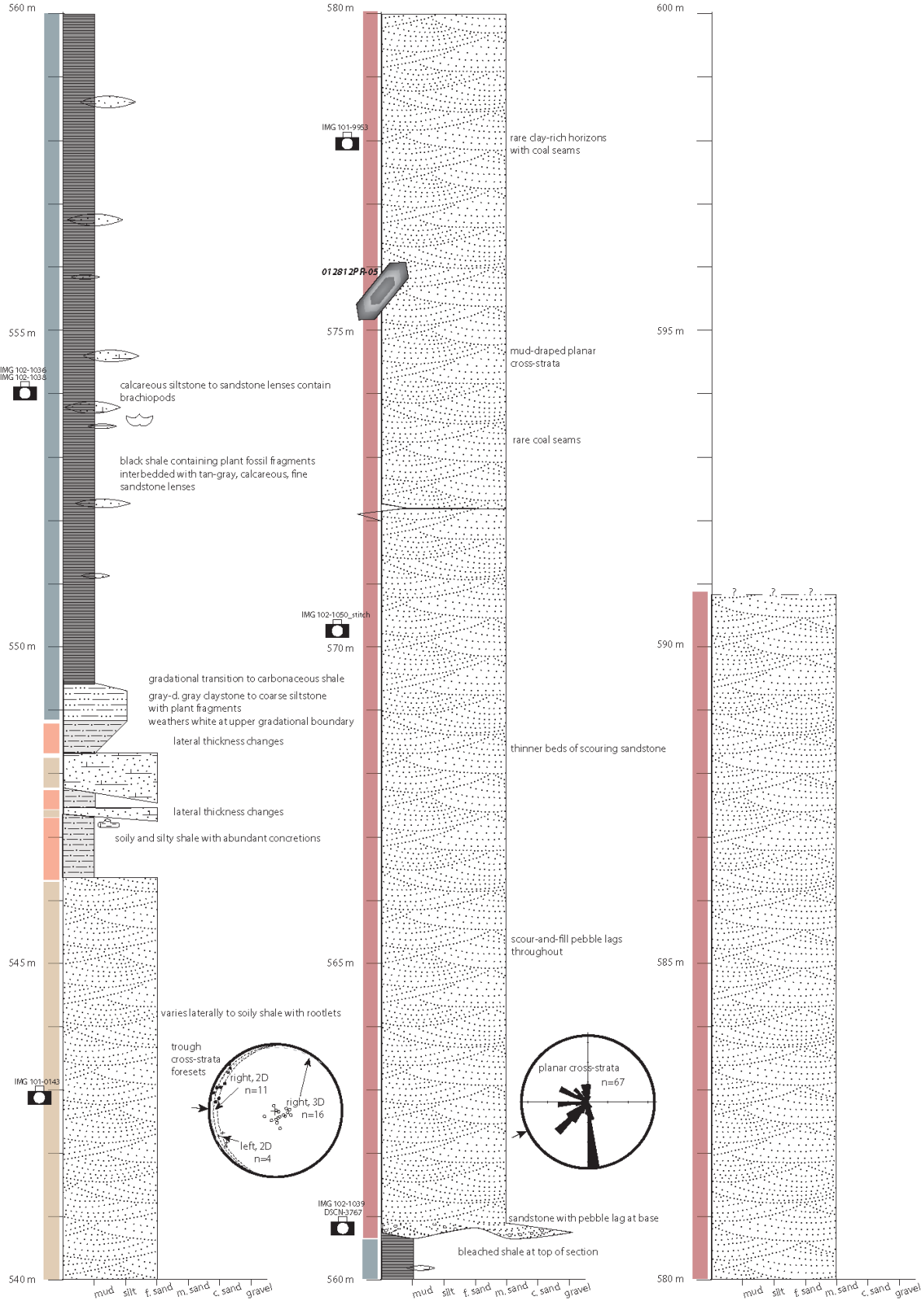
560 m
555 m
550 m
545 m
540 m
IMG 102-1036
IMG 102-1038
calcareous siltstone to sandstone lenses contain brachiopods
black shale containing plant fossil fragments interbedded with tan-gray, calcareous, fine sandstone lenses
gradational transition to carbonaceous shale
gray-d. gray claystone to coarse siltstone with plant fragments
weathers white at upper gradational boundary
lateral thickness changes
lateral thickness changes
soily and silty shale with abundant concretions
varies laterally to soily shale with rootlets
IMG 101-0143
trough cross-strata foresets
right, 2D n=11
right, 3D n=16
left, 2D n=4
mud
silt
f. sand
m. sand
c. sand
gravel
580 m
575 m
570 m
565 m
560 m
IMG 101-9953
012812PR-05
IMG 102-1050_stitch
IMG 102-1039
DSCN-3767
rare clay-rich horizons with coal seams
mud-draped planar cross-strata
rare coal seams
thinner beds of scouring sandstone
scour-and-fill pebble lags throughout
planar cross-strata n=67
sandstone with pebble lag at base
bleached shale at top of section
600 m
595 m
590 m
585 m
580 m
? ? ?

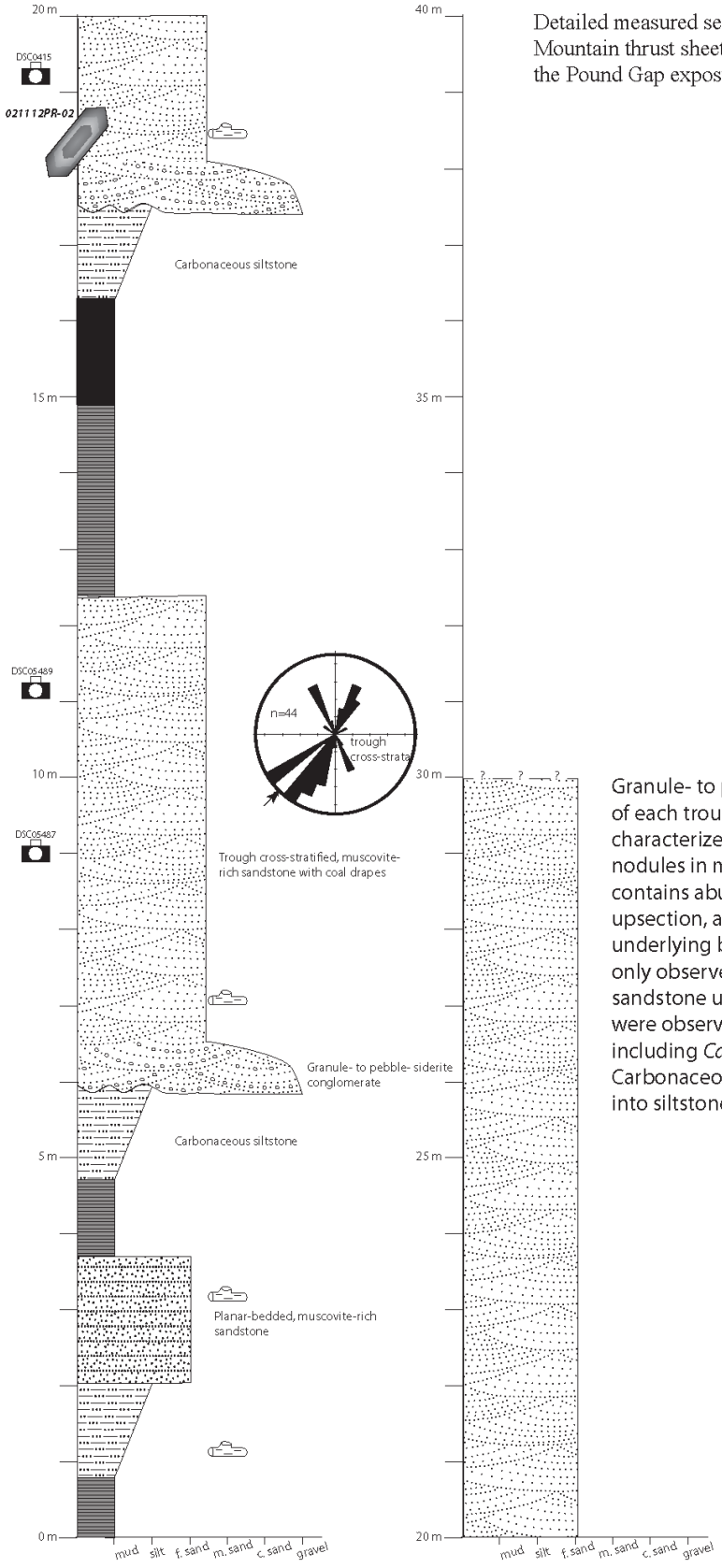

Detailed measured section from the footwall of the Pine Mountain thrust sheet exposed along U.S. Route 23 north of the Pound Gap exposure

Granule- to pebble-conglomerates at the base of each trough cross-stratified sandstone are characterized by subangular to rounded siderite nodules in micaceous, felsic sandstone which contains abundant, thin drapes of plant trash upsection, and a scour-and-fill boundary with underlying beds. Planar cross-stratification was only observed at the base of the topmost sandstone unit (~18 m). Abundant plant fossils were observed throughout the sandstone unit, including *Calamites* and *Lepidodendron*. Carbonaceous shale typically grades upward into siltstone.

Appendix B Subsurface geology of the Cumberland-Allegheny Plateau of eastern Kentucky. Distance betwen Natural Bridge State Park and Lexington is ~90 km. Mississippian strata are buried to depths of ~140 m in the footwall of the Pine Mountain thrust fault north of Pine Mountain and shallow northwestward. Well data from the Department of Mines and Minerals Oil and Gas Division, Kentucky Geological Survey. Big Lime also known as Newman Limestone

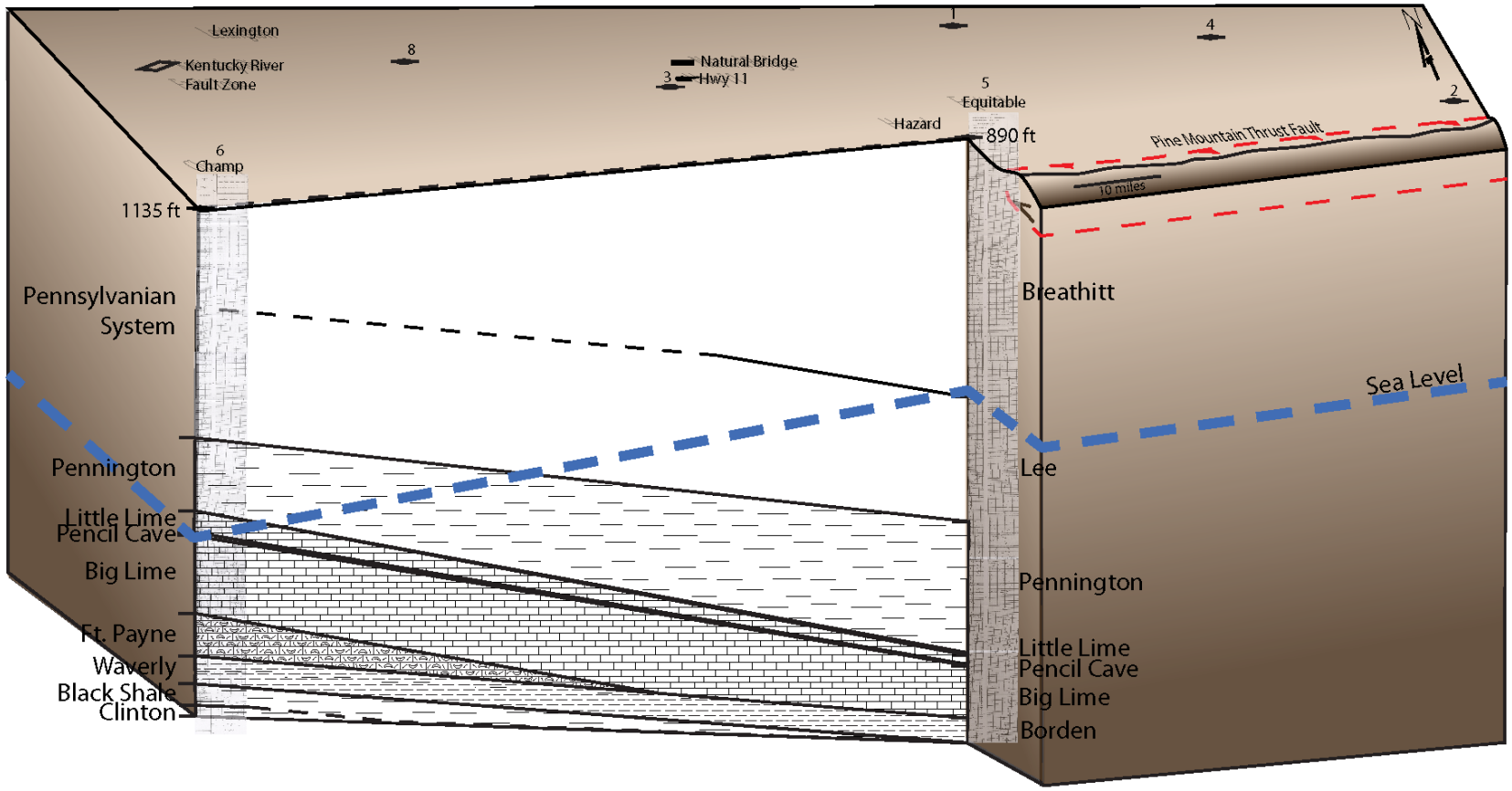

Appendix C Relative U-Pb age probability density and frequency plots for detrital zircons analyzed from Lower and Upper Mississippian sandstones sampled in the Appalachian basin

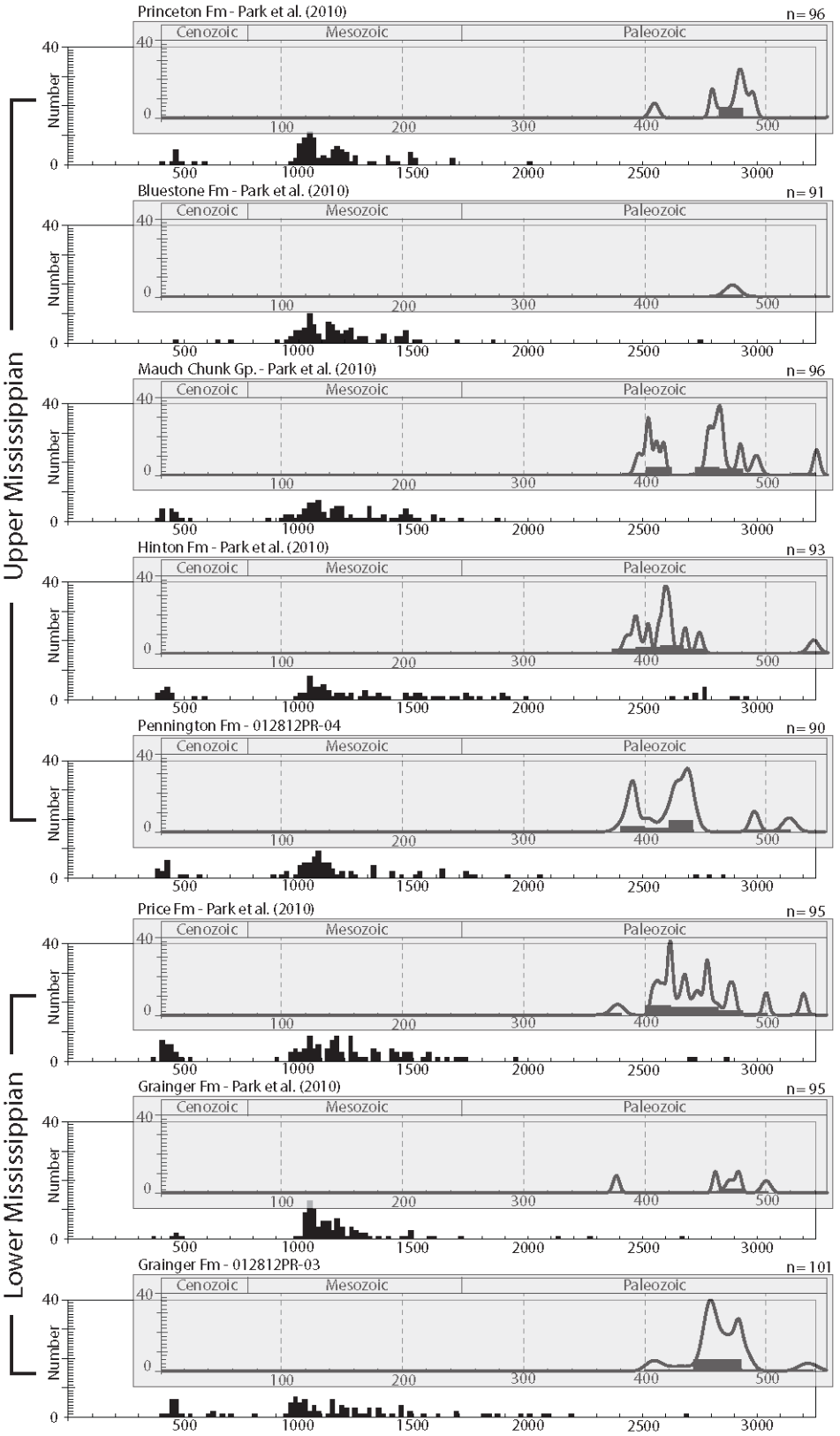

Appendix D Relative U-Pb age probability density and frequency plots for detrital zircons analyzed from Lower Pennsylvanian sandstones sampled in the Appalachian basin

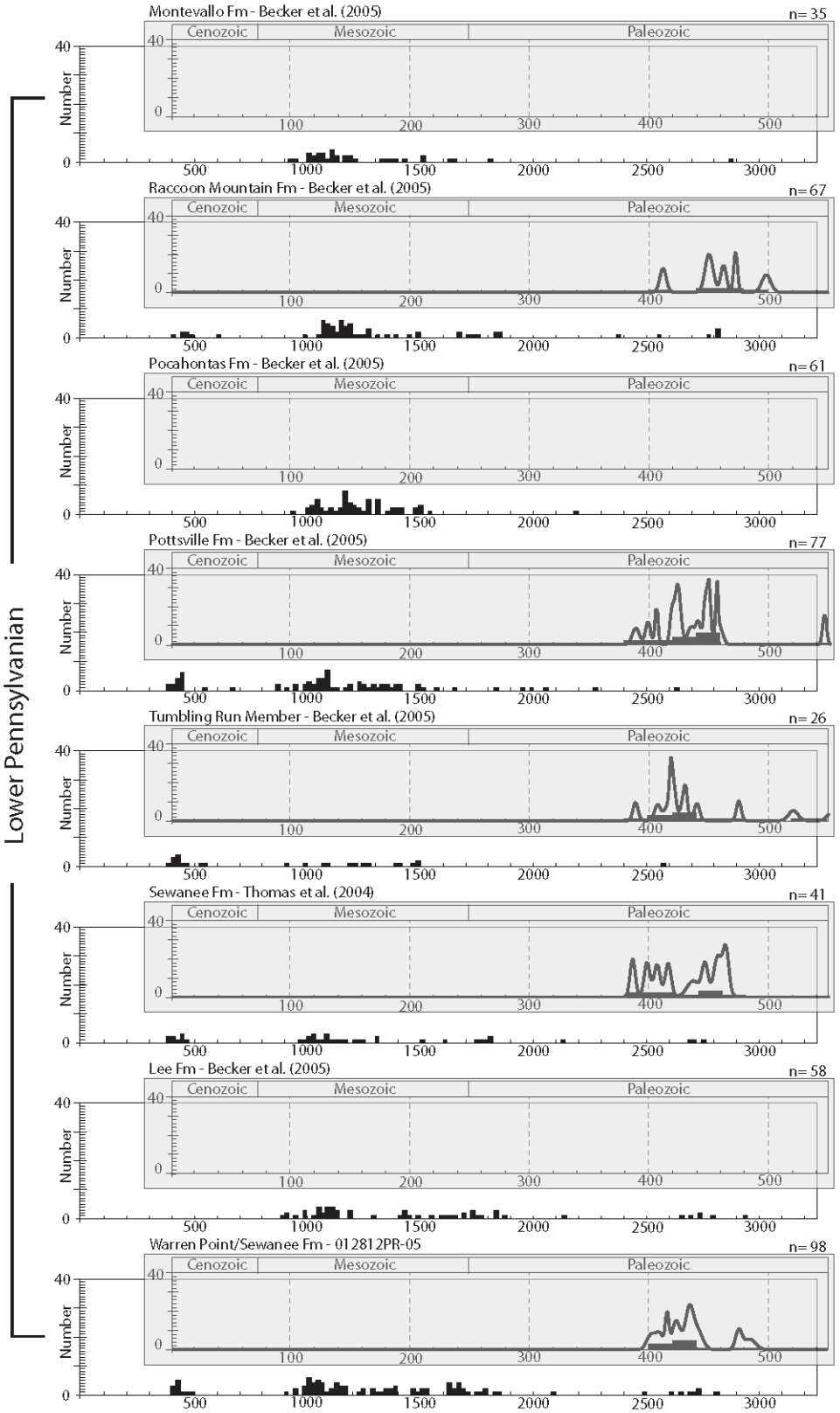

Appendix E Aerial photograph of Pine Mountain and the Pound Gap road exposure with geologic overlay

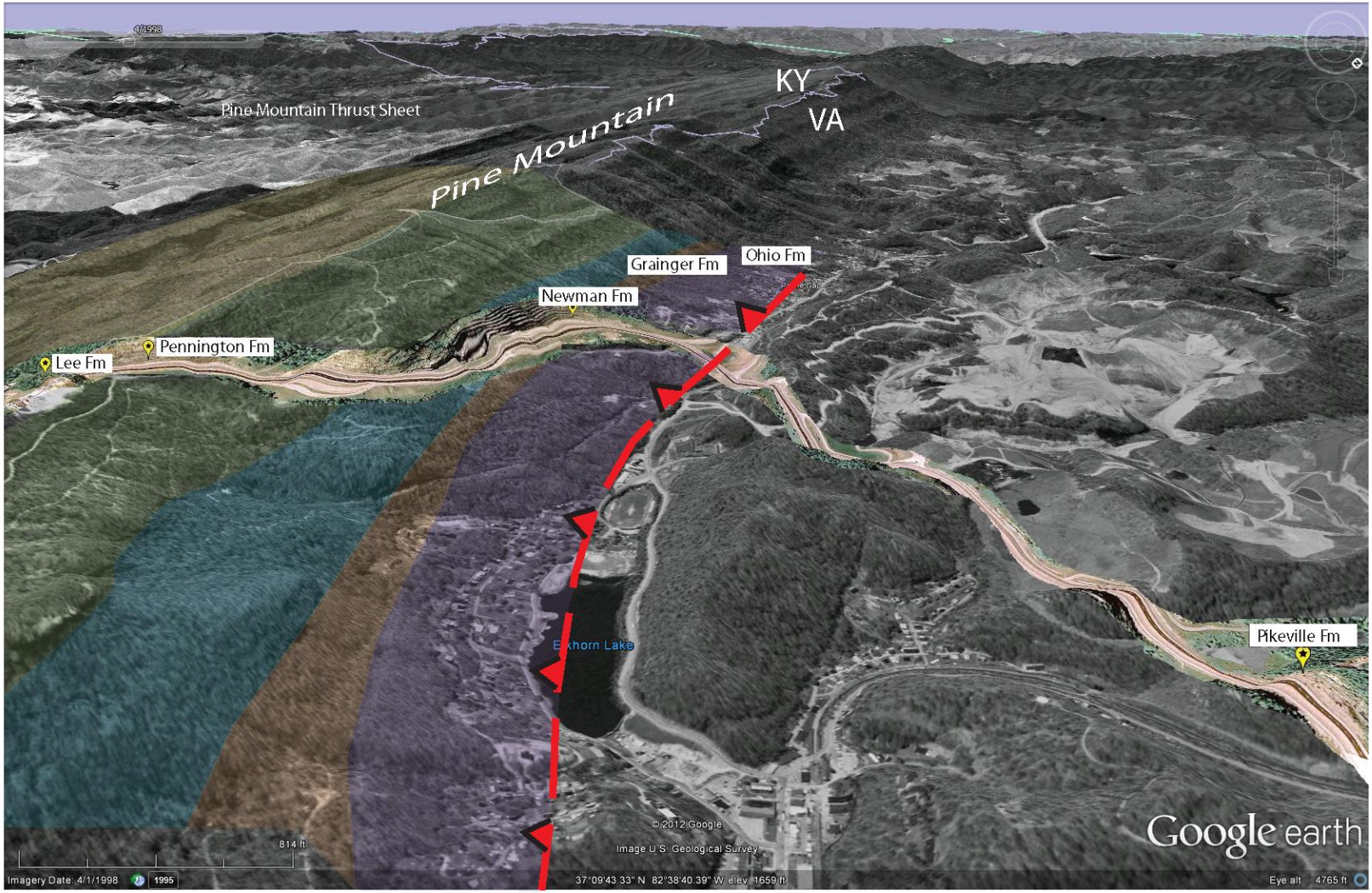

Appendix F Paleogeographic reconstructions with source terrane map overlay

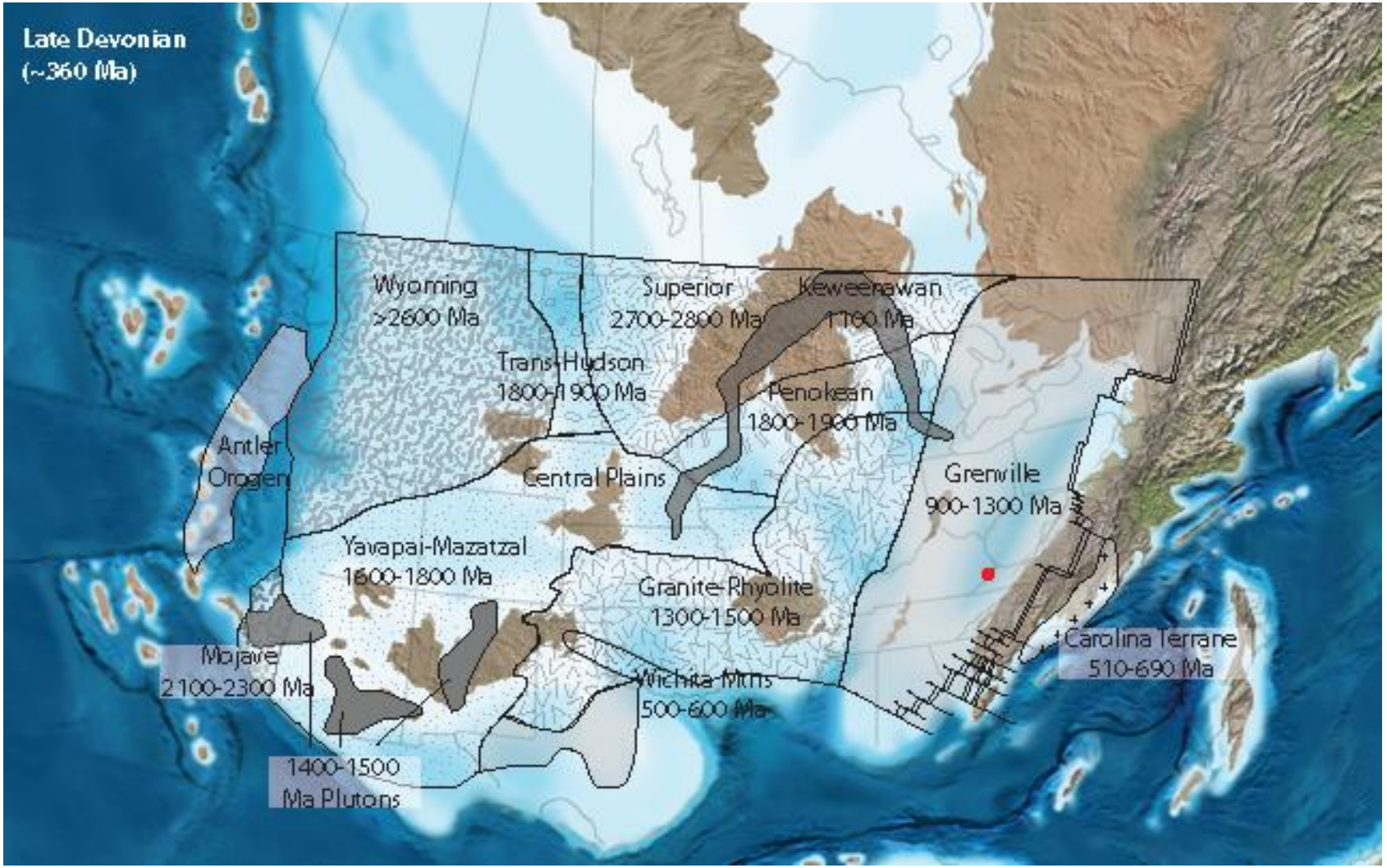

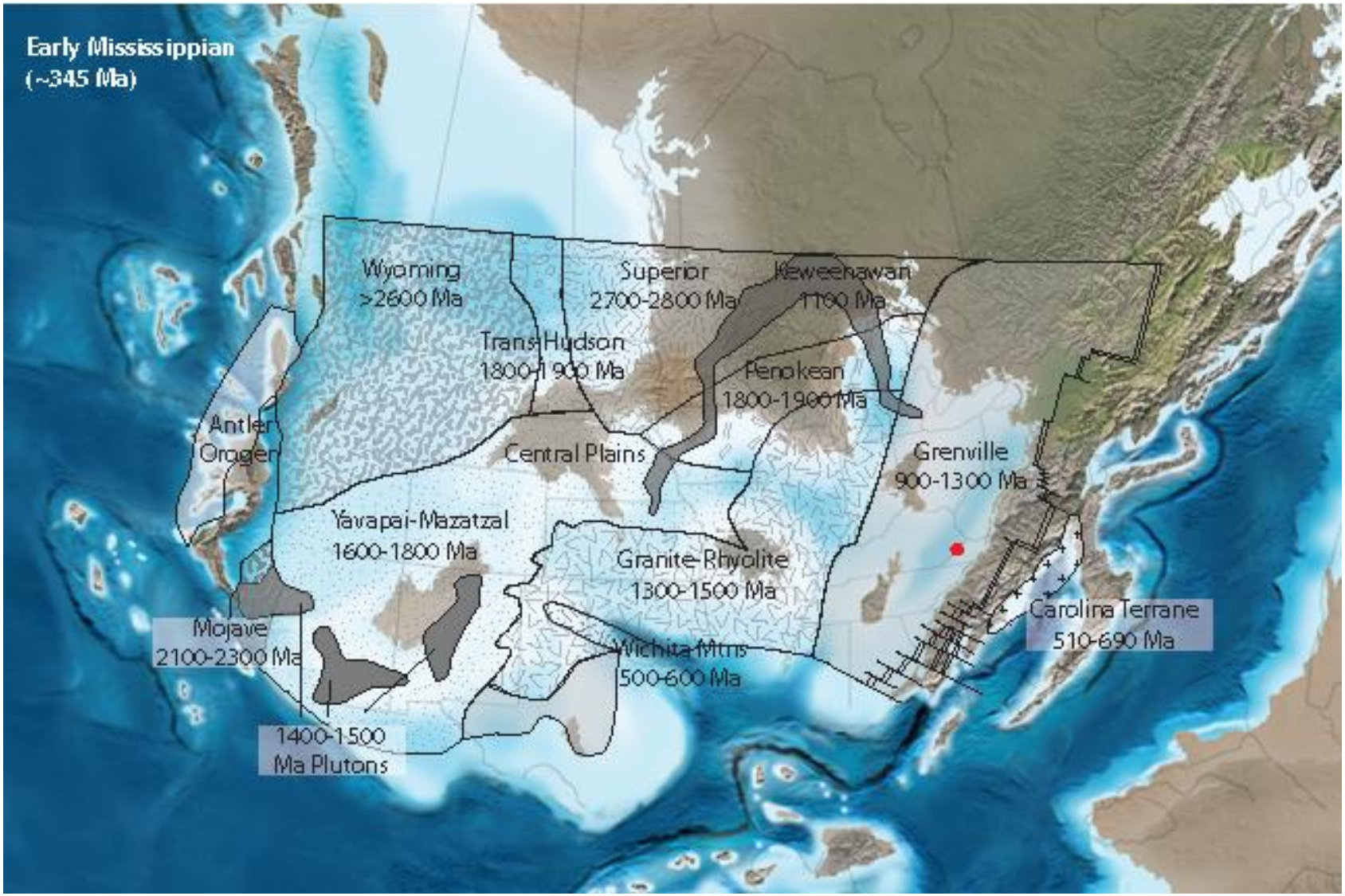
Early Mississippian
(~345 Ma)
Wyoming
>2600 Ma
Superior
2700-2800 Ma
Keweenawan
1100 Ma
Trans-Hudson
1800-1900 Ma
Penokean
1800-1900 Ma
Antler
Orogen
Central Plains
Grenville
900-1300 Ma
Yavapai-Mazatzal
1600-1800 Ma
Granite-Rhyolite
1300-1500 Ma
Carolina Terrane
510-690 Ma
Mojave
2100-2300 Ma
Wichita Mtns
500-600 Ma
1400-1500
Ma Plutons

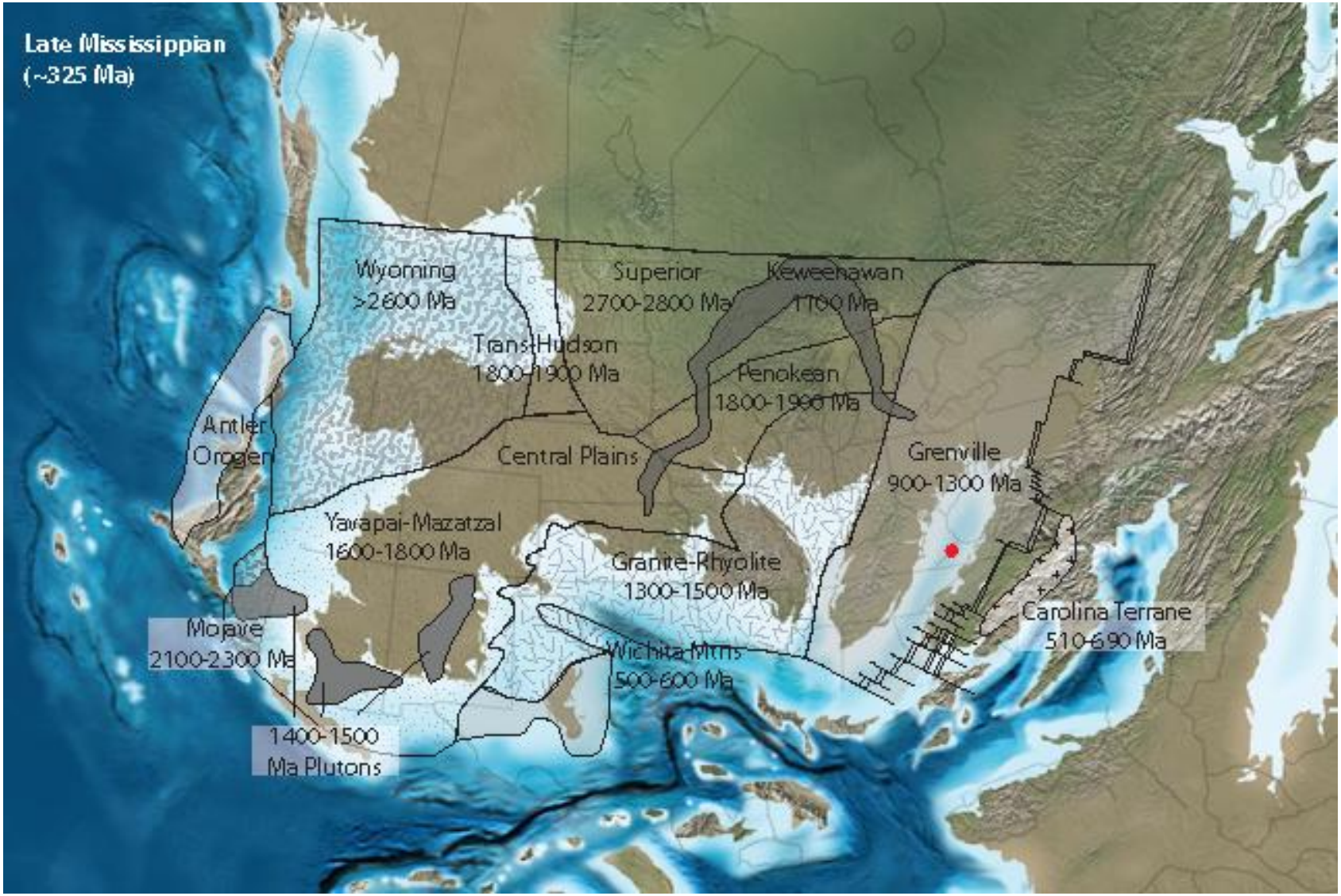
Late Mississippian
(~325 Ma)
Wyoming
>2600 Ma
Superior
2700-2800 Ma
Keweenawan
1100 Ma
Trans-Hudson
1800-1900 Ma
Penokean
1800-1900 Ma
Antler
Orogen
Central Plains
Grenville
900-1300 Ma
Yavapai-Mazatzal
1600-1800 Ma
Granite-Rhyolite
1300-1500 Ma
Carolina Terrane
510-690 Ma
Mojave
2100-2300 Ma
Wichita Mtns
500-600 Ma
1400-1500
Ma Plutons

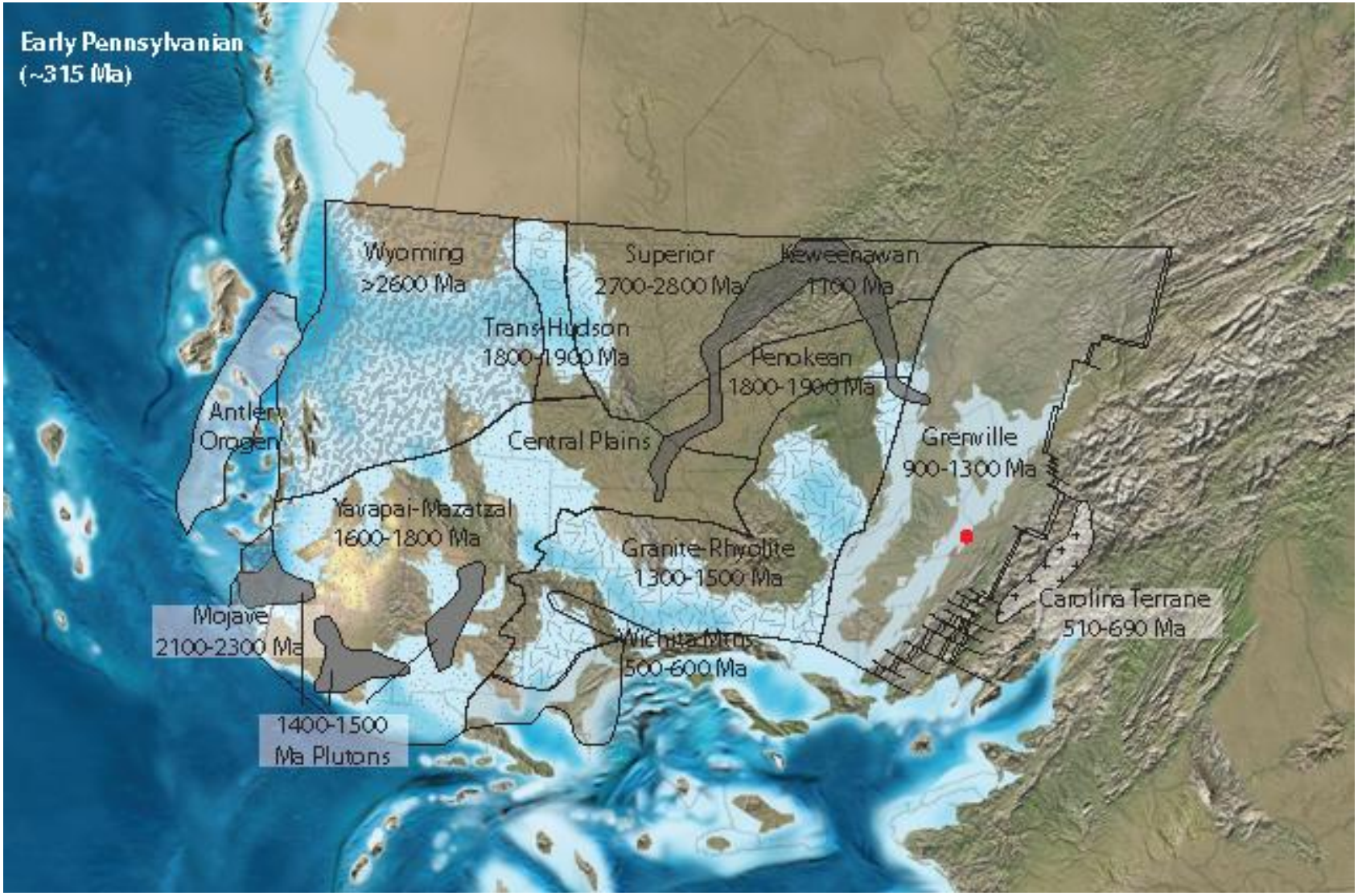
Early Pennsylvanian
(~315 Ma)
Wyoming
>2600 Ma
Superior
2700-2800 Ma
Keweenawan
1100 Ma
Trans-Hudson
1800-1900 Ma
Penokean
1800-1900 Ma
Antler
Orogen
Central Plains
Grenville
900-1300 Ma
Yavapai-Mazatzal
1600-1800 Ma
Granite-Rhyolite
1300-1500 Ma
Carolina Terrane
510-690 Ma
Mojave
2100-2300 Ma
Wichita Mtns.
500-600 Ma
1400-1500
Ma Plutons

Appendix G Bedding orientation data measured from the Pine Mountain thrust sheet strata at Pound Gap (n=35). Stereonets created using stereographic projection software GEOrient (version 9.5.0; Rod Holcombe, ©2011).

Strike Azimuth	Dip
58	24
47	21
70	30
52	24
65	25
68	24
68	29
69	24
72	25
65	25
74	26
72	24
68	29
72	27
67	27
52	23
64	28
65	26
61	19
57	22
64	24
61	28
61	19
62	20
57	25
61	32
50	33
51	32
57	27
69	24
54	27
68	27
54	25
60	31
66	28

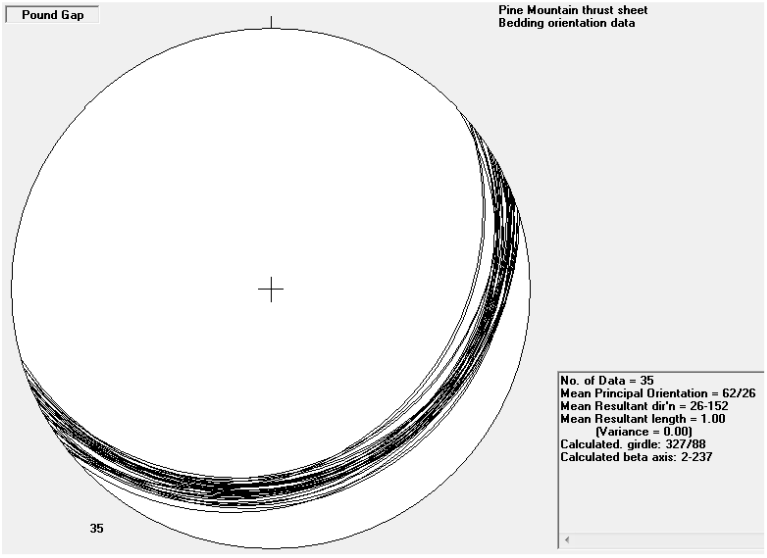

Appendix H Raw paleocurrent data from the Pine Mountain thrust sheet at Pound Gap, Grainger Formation groove casts.

Dip	Dip Direction
13	274
10	285
19	274
20	272
10	270
12	272
14	264
12	245
15	290
20	300
12	292
22	278
20	307
24	314
23	296
20	290
22	275
20	304
28	294
25	304
23	306
25	286
25	295
23	289
25	302
20	291
23	264
18	282
15	298
20	275
22	270
18	290
18	258
14	290
11	358
20	245
21	260
11	240
13	235

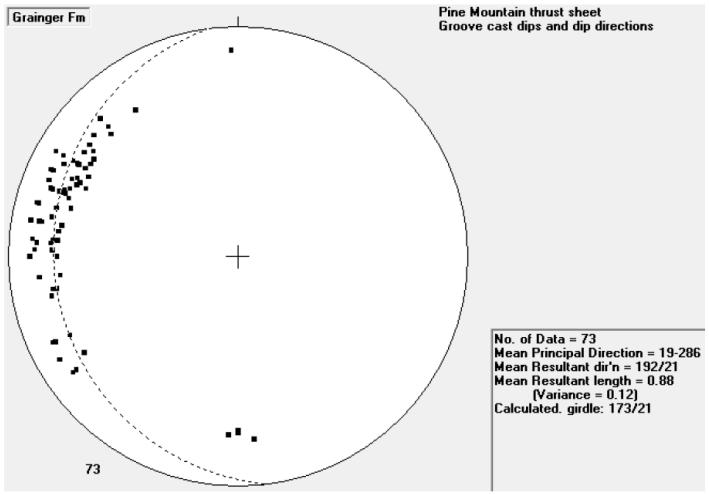

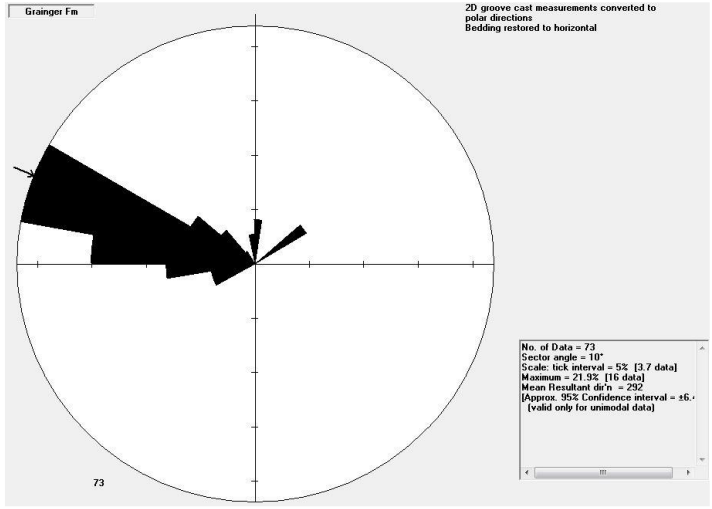

Dip	Dip Direction
16	315
21	300
13	300
23	325
21	315
25	180
24	180
21	175
23	183
21	295
12	295
09	300
18	300
19	310
09	280
11	295
13	280
11	275
14	280
19	285
11	285
21	290
19	290
23	280
22	238
19	290
21	290
19	260
27	298
24	294
22	292
24	300
15	235
13	245

Appendix I Raw paleocurrent data from the Pine Mountain thrust sheet at Pound Gap, Pennington Formation.

2D trough cross-strata foresets, meters 295-296

Dip	Dip direction
27	116
22	120
34	104
44	114
36	111
41	128
26	144
35	136
47	146
17	083
19	081
55	147
05	064
45	153
47	149
48	147
54	156
52	144
51	156
50	154
45	152
44	161
50	150
38	160
05	297
04	274
03	265
12	280
10	274
12	274
06	312
03	324
03	319
07	250
03	316
07	332
02	285

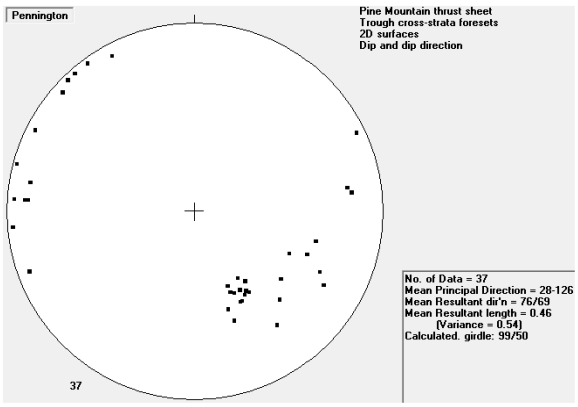

3D lateral accretion surfaces, meters 315-327

Strike Azimuth	Dip
064	52
052	25
067	53
069	58
060	45
056	55
054	57
099	45
055	33
049	41
071	55
049	35
060	49
055	45
060	32
070	39
055	51
060	20
059	18
059	18
057	25
050	24
072	24
061	39
029	35
041	28
318	15
034	14
354	20
051	19
042	38
013	28
012	27
019	34
019	37
016	29
350	12
345	13
333	08
011	10
014	29
004	36
014	35
019	27

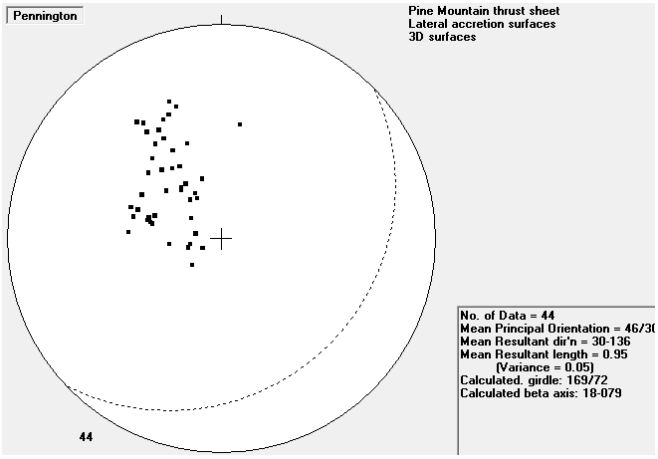

2D planar cross-strata foresets, meters 498-502

Dip	Dip direction
07	116
16	132
15	080
26	109
10	092
24	179
18	115
19	271
29	165
24	129

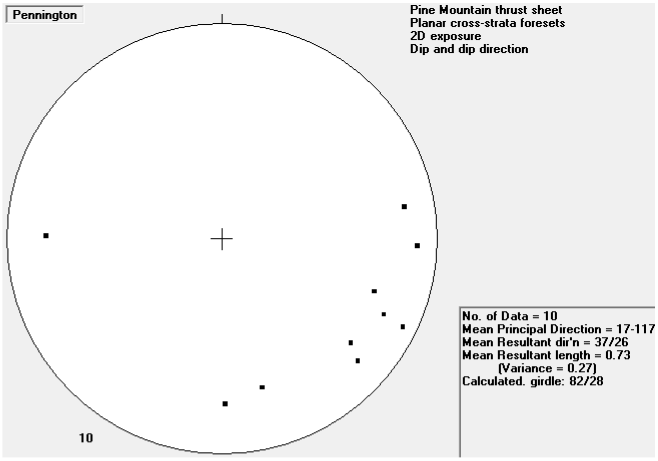

3D planar cross-strata foresets, meters 498-502

Strike Azimuth	Dip
046	41
042	46
024	41
044	40
035	45
057	45
054	33
062	30
044	42
018	45
049	42

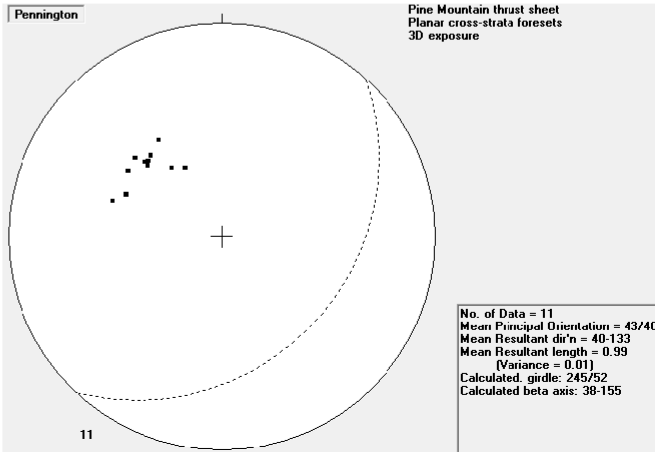

2D trough cross-strata foresets, meters 510-513

Dip	Dip direction
24	121
28	101
33	116
36	116
51	142
38	124
33	123
39	122
35	120
40	112
32	112

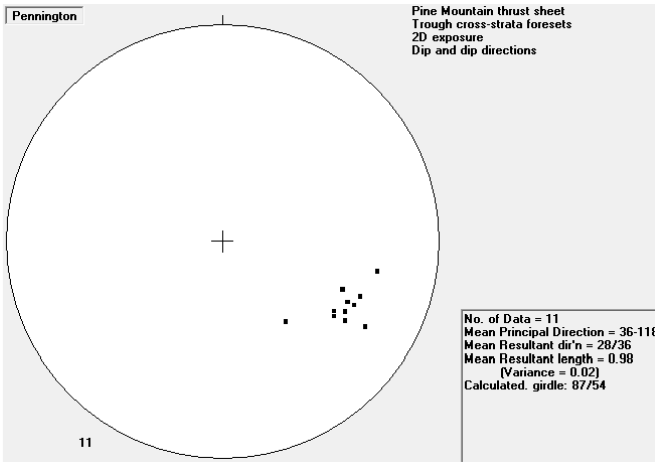

3D trough cross-strata foresets, meters 510-513

Strike Azimuth	Dip
047	19
074	33
043	30
055	19
061	21
056	12
051	27
012	14
039	23
020	18
039	44
050	41

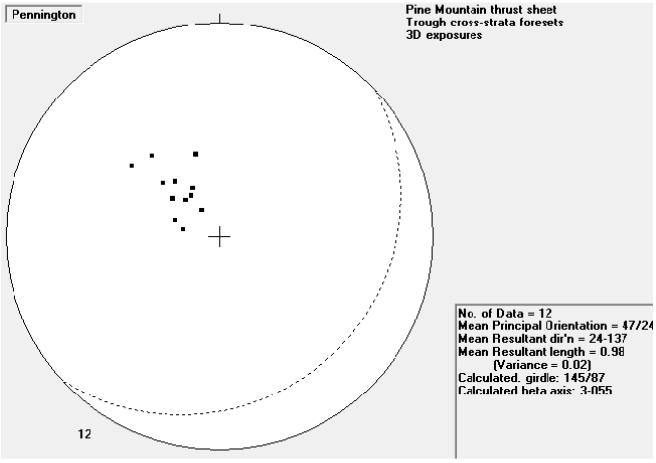

2D trough cross-strata foresets, meters 539-546

Dip	Dip direction
13	106
13	112
15	097
05	100
17	133
09	114
03	105
13	111
07	120
25	133
15	130
24	134
13	240
13	254
15	244
6	249

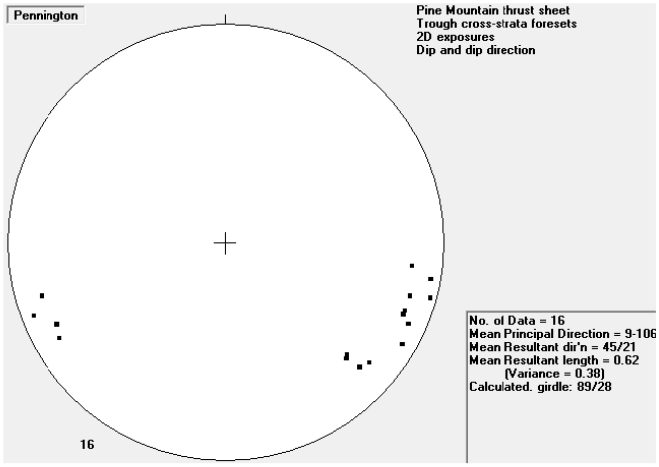

3D trough cross-strata foresets, meters 539-546

Strike Azimuth	Dip
32	30
114	19
104	25
51	17
43	13
69	17
61	17
69	24
34	20
95	26
100	21
88	18
92	17
66	26
66	33
14	6

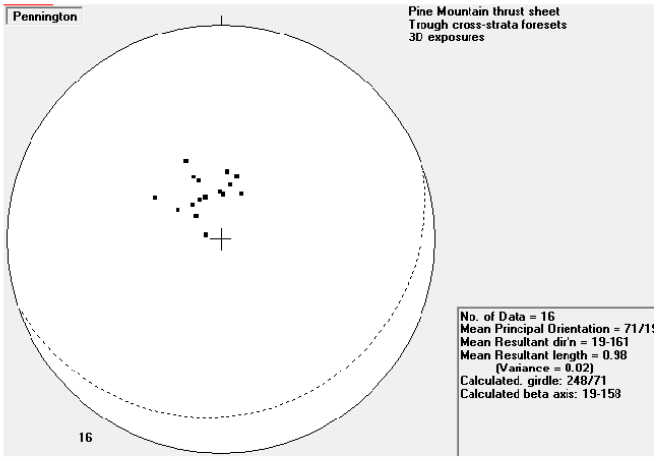

Appendix J Raw paleocurrent data from the Pine Mountain thrust sheet at Pound Gap, undivided Warren Point/Sewanee Formation.

3D trough cross-strata foresets

Strike azimuth	Dip
242	009
181	006
189	009
186	007
100	015
210	018
211	013
069	021
098	020
098	013
135	020
167	010
140	012
153	014
140	015
132	013
124	017
153	008
189	018
186	019
216	012
090	027
092	028
140	020
084	026
106	012
146	010
130	017
136	015
091	020
091	014
160	012
208	013
146	014
176	009
141	016
154	012
113	009

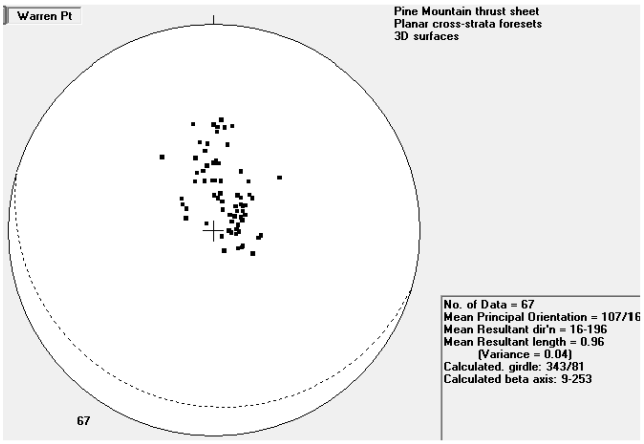

Strike azimuth	Dip
136	009
182	010
045	004
076	030
084	032
141	034
089	020
081	036
092	042
079	044
099	035
100	043
092	040
094	045
096	042
090	043
115	026
125	024
094	027
045	018
074	024
024	012
040	016
215	004
055	036
080	020
080	024
086	035
039	014

Appendix K Raw paleocurrent data from the footwall of the Pine Mountain thrust sheet at Pound Gap, Middle Pennsylvanian Pikeville Formation.

2D trough cross-strata foresets

Dip	Dip Direction
02	344
16	148
08	340
06	340
04	332
16	160
18	155
11	160
06	240
14	212
20	210
19	210
10	205
04	204
06	025
07	028
12	200
13	194
16	220
10	035
18	335
16	205
16	194
09	189
04	310
03	064
19	240
11	180
16	231
16	240
15	215
16	198
14	235
24	234
10	024
23	215

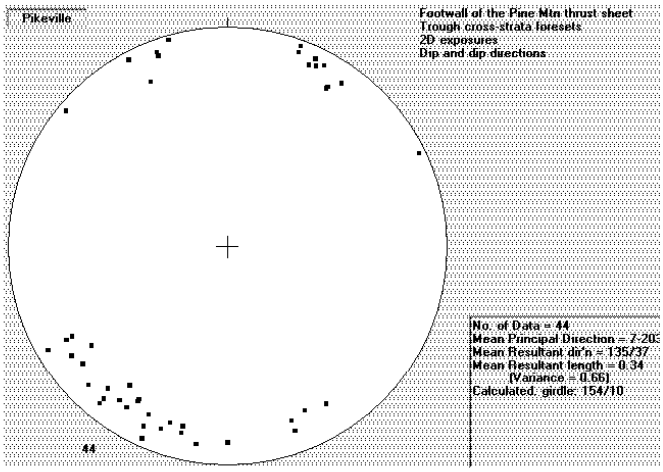

Two-dimensional surface orientation data for trough cross-strata measured in Middle Pennsylvanian Pikeville Formation in the footwall of the Pine Mountain thrust fault. Stereonet constructed using the stereographic projection software GEOrient (version 9.5.0; Rod Holcombe ©2011).

Dip	Dip Direction
09	026
06	020
03	020
11	225
11	219
08	219
15	032
16	032

Appendix L K-S tests comparing samples analyzed in this study to others analyzed by Thomas et al. (2004), Becker et al. (2005), and Park et al. (2010). Analysis run on: Wednesday, Dec 12, 2012 @ 12:15:35 PM. Version: 1.0.

K-S P-values using error in the CDF

	Pennington	Lee	Breathitt	Grainger	rainger (Par-	linton (Park_	ee (Becker	anee (Thomas)
Pennington		0.031	**0.091**	**0.860**	**0.193**	**0.057**	0.005	**0.708**
Lee	0.031		0.000	0.043	0.001	**0.957**	**0.670**	**0.474**
Breathitt	**0.091**	0.000		0.023	**0.316**	0.000	0.000	0.046
Grainger	**0.860**	0.043	0.023		0.009	**0.067**	0.004	**0.717**
Grainger (Park)	**0.193**	0.001	**0.316**	0.009		0.002	0.000	**0.241**
Hinton (Park)	**0.057**	**0.957**	0.000	**0.067**	0.002		**0.469**	**0.625**
Lee (Becker)	0.005	**0.670**	0.000	0.004	0.000	**0.469**		**0.160**
Sewanee (Thomas)	**0.708**	**0.474**	0.046	**0.717**	**0.241**	**0.625**	**0.160**	

K-S P-values for no error

	Pennington	Lee	Breathitt	Grainger	rainger (Par-	linton (Park_	ee (Becker	anee (Thomas)
Pennington		0.006	0.101	0.161	0.094	**0.018**	0.002	0.623
Lee	0.006		0.000	0.024	0.000	0.906	0.383	0.370
Breathitt	0.101	0.000		0.015	**0.020**	0.000	0.000	0.036
Grainger	0.161	0.024	0.015		0.000	**0.002**	0.001	0.621
Grainger (Park)	0.094	0.000	**0.020**	0.000		0.001	0.000	**0.027**
Hinton (Park)	**0.018**	0.906	0.000	**0.002**	0.001		0.439	0.173
Lee (Becker)	0.002	0.383	0.000	0.001	0.000	0.439		0.091
Sewanee (Thomas)	0.623	0.370	0.036	0.621	**0.027**	0.173	0.091	

Average K-S P-values using Monte-Carlo

	Pennington	Lee	Breathitt	Grainger	rainger (Par-	linton (Park_	ee (Becker	anee (Thomas)
Pennington		0.016	**0.065**	**0.446**	**0.123**	**0.027**	0.003	0.601
Lee	0.016		0.000	0.021	0.000	0.831	0.384	0.328
Breathitt	**0.065**	0.000		0.012	**0.096**	0.000	0.000	**0.033**
Grainger	**0.446**	0.021	0.012		0.006	**0.022**	0.002	0.589
Grainger (Park)	**0.123**	0.000	**0.096**	0.006		0.001	0.000	**0.149**
Hinton (Park)	**0.027**	0.831	0.000	**0.022**	0.001		0.429	0.293
Lee (Becker)	0.003	0.384	0.000	0.002	0.000	0.429		**0.086**
Sewanee (Thomas)	0.601	0.328	**0.033**	0.589	**0.149**	0.293	**0.086**	

D-values using error in the CDF

Pennington	Lee	Breathitt	Grainger	rainger (Par-	linton (Park_	ee (Becker'	anee (Thomas)
	0.211	0.177	0.087	0.159	0.197	0.294	0.132
0.211		0.376	0.196	0.291	0.074	0.120	0.157
0.177	0.376		0.206	0.134	0.357	0.435	0.252
0.087	0.196	0.206		0.234	0.187	0.293	0.129
0.159	0.291	0.134	0.234		0.272	0.366	0.192
0.197	0.074	0.357	0.187	0.272		0.142	0.141
0.294	0.120	0.435	0.293	0.366	0.142		0.229
0.132	0.157	0.252	0.129	0.192	0.141	0.229	

D-values for no error

Pennington	Lee	Breathitt	Grainger	rainger (Par-	linton (Park_	ee (Becker'	anee (Thomas)
	0.250	0.174	0.163	0.182	0.227	0.311	0.142
0.250		0.391	0.210	0.312	0.082	0.150	0.170
0.174	0.391		0.215	0.213	0.381	0.445	0.260
0.163	0.210	0.215		0.322	0.272	0.318	0.140
0.182	0.312	0.213	0.322		0.294	0.384	0.274
0.227	0.082	0.381	0.272	0.294		0.145	0.207
0.311	0.150	0.445	0.318	0.384	0.145		0.254
0.142	0.170	0.260	0.140	0.274	0.207	0.254	

Two std devs. of P-values using Monte-Carlo

Pennington	Lee	Breathitt	Grainger	rainger (Par-	linton (Park_	ee (Becker'	anee (Thomas)
	0.020	**0.068**	**0.399**	**0.203**	**0.040**	0.004	0.170
0.020		0.000	0.019	0.001	0.274	0.232	0.166
0.068	0.000		0.020	**0.165**	0.000	0.000	**0.023**
0.399	0.019	0.020		0.016	**0.032**	0.002	0.194
0.203	0.001	**0.165**	0.016		0.002	0.000	**0.102**
0.040	0.274	0.000	**0.032**	0.002		0.127	0.241
0.004	0.232	0.000	0.002	0.000	0.127		**0.075**
0.170	0.166	**0.023**	0.194	**0.102**	0.241	**0.075**	

Appendix M Detrital zircon U-Pb geochronologic analyses for Pound Gap sandstones

Grainger Formation

37°9'23.46"N						Isotope ratios					Apparent ages (Ma)								
82°38'46.38"W																			
Analysis	U	206Pb	U/Th	206Pb*	±	207Pb*	±	206Pb*	±	error	206Pb*	±	207Pb*	±	206Pb*	±	Best age	±	Conc
	(ppm)	204Pb		207Pb*	(%)	235U*	(%)	238U	(%)	corr.	238U*	(Ma)	235U	(Ma)	207Pb*	(Ma)	(Ma)	(Ma)	(%)
012812PR-03-41	397	66106	2.4	18.0177	3.7	0.4986	4.9	0.0652	3.3	0.67	406.9	13.0	410.7	16.6	432.4	81.6	406.9	13.0	94.1
012812PR-03-2	295	15366	4.7	17.9695	3.7	0.5263	7.1	0.0686	6.1	0.86	427.7	25.4	429.4	25.0	438.4	81.6	427.7	25.4	97.6
012812PR-03-47	305	31102	1.4	17.7954	4.4	0.5606	4.9	0.0724	2.2	0.44	450.3	9.5	451.9	18.0	460.0	98.0	450.3	9.5	97.9
012812PR-03-33	292	37243	1.1	18.1013	5.0	0.5541	5.6	0.0727	2.5	0.45	452.7	11.1	447.7	20.3	422.1	111.3	452.7	11.1	107.2
012812PR-03-63	105	22128	4.1	16.6928	10.5	0.6010	10.7	0.0728	2.2	0.20	452.8	9.4	477.9	40.7	600.2	227.0	452.8	9.4	75.4
012812PR-03-56	329	38133	2.3	17.5308	3.5	0.5751	3.9	0.0731	1.9	0.47	454.9	8.1	461.3	14.5	493.2	76.3	454.9	8.1	92.2
012812PR-03-37	191	17232	2.9	17.6708	6.0	0.5730	7.8	0.0734	5.0	0.64	456.8	22.1	459.9	28.8	475.6	132.3	456.8	22.1	96.1
012812PR-03-79	187	18548	2.1	18.4213	5.7	0.5502	6.4	0.0735	2.9	0.45	457.2	12.9	445.1	23.2	382.9	129.0	457.2	12.9	119.4
012812PR-03-45	415	47300	0.7	17.8058	2.1	0.5746	3.4	0.0742	2.7	0.79	461.5	11.9	461.0	12.6	458.8	46.1	461.5	11.9	100.6
012812PR-03-72	137	35167	1.2	17.7596	10.0	0.5790	10.8	0.0746	4.2	0.39	463.7	18.7	463.8	40.4	464.5	222.2	463.7	18.7	99.8
012812PR-03-1	105	4283	0.5	16.5743	8.1	0.6307	8.5	0.0758	2.6	0.31	471.1	12.0	496.5	33.5	615.6	175.6	471.1	12.0	76.5
012812PR-03-73	114	13318	1.7	17.9610	10.4	0.5852	10.8	0.0762	3.0	0.28	473.6	13.7	467.8	40.5	439.5	231.1	473.6	13.7	107.8
012812PR-03-82	242	29483	1.1	18.2425	5.5	0.5810	5.7	0.0769	1.2	0.22	477.4	5.7	465.1	21.1	404.7	123.8	477.4	5.7	118.0
012812PR-03-51	134	35585	1.1	19.1559	10.5	0.5542	11.1	0.0770	3.5	0.31	478.2	16.0	447.8	40.1	294.3	240.5	478.2	16.0	162.5
012812PR-03-66	359	74726	1.5	17.8563	2.6	0.6010	3.4	0.0778	2.3	0.67	483.2	10.7	477.9	13.1	452.5	56.8	483.2	10.7	106.8
012812PR-03-8	165	30059	1.9	17.9533	6.2	0.6645	6.9	0.0865	3.0	0.43	534.9	15.4	517.3	28.0	440.4	138.6	534.9	15.4	121.5
012812PR-03-29	110	42534	1.4	16.1379	6.0	0.8555	6.6	0.1001	2.9	0.43	615.2	16.7	627.7	30.9	672.9	127.6	615.2	16.7	91.4
012812PR-03-95	191	66865	1.8	16.1747	3.8	0.8720	4.2	0.1023	1.7	0.41	627.8	10.2	636.6	19.8	668.0	81.6	627.8	10.2	94.0
012812PR-03-6	124	15824	2.0	16.4727	6.7	0.8732	7.0	0.1043	2.0	0.28	639.7	12.0	637.3	33.1	628.8	144.5	639.7	12.0	101.7
012812PR-03-30	322	112791	3.0	15.3739	5.9	0.9757	11.2	0.1088	9.5	0.85	665.7	60.3	691.4	56.1	775.8	123.2	665.7	60.3	85.8
012812PR-03-15	313	47478	0.5	15.8354	2.1	1.0274	3.5	0.1180	2.8	0.80	719.0	19.2	717.6	18.0	713.3	44.3	719.0	19.2	100.8
012812PR-03-36	156	42999	1.5	15.1992	3.2	1.2224	4.5	0.1347	3.1	0.70	814.9	24.1	810.9	25.2	799.8	68.1	814.9	24.1	101.9
012812PR-03-61	99	72621	2.6	14.1085	5.1	1.5456	5.3	0.1582	1.5	0.29	946.5	13.2	948.7	32.5	953.9	103.4	953.9	103.4	99.2
012812PR-03-14	105	27107	2.4	14.0455	2.5	1.6562	3.2	0.1687	2.0	0.63	1005.0	18.8	991.9	20.3	963.1	51.0	963.1	51.0	104.4
012812PR-03-2 the first	100	23621	2.1	13.9985	1.7	1.6385	2.7	0.1664	2.1	0.77	992.0	19.6	985.1	17.3	969.9	35.6	969.9	35.6	102.3
012812PR-03-39	113	48811	1.9	13.9663	3.7	1.6582	4.4	0.1680	2.5	0.57	1000.9	23.3	992.7	28.1	974.6	74.5	974.6	74.5	102.7
012812PR-03-77	70	19732	2.7	13.9589	6.5	1.6985	6.9	0.1720	2.3	0.34	1022.9	21.9	1008.0	44.1	975.7	132.4	975.7	132.4	104.8
012812PR-03-83	122	62928	2.5	13.9327	2.7	1.5940	5.6	0.1611	5.0	0.88	962.7	44.4	967.9	35.3	979.5	54.9	979.5	54.9	98.3
012812PR-03-85	74	22536	3.2	13.9103	4.4	1.6413	4.9	0.1656	2.1	0.42	987.7	18.9	986.2	30.9	982.8	90.5	982.8	90.5	100.5

012812PR-03-34	171	109428	2.1	13.9034	1.4	1.6990	2.6	0.1713	2.1	0.83	1019.4	20.1	1008.2	16.3	983.8	28.8	983.8	28.8	103.6
012812PR-03-84	67	14725	1.9	13.8858	6.4	1.5838	7.2	0.1595	3.2	0.45	954.0	28.6	963.9	44.9	986.4	131.4	986.4	131.4	96.7
012812PR-03-92	104	28574	4.4	13.8667	3.2	1.7325	4.3	0.1742	2.9	0.67	1035.4	27.9	1020.7	27.9	989.2	65.2	989.2	65.2	104.7
012812PR-03-100	110	33428	4.1	13.8529	3.0	1.7323	3.3	0.1740	1.4	0.44	1034.3	13.9	1020.6	21.2	991.2	60.2	991.2	60.2	104.3
012812PR-03-31	221	46272	1.9	13.8502	2.2	1.6729	3.2	0.1680	2.3	0.73	1001.3	21.4	998.3	20.2	991.6	44.4	991.6	44.4	101.0
012812PR-03-81	42	15378	1.3	13.8135	5.3	1.7584	5.7	0.1762	2.2	0.38	1046.0	20.8	1030.3	36.8	997.0	106.9	997.0	106.9	104.9
012812PR-03-44	84	24709	1.9	13.7556	3.0	1.6947	6.4	0.1691	5.7	0.89	1007.0	52.8	1006.5	40.8	1005.5	60.0	1005.5	60.0	100.1
012812PR-03-88	95	34062	3.1	13.7411	4.9	1.7066	5.0	0.1701	1.1	0.23	1012.6	10.7	1011.0	32.0	1007.7	98.6	1007.7	98.6	100.5
012812PR-03-12	394	81526	1.6	13.7408	1.3	1.4128	3.4	0.1408	3.2	0.93	849.1	25.1	894.3	20.3	1007.7	26.0	1007.7	26.0	84.3
012812PR-03-32	90	25151	3.4	13.6903	3.1	1.6836	3.9	0.1672	2.3	0.60	996.5	21.3	1002.3	24.5	1015.2	62.5	1015.2	62.5	98.2
012812PR-03-69	56	13570	1.2	13.6797	7.7	1.6624	9.1	0.1649	4.8	0.53	984.2	43.5	994.3	57.5	1016.7	156.1	1016.7	156.1	96.8
012812PR-03-23	110	45504	4.3	13.6450	2.4	1.7737	6.3	0.1755	5.9	0.93	1042.5	56.6	1035.9	41.2	1021.9	48.2	1021.9	48.2	102.0
012812PR-03-35	166	39880	1.2	13.6361	2.1	1.7633	4.0	0.1744	3.4	0.85	1036.2	32.5	1032.1	26.0	1023.2	43.2	1023.2	43.2	101.3
012812PR-03-49	203	72050	3.2	13.5945	1.7	1.7785	1.9	0.1754	0.9	0.47	1041.6	8.7	1037.6	12.4	1029.4	34.0	1029.4	34.0	101.2
012812PR-03-55	409	111721	2.4	13.5528	0.9	1.7697	1.3	0.1740	0.9	0.69	1033.9	8.5	1034.4	8.3	1035.6	18.8	1035.6	18.8	99.8
012812PR-03-60	219	38457	17.3	13.5471	2.2	1.7734	2.8	0.1742	1.7	0.62	1035.5	16.5	1035.8	18.0	1036.4	43.6	1036.4	43.6	99.9
012812PR-03-17	175	46891	1.2	13.5263	1.5	1.7930	2.6	0.1759	2.2	0.81	1044.5	20.7	1042.9	17.3	1039.5	31.2	1039.5	31.2	100.5
012812PR-03-22	344	212286	2.2	13.5096	1.1	1.7368	1.9	0.1702	1.6	0.83	1013.1	14.7	1022.3	12.2	1042.0	21.4	1042.0	21.4	97.2
012812PR-03-46	273	58329	17.1	13.4096	1.5	1.7151	6.9	0.1668	6.7	0.98	994.4	62.1	1014.2	44.3	1057.1	30.8	1057.1	30.8	94.1
012812PR-03-93	110	53468	1.7	13.3185	3.3	1.7695	3.5	0.1709	1.0	0.28	1017.2	9.0	1034.3	22.5	1070.8	66.9	1070.8	66.9	95.0
012812PR-03-11	260	20012	3.1	13.2847	1.5	1.8748	3.0	0.1806	2.6	0.87	1070.4	25.3	1072.2	19.6	1075.9	29.5	1075.9	29.5	99.5
012812PR-03-40	75	23296	2.8	13.2616	5.0	1.8708	6.4	0.1799	4.0	0.62	1066.6	39.1	1070.8	42.5	1079.3	101.3	1079.3	101.3	98.8
012812PR-03-21	86	21289	1.2	13.2614	3.0	1.6319	5.0	0.1570	4.0	0.80	939.9	34.7	982.6	31.2	1079.3	59.5	1079.3	59.5	87.1
012812PR-03-58	137	70024	2.3	13.2092	2.7	1.8165	5.2	0.1740	4.5	0.86	1034.2	42.9	1051.4	34.3	1087.3	54.1	1087.3	54.1	95.1
012812PR-03-19	124	37163	1.7	13.1524	2.7	1.8766	4.5	0.1790	3.5	0.79	1061.6	34.3	1072.9	29.5	1095.9	54.9	1095.9	54.9	96.9
012812PR-03-57	342	250088	3.1	12.9237	1.2	2.0463	2.4	0.1918	2.0	0.85	1131.1	21.0	1131.1	16.2	1130.9	24.6	1130.9	24.6	100.0
012812PR-03-70	76	41017	1.7	12.8622	5.4	2.0855	7.7	0.1945	5.4	0.71	1146.0	56.8	1144.1	52.7	1140.4	108.2	1140.4	108.2	100.5
012812PR-03-27	52	21845	17.6	12.8316	6.0	2.1227	7.2	0.1975	4.0	0.55	1162.1	42.3	1156.2	49.7	1145.2	119.1	1145.2	119.1	101.5
012812PR-03-98	80	97677	1.4	12.8030	3.4	2.2088	3.8	0.2051	1.6	0.44	1202.7	18.1	1183.8	26.3	1149.6	67.1	1149.6	67.1	104.6
012812PR-03-94	444	194677	100.8	12.7956	5.0	1.8183	6.2	0.1687	3.6	0.58	1005.2	33.1	1052.1	40.4	1150.7	99.9	1150.7	99.9	87.3
012812PR-03-9	42	20506	1.6	12.7901	5.8	2.0121	6.2	0.1866	2.1	0.34	1103.2	21.4	1119.6	41.9	1151.6	115.3	1151.6	115.3	95.8
012812PR-03-76	276	89305	10.7	12.7779	1.0	2.1543	1.6	0.1997	1.2	0.76	1173.4	13.3	1166.4	11.3	1153.5	20.8	1153.5	20.8	101.7
012812PR-03-24	157	10754	1.3	12.6398	2.8	2.0588	3.5	0.1887	2.0	0.59	1114.5	20.8	1135.2	23.7	1175.0	55.6	1175.0	55.6	94.8
012812PR-03-64	116	60237	1.6	12.5767	3.1	2.2340	4.1	0.2038	2.6	0.64	1195.6	28.7	1191.8	28.7	1184.9	61.9	1184.9	61.9	100.9
012812PR-03-25	103	50024	1.5	12.5604	3.4	2.1221	4.0	0.1933	2.1	0.53	1139.3	22.5	1156.0	27.9	1187.5	67.7	1187.5	67.7	95.9
012812PR-03-97	527	166512	143.7	12.5547	0.9	2.2806	3.5	0.2077	3.4	0.96	1216.3	37.3	1206.3	24.6	1188.4	18.4	1188.4	18.4	102.4
012812PR-03-68	151	88500	2.5	12.5174	1.3	2.1281	3.9	0.1932	3.7	0.94	1138.7	38.6	1158.0	27.1	1194.2	25.6	1194.2	25.6	95.3
012812PR-03-1 the first	98	34669	1.4	12.4230	2.2	2.2909	3.3	0.2064	2.4	0.74	1209.7	26.6	1209.5	23.1	1209.2	43.2	1209.2	43.2	100.0
012812PR-03-10	199	84977	2.0	12.3738	1.4	2.2975	1.6	0.2062	0.8	0.52	1208.4	9.1	1211.5	11.2	1217.0	26.6	1217.0	26.6	99.3
012812PR-03-86	174	94981	1.8	12.3625	1.1	2.3491	2.1	0.2106	1.7	0.84	1232.1	19.3	1227.3	14.6	1218.7	22.2	1218.7	22.2	101.1
012812PR-03-18	165	79730	3.5	12.2218	1.2	2.4058	3.1	0.2132	2.8	0.92	1246.1	32.0	1244.3	21.9	1241.2	22.9	1241.2	22.9	100.4

012812PR-03-102	116	28327	4.6	12.1656	1.4	2.5508	2.3	0.2251	1.7	0.77	1308.6	20.7	1286.7	16.5	1250.3	28.0	1250.3	28.0	104.7
012812PR-03-38	184	61145	2.6	12.1132	1.3	2.5296	7.0	0.2222	6.9	0.98	1293.7	81.1	1280.6	51.3	1258.7	25.5	1258.7	25.5	102.8
012812PR-03-89	187	86247	1.5	12.0414	1.4	2.5212	1.8	0.2202	1.1	0.60	1282.8	12.7	1278.2	13.1	1270.3	28.1	1270.3	28.1	101.0
012812PR-03-59	187	53390	2.1	11.9632	1.6	2.6369	4.8	0.2288	4.6	0.94	1328.2	54.9	1311.0	35.6	1283.0	30.9	1283.0	30.9	103.5
012812PR-03-62	167	51647	2.6	11.8056	1.2	2.7208	3.5	0.2330	3.3	0.93	1350.0	40.1	1334.2	26.1	1308.8	24.3	1308.8	24.3	103.1
012812PR-03-78	606	362660	2.0	11.7543	0.5	2.7138	1.5	0.2314	1.4	0.95	1341.6	17.0	1332.2	11.0	1317.2	8.8	1317.2	8.8	101.8
012812PR-03-80	74	30607	2.1	11.7469	3.2	2.6633	4.2	0.2269	2.7	0.65	1318.2	32.2	1318.3	30.8	1318.5	61.8	1318.5	61.8	100.0
012812PR-03-20	115	76231	3.5	11.5928	1.6	2.7142	2.6	0.2282	2.0	0.79	1325.1	24.5	1332.3	19.3	1344.0	31.0	1344.0	31.0	98.6
012812PR-03-87	265	77034	1.2	11.5191	0.8	2.9235	2.6	0.2442	2.5	0.95	1408.7	31.3	1388.0	19.8	1356.3	16.2	1356.3	16.2	103.9
012812PR-03-71	207	241928	1.5	11.5187	1.5	2.7082	4.9	0.2262	4.6	0.95	1314.8	55.0	1330.7	36.1	1356.4	29.7	1356.4	29.7	96.9
012812PR-03-3	107	62922	1.1	11.4903	2.2	2.9002	4.8	0.2417	4.2	0.89	1395.5	53.2	1382.0	36.2	1361.1	42.9	1361.1	42.9	102.5
012812PR-03-103	97	40112	1.7	11.2569	2.4	3.0632	5.4	0.2501	4.9	0.90	1438.9	63.2	1423.5	41.7	1400.6	45.3	1400.6	45.3	102.7
012812PR-03-96	115	95399	2.6	11.0249	2.8	3.1654	3.1	0.2531	1.5	0.47	1454.5	18.9	1448.7	24.0	1440.4	52.6	1440.4	52.6	101.0
012812PR-03-74	182	79597	2.4	11.0165	1.8	3.1682	5.8	0.2531	5.5	0.95	1454.6	71.2	1449.4	44.6	1441.8	35.0	1441.8	35.0	100.9
012812PR-03-104	419	247468	1.5	10.9309	0.4	3.0959	3.2	0.2454	3.1	0.99	1414.9	39.8	1431.7	24.2	1456.7	7.4	1456.7	7.4	97.1
012812PR-03-4	201	86854	2.9	10.9296	1.2	3.1360	1.7	0.2486	1.2	0.70	1431.2	15.5	1441.6	13.3	1456.9	23.6	1456.9	23.6	98.2
012812PR-03-5	281	131885	5.3	10.7107	0.8	3.3910	2.1	0.2634	1.9	0.92	1507.3	25.5	1502.3	16.1	1495.3	14.9	1495.3	14.9	100.8
012812PR-03-13	32	9760	1.0	10.7100	5.1	3.2168	5.7	0.2499	2.7	0.47	1437.8	34.6	1461.2	44.4	1495.4	95.9	1495.4	95.9	96.1
012812PR-03-67	324	130866	1.9	10.4214	0.4	3.6632	1.6	0.2769	1.6	0.96	1575.6	21.8	1563.4	12.9	1546.9	8.2	1546.9	8.2	101.9
012812PR-03-50	167	90311	2.1	10.0372	0.9	3.9062	3.4	0.2844	3.3	0.97	1613.3	47.1	1615.0	27.6	1617.2	16.3	1617.2	16.3	99.8
012812PR-03-7	271	275514	1.2	9.6869	0.7	3.9763	2.8	0.2794	2.7	0.97	1588.1	38.7	1629.4	23.0	1683.0	12.6	1683.0	12.6	94.4
012812PR-03-16	151	59753	1.2	9.6099	1.1	4.1950	1.5	0.2924	1.0	0.65	1653.4	14.0	1673.0	12.1	1697.7	20.6	1697.7	20.6	97.4
012812PR-03-54	135	91927	2.2	9.0709	1.0	4.8982	2.1	0.3222	1.9	0.88	1800.7	29.6	1802.0	17.9	1803.4	18.1	1803.4	18.1	99.8
012812PR-03-105	112	42527	2.4	8.9753	1.2	5.2023	3.3	0.3386	3.0	0.92	1880.1	49.3	1853.0	27.9	1822.6	22.6	1822.6	22.6	103.2
012812PR-03-75	128	88480	0.7	8.6952	1.0	5.3022	4.1	0.3344	3.9	0.97	1859.6	63.6	1869.2	34.8	1880.0	18.4	1880.0	18.4	98.9
012812PR-03-90	123	60271	0.8	8.3116	0.8	6.0319	6.1	0.3636	6.1	0.99	1999.3	104.1	1980.5	53.3	1960.9	14.2	1960.9	14.2	102.0
012812PR-03-43	274	48514	5.4	8.1123	0.6	4.8195	2.4	0.2836	2.3	0.97	1609.3	33.2	1788.3	20.2	2004.1	10.7	2004.1	10.7	80.3
012812PR-03-53	226	232358	1.4	7.8578	0.5	6.6050	1.2	0.3764	1.1	0.91	2059.6	19.7	2060.0	10.8	2060.5	8.8	2060.5	8.8	100.0
012812PR-03-52	412	558243	8.6	7.7004	0.2	7.1059	1.9	0.3969	1.9	1.00	2154.5	34.1	2124.8	16.7	2096.1	3.1	2096.1	3.1	102.8
012812PR-03-48	75	34375	0.8	7.2659	1.3	7.8290	8.1	0.4126	8.0	0.99	2226.7	150.7	2211.6	73.1	2197.6	22.7	2197.6	22.7	101.3
012812PR-03-65	90	110266	1.4	5.4257	0.7	13.1182	1.4	0.5162	1.2	0.87	2683.1	26.9	2688.2	13.4	2692.0	11.7	2692.0	11.7	99.7

Pennington Formation

37°9'18.24"N						Isotope ratios					Apparent ages (Ma)								
82°38'5.10"W																			
Analysis	U	206Pb	U/Th	206Pb*	±	207Pb*	±	206Pb*	±	error	206Pb*	±	207Pb*	±	206Pb*	±	Best age	±	Conc
	(ppm)	204Pb		207Pb*	(%)	235U*	(%)	238U	(%)	corr.	238U*	(Ma)	235U	(Ma)	207Pb*	(Ma)	(Ma)	(Ma)	(%)
01812PR-04-45	548	17000	0.7	17.5142	6.3	0.4836	7.2	0.0614	3.5	0.48	384.3	12.9	400.5	23.8	495.3	139.0	384.3	12.9	NA
01812PR-04-16	92	23335	1.1	17.9002	7.3	0.4778	7.6	0.0620	2.1	0.27	387.9	7.7	396.5	24.8	447.0	161.9	387.9	7.7	NA
01812PR-04-13	476	95344	1.3	18.1072	1.8	0.4757	2.4	0.0625	1.6	0.68	390.7	6.1	395.1	7.8	421.4	39.3	390.7	6.1	NA
01812PR-04-15	75	14828	1.4	17.0517	9.4	0.5208	9.9	0.0644	2.9	0.30	402.4	11.4	425.7	34.4	553.9	206.2	402.4	11.4	72.6
01812PR-04-26	134	21735	0.9	18.0325	8.5	0.5127	8.9	0.0670	2.4	0.27	418.3	9.8	420.2	30.6	430.6	190.7	418.3	9.8	97.2
01812PR-04-88	259	59015	2.3	18.5534	2.0	0.5057	2.6	0.0680	1.6	0.61	424.4	6.4	415.5	8.7	366.8	45.7	424.4	6.4	115.7
01812PR-04-31	169	57240	0.8	18.3421	4.5	0.5177	4.8	0.0689	1.6	0.34	429.3	6.8	423.6	16.6	392.5	100.8	429.3	6.8	109.4
01812PR-04-5	86	18941	1.5	18.1222	6.8	0.5255	7.7	0.0691	3.7	0.48	430.5	15.5	428.8	27.1	419.5	151.5	430.5	15.5	102.6
01812PR-04-90	107	30433	0.5	18.5020	7.2	0.5207	7.3	0.0699	1.5	0.21	435.4	6.5	425.6	25.4	373.0	161.2	435.4	6.5	116.7
01812PR-04-32	106	27570	1.3	17.7216	4.2	0.5461	4.8	0.0702	2.5	0.51	437.3	10.5	442.4	17.4	469.3	92.1	437.3	10.5	93.2
01812PR-04-11	364	77275	0.6	18.0050	1.3	0.5388	2.6	0.0704	2.3	0.87	438.3	9.7	437.6	9.4	434.0	29.2	438.3	9.7	101.0
01812PR-04-87	289	33466	1.3	17.6987	2.5	0.6160	2.9	0.0791	1.6	0.54	490.6	7.5	487.3	11.3	472.1	54.4	490.6	7.5	103.9
01812PR-04-36	62	17700	1.3	17.0190	9.0	0.6798	9.2	0.0839	2.2	0.24	519.4	11.0	526.6	38.0	558.1	196.3	519.4	11.0	93.1
01812PR-04-44	244	72014	1.2	17.1025	2.2	0.7448	2.6	0.0924	1.4	0.53	569.6	7.6	565.2	11.3	547.4	48.0	569.6	7.6	104.1
01812PR-04-85	78	42013	1.2	14.5445	5.0	1.4480	5.3	0.1527	1.7	0.32	916.3	14.3	909.1	31.8	891.4	103.7	891.4	103.7	102.8
01812PR-04-28	40	29989	2.2	14.2247	6.4	1.5749	6.6	0.1625	1.5	0.22	970.5	13.3	960.4	41.1	937.1	132.4	937.1	132.4	103.6
01812PR-04-52	45	22063	1.7	14.1389	6.3	1.6056	6.5	0.1646	1.5	0.23	982.6	13.5	972.4	40.8	949.5	129.9	949.5	129.9	103.5
01812PR-04-98	117	93060	9.5	14.0862	1.8	1.5787	2.1	0.1613	1.1	0.53	963.9	9.8	961.8	13.0	957.2	36.4	957.2	36.4	100.7
01812PR-04-67	248	95259	3.2	13.8223	2.0	1.6053	3.9	0.1609	3.3	0.86	961.9	29.9	972.3	24.4	995.7	40.7	995.7	40.7	96.6
01812PR-04-43	28	18119	2.4	13.7766	6.8	1.5960	7.5	0.1595	3.2	0.43	953.8	28.3	968.6	46.9	1002.4	138.2	1002.4	138.2	95.1
01812PR-04-8	49	21317	1.6	13.7068	3.5	1.6127	4.8	0.1603	3.2	0.68	958.6	28.9	975.2	29.8	1012.7	70.4	1012.7	70.4	94.7
01812PR-04-101	109	45600	2.9	13.6704	2.0	1.7631	2.2	0.1748	0.8	0.35	1038.5	7.3	1032.0	14.0	1018.1	40.8	1018.1	40.8	102.0
01812PR-04-62	57	29960	1.1	13.6673	3.2	1.7210	3.8	0.1706	2.1	0.54	1015.4	19.3	1016.4	24.4	1018.6	64.9	1018.6	64.9	99.7
01812PR-04-25	146	271831	2.9	13.6421	1.3	1.7531	1.8	0.1735	1.3	0.71	1031.1	12.3	1028.3	11.8	1022.3	26.1	1022.3	26.1	100.9
01812PR-04-104	153	79997	1.5	13.6181	1.4	1.7277	2.4	0.1706	2.0	0.81	1015.6	18.5	1018.9	15.7	1025.9	29.3	1025.9	29.3	99.0
01812PR-04-55	49	36196	1.4	13.5809	5.8	1.7927	6.4	0.1766	2.6	0.41	1048.2	25.0	1042.8	41.6	1031.4	117.9	1031.4	117.9	101.6
01812PR-04-75	35	15005	2.1	13.5516	7.3	1.7646	8.2	0.1734	3.8	0.47	1031.0	36.7	1032.5	53.3	1035.8	146.7	1035.8	146.7	99.5
01812PR-04-53	129	53571	3.5	13.5340	1.7	1.7580	2.7	0.1726	2.1	0.77	1026.2	19.5	1030.1	17.2	1038.4	34.1	1038.4	34.1	98.8
01812PR-04-96	68	14076	1.4	13.5059	2.7	1.8083	2.9	0.1771	1.0	0.36	1051.3	10.0	1048.5	19.0	1042.6	54.7	1042.6	54.7	100.8
01812PR-04-20	128	72275	2.6	13.4681	1.3	1.7407	1.5	0.1700	0.8	0.55	1012.3	7.7	1023.7	9.7	1048.3	25.5	1048.3	25.5	96.6
01812PR-04-9	24	9279	2.9	13.4655	7.0	1.8059	7.4	0.1764	2.4	0.33	1047.1	23.3	1047.6	48.2	1048.7	140.6	1048.7	140.6	99.8

01812PR-04-37	32	1574	3.2	13.4485	6.3	1.6885	10.4	0.1647	8.3	0.79	982.8	75.4	1004.2	66.6	1051.2	128.1	1051.2	128.1	93.5
01812PR-04-83	99	32501	3.3	13.4352	2.1	1.7685	4.3	0.1723	3.8	0.87	1024.9	35.6	1034.0	28.1	1053.2	43.3	1053.2	43.3	97.3
01812PR-04-24	21	17424	2.1	13.3737	9.3	1.9254	9.9	0.1868	3.3	0.34	1103.8	33.9	1089.9	66.1	1062.4	187.3	1062.4	187.3	103.9
01812PR-04-3	59	42912	1.7	13.3407	5.1	1.7413	5.6	0.1685	2.2	0.40	1003.7	20.6	1023.9	36.2	1067.4	103.5	1067.4	103.5	94.0
01812PR-04-12	29	16976	2.7	13.2982	9.2	1.8290	9.3	0.1764	1.8	0.19	1047.3	17.0	1055.9	61.3	1073.8	184.2	1073.8	184.2	97.5
01812PR-04-14	89	49081	2.0	13.2977	2.2	1.8538	2.7	0.1788	1.5	0.57	1060.3	15.1	1064.8	17.8	1073.9	44.5	1073.9	44.5	98.7
01812PR-04-34	211	39909	1.7	13.2865	0.8	1.8767	1.3	0.1808	1.0	0.77	1071.6	9.9	1072.9	8.6	1075.6	16.7	1075.6	16.7	99.6
01812PR-04-54	63	28471	1.3	13.2746	4.0	1.8247	4.3	0.1757	1.4	0.33	1043.3	13.7	1054.4	28.0	1077.4	80.8	1077.4	80.8	96.8
01812PR-04-93	304	208949	1.8	13.2731	0.8	1.8895	2.2	0.1819	2.1	0.94	1077.3	20.6	1077.4	14.7	1077.6	15.7	1077.6	15.7	100.0
01812PR-04-6	167	124149	1.0	13.2192	1.1	1.8384	1.6	0.1763	1.1	0.72	1046.5	11.0	1059.3	10.4	1085.7	22.1	1085.7	22.1	96.4
01812PR-04-60	102	42708	2.3	13.2120	2.5	1.8176	3.6	0.1742	2.6	0.72	1035.0	24.6	1051.8	23.3	1086.9	49.5	1086.9	49.5	95.2
01812PR-04-99	93	30915	1.0	13.2047	2.4	1.8699	2.8	0.1791	1.4	0.49	1061.9	13.3	1070.5	18.3	1088.0	48.2	1088.0	48.2	97.6
01812PR-04-80	158	70692	0.9	13.2002	1.0	1.8895	1.4	0.1809	1.0	0.72	1071.9	9.9	1077.4	9.2	1088.6	19.2	1088.6	19.2	98.5
01812PR-04-51	49	1477	2.2	13.1731	7.5	1.6944	8.1	0.1619	3.1	0.38	967.2	27.8	1006.4	51.7	1092.7	150.1	1092.7	150.1	88.5
01812PR-04-94	46	21807	2.1	13.1630	4.8	1.9540	5.1	0.1865	1.8	0.36	1102.6	18.4	1099.8	34.3	1094.3	95.5	1094.3	95.5	100.8
01812PR-04-40	88	30720	3.0	13.1554	2.1	1.9976	2.5	0.1906	1.3	0.52	1124.6	13.5	1114.7	16.8	1095.5	42.4	1095.5	42.4	102.7
01812PR-04-48	198	94106	3.8	13.1422	0.9	1.9716	2.4	0.1879	2.2	0.92	1110.2	22.4	1105.9	16.1	1097.5	18.5	1097.5	18.5	101.2
01812PR-04-78	96	110140	3.7	13.1319	2.5	1.9946	5.7	0.1900	5.1	0.90	1121.2	53.0	1113.7	38.6	1099.0	49.6	1099.0	49.6	102.0
01812PR-04-30	187	15713	0.9	13.1054	1.1	1.8878	1.6	0.1794	1.1	0.72	1063.9	11.2	1076.8	10.5	1103.1	21.9	1103.1	21.9	96.4
01812PR-04-69	73	103053	1.3	13.0980	1.9	2.0295	2.4	0.1928	1.5	0.62	1136.5	15.7	1125.5	16.5	1104.2	38.0	1104.2	38.0	102.9
01812PR-04-1	32	20865	3.4	13.0968	5.4	1.9362	5.8	0.1839	2.0	0.34	1088.3	19.7	1093.7	38.7	1104.4	108.6	1104.4	108.6	98.5
01812PR-04-95	376	59913	2.6	13.0349	0.5	2.0041	1.1	0.1895	1.0	0.90	1118.5	10.0	1116.9	7.3	1113.8	9.5	1113.8	9.5	100.4
01812PR-04-23	210	93458	3.3	13.0077	1.1	2.0507	1.5	0.1935	1.1	0.72	1140.1	11.6	1132.5	10.5	1118.0	21.3	1118.0	21.3	102.0
01812PR-04-21	262	279316	1.4	12.9769	0.6	2.0419	1.0	0.1922	0.7	0.75	1133.1	7.7	1129.6	6.7	1122.7	12.9	1122.7	12.9	100.9
01812PR-04-29	71	78260	1.2	12.9652	2.3	2.0472	3.1	0.1925	2.1	0.67	1134.9	21.5	1131.4	21.0	1124.6	45.5	1124.6	45.5	100.9
01812PR-04-82	47	20634	1.9	12.9342	4.5	2.0792	4.7	0.1950	1.6	0.33	1148.6	16.4	1142.0	32.4	1129.3	88.8	1129.3	88.8	101.7
01812PR-04-47	229	59988	1.3	12.9201	0.9	2.0426	1.9	0.1914	1.6	0.86	1129.0	16.6	1129.8	12.7	1131.5	18.9	1131.5	18.9	99.8
01812PR-04-65	114	59817	2.3	12.8880	1.4	2.0809	2.3	0.1945	1.8	0.79	1145.8	18.8	1142.5	15.6	1136.5	28.0	1136.5	28.0	100.8
01812PR-04-84	92	65412	2.8	12.8555	1.4	2.1104	1.8	0.1968	1.1	0.60	1157.9	11.5	1152.2	12.4	1141.4	28.6	1141.4	28.6	101.4
01812PR-04-50	45	31504	1.8	12.8510	4.0	2.0563	4.5	0.1917	2.0	0.45	1130.3	21.0	1134.4	30.7	1142.2	79.9	1142.2	79.9	99.0
01812PR-04-42	224	185470	1.8	12.8011	0.6	2.1770	1.2	0.2021	1.1	0.88	1186.7	11.9	1173.7	8.7	1149.9	11.8	1149.9	11.8	103.2
01812PR-04-18	162	156924	2.4	12.7163	1.2	2.1175	3.8	0.1953	3.7	0.95	1150.0	38.6	1154.5	26.5	1163.1	23.2	1163.1	23.2	98.9
01812PR-04-71	131	53700	2.9	12.5950	1.2	2.1614	1.7	0.1974	1.2	0.69	1161.5	12.4	1168.7	11.8	1182.1	24.3	1182.1	24.3	98.3
01812PR-04-63	17	8587	2.7	12.4924	9.1	2.1338	10.2	0.1933	4.6	0.45	1139.4	47.6	1159.8	70.5	1198.2	179.9	1198.2	179.9	95.1
01812PR-04-66	381	212583	2.9	12.2783	0.5	2.4137	1.9	0.2149	1.9	0.96	1255.1	21.4	1246.7	14.0	1232.2	10.1	1232.2	10.1	101.9
01812PR-04-38	25	18677	1.0	12.2311	3.9	2.4390	4.7	0.2164	2.5	0.54	1262.6	28.8	1254.2	33.5	1239.8	76.9	1239.8	76.9	101.8
01812PR-04-97	82	60185	1.8	12.1053	2.0	2.4314	3.3	0.2135	2.6	0.79	1247.2	29.6	1251.9	23.9	1260.0	39.9	1260.0	39.9	99.0
01812PR-04-61	211	42858	2.9	11.7005	1.7	2.5221	3.1	0.2140	2.6	0.84	1250.2	30.0	1278.4	22.7	1326.1	32.5	1326.1	32.5	94.3
01812PR-04-59	519	264438	1.8	11.6686	0.5	2.6887	1.4	0.2275	1.3	0.93	1321.6	15.6	1325.4	10.4	1331.4	10.1	1331.4	10.1	99.3
01812PR-04-72	162	86328	1.4	11.6679	1.1	2.7164	1.7	0.2299	1.3	0.75	1333.8	15.5	1332.9	12.7	1331.5	21.8	1331.5	21.8	100.2
01812PR-04-2	168	385954	0.9	11.6226	1.1	2.6093	1.6	0.2200	1.1	0.71	1281.6	13.2	1303.3	11.7	1339.1	21.8	1339.1	21.8	95.7

01812PR-04-103	90	78404	2.2	11.2601	1.1	2.9666	1.8	0.2423	1.4	0.76	1398.5	17.1	1399.1	13.5	1400.0	22.0	1400.0	22.0	99.9
01812PR-04-58	30	12711	1.6	11.1919	2.3	3.0299	3.0	0.2459	2.0	0.67	1417.5	26.0	1415.2	23.2	1411.7	43.2	1411.7	43.2	100.4
01812PR-04-77	47	40916	1.3	10.9170	2.1	3.3311	3.0	0.2637	2.1	0.70	1509.0	28.3	1488.4	23.4	1459.1	40.7	1459.1	40.7	103.4
01812PR-04-74	131	111691	1.8	10.6578	0.8	3.3587	2.4	0.2596	2.2	0.94	1487.9	29.3	1494.8	18.4	1504.6	15.4	1504.6	15.4	98.9
01812PR-04-49	362	4907	2.0	10.5638	1.5	3.1079	2.7	0.2381	2.2	0.82	1376.9	27.2	1434.6	20.6	1521.4	29.2	1521.4	29.2	90.5
01812PR-04-41	249	177606	2.9	10.4615	0.3	3.5426	0.9	0.2688	0.9	0.94	1534.7	11.9	1536.8	7.3	1539.7	5.8	1539.7	5.8	99.7
01812PR-04-22	116	37325	2.8	9.9930	0.9	4.0994	4.7	0.2971	4.6	0.98	1677.0	67.4	1654.2	38.1	1625.4	17.4	1625.4	17.4	103.2
01812PR-04-89	43	65481	2.0	9.9692	2.3	4.0099	2.9	0.2899	1.8	0.63	1641.2	26.6	1636.2	23.7	1629.8	42.2	1629.8	42.2	100.7
01812PR-04-92	124	134727	1.5	9.9195	0.8	4.0807	1.6	0.2936	1.5	0.89	1659.4	21.3	1650.5	13.4	1639.1	14.2	1639.1	14.2	101.2
01812PR-04-64	97	110664	1.5	9.4233	0.7	4.4926	3.3	0.3070	3.2	0.97	1726.2	49.0	1729.6	27.6	1733.8	13.6	1733.8	13.6	99.6
01812PR-04-105	59	159370	2.8	9.4189	1.0	4.2827	1.9	0.2926	1.7	0.86	1654.3	24.3	1690.0	15.9	1734.6	18.1	1734.6	18.1	95.4
01812PR-04-102	142	144100	2.9	9.3459	0.9	4.5934	2.3	0.3114	2.1	0.92	1747.4	32.4	1748.1	19.2	1748.9	16.8	1748.9	16.8	99.9
01812PR-04-56	27	41611	1.6	9.2846	3.5	4.5510	4.0	0.3065	1.8	0.46	1723.2	27.8	1740.3	33.2	1760.9	64.6	1760.9	64.6	97.9
01812PR-04-73	246	738277	1.7	8.5706	0.3	5.5930	0.9	0.3477	0.9	0.96	1923.4	14.6	1915.0	7.9	1905.9	4.9	1905.9	4.9	100.9
01812PR-04-100	19	4515	1.3	7.8638	2.8	5.7301	5.5	0.3268	4.7	0.86	1822.9	74.9	1935.9	47.2	2059.1	48.6	2059.1	48.6	88.5
01812PR-04-46	45	57070	0.7	5.3121	0.8	13.7663	1.1	0.5304	0.8	0.70	2743.0	17.2	2733.8	10.4	2726.9	12.8	2726.9	12.8	100.6
01812PR-04-81	117	67338	1.0	5.1182	0.3	15.0201	4.3	0.5576	4.3	1.00	2856.5	98.8	2816.5	40.9	2788.0	5.2	2788.0	5.2	102.5
01812PR-04-79	109	146746	1.1	4.9504	0.7	15.6621	4.9	0.5623	4.9	0.99	2876.2	113.1	2856.4	47.1	2842.4	11.7	2842.4	11.7	101.2

Warren Point/Sewanee Formation

37°9'16.44"N						Isotope ratios					Apparent ages (Ma)								
82°37'58.50"W																			
Analysis	U	206Pb	U/Th	206Pb*	±	207Pb*	±	206Pb*	±	error	206Pb*	±	207Pb*	±	206Pb*	±	Best age	±	Conc
	(ppm)	204Pb		207Pb*	(%)	235U*	(%)	238U	(%)	corr.	238U*	(Ma)	235U	(Ma)	207Pb*	(Ma)	(Ma)	(Ma)	(%)
012812PR-05-05	163	32143	1.5	17.9406	2.4	0.4937	3.0	0.0642	1.8	0.60	401.3	7.1	407.4	10.2	442.0	53.7	401.3	7.1	90.8
012812PR-05-21	292	21262	1.1	18.1887	3.6	0.4962	4.0	0.0655	1.7	0.42	408.7	6.6	409.1	13.4	411.4	80.9	408.7	6.6	99.4
012812PR-05-92	166	35733	1.4	17.9358	2.5	0.5111	2.6	0.0665	0.7	0.29	415.0	3.0	419.2	8.9	442.6	55.5	415.0	3.0	93.8
012812PR-05-03	69	19604	2.1	18.3842	7.8	0.5071	8.0	0.0676	1.5	0.18	421.8	6.0	416.5	27.3	387.4	176.3	421.8	6.0	108.9
012812PR-05-16	166	75053	1.6	18.3394	4.3	0.5114	4.7	0.0680	1.9	0.40	424.2	7.8	419.4	16.1	392.9	96.0	424.2	7.8	108.0
012812PR-05-41	915	12952	1.9	17.3115	6.2	0.5517	6.3	0.0693	1.3	0.21	431.7	5.6	446.1	22.8	520.8	135.2	431.7	5.6	82.9
012812PR-05-73	184	66820	1.8	17.8779	1.7	0.5378	2.0	0.0697	1.2	0.58	434.5	5.0	437.0	7.3	449.8	37.0	434.5	5.0	96.6
012812PR-05-25	93	26714	1.0	17.8694	4.4	0.5424	4.8	0.0703	1.9	0.40	437.9	8.1	440.0	17.3	450.8	98.6	437.9	8.1	97.1
012812PR-05-82	301	20992	1.3	16.8046	6.5	0.5812	6.8	0.0708	2.1	0.30	441.2	8.8	465.2	25.4	585.7	141.0	441.2	8.8	75.3
012812PR-05-02	211	63074	1.2	17.8217	2.3	0.5917	2.6	0.0765	1.2	0.46	475.1	5.4	471.9	9.7	456.8	50.4	475.1	5.4	104.0
012812PR-05-88	sitt58	32363	1.7	16.7280	5.9	0.6433	6.2	0.0780	2.1	0.33	484.5	9.7	504.3	24.8	595.6	127.7	484.5	9.7	81.3
012812PR-05-97	51	21318	2.6	14.4400	3.7	1.4877	4.5	0.1558	2.5	0.56	933.4	21.7	925.4	27.2	906.2	76.5	906.2	76.5	103.0
012812PR-05-87	177	88228	1.0	14.1032	1.3	1.5412	1.8	0.1576	1.3	0.71	943.7	11.5	947.0	11.4	954.7	26.6	954.7	26.6	98.8
012812PR-05-23	184	103183	4.0	14.0671	1.0	1.5544	1.7	0.1586	1.4	0.81	948.9	12.4	952.3	10.7	960.0	20.8	960.0	20.8	98.9
012812PR-05-83	78	122926	1.6	13.9232	1.9	1.6155	2.6	0.1631	1.7	0.65	974.2	15.2	976.2	16.1	980.9	39.6	980.9	39.6	99.3
012812PR-05-46	36	22490	1.1	13.8867	3.5	1.7200	4.0	0.1732	1.9	0.47	1029.9	18.0	1016.0	25.6	986.2	71.6	986.2	71.6	104.4
012812PR-05-48	367	197379	4.5	13.8438	0.4	1.6814	2.2	0.1688	2.2	0.99	1005.6	20.4	1001.5	14.2	992.6	7.3	992.6	7.3	101.3
012812PR-05-72	53	37462	0.5	13.7619	4.0	1.7399	4.4	0.1737	1.7	0.39	1032.3	16.2	1023.4	28.3	1004.6	82.1	1004.6	82.1	102.8
012812PR-05-81	300	140054	2.8	13.7618	1.1	1.6849	2.4	0.1682	2.2	0.90	1002.0	20.3	1002.9	15.5	1004.6	21.3	1004.6	21.3	99.7
012812PR-05-30	62	23493	0.7	13.7411	2.4	1.6655	2.7	0.1660	1.1	0.43	989.9	10.5	995.5	16.8	1007.7	48.6	1007.7	48.6	98.2
012812PR-05-19	102	13287	1.6	13.7214	1.3	1.5745	2.2	0.1567	1.7	0.80	938.4	15.1	960.2	13.4	1010.6	26.3	1010.6	26.3	92.9
012812PR-05-85	428	194944	3.5	13.6966	0.5	1.6736	1.3	0.1663	1.2	0.94	991.4	11.5	998.6	8.5	1014.2	9.4	1014.2	9.4	97.8
012812PR-05-78	113	179252	2.3	13.6693	1.5	1.7278	1.9	0.1713	1.1	0.58	1019.2	10.2	1018.9	12.1	1018.3	30.9	1018.3	30.9	100.1
012812PR-05-38	107	57212	3.1	13.5831	1.6	1.8128	2.1	0.1786	1.4	0.65	1059.3	13.5	1050.1	14.0	1031.1	33.0	1031.1	33.0	102.7
012812PR-05-95	69	45772	2.7	13.5575	2.6	1.7433	3.2	0.1714	1.8	0.57	1019.9	17.1	1024.7	20.4	1034.9	52.4	1034.9	52.4	98.6
012812PR-05-47	40	26412	1.2	13.5465	4.9	1.8324	5.4	0.1800	2.2	0.41	1067.2	21.4	1057.2	35.2	1036.5	98.8	1036.5	98.8	103.0
012812PR-05-57	99	72119	1.0	13.5297	1.5	1.8163	1.6	0.1782	0.7	0.45	1057.3	7.1	1051.3	10.7	1039.0	29.5	1039.0	29.5	101.8
012812PR-05-75	57	40371	1.6	13.4981	3.5	1.8816	3.8	0.1842	1.5	0.39	1089.9	15.0	1074.6	25.5	1043.7	71.4	1043.7	71.4	104.4
012812PR-05-04	106	122775	1.0	13.4672	1.3	1.8183	2.0	0.1776	1.5	0.74	1053.9	14.2	1052.1	12.9	1048.4	26.7	1048.4	26.7	100.5
012812PR-05-51	62	65249	2.4	13.4443	1.6	1.7559	2.4	0.1712	1.8	0.73	1018.8	16.7	1029.3	15.6	1051.8	33.2	1051.8	33.2	96.9
012812PR-05-43	248	214771	1.9	13.4228	0.6	1.8597	1.6	0.1810	1.5	0.94	1072.7	14.7	1066.9	10.5	1055.1	11.4	1055.1	11.4	101.7

012812PR-05-07	100	54360	1.7	13.4130	1.6	1.8070	2.5	0.1758	1.8	0.75	1043.9	17.8	1048.0	16.1	1056.5	32.9	1056.5	32.9	98.8
012812PR-05-94	86	55979	2.1	13.3840	1.7	1.8688	2.3	0.1814	1.6	0.67	1074.6	15.4	1070.1	15.4	1060.9	35.1	1060.9	35.1	101.3
012812PR-05-84	96	22556	2.5	13.3768	1.7	1.7911	3.0	0.1738	2.5	0.83	1032.8	23.5	1042.2	19.5	1062.0	33.9	1062.0	33.9	97.3
012812PR-05-20	164	8026	1.7	13.3701	1.7	1.8427	2.3	0.1787	1.5	0.67	1059.8	14.7	1060.8	14.9	1063.0	33.9	1063.0	33.9	99.7
012812PR-05-42	248	113560	2.7	13.3017	0.7	1.9252	3.1	0.1857	3.0	0.97	1098.2	30.4	1089.9	20.7	1073.3	14.6	1073.3	14.6	102.3
012812PR-05-68	30	27862	1.3	13.2558	5.4	1.8270	6.1	0.1757	2.8	0.46	1043.2	27.1	1055.2	40.0	1080.2	108.5	1080.2	108.5	96.6
012812PR-05-29	77	45794	2.2	13.1254	1.5	1.9789	2.4	0.1884	1.9	0.77	1112.6	19.2	1108.3	16.4	1100.0	30.7	1100.0	30.7	101.1
012812PR-05-55	58	41602	3.0	13.0381	3.4	1.9803	3.8	0.1873	1.7	0.44	1106.5	17.1	1108.8	25.6	1113.3	68.1	1113.3	68.1	99.4
012812PR-05-45	106	83071	2.1	12.9935	0.9	2.0596	2.3	0.1941	2.1	0.92	1143.5	22.5	1135.5	15.9	1120.2	17.9	1120.2	17.9	102.1
012812PR-05-65	149	128921	1.7	12.9642	0.8	2.0433	2.3	0.1921	2.2	0.94	1132.9	22.5	1130.1	15.6	1124.7	15.0	1124.7	15.0	100.7
012812PR-05-28	39	34384	3.0	12.9592	2.8	2.0132	3.5	0.1892	2.2	0.61	1117.1	22.2	1120.0	23.9	1125.5	55.3	1125.5	55.3	99.3
012812PR-05-58	161	453098	1.8	12.8698	0.9	1.9925	1.6	0.1860	1.3	0.81	1099.6	13.1	1113.0	10.8	1139.2	18.6	1139.2	18.6	96.5
012812PR-05-12	244	182616	5.3	12.7834	0.4	2.1147	1.9	0.1961	1.8	0.97	1154.1	19.2	1153.6	12.9	1152.6	8.6	1152.6	8.6	100.1
012812PR-05-42	30	33165	1.6	12.7777	6.5	2.1491	6.6	0.1992	1.1	0.17	1170.8	12.2	1164.8	45.7	1153.5	129.1	1153.5	129.1	101.5
012812PR-05-99	206	108993	1.5	12.7557	0.7	2.1531	1.6	0.1992	1.5	0.90	1171.0	15.9	1166.1	11.4	1156.9	14.0	1156.9	14.0	101.2
012812PR-05-96	292	257360	2.8	12.7261	0.6	2.1786	2.1	0.2011	2.1	0.96	1181.1	22.3	1174.2	14.9	1161.5	11.2	1161.5	11.2	101.7
012812PR-05-90	291	6104	2.8	12.6400	0.7	2.1025	2.3	0.1927	2.2	0.95	1136.2	22.8	1149.6	15.8	1175.0	13.9	1175.0	13.9	96.7
012812PR-05-36	198	2683	2.5	12.6339	1.5	2.0761	2.9	0.1902	2.5	0.86	1122.6	25.7	1141.0	19.8	1176.0	29.1	1176.0	29.1	95.5
012812PR-05-06	369	416266	1.9	12.2379	0.4	2.3559	2.7	0.2091	2.7	0.99	1224.0	30.1	1229.3	19.5	1238.7	7.8	1238.7	7.8	98.8
012812PR-05-01	91	44536	2.0	12.1879	1.2	2.3829	2.9	0.2106	2.6	0.91	1232.2	29.6	1237.5	20.7	1246.7	23.3	1246.7	23.3	98.8
012812PR-05-40	244	217471	4.0	12.1536	0.8	2.4205	2.7	0.2134	2.6	0.96	1246.7	29.7	1248.7	19.7	1252.2	15.2	1252.2	15.2	99.6
012812PR-05-34	56	41319	1.1	11.9643	1.9	2.5811	2.3	0.2240	1.3	0.58	1302.8	15.6	1295.3	16.7	1282.8	36.3	1282.8	36.3	101.6
012812PR-05-63	160	308086	2.7	11.8671	0.8	2.5041	2.3	0.2155	2.1	0.94	1258.2	24.3	1273.2	16.5	1298.7	15.5	1298.7	15.5	96.9
012812PR-05-66	44	1781	1.4	11.8353	2.1	2.1761	2.7	0.1868	1.6	0.60	1104.0	16.1	1173.4	18.5	1303.9	41.6	1303.9	41.6	84.7
012812PR-05-64	365	305782	9.9	11.6500	1.2	2.4942	3.7	0.2107	3.5	0.95	1232.8	38.7	1270.3	26.5	1334.5	23.1	1334.5	23.1	92.4
012812PR-05-14	63	74240	2.5	11.5745	1.6	2.7917	2.2	0.2343	1.5	0.69	1357.3	18.2	1353.3	16.2	1347.1	30.3	1347.1	30.3	100.8
012812PR-05-49	32	23675	1.3	11.5060	4.8	2.8206	5.6	0.2354	2.7	0.49	1362.6	33.7	1361.0	41.8	1358.5	93.5	1358.5	93.5	100.3
012812PR-05-44	91	162394	2.6	11.4953	1.3	2.8371	2.3	0.2365	1.8	0.82	1368.7	22.7	1365.4	16.9	1360.3	25.1	1360.3	25.1	100.6
012812PR-05-80	93	168354	1.6	11.4706	1.7	2.6223	2.1	0.2182	1.2	0.56	1272.1	13.5	1306.9	15.2	1364.4	33.0	1364.4	33.0	93.2
012812PR-05-53	124	142780	3.9	11.3639	0.9	2.6900	1.8	0.2217	1.6	0.87	1290.9	18.2	1325.7	13.3	1382.4	17.1	1382.4	17.1	93.4
012812PR-05-70	133	142872	2.6	11.3452	0.8	2.9318	2.8	0.2412	2.7	0.96	1393.1	33.6	1390.2	21.2	1385.6	15.5	1385.6	15.5	100.5
012812PR-05-39	308	59679	0.9	11.2963	0.6	2.8997	2.3	0.2376	2.3	0.97	1374.1	28.2	1381.8	17.7	1393.9	10.7	1393.9	10.7	98.6
012812PR-05-79	151	137884	2.4	10.8752	0.6	3.2030	1.5	0.2526	1.4	0.93	1452.1	18.2	1457.9	11.7	1466.4	10.5	1466.4	10.5	99.0
012812PR-05-89	127	89365	1.5	10.8241	0.5	3.2752	3.2	0.2571	3.1	0.99	1475.1	41.2	1475.2	24.6	1475.3	8.6	1475.3	8.6	100.0
012812PR-05-22	263	320338	2.4	10.7230	0.4	3.2724	3.5	0.2545	3.5	0.99	1461.6	45.3	1474.5	27.1	1493.1	7.7	1493.1	7.7	97.9
012812PR-05-13	242	266893	3.7	10.6703	0.3	3.4180	1.2	0.2645	1.2	0.98	1512.9	15.8	1508.5	9.5	1502.4	5.0	1502.4	5.0	100.7
012812PR-05-100	599	44168	3.7	10.6217	0.2	3.4114	2.7	0.2628	2.6	1.00	1504.2	35.5	1507.0	20.9	1511.1	4.2	1511.1	4.2	99.5
012812PR-05-15	185	39541	1.8	10.5683	0.7	3.4844	1.9	0.2671	1.8	0.94	1525.9	24.3	1523.7	15.1	1520.6	12.5	1520.6	12.5	100.4
012812PR-05-09	54	17836	1.7	10.5214	1.7	3.1744	4.2	0.2422	3.9	0.92	1398.3	48.8	1451.0	32.6	1528.9	31.3	1528.9	31.3	91.5
012812PR-05-52	85	107482	2.0	9.9778	0.7	3.8449	2.0	0.2782	1.9	0.93	1582.5	26.5	1602.2	16.3	1628.2	13.5	1628.2	13.5	97.2
012812PR-05-74	515	31914	1.5	9.9518	0.3	3.9262	2.5	0.2834	2.5	0.99	1608.4	35.3	1619.1	20.2	1633.0	5.5	1633.0	5.5	98.5

012812PR-05-59	133	200648	2.6	9.9209	0.4	3.9826	1.5	0.2866	1.5	0.97	1624.3	21.4	1630.7	12.5	1638.8	6.9	1638.8	6.9	99.1
012812PR-05-56	336	243346	2.8	9.9190	0.2	4.1104	1.8	0.2957	1.8	0.99	1670.0	26.2	1656.4	14.6	1639.2	3.4	1639.2	3.4	101.9
012812PR-05-11	345	470228	3.1	9.9031	0.1	4.0749	1.5	0.2927	1.5	1.00	1654.9	21.2	1649.3	11.9	1642.2	2.5	1642.2	2.5	100.8
012812PR-05-86	74	65993	1.0	9.8923	1.2	3.9106	1.5	0.2806	0.9	0.61	1594.2	13.3	1615.9	12.5	1644.2	22.8	1644.2	22.8	97.0
012812PR-05-27	99	187539	1.4	9.7694	0.3	4.2529	1.5	0.3013	1.5	0.97	1697.9	22.0	1684.3	12.4	1667.3	6.2	1667.3	6.2	101.8
012812PR-05-98	194	210240	1.1	9.7653	0.4	4.3009	1.9	0.3046	1.8	0.98	1714.1	27.4	1693.5	15.3	1668.1	6.5	1668.1	6.5	102.8
012812PR-05-93	109	133071	1.2	9.7170	0.9	4.1784	2.3	0.2945	2.2	0.93	1663.8	31.9	1669.8	19.2	1677.3	15.8	1677.3	15.8	99.2
012812PR-05-77	164	3856	1.3	9.7056	2.4	4.0941	2.8	0.2882	1.5	0.55	1632.5	22.2	1653.1	22.9	1679.5	43.5	1679.5	43.5	97.2
012812PR-05-62	450	284940	0.6	9.6999	0.3	4.0947	1.7	0.2881	1.7	0.98	1631.9	24.3	1653.3	14.0	1680.5	6.4	1680.5	6.4	97.1
012812PR-05-26	89	128874	0.9	9.6925	0.6	4.2882	2.7	0.3014	2.6	0.97	1698.5	38.7	1691.1	21.9	1681.9	11.1	1681.9	11.1	101.0
012812PR-05-24	26	47443	2.7	9.5618	1.4	4.3573	2.5	0.3022	2.1	0.83	1702.1	30.9	1704.3	20.7	1707.0	26.0	1707.0	26.0	99.7
012812PR-05-71	227	167801	2.8	9.3051	0.3	4.6200	0.9	0.3118	0.8	0.95	1749.5	12.9	1752.9	7.4	1756.9	4.9	1756.9	4.9	99.6
012812PR-05-69	92	134982	3.2	9.1941	0.9	4.6598	1.9	0.3107	1.7	0.89	1744.3	26.1	1760.1	16.0	1778.8	15.7	1778.8	15.7	98.1
012812PR-05-37	183	362614	3.9	9.1563	0.5	4.9758	1.7	0.3304	1.7	0.97	1840.5	26.9	1815.2	14.7	1786.3	8.2	1786.3	8.2	103.0
012812PR-05-10	166	114403	11.0	9.0978	0.5	4.8315	3.5	0.3188	3.4	0.99	1783.9	53.4	1790.4	29.1	1798.0	8.9	1798.0	8.9	99.2
012812PR-05-18	164	150617	2.0	8.9542	0.4	4.9984	1.2	0.3246	1.1	0.94	1812.2	18.1	1819.0	10.3	1826.9	7.5	1826.9	7.5	99.2
012812PR-05-67	411	37939	3.4	8.8598	0.2	5.0283	2.9	0.3231	2.9	1.00	1804.9	45.8	1824.1	24.7	1846.1	4.0	1846.1	4.0	97.8
012812PR-05-60	75	118726	2.7	7.7116	0.6	6.8061	2.0	0.3807	1.9	0.96	2079.4	34.6	2086.5	17.9	2093.6	9.8	2093.6	9.8	99.3
012812PR-05-08	379	127988	1.6	6.1054	0.1	10.6413	1.5	0.4712	1.5	1.00	2488.8	30.2	2492.3	13.7	2495.1	2.3	2495.1	2.3	99.7
012812PR-05-35	224	53251	1.5	5.7158	1.2	11.8890	2.6	0.4929	2.3	0.88	2583.0	48.4	2595.7	24.3	2605.6	20.7	2605.6	20.7	99.1
012812PR-05-50	43	68720	1.1	5.5866	0.7	12.7088	1.8	0.5149	1.7	0.93	2677.6	36.3	2658.3	16.8	2643.6	11.0	2643.6	11.0	101.3
012812PR-05-76	42	58213	0.4	5.4267	0.5	12.9943	1.6	0.5114	1.6	0.94	2662.7	33.9	2679.2	15.5	2691.7	9.1	2691.7	9.1	98.9
012812PR-05-31	48	54486	1.4	5.3861	2.1	12.7159	3.0	0.4967	2.1	0.71	2599.7	45.4	2658.8	28.1	2704.1	34.6	2704.1	34.6	96.1
012812PR-05-33	65	81866	0.9	5.3028	0.2	14.1420	1.5	0.5439	1.5	0.99	2799.7	33.6	2759.3	14.1	2729.8	2.8	2729.8	2.8	102.6
012812PR-05-61	92	87709	0.8	5.2923	0.3	13.6560	1.3	0.5242	1.3	0.97	2716.8	28.7	2726.1	12.6	2733.1	5.0	2733.1	5.0	99.4
012812PR-05-91	82	8600	1.1	5.0478	0.6	12.0236	1.9	0.4402	1.8	0.95	2351.5	35.3	2606.3	17.7	2810.6	9.6	2810.6	9.6	83.7

Pikeville Formation

37°10'6.24"N						Isotope ratios					Apparent ages (Ma)								
82°38'43.08"W																			
Analysis	U	206Pb	U/Th	206Pb*	±	207Pb*	±	206Pb*	±	error	206Pb*	±	207Pb*	±	206Pb*	±	Best age	±	Conc
	(ppm)	204Pb		207Pb*	(%)	235U*	(%)	238U	(%)	corr.	238U*	(Ma)	235U	(Ma)	207Pb*	(Ma)	(Ma)	(Ma)	(%)
021112PR-01-71	665	182150	5.3	18.2525	0.9	0.4855	1.3	0.0643	1.0	0.74	401.5	3.9	401.8	4.5	403.5	20.2	401.5	3.9	99.5
021112PR-01-26	502	90632	22.6	17.6717	0.6	0.5815	1.6	0.0745	1.5	0.93	463.4	6.6	465.4	5.9	475.5	12.6	463.4	6.6	97.4
021112PR-01-70	129	2139	1.1	15.7366	11.9	0.6704	14.1	0.0765	7.7	0.54	475.3	35.1	521.0	57.6	726.5	252.3	475.3	35.1	65.4
021112PR-01-77	1602	40808	1.7	13.4360	0.3	0.8788	1.4	0.0856	1.3	0.97	529.7	6.8	640.3	6.5	1053.1	6.8	529.7	6.8	50.3
021112PR-01-100	96	20574	1.0	16.8038	4.2	0.7604	4.4	0.0927	1.3	0.29	571.3	7.0	574.3	19.4	585.8	91.9	571.3	7.0	97.5
021112PR-01-11	127	32951	1.6	16.4095	2.8	0.7887	6.3	0.0939	5.7	0.90	578.4	31.3	590.4	28.2	637.1	59.5	578.4	31.3	90.8
021112PR-01-44	135	34415	1.3	16.8834	3.7	0.7698	4.4	0.0943	2.3	0.53	580.7	12.9	579.6	19.4	575.5	80.7	580.7	12.9	100.9
021112PR-01-10	221	88885	1.1	16.4116	1.1	0.8586	1.6	0.1022	1.1	0.70	627.3	6.8	629.4	7.6	636.9	24.6	627.3	6.8	98.5
021112PR-01-6	656	209918	2.5	14.3748	0.3	1.2247	1.6	0.1277	1.6	0.98	774.6	11.6	811.9	9.1	915.6	6.9	774.6	11.6	84.6
021112PR-01-2	181	82412	1.2	14.5925	1.7	1.3898	2.1	0.1471	1.3	0.59	884.7	10.5	884.6	12.7	884.6	35.8	884.7	10.5	100.0
021112PR-01-69	81	29296	2.7	14.3120	2.0	1.4879	2.6	0.1544	1.6	0.62	925.8	13.9	925.5	15.7	924.6	41.7	924.6	41.7	100.1
021112PR-01-104	85	52573	3.2	14.1343	2.8	1.5458	4.1	0.1585	3.0	0.72	948.2	26.2	948.8	25.3	950.2	57.9	950.2	57.9	99.8
021112PR-01-53	337	163002	3.0	14.0930	0.6	1.5897	1.4	0.1625	1.2	0.90	970.6	11.1	966.2	8.5	956.2	12.4	956.2	12.4	101.5
021112PR-01-15	40	27032	1.3	14.0778	3.6	1.5797	4.5	0.1613	2.6	0.58	963.9	23.2	962.2	27.8	958.4	74.5	958.4	74.5	100.6
021112PR-01-50	58	30234	2.9	14.0032	3.0	1.6041	3.5	0.1629	1.8	0.51	972.9	15.9	971.8	21.8	969.3	61.2	969.3	61.2	100.4
021112PR-01-46	36	30767	1.8	13.9693	2.6	1.6708	3.1	0.1693	1.6	0.53	1008.1	15.2	997.5	19.5	974.2	53.0	974.2	53.0	103.5
021112PR-01-32	124	94656	1.0	13.9301	0.8	1.6483	2.2	0.1665	2.0	0.92	992.9	18.7	988.9	13.9	979.9	17.0	979.9	17.0	101.3
021112PR-01-68	91	87249	1.7	13.8965	3.2	1.6459	3.9	0.1659	2.3	0.58	989.4	20.8	988.0	24.6	984.8	64.4	984.8	64.4	100.5
021112PR-01-82	50	25147	2.6	13.8916	3.6	1.6599	4.8	0.1672	3.2	0.66	996.9	29.1	993.3	30.2	985.6	72.7	985.6	72.7	101.1
021112PR-01-7	71	32752	3.0	13.8668	2.4	1.6190	2.9	0.1628	1.5	0.53	972.5	13.8	977.6	18.0	989.2	49.2	989.2	49.2	98.3
021112PR-01-9	25	17933	2.8	13.8640	8.0	1.5962	8.5	0.1605	2.8	0.33	959.5	25.2	968.7	52.9	989.6	162.5	989.6	162.5	97.0
021112PR-01-7	34	22599	1.6	13.8563	5.4	1.6321	5.9	0.1640	2.4	0.41	979.1	21.8	982.7	37.0	990.7	109.2	990.7	109.2	98.8
021112PR-01-1	120	102419	1.2	13.7720	1.2	1.6755	2.2	0.1674	1.9	0.86	997.5	17.7	999.3	14.2	1003.1	23.4	1003.1	23.4	99.4
021112PR-01-98	55	30614	1.5	13.7692	3.6	1.7273	4.1	0.1725	1.9	0.48	1025.8	18.4	1018.7	26.1	1003.5	72.5	1003.5	72.5	102.2
021112PR-01-80	99	40819	1.5	13.7559	1.4	1.6922	2.4	0.1688	1.9	0.81	1005.7	18.1	1005.6	15.2	1005.5	28.1	1005.5	28.1	100.0
021112PR-01-59	149	63726	3.7	13.7476	1.3	1.6669	1.9	0.1662	1.4	0.74	991.2	12.8	996.0	11.9	1006.7	25.6	1006.7	25.6	98.5
021112PR-01-79	122	82498	7.4	13.7314	1.4	1.6948	2.0	0.1688	1.4	0.73	1005.4	13.5	1006.6	12.7	1009.1	27.8	1009.1	27.8	99.6
021112PR-01-86	112	105360	1.5	13.6862	1.3	1.7369	2.6	0.1724	2.3	0.87	1025.3	21.4	1022.3	16.6	1015.8	25.5	1015.8	25.5	100.9
021112PR-01-4	129	67485	4.6	13.6834	0.5	1.7218	1.7	0.1709	1.7	0.96	1016.9	15.7	1016.7	11.1	1016.2	9.3	1016.2	9.3	100.1
021112PR-01-49	102	89442	1.9	13.6442	1.8	1.7491	3.1	0.1731	2.5	0.81	1029.1	24.0	1026.8	20.2	1022.0	37.2	1022.0	37.2	100.7
021112PR-01-102	44	21153	0.8	13.6198	3.0	1.6799	3.6	0.1659	2.0	0.55	989.7	18.2	1000.9	23.0	1025.6	61.1	1025.6	61.1	96.5

021112PR-01-72	45	52922	1.1	13.6162	3.5	1.8278	4.1	0.1805	2.2	0.53	1069.7	21.5	1055.5	26.9	1026.2	70.2	1026.2	70.2	104.2
021112PR-01-19	514	362377	2.2	13.6037	0.4	1.7568	1.4	0.1733	1.4	0.96	1030.4	13.1	1029.7	9.2	1028.0	7.6	1028.0	7.6	100.2
021112PR-01-36	22	8360	1.8	13.5900	8.3	1.7492	8.6	0.1724	2.3	0.26	1025.3	21.5	1026.9	55.8	1030.1	168.4	1030.1	168.4	99.5
021112PR-01-24	40	17594	1.3	13.5896	3.6	1.7147	4.5	0.1690	2.7	0.59	1006.6	24.8	1014.0	28.8	1030.1	73.0	1030.1	73.0	97.7
021112PR-01-5	79	70934	4.6	13.5705	0.9	1.7129	1.9	0.1686	1.7	0.87	1004.3	15.7	1013.4	12.4	1033.0	19.0	1033.0	19.0	97.2
021112PR-01-41	93	48470	1.3	13.5429	1.8	1.7222	2.6	0.1692	1.9	0.72	1007.5	17.6	1016.8	16.9	1037.1	37.0	1037.1	37.0	97.1
021112PR-01-21	88	64375	2.9	13.5288	2.4	1.7295	3.3	0.1697	2.2	0.68	1010.5	20.7	1019.6	21.0	1039.2	48.3	1039.2	48.3	97.2
021112PR-01-8	76	39979	1.5	13.5161	2.2	1.8098	2.9	0.1774	1.9	0.65	1052.8	18.3	1049.0	18.8	1041.1	43.9	1041.1	43.9	101.1
021112PR-01-45	93	31507	1.7	13.4996	1.9	1.7674	2.5	0.1730	1.5	0.62	1028.9	14.7	1033.6	16.0	1043.5	39.0	1043.5	39.0	98.6
021112PR-01-74	117	62319	2.1	13.4977	1.3	1.7853	2.4	0.1748	2.1	0.86	1038.3	19.9	1040.1	15.8	1043.8	25.3	1043.8	25.3	99.5
021112PR-01-3	64	87403	1.8	13.4967	2.8	1.7543	3.5	0.1717	2.0	0.59	1021.6	19.2	1028.7	22.3	1044.0	56.2	1044.0	56.2	97.9
021112PR-01-17	301	208518	2.5	13.4900	0.4	1.7432	1.6	0.1705	1.6	0.97	1015.1	15.0	1024.6	10.6	1045.0	8.4	1045.0	8.4	97.1
021112PR-01-75	280	97934	0.4	13.4786	1.0	1.7475	2.1	0.1708	1.9	0.88	1016.7	17.6	1026.3	13.7	1046.7	20.2	1046.7	20.2	97.1
021112PR-01-28	241	110675	3.2	13.4687	0.7	1.7794	1.6	0.1738	1.4	0.91	1033.1	13.6	1037.9	10.2	1048.2	13.2	1048.2	13.2	98.6
021112PR-01-73	120	243103	2.9	13.4616	1.6	1.7967	7.5	0.1754	7.4	0.98	1041.9	70.8	1044.3	49.2	1049.3	32.9	1049.3	32.9	99.3
021112PR-01-13	56	31014	2.1	13.4458	2.3	1.6886	4.9	0.1647	4.4	0.89	982.7	40.0	1004.2	31.5	1051.6	45.6	1051.6	45.6	93.4
021112PR-01-55	64	33177	1.0	13.4088	1.4	1.7291	2.5	0.1682	2.0	0.83	1001.9	18.9	1019.4	15.9	1057.2	27.9	1057.2	27.9	94.8
021112PR-01-85	57	39615	1.4	13.4041	2.1	1.8548	3.2	0.1803	2.4	0.75	1068.7	23.5	1065.1	21.0	1057.9	42.4	1057.9	42.4	101.0
021112PR-01-95	119	130251	2.3	13.3999	1.1	1.8274	1.7	0.1776	1.3	0.76	1053.8	12.4	1055.3	10.9	1058.5	21.6	1058.5	21.6	99.6
021112PR-01-91	23	15802	2.6	13.3813	5.9	1.7262	7.4	0.1675	4.5	0.60	998.5	41.3	1018.3	47.8	1061.3	119.6	1061.3	119.6	94.1
021112PR-01-27	225	119540	3.0	13.3736	0.6	1.8086	1.6	0.1754	1.5	0.92	1042.0	14.6	1048.6	10.8	1062.5	12.9	1062.5	12.9	98.1
021112PR-01-92	79	65696	2.1	13.3445	1.7	1.8604	2.1	0.1801	1.2	0.58	1067.3	11.8	1067.1	13.8	1066.8	34.4	1066.8	34.4	100.0
021112PR-01-56	49	37548	1.9	13.2935	2.9	1.7718	3.4	0.1708	1.7	0.51	1016.7	16.5	1035.2	22.1	1074.5	58.6	1074.5	58.6	94.6
021112PR-01-84	165	212424	2.8	13.2889	1.4	1.8913	3.4	0.1823	3.2	0.92	1079.5	31.5	1078.0	22.9	1075.2	27.4	1075.2	27.4	100.4
021112PR-01-29	116	61017	2.8	13.2858	1.5	1.8374	2.4	0.1770	1.9	0.79	1050.8	18.5	1058.9	16.0	1075.7	30.1	1075.7	30.1	97.7
021112PR-01-51	114	46351	2.1	13.2612	1.3	1.8756	3.1	0.1804	2.8	0.90	1069.1	27.6	1072.5	20.6	1079.4	26.8	1079.4	26.8	99.1
021112PR-01-101	211	85715	3.5	13.1689	0.9	1.9096	2.0	0.1824	1.8	0.90	1080.0	17.6	1084.4	13.1	1093.4	17.1	1093.4	17.1	98.8
021112PR-01-34	253	105731	1.6	13.1566	0.7	1.8703	2.2	0.1785	2.1	0.95	1058.6	20.9	1070.6	14.9	1095.3	13.5	1095.3	13.5	96.6
021112PR-01-20	85	52181	3.6	13.1482	0.7	1.9440	2.1	0.1854	1.9	0.94	1096.3	19.4	1096.4	13.8	1096.5	14.4	1096.5	14.4	100.0
021112PR-01-2	42	35711	1.0	13.1241	4.1	1.8861	4.8	0.1795	2.4	0.51	1064.4	23.9	1076.2	31.6	1100.2	81.8	1100.2	81.8	96.7
021112PR-01-14	61	110905	1.6	13.1017	2.1	1.7858	4.1	0.1697	3.6	0.86	1010.4	33.2	1040.3	26.9	1103.6	42.2	1103.6	42.2	91.6
021112PR-01-31	308	207784	2.5	13.0786	1.3	1.9967	5.4	0.1894	5.2	0.97	1118.1	53.8	1114.4	36.5	1107.2	25.8	1107.2	25.8	101.0
021112PR-01-47	211	91016	5.1	13.0726	1.5	1.9050	2.8	0.1806	2.4	0.85	1070.3	23.3	1082.8	18.5	1108.1	29.5	1108.1	29.5	96.6
021112PR-01-3	248	162475	3.1	13.0463	1.1	2.0454	4.7	0.1935	4.5	0.97	1140.5	47.4	1130.8	31.9	1112.1	22.5	1112.1	22.5	102.6
021112PR-01-65	266	93135	6.5	13.0061	0.6	2.0108	2.1	0.1897	2.0	0.96	1119.7	21.0	1119.2	14.4	1118.3	11.3	1118.3	11.3	100.1
021112PR-01-25	105	69052	1.9	12.9844	1.3	2.0470	4.0	0.1928	3.8	0.94	1136.4	39.6	1131.3	27.5	1121.6	26.6	1121.6	26.6	101.3
021112PR-01-87	124	68194	2.4	12.9433	0.9	1.9958	3.0	0.1874	2.9	0.95	1107.0	29.4	1114.1	20.5	1127.9	18.1	1127.9	18.1	98.1
021112PR-01-22	33	22314	1.3	12.9384	2.9	2.1061	4.8	0.1976	3.9	0.80	1162.6	41.1	1150.8	33.2	1128.7	57.1	1128.7	57.1	103.0
021112PR-01-76	131	94500	1.3	12.9378	1.1	1.9598	2.9	0.1839	2.7	0.93	1088.2	26.6	1101.8	19.3	1128.8	21.6	1128.8	21.6	96.4
021112PR-01-58	134	81804	3.6	12.9189	0.9	1.8466	3.8	0.1730	3.6	0.97	1028.8	34.7	1062.2	24.8	1131.7	18.6	1131.7	18.6	90.9
021112PR-01-54	90	83972	2.9	12.8886	1.9	1.9734	2.2	0.1845	1.2	0.54	1091.3	11.9	1106.5	14.9	1136.4	37.1	1136.4	37.1	96.0

021112PR-01-30	173	251836	3.7	12.8394	0.8	2.0561	2.0	0.1915	1.9	0.91	1129.3	19.4	1134.3	14.0	1143.9	16.5	1143.9	16.5	98.7
021112PR-01-88	221	419855	3.9	12.8351	0.3	2.0845	1.0	0.1940	1.0	0.97	1143.2	10.1	1143.7	6.8	1144.6	5.0	1144.6	5.0	99.9
021112PR-01-60	336	192473	5.8	12.8268	0.3	2.0557	1.0	0.1912	0.9	0.94	1128.1	9.3	1134.2	6.5	1145.9	6.2	1145.9	6.2	98.4
021112PR-01-57	207	328788	3.0	12.8187	0.9	2.1054	2.1	0.1957	1.9	0.90	1152.4	20.1	1150.6	14.6	1147.1	18.2	1147.1	18.2	100.5
021112PR-01-83	57	39695	1.0	12.8123	2.8	2.0774	3.4	0.1930	2.0	0.58	1137.8	20.8	1141.4	23.6	1148.1	55.9	1148.1	55.9	99.1
021112PR-01-4	46	34221	4.1	12.8108	4.0	2.1019	4.2	0.1953	1.3	0.31	1150.0	13.6	1149.4	28.9	1148.4	79.4	1148.4	79.4	100.1
021112PR-01-103	67	114351	2.7	12.8071	1.4	2.0917	2.0	0.1943	1.5	0.73	1144.6	15.2	1146.1	13.7	1149.0	27.0	1149.0	27.0	99.6
021112PR-01-9	113	214869	2.5	12.7803	1.1	2.0737	3.8	0.1922	3.6	0.95	1133.4	37.8	1140.2	26.1	1153.1	22.7	1153.1	22.7	98.3
021112PR-01-40	55	35212	1.3	12.7738	1.4	1.9238	3.0	0.1782	2.7	0.89	1057.3	26.1	1089.4	20.2	1154.1	27.7	1154.1	27.7	91.6
021112PR-01-33	24	29717	1.6	12.7629	5.8	1.9936	6.1	0.1845	1.8	0.30	1091.7	18.2	1113.4	41.3	1155.8	115.6	1155.8	115.6	94.5
021112PR-01-99	69	58029	1.4	12.7551	2.1	2.1011	3.6	0.1944	2.8	0.80	1145.0	29.8	1149.2	24.5	1157.0	42.5	1157.0	42.5	99.0
021112PR-01-62	130	107778	1.4	12.7392	1.1	2.1855	2.3	0.2019	2.1	0.88	1185.7	22.4	1176.4	16.3	1159.5	21.6	1159.5	21.6	102.3
021112PR-01-11	117	141589	3.0	12.7117	1.2	2.0649	2.9	0.1904	2.7	0.91	1123.4	27.7	1137.3	20.1	1163.8	23.5	1163.8	23.5	96.5
021112PR-01-5	85	72079	2.4	12.6410	1.8	2.1692	3.2	0.1989	2.6	0.82	1169.3	28.2	1171.2	22.4	1174.9	36.5	1174.9	36.5	99.5
021112PR-01-10	102	83635	2.3	12.6402	1.6	2.1280	2.7	0.1951	2.2	0.80	1148.9	23.0	1157.9	18.9	1175.0	32.6	1175.0	32.6	97.8
021112PR-01-37	115	43510	1.1	12.6311	1.2	2.1001	3.1	0.1924	2.9	0.92	1134.3	30.0	1148.8	21.5	1176.4	23.7	1176.4	23.7	96.4
021112PR-01-42	32	22602	2.6	12.6111	3.7	2.0986	5.0	0.1919	3.4	0.68	1131.9	35.4	1148.3	34.7	1179.5	73.6	1179.5	73.6	96.0
021112PR-01-63	59	54823	2.5	12.5973	1.8	2.1569	2.4	0.1971	1.6	0.68	1159.5	17.2	1167.3	16.6	1181.7	34.8	1181.7	34.8	98.1
021112PR-01-81	103	72852	1.4	12.5369	1.3	2.1750	1.9	0.1978	1.3	0.72	1163.3	14.3	1173.1	12.9	1191.2	25.3	1191.2	25.3	97.7
021112PR-01-94	99	60972	2.3	12.5244	0.7	2.2249	2.2	0.2021	2.1	0.95	1186.6	23.1	1188.9	15.6	1193.2	13.1	1193.2	13.1	99.4
021112PR-01-93	123	86181	3.1	12.4422	1.1	2.3089	2.0	0.2083	1.6	0.81	1220.0	17.8	1215.0	13.9	1206.1	22.4	1206.1	22.4	101.2
021112PR-01-23	56	46161	1.2	12.4412	1.7	2.1910	2.6	0.1977	1.9	0.76	1162.9	20.7	1178.2	17.8	1206.3	32.6	1206.3	32.6	96.4
021112PR-01-78	32	14566	2.4	12.4021	4.6	2.1228	5.7	0.1909	3.3	0.58	1126.5	34.3	1156.2	39.4	1212.5	91.3	1212.5	91.3	92.9
021112PR-01-39	60	33891	2.2	12.3585	2.8	2.1775	3.3	0.1952	1.8	0.55	1149.3	19.5	1173.9	23.3	1219.4	54.9	1219.4	54.9	94.3
021112PR-01-35	107	126483	3.4	12.3020	0.9	2.2767	1.3	0.2031	0.9	0.70	1192.1	9.6	1205.1	8.9	1228.4	17.7	1228.4	17.7	97.1
021112PR-01-16	137	191786	3.3	12.2531	0.8	2.3742	1.7	0.2110	1.5	0.89	1234.1	17.0	1234.9	12.1	1236.2	15.0	1236.2	15.0	99.8
021112PR-01-12	560	623301	2.8	12.2053	0.3	2.4303	1.5	0.2151	1.5	0.98	1256.1	17.2	1251.6	11.0	1243.9	5.2	1243.9	5.2	101.0
021112PR-01-67	110	59250	1.5	12.1629	1.1	2.3895	2.5	0.2108	2.2	0.89	1233.0	24.7	1239.5	17.6	1250.7	21.7	1250.7	21.7	98.6
021112PR-01-66	84	42988	2.1	12.1214	1.3	2.3307	3.2	0.2049	2.9	0.91	1201.6	31.5	1221.7	22.5	1257.4	25.8	1257.4	25.8	95.6
021112PR-01-43	119	25146	1.0	11.9198	1.5	2.5111	2.9	0.2171	2.5	0.87	1266.5	28.9	1275.3	21.1	1290.1	28.3	1290.1	28.3	98.2
021112PR-01-38	257	23736	1.9	11.5413	3.1	2.5212	7.6	0.2110	7.0	0.92	1234.3	78.7	1278.2	55.6	1352.6	59.0	1352.6	59.0	91.3
021112PR-01-64	80	71951	2.8	11.3734	1.0	2.8716	2.7	0.2369	2.5	0.93	1370.4	30.5	1374.5	20.0	1380.8	18.6	1380.8	18.6	99.2
021112PR-01-97	109	88318	2.3	11.1465	0.8	2.9697	2.8	0.2401	2.7	0.95	1387.1	33.3	1399.9	21.3	1419.4	16.2	1419.4	16.2	97.7
021112PR-01-11	42	4110	1.5	11.0658	5.3	2.8342	7.2	0.2275	4.9	0.68	1321.2	58.6	1364.6	54.1	1433.3	100.8	1433.3	100.8	92.2
021112PR-01-96	77	62331	1.8	10.9454	1.2	3.1292	2.1	0.2484	1.7	0.83	1430.3	22.4	1439.9	16.1	1454.1	21.9	1454.1	21.9	98.4
021112PR-01-6	60	70047	2.6	10.9214	1.3	3.1432	1.8	0.2490	1.3	0.71	1433.2	16.7	1443.3	14.1	1458.3	24.7	1458.3	24.7	98.3
021112PR-01-90	10	14364	1.1	10.7263	10.0	3.0206	10.6	0.2350	3.6	0.34	1360.6	44.4	1412.8	81.3	1492.5	189.7	1492.5	189.7	91.2
021112PR-01-61	392	321050	0.9	10.4719	0.2	3.5469	1.2	0.2694	1.2	0.99	1537.7	16.3	1537.7	9.6	1537.8	3.6	1537.8	3.6	100.0

Appendix N Detrital zircon concordia diagrams for U-Pb systems

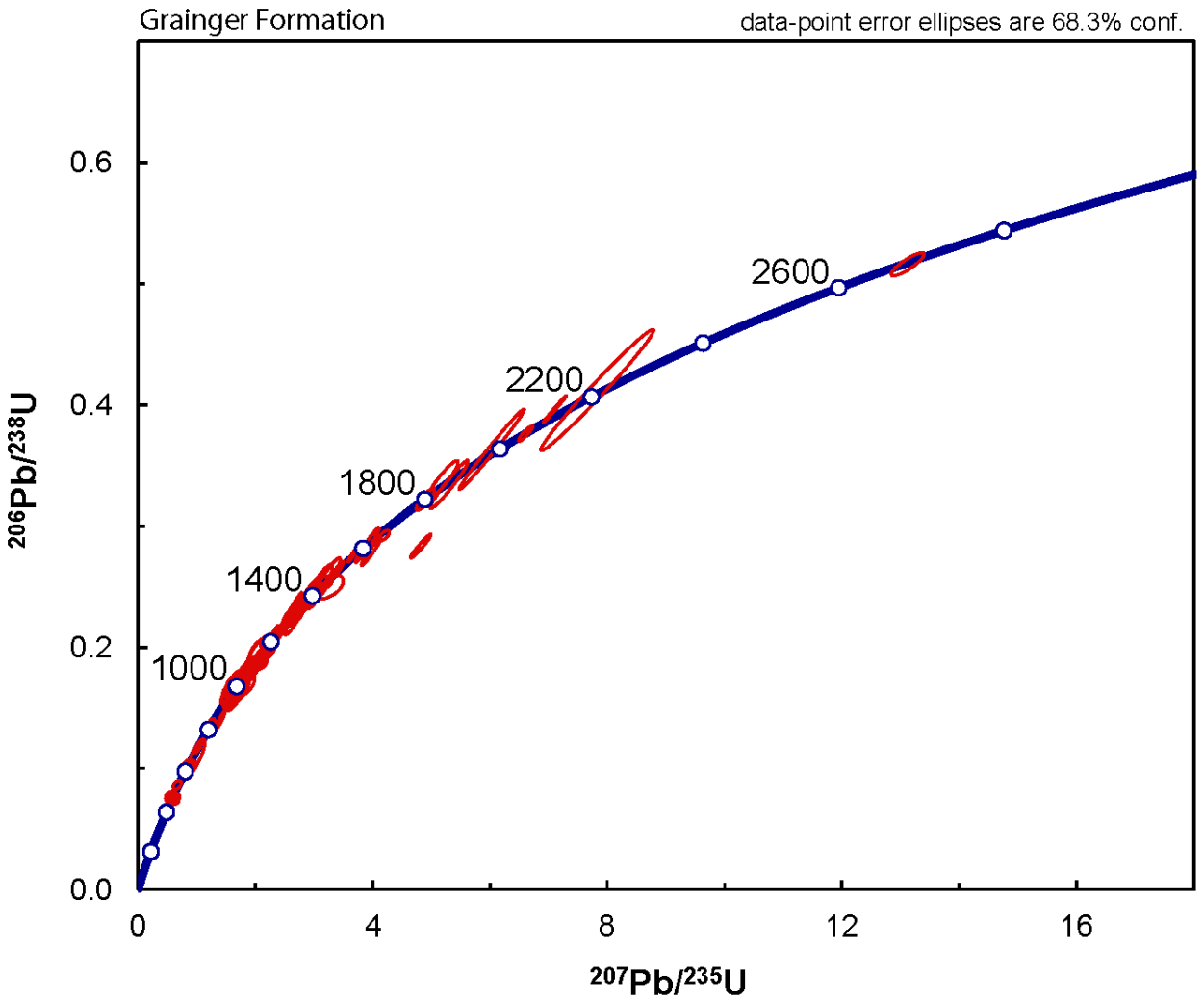

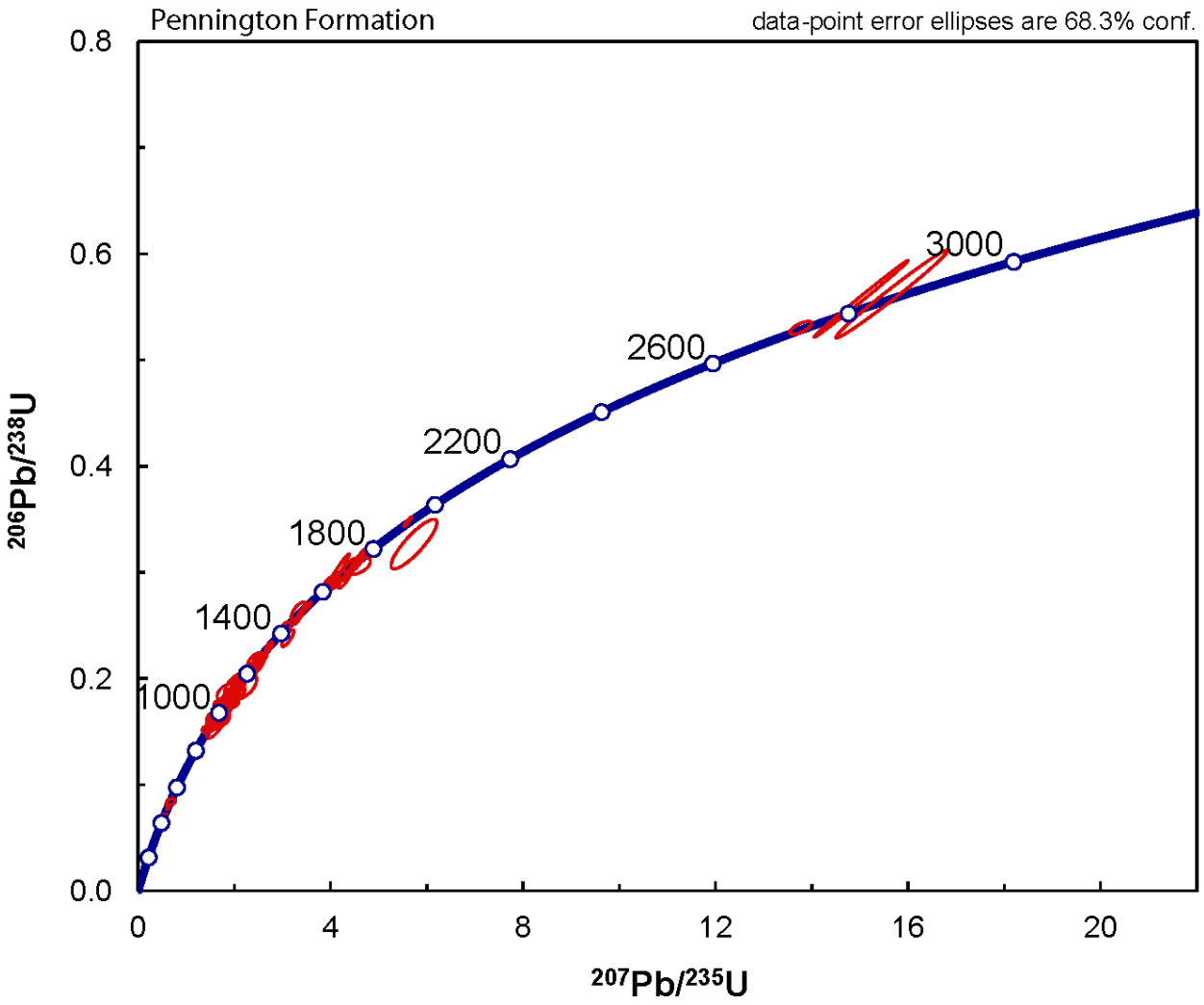
Pennington Formation
data-point error ellipses are 68.3% conf.
0.8
0.6
0.4
0.2
0.0
0
4
8
12
16
20
1000
1400
1800
2200
2600
3000
206Pb/238U
207Pb/235U

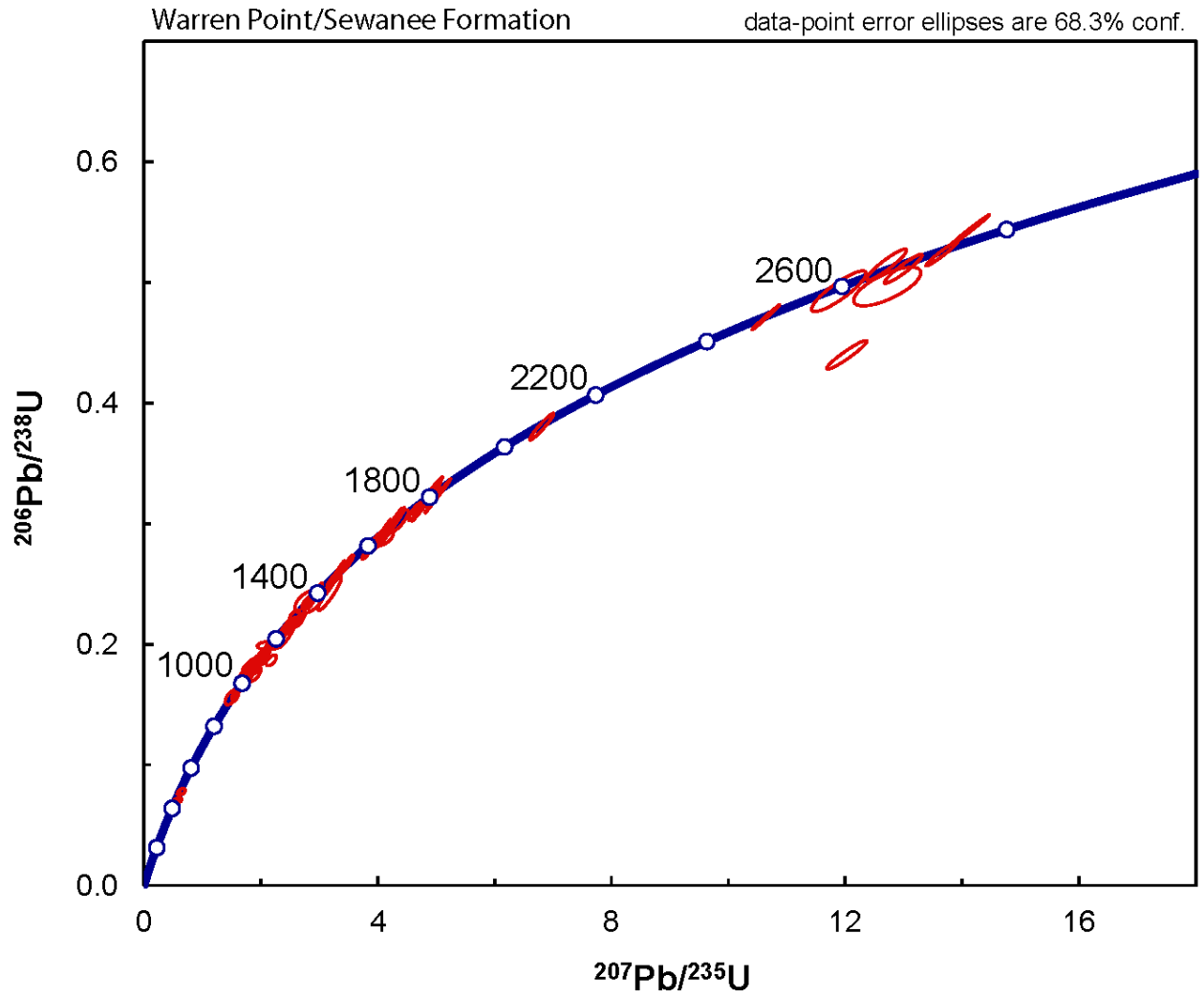
Warren Point/Sewanee Formation
data-point error ellipses are 68.3% conf.
0.6
0.4
0.2
0.0
206Pb/238U
2600
2200
1800
1400
1000
0
4
8
12
16
207Pb/235U

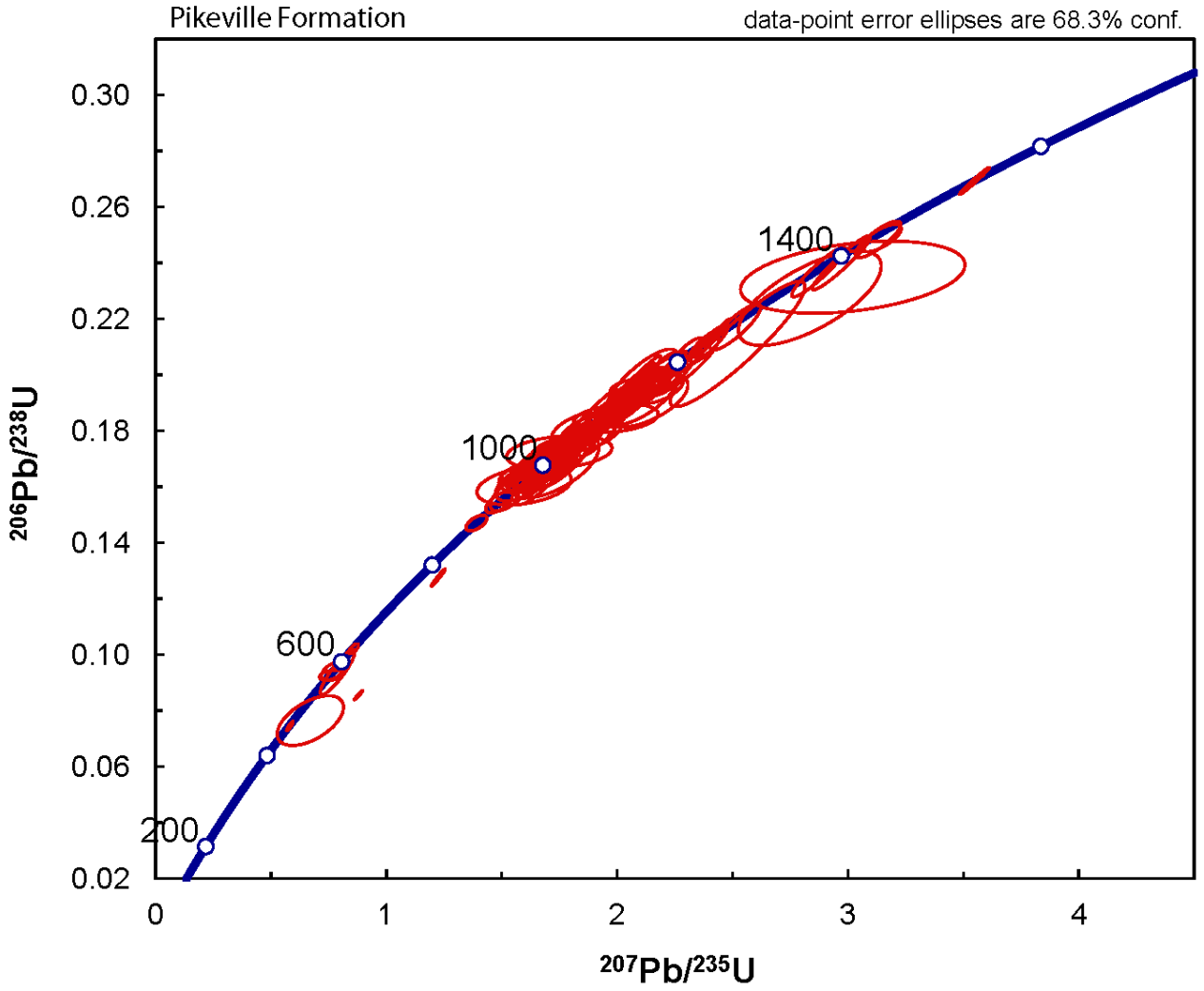
Pikeville Formation
data-point error ellipses are 68.3% conf.
0.30
0.26
0.22
0.18
0.14
0.10
0.06
0.02
206Pb/238U
0
1
2
3
4
207Pb/235U
200
600
1000
1400